Ontwikkeling van een numeriek kader
voor het evalueren van de invloed van connectie-eigenschappen
op de performantie-index van geschroefde OCTG-connecties

Development of a Numerical Framework
to Assess the Influence of Connection Characteristics
on the Performance-Rating of OCTG Threaded Connections

Timothy Galle

Promotoren: prof. dr. ir. W. De Waele, prof. dr. ir. P. De Baets
Proefschrift ingediend tot het behalen van de graad van
Doctor in de Ingenieurswetenschappen: Werktuigkunde-Elektrotechniek

Vakgroep Elektrische Energie, Systemen en Automatisering
Voorzitter: prof. dr. ir. J. Melkebeek
Faculteit Ingenieurswetenschappen en Architectuur
Academiejaar 2015 - 2016

ISBN 978-90-8578-890-4
NUR 929
Wettelijk depot: D/2016/10.500/22

Supervisors

prof. dr. ir. P. De Baets
prof. dr. ir. W. De Waele

Ghent University
Faculty of Engineering and Architecture
Department of Electrical Energy, Systems and Automation

Examination Committee

Prof. P. De Baets	-	*Ghent University*
Prof. W. De Waele	-	*Ghent University*
Prof. S. Hertelé	-	*Ghent University*
Dr. F. Van den Abeele	-	*Subseawolf*
Prof. R. Van de Walle	-	*Ghent University*
Eur. Ing. H. Van Rijzingen	-	*National Oilwell Varco*
Dr. J. Van Wittenberghe	-	*OCAS nv / Arcelor Mittal*
Prof. P. Verleysen	-	*Ghent University*

Research Institute

Ghent University
Department of Electrical Energy, Systems and Automation
Soete Laboratory

Technologiepark 903
B-9052 Zwijnaarde
Belgium

Tel. +32 9 331 04 99
Fax +32 9 331 04 90
Mail Timothy.Galle@UGent.be

www.SoeteLaboratory.UGent.be

"Life [A PhD] is full of disappointments;
as one reaches one ridge there is always another
and a higher one beyond which blocks the view"

- Fridtjof Nansen
explorer, scientist and diplomat

Acknowledgements

Prior to presenting an overview of the research I conducted, I would like to take the time to implicitly and explicitly thank the many people who made this possible.

First of all, I would like to thank my supervisors, prof. P. De Baets and prof. W. De Waele for allowing me to conduct this research at Ghent University, Soete Laboratory. In addition, my gratitude goes towards Jeroen Van Wittenberghe who introduced me into the subject of threaded connections. In addition, this research wouldn't have been possible without the financial support of OCAS NV/ArcelorMittal Global R&D Gent.

Next, I would like to thank all people who provided topic-related feedback, information and with whom I could discuss various matters from an industrial point of view. In particular, I would like to thank the following people:

- *François Conrad (Vallourec)*
- *Sebastián Cravero (Tenaris)*
- *Ahmed El Saghier (Independent Consultant OCTG & Linepipe)*
- *Jacques Schueremans (Soconord)*
- *Filip Van den Abeele (Subseawolf),*
- *Hans Van Rijzingen (National Oilwell Varco)*
- *Larry W. Vincent (High Performance Tubular Goods)*

Subsequently, my gratitude goes towards all people involved in any of my spare time occupations. I'd like to thank all of my hyper active, normal active and less active fellow runners. In order to take my mind off my research, I had to have a run once in a while. As it turned out, these runs were required to be quite far in order to have the desired effect… Nevertheless, these people made sure the running through forests, over mountains, through rivers,… remained enjoyable.

Also the people of Belgian Red Cross deserve a 'thank you'. They gave/give me the ability to spend a part of my spare time doing something of value for the society. While the knowledge gathered during a PhD may (indirectly) contribute to people's comfort in the long term; it is enjoyable to help people directly. Additionally, this bunch of people is not just a group of Red Cross colleagues, but a group of Red Cross friends with whom you can just relax and have a great time.

Next, I would like to thank all people I met during any of my (initiations to) polar trips. These people made me rediscover the magnitude and the beauty nature has to offer. This is something which is often overlooked when spending a considerable amount of time sitting on a chair… in an office… behind a computer. They made me realize that if you can dream it and you want it, you can do it. While a PhD may be an important realization, something to be proud of, there are other things in life which are more ambitious, more difficult and much more rewarding for you, as a person.

Finally, I would like to thank all colleagues for making life at the office possible and for allowing me to conduct all the research I could ever wish for. Also my friends deserve a special word of thanks. Without them, everyday life would be boring and after all, nothing beats a good laugh! Last but not least, I would like to thank my family. Without them, not only the PhD, but anything of the things described above would be possible.

To conclude, I would like to take the time to thank my mother who, unfortunately, passed away during the completion of this PhD but who, I'm sure, would have believed in the successful completion of this research.

This being said, I'd like to urge you to read the dissertation. While not everything may be mind-blowing, I'm sure there are some things which could be helpful if you're interested in threaded connections and their design.

Timothy Galle

Ghent, 2016

Summary

When establishing wells to collect gas and oil, threaded connections are indispensable when creating the required drill-, casing- and tubing strings because of their ability to rapidly connect pipes with each other. Also their ability to disconnect and reuse the equipment results in the preference of using threaded connections over welded connections. Among these connections, various types containing a variety of features depending on the intended application exist. Within this research, connections containing only a tapered thread are considered. However, this does not mean that the proposed methodologies and approaches are solely limited to connections of this type.

Currently, the ultimate design objective for these connections is to acquire a connection having the same or even higher strength compared to the pipe body of the pipes it connects without increasing the outer diameter, resulting in a flush-like transition between the pipes. The first objective is required to ensure that the connection is not the weakest part of the string, while the latter reduces the need for additional clearance when installing pipes. This also lowers the probability of getting stuck down hole, being economically beneficial. In order to work towards this design objective, it is crucial to know the effects of small changes to the various parameters of the connection, and in particular of the thread itself.

In order to analyze the effects of small changes on the mechanical performance of the connection when subjected to internal pressure and axial tension, the numerical script "*ThreadGenBT*" is developed. This python script allows the generation of 2D axisymmetric, numerical models of couplings containing tapered, trapezoidal threads and results in an increased efficiency when conducting parametric studies. While the use of these 2D axisymmetric models is generally accepted, the method of applying the initial preload (make-up) is counterintuitive and additional validation is performed. For this reason, the **2D axisymmetric model is compared with a full 3D model** to evaluate the initially applied preload. This numerical comparison has not yet been conducted in available literature for these types of connections and it is concluded that the increased accuracy associated with the complex 3D models does not outweigh the benefits of reduced calculation times and simplicity

using the 2D axisymmetric models. By using a simple modification taking into account the internal energy of the connection, the make-up torque obtained by the 2D model matches the one obtained by the 3D model. In addition, stress-strain fields prove to be identical.

While the numerical comparison of a full 3D model with the used 2D axisymmetric model is limited to only the preload during assembly stage, the experimental procedure contains, in addition to make-up, workloads consisting of internal pressure combined with axial tension. Since the experimental tests are only applied to validate the numerical modeling approach, full scale testing is not required and therefore, small scale connections with an outer diameters of about 50 mm are used. In order to conduct reliable and realistic tests, the testing procedures described in the ISO 13679 standard are used as a guideline and consist of: a make-up, a test load envelope (TLE) and a limit load test. Using the make-up tests, it is found that a **better approximation of the torque-turn diagram** during assembly is possible when combining the calculated contact pressure over the threaded region with the contact pressure dependent coefficient of friction of the applied thread compound. Furthermore, when conducting a test load envelope (TLE), the strains which are monitored using strain gauges and digital image correlation match the numerically predicted ones and differences with a less than 5% error margin, increasing the reliability of the numerical methodology. In addition to these strains, **temperatures are monitored** using thermocouples and infrared monitoring. While limited temperature variations occur when combined loads below the connection's yield strength are applied (during the TLE test), significant temperature increases are observed when testing the connection up to failure due to the induced plastic deformation. Using these observations, a new methodology using the same model is suggested to **accurately approximate the connection's weakest section when axial loads exceeding the yield strength** are applied. In addition to the ability of more accurately predicting post-yield fracture, the observed temperatures can be used as an indirect indication for contact pressure during make-up and even for misalignment.

Once the finite element model is considered to be sufficiently validated, a parametric study is conducted to investigate the **effect of various connection variables on its mechanical performance**. In order to do this, three performance parameters are defined: the load distribution over the threads, the thread clearance between the opposing flanks and the overall plasticity of the joint. During this study, the effects of changing the thread angles are not reflected in the resulting performance parameters when sufficient initial preload was applied. In contrast, modifying the thread taper, wall thickness or scaling the threads has significant effects on the performance of the coupling. Apart from geometrical features, changing the material characteristics of at least one of the members is considered. This can be beneficial for the mechanical performance until both members have a similar strength. In

contrast, increasing the strength of the material of the entire connection does not result in significant performance enhancement when considering the applied load relative to the material's yield strength.

Using the developed, validated numerical script in combination with the conducted parametric study, a **new connection named "LS95R"** is developed using a standard API Buttress connection as the initial starting point. While this enhanced design is not subjected to experimental testing, the numerical analysis suggests that the internal pressure resistance of the LS95R is likely to be higher than the accepted maximum of 175 bars for standard API Buttress connections. In addition, the axial tensile strength is believed to be at least 95% of the pipe body strength, which is similar than the standard connections. Nevertheless, a significant reduction of the outer diameter results in a design which is one step closer towards the ultimate design objective in which a connection is achieved with a 100% mechanical efficiency relative to the pipe body without locally increasing the outer diameter of the string.

To conclude, some remarks are made suggesting plausible methods to **better approximate occurring contact pressures** using thermography. This approach could particularly be interesting for studies investigating galling. In addition, a possible approach is suggested which would allow the implementation of **dopefree and premium connections** by implementing a coating layer, a torque shoulder and/or a sealing surface.

Samenvatting (Dutch summary)

Bij het exploiteren van olie- en gasbronnen worden schroefverbindingen gebruikt voor het assembleren van boor-, behuizings- en transportpijpen, welke typisch een lengte hebben tot 16 m, om zo hun respectievelijke stringen te maken. Het voordeel van dit type connecties ten opzichte van het gebruik van gelaste verbindingen wordt gekenmerkt door de snelheid waarbij deze verbindingen tot stand komen. Vervolgens primeert ook de mogelijkheid om de verbindingen uit te breken om zo de pijpen te hergebruiken. Momenteel is er een groot aanbod geschroefde verbindingen commercieel beschikbaar en wordt er gekozen op basis van de toepassing en de verwachte belastingen. Tijdens dit onderzoek worden enkel standaardverbindingen met een conische, trapeziumvormige schroefdraad onderzocht. Dit impliceert echter niet dat de voorgestelde methodologie en aanpak gelimiteerd is tot dit soort verbindingen.

Op industrieel niveau bestaat het ultieme doel er momenteel uit om een verbinding te ontwerpen met eenzelfde, of zelfs hogere, sterkte dan die van de buizen die verbonden worden zonder de buitendiameter te vergroten. Het eerste deel van deze doelstelling verzekert dat de verbinding niet het zwakste deel van de string is. De vloeiende overgang tussen de pijpen laat toe mogelijke speling te verkleinen wanneer strings geïnstalleerd worden, hetgeen resulteert in een kleiner boorgat. Bovendien vermindert ook het risico om tijdens installatie vast te komen te zitten. Vooraleer naar dit doel toegewerkt kan worden is het belangrijk dat de effecten van kleine wijzigingen aan de geometrie van de verbinding op het gedrag ervan (na aanleg van belasting) gekend zijn.

Om de effecten van kleine veranderingen aan de verbinding onder invloed van een combinatie van inwendige druk en axiale trekkracht te analyseren, wordt het numerieke script "ThreadGenBT" ontwikkeld. Dit python script maakt het mogelijk 2D axisymmetrische, numerieke modellen te genereren van geschroefde verbindingen welke een conische, trapeziumvormige schroefdraad bevatten. Dit resulteert in een verhoogde efficiëntie bij het uitvoeren van parameterstudies. Niettegenstaande dat het gebruik van deze 2D axisymmetrische modellen algemeen aanvaard wordt, is de wijze waarop de initiële opmaak gesimuleerd wordt contra-intuïtief en vereist daarom extra

controle. Daarom wordt het gebruik van het **2D axisymmetrisch modellen vergeleken met een volledig 3D model**. Deze vergelijking is nog niet beschreven in de beschikbare literatuur voor dit type verbinding en leidt tot de conclusie dat de voordelen van het simuleren van de schroefdraad helix, welke aanwezig is in het complexe 3D-model, niet opweegt tegenover de voordelen van snel rekenende, eenvoudigere 2D-axisymmetrische modellen. Door een kleine aanpassing welke gebruik maakt van de resulterende inwendige energie van de koppeling is het mogelijk het opmaakkoppel, verkregen met het 3D model, accuraat te benaderen aan de hand van de 2D resultaten. Bovendien blijkt het spanning-rek veld voor beide modellen quasi identiek te zijn.

Terwijl de numerieke vergelijking van het volledige 3D model met het gebruikte 2D axisymmetrische model beperkt is tot de opmaak procedure, bevat het experimentele gedeelte ook externe belastingen bestaande uit een combinatie van inwendige druk en axiale rek. Daar de experimentele testen alleen uitgevoerd worden om de numerieke methodologie te valideren, volstaat het om kleinschalige, niet-gestandaardiseerde verbindingen met een buitendiameter van ongeveer 50 mm te gebruiken. Om betrouwbare en realistische experimenten uit te voeren, worden de testprocedures uit de ISO 13679 norm als leidraad gebruikt. Deze procedure bestaat uit: een opmaak test, een test enveloppe (TLE) en een faaltest. Gebaseerd op de resultaten van de opmaaktesten blijkt een **betere benadering van de koppel-rotatie diagram** mogelijk te zijn wanneer de contactdrukafhankelijke wrijvingscoëfficiënt van het gebruikte smeeringmiddel in rekening gebracht wordt. Bij het uitvoeren van de TLE testen, vallen de numeriek voorspelde rekken binnen een 5% foutenmarge wanneer deze vergeleken worden met de opgemeten rekken. Het opmeten gebeurde zowel met conventionele rekstrookjes als met meer geavanceerde, optische, digitale beeldcorrelatie (DIC). Naast rekken wordt ook **de temperatuurverdeling aan de buitenzijde van de verbinding gemonitord** met behulp van thermokoppels en infrarood technologie. Hoewel beperkte temperatuurvariaties merkbaar zijn gedurende de TLE test, zijn significante stijgingen ten gevolge van wrijvingsenergie en plastische vervormingen enkel waarneembaar tijdens respectievelijk de opmaak test en de faaltest. Met behulp van deze waarnemingen wordt de nieuwe methodologie op punt gezet om, gebruik makend van het 2D model, het **zwakste gedeelte van de verbinding te identificeren wanneer een axiale belasting aangelegd wordt die de vloeigrens overschrijdt**. Naast het vermogen om nauwkeuriger te voorspellen waar breuk zal optreden, kan de waargenomen temperaturen ook gebruikt worden als een indirecte indicatie voor contactdruk en eventuele voor het detecteren van een foutieve uitlijning tijdens de opmaak van de verbinding.

Na het eindige elementen model voldoende gevalideerd te hebben, wordt een parametrische studie uitgevoerd om het **effect van wijzigingen van de connectieparameters op de mechanische performantie** te onderzoeken. Deze

performantie wordt gedefinieerd aan de hand van drie karakteristieken: de lastverdeling over de tanden, de speling tussen de aanliggende tandflanken en de totale plasticiteit van de connectie. Tijdens dit onderzoek blijkt dat het effect van veranderende tandflankhoeken niet weerspiegeld wordt in de vooropgestelde karakteristieken indien er voldoende initiële voorspanning werd aangelegd tijdens de opmaak. In contrast hebben wijziging van de coniciteit, wanddikte en tandgrootte wel een merkbare invloed op de performantie van de connectie. Naast geometrische wijzigingen wordt ook de invloed van de materiaalsterkte beschouwd. Hieruit kan besloten worden dat het wijzigen van het materiaal van één van de leden gunstig kan zijn voor de mechanische prestaties tot wanneer beide leden een vergelijkbare sterkte hebben. Daarentegen leidt het verhogen van de materiaalsterkte van de gehele verbinding niet tot significante voordelen wanneer de uitgeoefende belasting relatief ten opzichte van de vloeigrens van het materiaal beschouwd wordt.

Gebruik makend van het gevalideerde, numerieke script in combinatie met de gevonden prestatieverbeteringen ten gevolge van variërende geometrische parameters en materialen wordt een **nieuwe verbinding, genaamd "LS95R"**, ontwikkeld op basis van de standaard API Buttress verbinding. Hoewel dit geoptimaliseerde ontwerp niet experimenteel gevalideerd is, suggereert de numerieke analyse dat de maximale inwendige druk vermoedelijk hoger is dan 175 bar, welke momenteel geldt voor de standaard API Buttress verbindingen. Bovendien kan een axiale belasting tot minstens 95% van de maximale treksterkte van de verbonden pijpen aangelegd worden, hetwelk vergelijkbaar is voor de standaard verbindingen. Niettemin is een aanzienlijke vermindering van de resulterende buitendiameter een belangrijke stap dichter bij het ultieme industriële ontwerpdoel.

Tot slot wordt een methode aangereikt welke toelaat om **de optredende contactdrukken beter te benadering** met behulp van infrarood thermografie. Dit zou kunnen bijdragen bij onderzoek naar het ontstaan van koudlassen in de contactzones van de geschroefde verbinding. Daarnaast wordt een mogelijke aanpak beschreven om het gebruik van de beschreven methodologie verder uit te breiden naar **geavanceerde verbindingen** welke een torsieschouder, afdichtsoppervlak en/of vaste coating over de tanden kunnen hebben.

Publications

A1 Peer reviewed journal publications included in Science Citation Index

1. **Galle, T.**, De Waele, W., and De Baets, P. (2013). Effect of Make-up on the Structural Performance of Standard Buttress Connections Subjected to Tensile Loading. *JOURNAL OF PRESSURE VESSEL TECHNOLOGY*. *(under review)*
2. **Galle, T.**, De Pauw, J., De Waele, W., Van Wittenberghe, J., and De Baets, P. (2014). Validating numerically predicted make-up of threaded connections using digital image correlation and infrared monitoring. *JOURNAL OF STRAIN ANALYSIS FOR ENGINEERING DESIGN*, *49*(7), 492–500. *(published)*
3. **Galle, T.**, De Waele, W., Van Wittenberghe, J., and De Baets, P. (2014). Optimal Make-up Torque for Trapezoidal Threaded Connections Subjected to Combined Axial Tension and Internal Pressure. *JOURNAL OF PRESSURE VESSEL TECHNOLOGY*. *(under review)*
4. **Galle, T.**, De Waele, W., Van Wittenberghe, J., and De Baets, P. (2015). Evaluation of a numerical model for tapered threaded connections subjected to combined loading using enhanced experimental measurement techniques. *JOURNAL OF STRAIN ANALYSIS FOR ENGINEERING DESIGN*. *(published)*
5. **Galle, T.**, De Waele, W., and De Baets, P. (2015). Enhancing trapezoidal Threads using a Parametris Numerical Approach. *JOURNAL OF PRESSURE VESSEL TECHNOLOGY*. *(under review)*
6. Rodriguez, V., Sukumaran, J., **Galle, T.**, Schlarb, A.K., Fekete, G., and De Baets, P. (2016). Sliding Behaviour of Low and High Viscosity Grade

Polyetheretherketone (PEEK) Polymer Under Different Conditions. ACTA POLYTECHNICA HUNGARICA. *(under review)*

A2 Peer reviewed journal publications

1. **Galle, T.**, De Waele, W., De Baets, P., and Van Wittenberghe, J. (2011). Experimental procedure for evaluation of the structural integrity of threaded API line pipe couplings. (I. Szabó & G. Kalácska, Eds.), *MECHANICAL ENGINEERING LETTERS*, *5*, 128–134. *(published)*
2. Van Wittenberghe, J., **Galle, T.**, De Baets, P., and De Waele, W. (2011). Numerical modelling and experimental validation of a threaded pipe connection under axial tension. (I. Szabó & G. Kalácska, Eds.), *MECHANICAL ENGINEERING LETTERS*, *5*, 89–94. *(published)*

C/P Conference proceedings

1. **Galle, T.**, De Waele, W., De Baets, P., and Van Wittenberghe, J. (2011). Influence of design features on the structural integrity of threaded pipe connections. In J. Van Wittenberghe (Ed.), SUSTAINABLE CONSTRUCTION AND DESIGN (Vol. 2, pp. 237–245). Presented at the Sustainable Construction and Design 2011 (SCAD), Ghent, Belgium: Ghent University, Laboratory Soete. *(published)*
2. Van Wittenberghe, J., De Baets, P., De Waele, W., **Galle, T.**, Bui, T. T., and De Roeck, G. (2011). Design characteristics that improve the fatigue life of threaded pipe connections. In J. Van Wittenberghe (Ed.), SUSTAINABLE CONSTRUCTION AND DESIGN (Vol. 2, pp. 334–341). Presented at the Sustainable Construction and Design 2011 (SCAD), Ghent, Belgium: Ghent University, Laboratory Soete. *(published)*
3. Seys, J., Roeygens, K., Van Wittenberghe, J., **Galle, T.**, De Baets, P., and De Waele, W. (2011). Failure behaviour of preloaded API line pipe threaded connections. In J. Van Wittenberghe (Ed.), SUSTAINABLE CONSTRUCTION AND DESIGN (Vol. 2, pp. 407–415). Presented at the Sustainable Construction and Design 2011 (SCAD), Ghent, Belgium: Ghent University, Laboratory Soete. *(published)*

4. Van Wittenberghe, J., **Galle, T.**, De Baets, P., and De Waele, W. (2011). Numerical modelling and experimental validation of a threaded pipe connection under axial tension. In Z. Kurják & L. Magó (Eds.), Synergy in the technical development of agriculture and food industry (Synergy2011). Presented at the 2nd International conference on Agricultural Engineering (Synergy 2011) : Synergy in the technical development of agriculture and food industry, Gödöllö, Hungary: Szent István University. Faculty of Mechanical Engineering. *(published)*

5. Van Wittenberghe, J., **Galle, T.**, De Baets, P., and De Waele, W. (2011). Numerical modelling and experimental validation of a threaded pipe connection under axial tension. In Z. Kurják & L. Magó (Eds.), Synergy in the technical development of agriculture and food industry (Synergy2011) (pp. 51–51). Presented at the 2nd International conference on Agricultural Engineering (Synergy 2011) : Synergy in the technical development of agriculture and food industry, Gödöllö, Hungary: Szent István University. Faculty of Mechanical Engineering. *(published)*

6. **Galle, T.** (2011). Design and evaluation of high integrity threaded couplings. FEA PhD symposium, 12th. Presented at the 12th FEA PhD Symposium, Ghent, Belgium: Ghent University. Faculty of Engineering and Architecture. *(published)*

7. Loncke, K., De Waele, W., Van Wittenberghe, J., **Galle, T.**, and De Baets, P. (2012). Crack growth around stress concentrations in pipes and tubes. In J. Van Wittenberghe (Ed.), SUSTAINABLE CONSTRUCTION AND DESIGN (Vol. 3, pp. 59–69). Presented at the Sustainable Construction and Design (SCAD - 2012), Ghent, Belgium: Ghent University, Laboratory Soete. *(published)*

8. Staelens, Seppe, **Galle, T.**, De Waele, W., and De Baets, P. (2012). Analysis of API 5C3 failure prediction formulae for casing and tubing. In S. Hertelé (Ed.), SUSTAINABLE CONSTRUCTION AND DESIGN (Vol. 3, pp. 80–88). Presented at the Sustainable Construction and Design (SCAD - 2012), Ghent, Belgium: Ghent University, Laboratory Soete. *(published)*

9. Van Wittenberghe, J., **Galle, T.**, De Waele, W., and De Baets, P. (2012). Experimental analysis of the fatigue life of threaded pipe connections under cyclic bending. In S. Hertelé (Ed.), SUSTAINABLE CONSTRUCTION AND DESIGN (Vol. 3, pp. 89–97). Presented at the

Sustainable Construction and Design (SCAD - 2012), Ghent, Belgium: Ghent University, Laboratory Soete. *(published)*

10. Jula, F. C., **Galle, T.**, De Waele, W., and Borzan, M. (2012). FEA modeling of orthogonal cutting of steel: a review. In S. Hertelé (Ed.), SUSTAINABLE CONSTRUCTION AND DESIGN (Vol. 3, pp. 98–105). Presented at the Sustainable Construction and Design (SCAD - 2012), Ghent, Belgium: Ghent University, Laboratory Soete. *(published)*
11. **Galle, T.**, De Waele, W., and De Baets, P. (2013). Effect of make-up on the structural performance of standard buttress connections subjected to tensile loading. ASME 2013 Pressure Vessels & Piping Conference, Proceedings. Presented at the ASME 2013 Pressure Vessels & Piping Conference (PVP - 2013). *(published)*
12. **Galle, T.**, Van Wittenberghe, J., Jula, F. C., De Waele, W., and De Baets, P. (2013). Effect of load flank angle modifications on the structural integrity of buttress threaded connections. SUSTAINABLE CONSTRUCTION AND DESIGN (Vol. 4). Presented at the Sustainable Construction and Design 2013. *(published)*
13. **Galle, T.**, De Waele, W., van wittenberghe, jeroen, and De Baets, P. (2014). Optimal make-up torque for trapezoidal threaded connections subjected to combined axial tension and internal pressure loading. ASME 2014 Pressure Vessels & Piping Conference, Proceedings. Presented at the ASME 2014 Pressure Vessels & Piping Conference (PVP - 2014). *(published)*
14. **Galle, T.**, De Waele, W., and De Baets, P. (2015). Enhancing trapezoidal threads using a parametric numerical approach. Pressure Vessels and Piping Conference, Proceedings (pp. 1–14). Presented at the Pressure Vessels and Piping Conference. *(published)*

Honors and Awards

Best Poster Award (2011)

Awarded by: Szent István University
Conference: Synergy International Conference
Paper: Experimental procedure for evaluation of the structural integrity of threaded API line pipe couplings

Honorable Mention (2013)

Awarded by: American Society of Mechanical Engineers (ASME)
Conference: Pressure Vessels and Piping Conference (PVP 2013)
Paper: Effect of Make-up on the Structural Performance of Standard Buttress Connections Subjected to Tensile Loading

Finalist Paper (2015)

Awarded by: American Society of Mechanical Engineers (ASME)
Conference: Pressure Vessels and Piping Conference (PVP 2015)
Paper: Enhancing Trapezoidal Threads Using a Parametric Numerical Approach

Second Runner-Up Award (2015)

Awarded by: American Society of Mechanical Engineers (ASME)
Conference: Pressure Vessels and Piping Conference (PVP 2015)
Paper: Enhancing Trapezoidal Threads Using a Parametric Numerical Approach

Contents

Chapter 2: Design process

Chapter 3: Experimental testing

Chapter 4: Numerical model: ThreadGenBT

Chapter 5: Numerical study using ThreadGenBT

Chapter 6: Development of the 'LS95R'

Chapter 7: Conclusions, future work and personal reflections

Appendix A: Numerical model: 3D - Model

Appendix B: Numerical model: Fracture estimation

Symbols and acronyms

Symbols

$A_{S,Axi}$	Surface area of stab flank (axisymmetric)	mm²
$A_{S,Heli}$	Surface area of stab flank (helix)	mm²
$C_{p,AVG}$	Average contact pressure	MPa
D_o	Outer diameter	mm
D_i	Inner diameter	mm
e	Engineering strain	- (%)
E	Young's modulus	MPa
E_i	Internal energy	mJ
F_a	Axial force	N
$F_{a,a}$	Total axial force (axisymmetric)	N/mm
$F_{ar,i}$	Relative axial load in section *i*	- (%)
F_{a,S_i}	Axial force in section *i* (axisymmetric)	N/mm
$\overrightarrow{F_C}$	Contact force perpendicular on crest	N
$F_{C,R}$	Combined force on crest and root	N
F_F	Frictional force	N
$\overrightarrow{F_R}$	Contact force perpendicular on root	N
$h_{ini,k}$	Initial location of point *k* along axis	mm
H_k	Actual height of point *k*	mm
h_t	Height of thread	mm
k	Frictional force multiplier	-
L_4	Threaded length (see API5B)	mm
l_C	Contact length	mm
MU	Applied make-up	rad
n	Number of rotations	turns
N	Normal load	N
n_N	Number of make-up turns	turns
p	Pitch length	mm
P_C	Contact pressure	MPa
p_i	Internal pressure	MPa

$R_{ini,k}$	Initial radius of point *k*	mm
R_k	Actual radius of point *k*	mm
R_{rY}	Relative yield ratio between pin and box	- (%)
R_{wt}	Wall thickness ratio between pin and box	- (%)
R_Y	Yield ratio	- (%)
s	Engineering stress	MPa
t	Wall thickness	mm
T_{2D}	Estimated torque using a 2D model	Nmm
T_{3D}	Estimated torque using a 3D model	Nmm
T_{calc}	Calculated temperature	K
T_F	Frictional torque	Nmm
T_{FEA}	Simulated temperature	K
T_{ini}	Initial temperature	K
α	Crest angle	rad
α_{ext}	Extrapolation parameter	-
β	Root angle	rad
δ	Radial overlap	mm
ε	Taper angle	rad
ε_{el}	Elastic strain	- (%)
ϵ	True strain	- (%)
ϵ_m	Maximum strain	- (%)
σ	True stress	MPa
σ_a	Axial stress	MPa
σ_h	Hoop stress	MPa
σ_m	Maximum stress	MPa
σ_r	Radial stress	MPa
σ_{VME}	Von Mises stress	MPa
σ_{YS}	Yield strength	MPa
μ	Coefficient of friction	-
μ_g	Global coefficient of friction	-

Acronyms

API	American petroleum institute
BTC	Buttress threaded connection
CAL	Connection application level
CPRESS	Contact pressure
CPRESSERI	Contact pressure accuracy
CTRQ	Friction independent holding torque
DF	Design factor
DIC	Digital image correlation
DIS	Draft international standard
DWC	Drilling with casing
ERD	Extended-reach drilling
FEA	Finite element analysis
FET	First engaged thread
FMU	Final make-up
HC	High collapse
HPHT	High pressure high temperature
IEU	Internal and external upset
IR	Infrared
ISO	International organization for standardization
LET	Last engaged thread
LF	Load factor
LLT	Limit load test
LPx	Load path x (with x being a number)
LRFD	Load resistance factor design
MBG	Make-up/break-out test for galling resistance
MBOE	Million barrels of oil equivalent
MBT	Make-and-break test
MU	Make-up
NDT	Non-destructive testing
NETD	Noise-equivalent temperature difference
NPT	Non-productive time
OD	Outer diameter
PEEQ	Plastic equivalent strain
QRA	Quantitative risk analysis
RBD	Reliability based design
RP	Reference point
SF	Safety factor
SG	Strain gauge
SI	Seal index
SL	Seal interference
SMYS	Specified minimum yield strength

S*x*	Specimen *x* (with *x* being a number)
T&C	Threaded and coupled
TC	Thermocouple
TLE	Test load envelope
TPI	Threads per inch
TPS	Thin plate spline
UNC	Unified screw thread - coarse
UNF	Unified screw thread - fine
UTS	Ultimate tensile strength
VME	Von Mises equivalent
WEC	World energy council

Chapter 1

Introduction

<< *This page intentionally left blank* >>

Table of Contents

1 Current trends of oil availability and usage

1.1 Oil resources and production

Oil has been dominating the world energy mix starting from the Second World War. In the beginning of the 21st century, oil accounted for about 40% of the total energy consumption and is currently slightly decreasing in percentage [1.1], but not in absolute values as can be seen in Figure 1-1. This is mainly due to oil's unique combination of properties such as sufficiency, accessibility, versatility, ease of transport and, in many areas, low costs. In addition, advances in technology make oil a cleaner, safer and more efficient fuel.

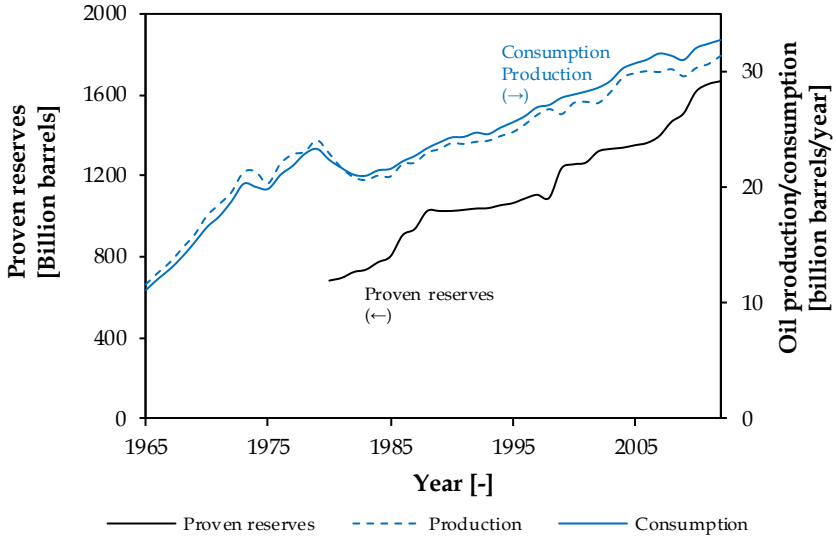

Figure 1-1: Overview of the yearly production/consumption together with the currently proven conventional reserves. (Adopted from [1.1]).

As a prospective, there should be plenty of oil around for decades to come. When considering the world's currently proven reserves of around 1600 billion barrels, there will be enough to meet the global demand for around 45 years assuming current production rates. However, in reality, the situation is more nuanced. After these expected 45 years, production will not suddenly stop, but a gradual transition lasting many decades will take place towards other energy resources as was seen during the transition of coal towards oil. In addition to the likely discoveries of new oil reserves, recovery rates will also improve through enhanced technology, improved infrastructure and better accessibility. It is of utmost importance to mention that these assumptions are solely based on the use of *conventional oil* only (see section 1.3.1) [1.2].

In addition to the conventional oil, there are still huge supplies of *unconventional oil* (see section 1.3.2), such as tar sands, oil shale and heavy oil, and their exploitation is expected to rise steadily in the future.

1.2 Completion of wells

When it comes to trends observed in drilling new oil wells, four major changes can be observed: longer vertical lengths (deeper), longer horizontal distances (further), higher temperatures and more pressure.

Figure 1-2 indicates that there is a growing tendency to go deeper and further, increasing the length of the applied strings and reducing the amount of clearance between the tubulars and the drilling and completion tools [1.4]. The deepest well to date (2015) is known by the name *Z-44 Chayvo* and reached a depth of 12,376 meters in 2012 [1.5]. In order to reach such depths, specific tubulars such as heavy wall, non-standardized tubes with high collapse ratings are required. Additionally, by applying new technologies such as directional drilling, it is possible to bend the vertical strings to a horizontal direction. Using this method, it is possible to significantly increase production capacity and to reach different oil reservoirs using the same well. With the current string materials, the pipes often need to be chosen based on the local geology and on the intention to drill horizontally extended, shallow wells or deep, quasi-vertical wells. This has stressed current materials to their limits and better equipment is currently required in order to further extend the 'very extended range' illustrated in Figure 1-2. This *Extended-Reach Drilling* (ERD) requires better connections able to, for example, resist higher make-up torque levels (see section 3.3).

In addition to land based drill sites, an important focus shift towards offshore drilling is noticeable. In 2013 for example, an offshore well was drilled at a depth of 2,900 meters [1.6]. When drilling at such extremes depths, both internal and external pressures drastically increase. By increasing the depth of the well, the temperature increases as well, about 25 °C every 1,000 meters [1.7]. Once temperatures higher than 150 °C and pressures exceeding 700 bars are reached, they are classified as *High Pressure High Temperature* (HPHT) wells. Within the HPHT wells, various classifications are made as illustrated in Figure 1-3. From this figure, it is obvious that more extreme HPHT wells will be drilled in the future since most of the exploratory wells, which are used to gather information to determine whether or not exploitation is profitable, are located in the 'extreme' and 'ultra' classifications.

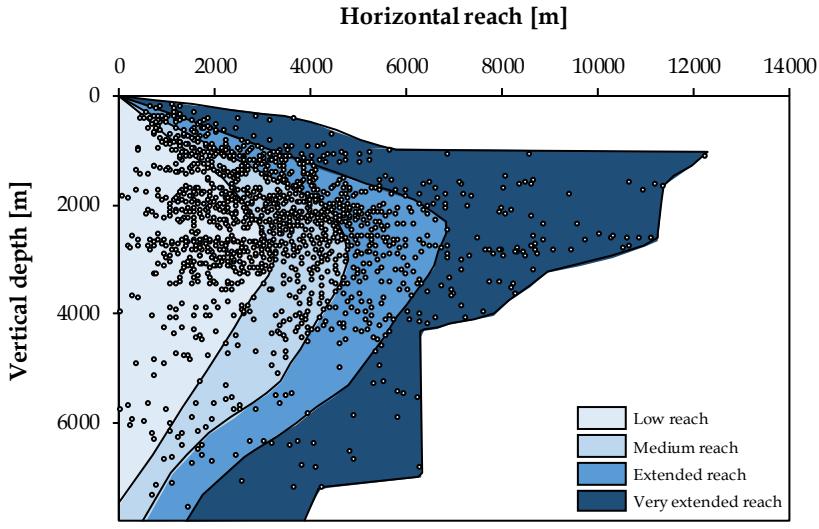

Figure 1-2: Overview of drilled wells (2009).
The use of directional drilling leads towards the tendency of reaching further in a horizontal direction, maximizing production output and increasing the length of the strings (Adopted from [1.3]).

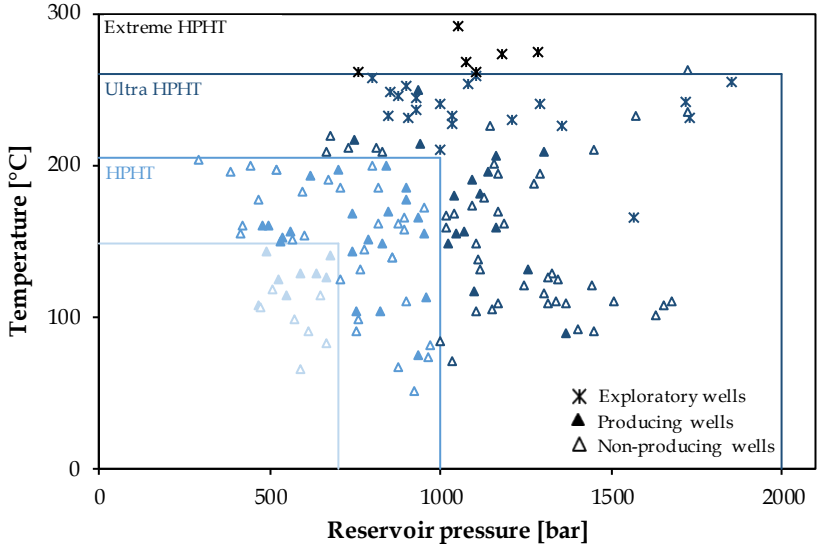

Figure 1-3: Overview of recent HPHT wells (2012).
It is visible that focus shifts towards deeper wells with higher temperatures and pressures. This shift results in the need of enhanced mechanical requirements (Adopted from [1.8]).

1.3 Projections for the future

1.3.1 Conventional oil

The conventional oils can be defined as a category of oil that includes crude oil, gas liquids and condensate liquids that are extracted from natural gas production. These types of oil can be extracted by using fairly low-tech equipment and are often pushed to the surface due to overpressure in the reservoir. Figure 1-4 gives a graphical overview of the approximate total amount and location of crude oil currently estimated by the World Energy Council (WEC) [1.10].

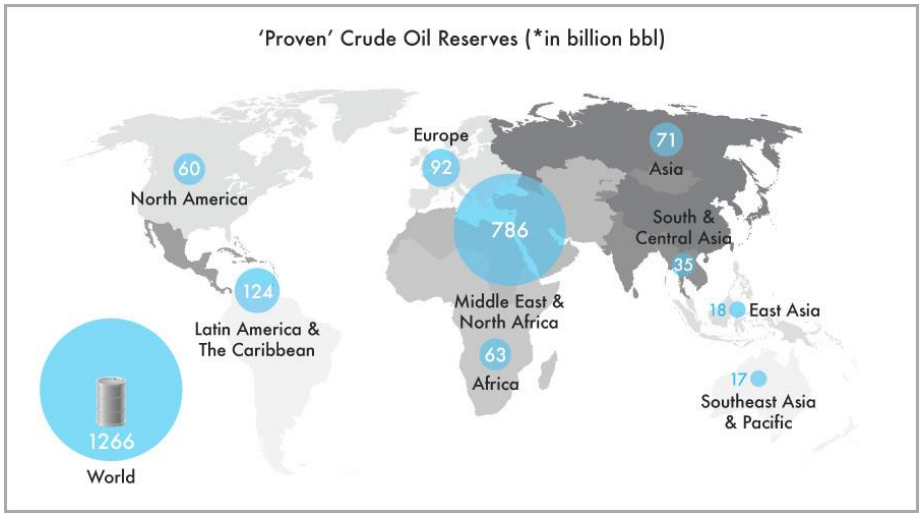

Figure 1-4: Proven crude oil reserves (2013) [1.9].

These numbers are very dynamic because there is a constant search for new and profitable reservoirs. When comparing the discoveries of the giant conventional petroleum reservoirs (defined as fields with a recoverable reservoir of 500 *Million Barrels of Oil Equivalent* (Mboe) or more) in the previous decades, three important discovery trends can be observed [1.11]:

- Deep and ultradeep water has been increasing in importance as the domain for discovering new giant fields. This evolution from 1900 till 2012 can be seen in Figure 1-5.
- More giant gas fields have been discovered: 68 giant gas fields (29,400 km^3) compared to 52 giant oil fields (10.4 km^3).
- More giant fields and more reserves are discovered in deep reservoirs with a burial depth of 5,000m or more.

By taking these trends, projected in Figure 1-5, into consideration, it can be assumed that future wells will have to reach deeper and be located in more

hostile environments than ever before. The latest deep water reservoir was discovered in October 2014 by BP at a depth of over 10,000 meters located about 300 km off the Louisiana coast in the Gulf of Mexico [1.12]. It is likely that future reservoirs will be located even deeper and at locations which are even harder to reach. Since operators are currently working near the material limits of current tools, an evolution in mechanical characteristics of rig equipment is required.

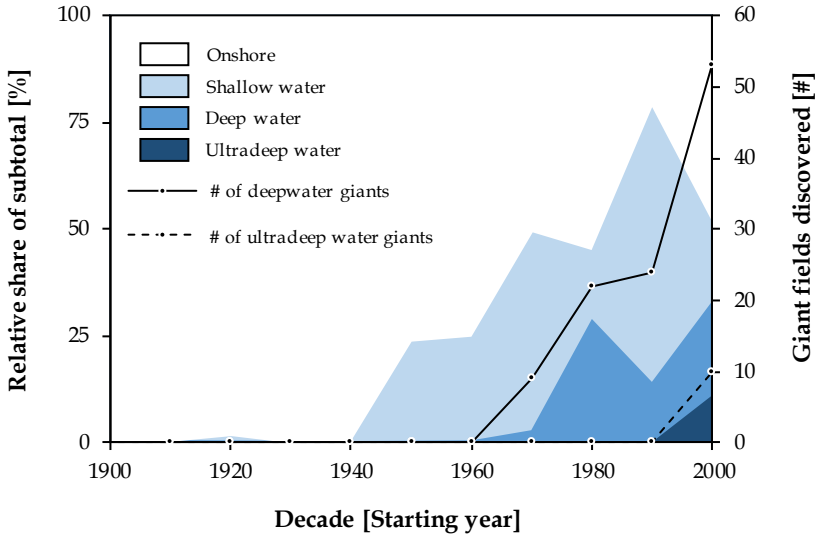

Figure 1-5: Tendency in the discovery of reservoirs (Adopted from [1.11]).

1.3.2 Unconventional oil

In addition to the commonly known conventional oil sources, *unconventional oils* exist. They include heavy oils, oil sands, oil shale and tar sands. Until recently, unconventional oil sources remained fairly untouched due to the increasing technical challenges and increased production costs. These types of oils need further refinement because they are not as homogeneous as the conventional ones. However, since these types count for about 70% of the world supply and the conventional oils are believed to become exhausted or too expensive to reach, unconventional oils are expected to continue gaining interest. Furthermore, it should be mentioned that the types currently defined as unconventional can become conventional when technology permits. One of the examples are the thick viscosity oils. While it was earlier not possible to extract these types of oils using conventional methods, the introduction of steam injection to lower viscosity transformed these types into conventional ones.

Figure 1-6 shows the total worldwide estimation of the available unconventional resources. When compared to the conventional oils (given in

Figure 1-4), it can be seen that their total amount is four times higher. Another important observation is that almost 60% is present in North America. This is in contrast with the conventional resources which are predominantly present in the Middle East and North Africa. This is the reason why the use of unconventional technology such as fracking is already initiated in American oilfields such as Bakken in North Dakota, Eagle Ford in Texas and the Marcellus in Pennsylvania and West Virginia [1.13].

Despite the large amount of estimated, available unconventional oil, it should be noted that a strong regulatory aspect is driven by national governments since excavation of these resources tends to push environmental and safety rules. This also requires more reliable technologies, especially in terms of performance variation.

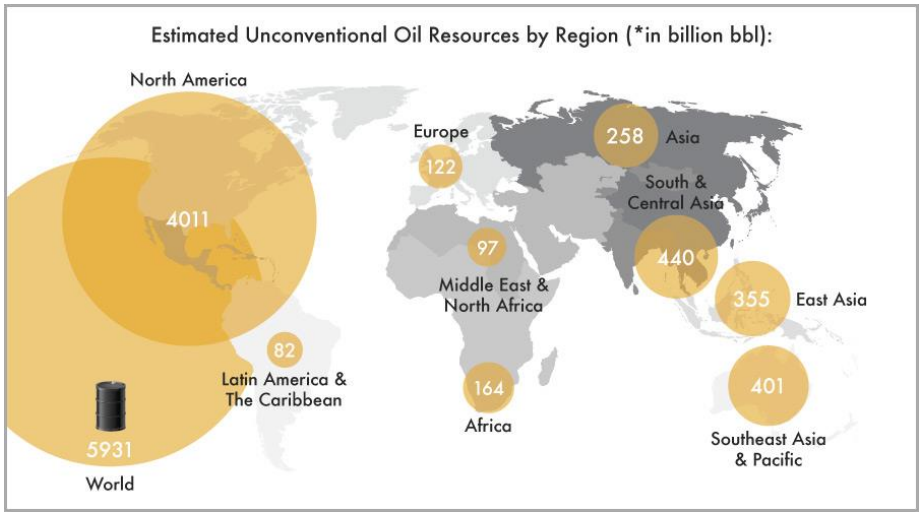

Figure 1-6: Estimated unconventional oil reserves (2013) [1.9].

2 Reaching reservoirs

In order to reach the available gas and oil reserves, wells have to be drilled. Considering the history of the average depth per well in the US, illustrated in Figure 1-7, an increasing trend can be observed. This inevitable means that more complex load cases and increasing absolute load values are encountered. An overview of the load types encountered at various depths is shown in Figure 1-8.

In order to create a string to access the gas and/or oil reservoir, many individual tubulars with a length of about 10 meters need to be joined. With average depths exceeding 2,000 meters, a huge number of connections have to be established. Since it is not time-efficient to weld the pipes together, threaded connections are used.

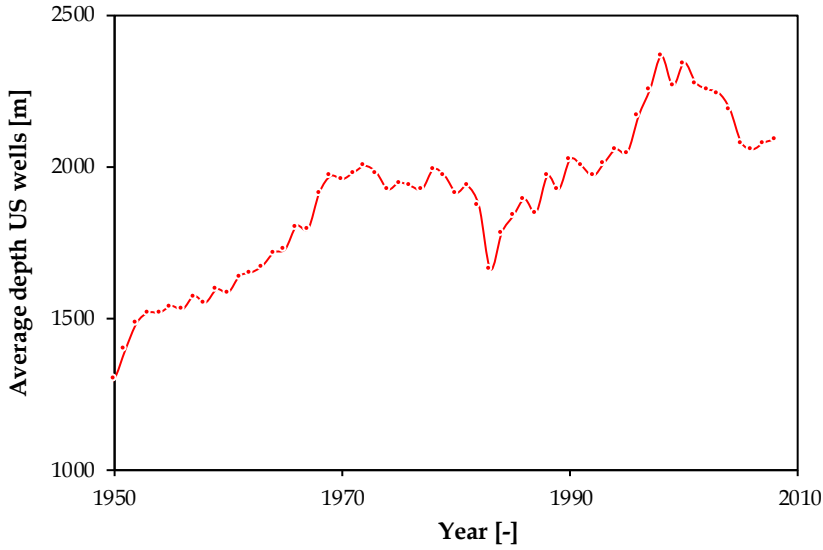

Figure 1-7: Overview of the depth of the average oil well in the US (Adopted from [1.14]).

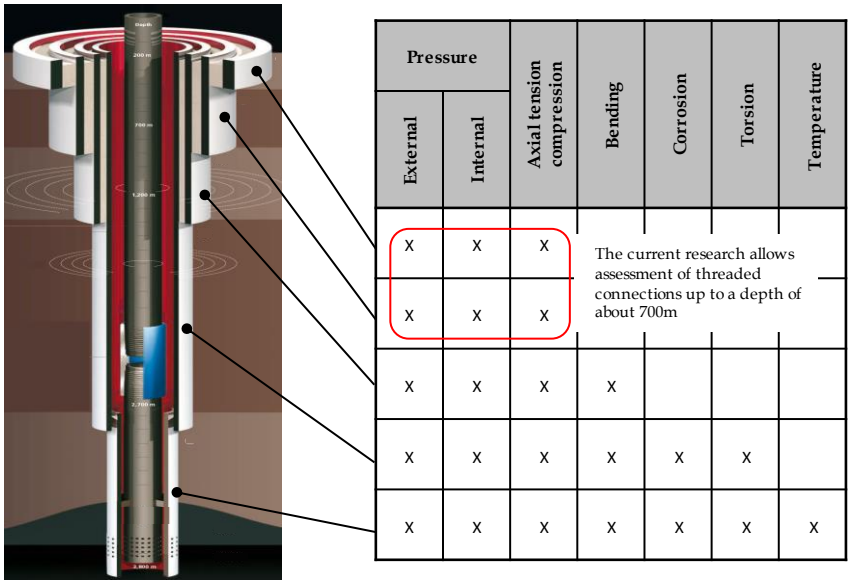

Figure 1-8: Load conditions increase with increasing depths. (Adopted from [1.15]).

3 What is a threaded connection?

3.1 Classification and configuration

Within the scope of this research, a threaded connection is defined as a mechanical joint of two pipe sections. This assembly consists of at least one externally threaded member, defined as the pin, and exactly one internally threaded member, defined as the box. They are joined together by applying a relative rotational movement between pin and box.

In general, threaded connections can be categorized in three types based on their geometrical features. When only a threaded region is present, they are considered standard connections (see Figure 1-9.A). A more advanced version is the semi-premium connection (see Figure 1-9.B1 and B2) which incorporates a torque shoulder to enhance make-up conditions. The torque shoulder is a feature used to geometrically position the metal-to-metal seal which is located in its vicinity and to prevent plastic deformation at the seal when over-torqueing the connection. In addition, low circumferential stress levels are maintained within the threaded section(s) of the connection and externally applied torque is resisted by the limited relative axial displacement between pin and box. This feature can be incorporated using two different methods. First, torque shoulder geometry can be manufactured within the connection, meaning a female part in the box and a male part in the pin (as illustrated in Figure 1-9.B1). As an alternative, two pins can be used in which one pin acts as the counter surface for the other, shown in Figure 1-9.B2. When a metal-to- metal sealing surface is added to the geometry, the connection is categorized as a premium connection (Figure 1-9.D).

The aforementioned types of threaded couplings can be consolidated in various configurations. Two major classes are being distinguished: *integral* and *threaded and coupled* (T&C) connections. While T&C configurations require an additional part to assemble the pipes, the integral connections have an internally and externally threaded end on the pipe. Depending on the ratio of outer diameter (OD) of the pipe to outer diameter of the connection, a further distinction can be made between flush (OD pipe = OD connection), semi-flush (OD pipe ≈ OD connection) and upset (OD pipe < OD connection) connection. These configurations are illustrated in Figure 1-10.

Finally, a last distinction can be made based on the application of the connection. Within the oilfield, threaded connections are mainly used for casing, tubing, drilling and offshore risers. From these applications, casing and tubing connections are used during well completion and are usually designed taking into account static loads. In contrast, the drilling and offshore riser connections are also susceptible to fatigue loads as a result of rotational forces and sea waves. Therefore, fatigue life extension is one of the main concerns for these applications. This research focusses on tubing and casing connections.

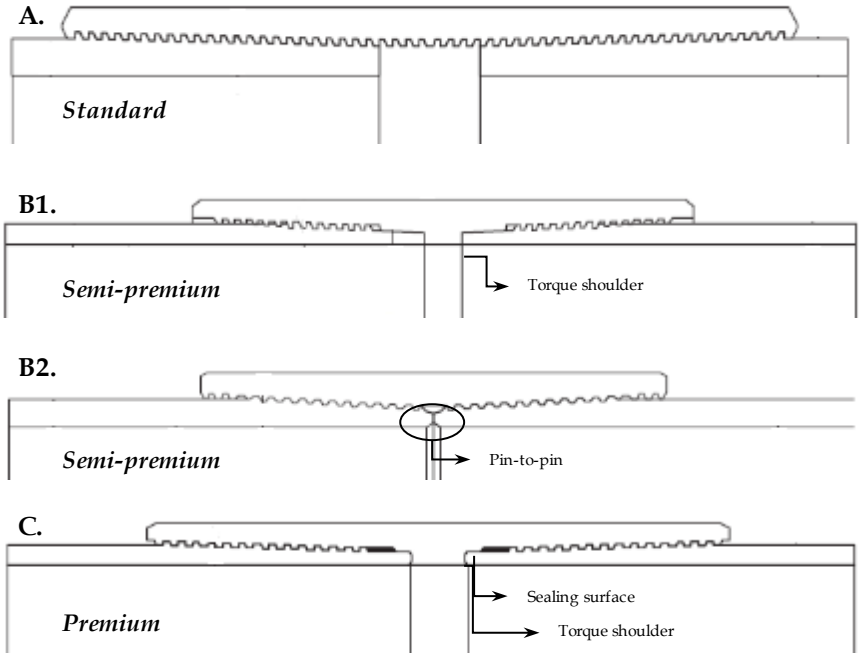

Figure 1-9: Different configurations of threaded connections (Adopted from [1.16]).

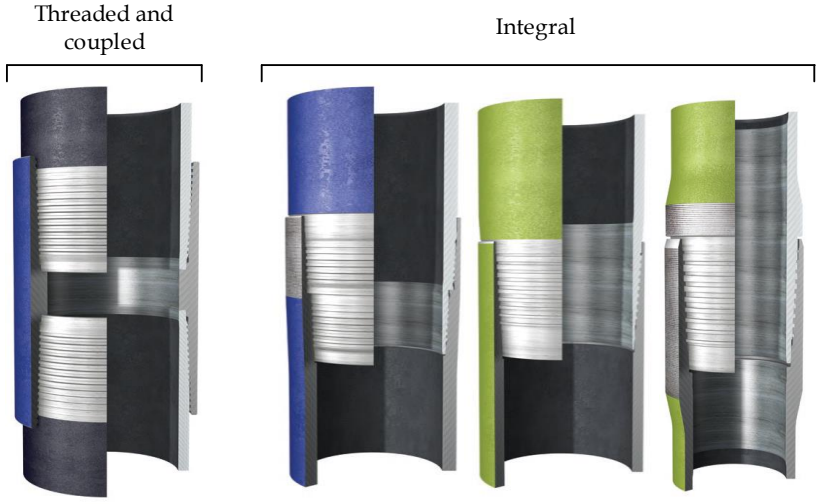

Figure 1-10: Connection classes with (left to right): threaded and coupled, integral semi flush, integral flush and integral upset geometry. [1.17].

3.2 Thread geometry

While triangular threads are defined by two flanks known as the stab and load flanks, the trapezoidal thread form is characterized by four angles and matching flanks as is illustrated in Figure 1-11.

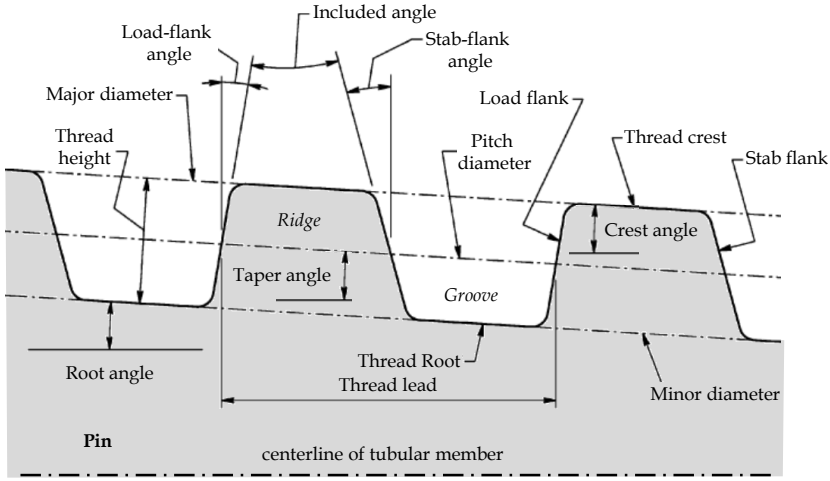

Figure 1-11: Overview of the terminology related to trapezoidal threads.

The top and bottom flanks of the thread are named the *root* and *crest* for the pin and the opposite for the box. From these two flanks, the root flank is defined as the flank which is closest to the base material of the pipe on which the thread has been cut [1.18]. This corresponds with the inner diameter for the pin and the outer diameter for the box. The *stab* flank is defined as the flank that makes initial contact during stabbing (see further in section 3.3) when making up the connection. It is the flank facing the tip of the pin or box. The fourth and last flank is defined as the *load* flank and is the flank that takes most of the load when applying high axial tensile forces to the connection. The four introduced *flank angles* are taken as positive as illustrated in Figure 1-11. The *included angle* is the algebraic sum of both load and stab flank.

When defining the thread geometry, the size of thread ridge and groove is often defined using the *pitch diameter*. The pitch diameter is an imaginary line on the thread form profile that intersects the stab flank and the load flank. In the case of a standard buttress connection, the axial width of the thread ridge equals the axial width of the thread groove. In a conventional thread, the included angle is positive. This means that the width of the thread crest is less than the width of the thread groove with which it is initially engaged, resulting in an axial clearance between load and/or stab flanks which facilitates the assembling process.

In order to be able to tighten the connection (make-up), a tapered thread profile is required. The *thread taper* is defined as the angle between the axis of the tubular member and the pitch line. Due to the tapered geometry, the threaded region of the pin can be divided in two sections: a section with perfect, complete threads near the pin tip and a section with incomplete threads. These threads are often called the vanishing threads. In contrast, the box does not usually include incomplete threads.

3.3 Assembling connections

The lifecycle of threaded connections consists of two major parts which have to be taken into consideration in the design stage. The most important part is the operational period during which high pressures, axial loading, temperature and other conditions are applied to the connection (see Figure 1-8). However, before reaching the operational lifecycle, the connection has to undergo the assembly stage. Despite the extremely short period of time compared to the entire lifetime of connections, this stage is not negligible.

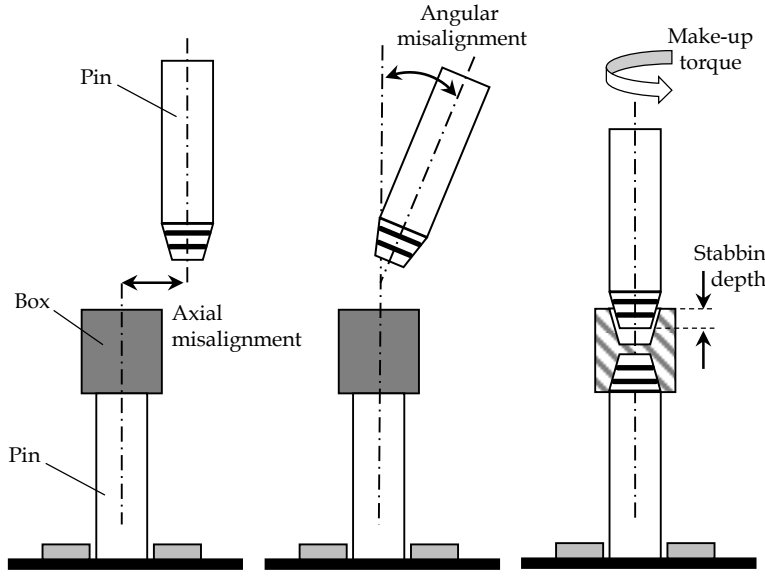

Figure 1-12: Assembling a threaded T&C connection.

During assembly, the pin and box members are first *stabbed* together (see Figure 1-12). Stabbing is a process that consists of two stages. First, both pin and box are axially and angularly aligned to prevent cross-threading. Because the pipe segments often have large diameters and are over 10m long, oscillations of the swinging pipe section have to be avoided. Once the alignment is ensured, the pin is carefully lowered in precise alignment with the section to which it is to be joined. Once the two parts make contact, a relative rotation is applied until a *hand-tight position* is reached. This is the

position to which the pin can be rotated in the box by applying a limited amount of torque and can often be applied manually using a torque wrench or similar. The torque corresponding with the hand tight position is defined in standardized tables depending on the geometry of the connection [1.19]. Subsequent to the hand-tight assembly of the connection, a number of power-turns is applied as defined in the API 5B standard [1.20]. This stage is known as the *make-up* of the connection and requires a considerable amount of torque. During this procedure, the tapered thread geometry will cause deformation of both pin and box member, initiating a certain pre-stress state which ought to be favorable when taking into account the expected working conditions. It is during this stage that special attention should be given to the possible occurrence of *galling*. According to reference [1.21], galling is described as follows: when a connection is made-up, the relative movement between the contacting faces may result in tiny high spots or thin metal slivers being formed on the faces opposite one another. The dope lubricant that was placed on these faces is slowly removed from between these high spots. The heat caused from the friction of these metal-to-metal contacts causes these tiny high spots to weld together. Once further relative movement occurs, the welds are torn apart and damage is induced. Despite being an industrial relevant and frequently occurring problem, the investigation of galling is not considered to be a focus of the current research.

4 Historical overview

4.1 The first threaded connections

The first patented connection matching the aforementioned definition can be traced back to as early as 1876 [1.22] and is shown in Figure 1-13.A. Even before the use of standardized threads was introduced, attempts to increase the tightness of connections was considered and solutions such as coating the threaded surfaces were patented as early as 1879 [1.23]. A few years later, an internally tapered thread, providing significant resistance to loosening, was introduced by Morse [1.24].

Once the American National Standard for tapered threaded pipe joints, which is currently still in use in the US and Canada, was formulated in the year 1882 by Robert Briggs [1.25], patented assemblies describing both internally and externally threaded members were published. The first patent defining both members of the connection can be considered the pipe coupling of Bole [1.26], shown in Figure 1-13.B. This patent dates back from 1885.

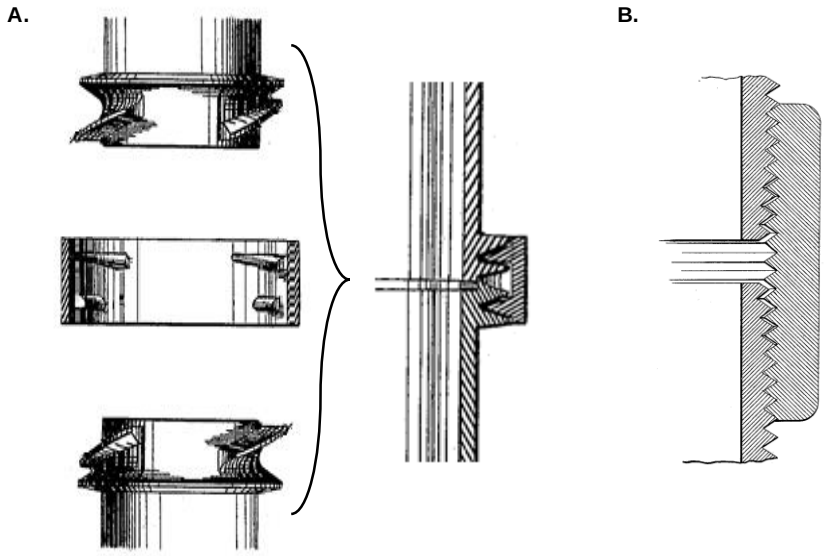

Figure 1-13: First pipe coupling matching the definition of threaded coupling by O'Neill (1876) (A) and the first connection defining both pin and box by Bole (1885) (B) (adopted from [1.22] and [1.24]).

4.2 The quest for premium connections

Initially, the tubular connections used for casing and tubing consisted of standard connections with a tapered thread. When using tapered threads, an additional make-up is applied after reaching a handtight position to ensure tightness and rigidity. As a result of the uncertainties related to the determination of the required amount of make-up such as the unknown coefficient of friction, tolerances, …, the applied make-up (or '*stand-off*') was often insufficient, causing the connection to loosen [1.28,29]. For this reason, an additional feature was introduced: the torque shoulder. In the early days, this shoulder consisted of an additional polymeric ring and was first introduced by Montgomery in 1932 [1.29] and is illustrated in Figure 1-14.A. By applying this additional polymeric ring at the end of the pin, less make-up turns were required and an increased sealing capacity was obtained. In addition, shock forces which were occasionally acting on the string were damped by these flexible rings. In response to this increased sealing capacity, a connection replacing the polymeric ring by a metallic ring was suggested by Reimschissel five years later [1.30], becoming the first metal-to-metal seal in a threaded connection, relieving the threaded region of its sealing function. The ability of enhancing leak tightness by introducing geometric changes in connections was not extensively studied during the following years. Instead, the studies related to leak issues focused on thread surface contact and the plugging of thread voids using thread compounds [1.31]. These studies

included an initial bridging theory by using solid particles and an analysis to determine adequate preload (contact pressure) to seal pressure under axial tension. One of the conclusions of these early studies conducted prior to World War II included that 3 to 3-1/2 turns of makeup were required to seal J55 connections containing an API round thread (API 8rd), which were then the common industrial connections, up to 69 bars (1,000 psi) [1.32]. Another observation was that when the gap size between the threads is less than twice the size of the particles found in the applied thread compound, the "bridge" is unconditionally stable and sealing is assured [1.33]. The particle sizes of the *API-modified* thread compound developed in the 1950's measure from 43 μm (0.0017") to 178 μm (0.0070"). These are in the same order of magnitude of the gaps that need to be plugged for API 8rd connections, which were still often used after the introduction of the trapezoidal API Buttress thread by Webb in 1956 [1.34]. This trapezoidal thread was introduced after it became apparent that triangular threads such as API LinePipe and API 8rd threads were vulnerable to failure by jump-out. Jump-out is defined as the occurrence where the pin end radially collapses and/or the box end expands sufficiently to allow the threaded portions to disengage from each other [1.35]. In order to eliminate this failure mechanism, triangular threads were often replaced by trapezoidal threads [1.36]. Until today, the vast majority of patented threaded connections consist of or include the possibility of using some sort of trapezoidal or more complex thread geometries (see section 4.3).

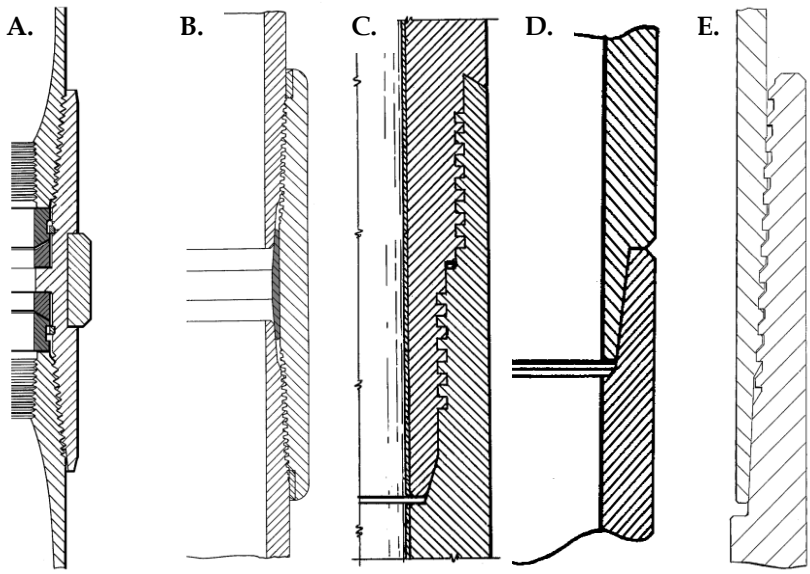

Figure 1-14: Connection designs by Montgomery (A; first polymeric seal [1.29]), Reimschissel (B; first metallic seal [1.30]), Macarthur (C; Hydril connection [1.37]), Van der Wissel (D; first semi-premium connection [1.38]) and Blose (E; first premium connection [1.40]).

In 1950, the Hydril Corporation came up with a revolutionary design [1.37] which would become known as the Hydril-type connection. A Hydril tubular connection can be defined as a pressure tight pipe connection and more particularly as a stepped, straight, buttress-like (see further section 4.3) threaded connection with internal and external tapered metal-to-metal seals. In addition, a perpendicular, positive torque shoulder and cylindrical alignment lands adjacent to the seals are included. This connection can be considered to be the first connection containing all functional features. However, the demand for this type of high performance couplings did not exist during that period and it would take many more years until the late 1980s before the overall design of this connection would become the focus.

In addition to jump-out, the requirement of resisting bending moments, both deliberate and undeliberate, increases with the increased use of directional drilling. In a response to this tendency, Van der Wissel proposed in 1956 to use a torque shoulder to withstand these bending moments [1.38]. This was the first connection that provided a torque shoulder not as an additional ring, but incorporated in the pin and box design. It can be considered as the first semi-premium connection.

In the early 1960s, threaded connections were required to comply with a whole set of prerequisites before even being considered to be used in the oil and gas fields. At that time, as a result of accessing deeper wells, the joints needed to have [1.39]:

- good compressive strength;
- high joint efficiency in tension;
- good and repeatable make-up performance;
- leak tightness at high gas pressures;
- outer wall thickness of the coupling as small as possible.

In order to meet the above mentioned specifications and to be applicable to well depths exceeding 6,000m, a new type of connection was introduced by Blose in 1965 [1.40]. By combining the featured torque shoulder and metal-to-metal sealing surface, this connection can be considered the first patented connection incorporating all premium features using the modern-day look. Despite this early introduction of high performance premium connections, applying sealing surfaces directly on the threaded members remained expensive and because of the manageable pressure levels (below 1,034 bars (15,000 psi)) [1.41] and low temperatures within wells, the use of polymer sealing rings was a cheaper and adequate solution to obtain a sealing connection. Up to the late 1970s, different designs using seal rings were patented. These seal rings could be located in a groove in the box [1.42-48], in a groove of the tapered part of the pin [1.49] or in a groove in the large diameter end of the tapered pin [1.50]. Even the use of multiple sealing rings [1.51,52] or the use of seal rings in the threaded area [1.53] can be found. Once the

internal pressure and the temperatures in the drilled wells increased, the use of polymer or plastic sealing rings and thread seals became unreliable and the use of metal-to-metal seals became the new standard. Initially, these seals where *frustoconically* shaped. This means that the sealing surface is shaped as a sequence of two cones with different tapers [1.54]. Initially, the machining grooves of these surfaces provided the sealing capacities. During the following years, various geometries of metal-to-metal seals incorporated in the overall geometry of the connection itself were invented [1.55]. In order to apply enough pressure on the sealing surface, they are usually located near the torque shoulder. When a negative shoulder angle is applied, the sealing surface is energized as a result of outward forces. Based on the growing number of filed patents incorporating this feature, a shift in research focus towards enhancing leak resistance can be observed.

The need for enhanced sealing performance did not show up until the late 1970s, beginning of the 1980s as the result of the introduction of CNC lathes which allowed for a precision thread form and a tight dimensional control. Due to stricter tolerances, connection types such as the buttress connection started to leak under load conditions in which they used to seal. This initiated a series of new studies towards leak resistance of threaded connections investigating various aspects such as thread compounds [1.32,56], effect of contact pressure [1.57] and make-up torque [1.58]. Based on these studies, the industry tended to avoid API modified thread compounds and started using other commercial thread compounds such as '*Best-O-Life 2000*' [1.59] when enhanced sealing capabilities were required. It is estimated that about 80% of the API connections were assembled using this enhanced thread compound which included larger particles, compared to the *API modified* thread compound, and polymer additives increasing the reliability of the seal. A study performed in 1982 [1.60] focused on specifying a seal ring combined with sufficient contact pressures applied by a limited amount of make-up. The intention of reducing make-up combined with a sealing surface included in the connection geometry are typically the requirements for modern premium connections.

From this study onwards, almost 30 years after its first introduction, most patents claiming to present high performance tubular connections incorporate a torque shoulder and sealing surface together with a certain thread geometry.

4.3 The search for the ideal thread type

In the late 1980s, the supply of premium connections was booming. The main reason was based upon the fact that the high well pressures excluded the possibility of using polymer sealing rings to create a reliable leak tight connection. As a result, the need for premium connections kept increasing.

Generally, three basic trapezoidal thread shapes can be distinguished: buttress, modified buttress and dovetail threads. Buttress threads can be

recognized by their positive load and stab flank angles. Modified buttress threads are defined as regular buttress threads of which one of the flank angles is modified, e.g. having a negative load-flank angle [1.61]. Finally, dovetail threads [1.62] are defined as a thread geometry having both a negative load and stab flank angle. The latter was initially introduced to remove the clearance between the stab flanks which is usually the case when using the first two thread types and solves major problems that were encountered using the early premium connections. The initial premium connections were lacking the ability to resist compressive forces. Increasing compressive forces caused plastic deformation at the pin tip and the accompanying metal-to-metal sealing surface [1.63]. By deforming the sealing surfaces, sealing capabilities of the assembly cannot be assured. For this reason, more recent patents focus on the thread geometry in an effort to relief the sealing surface and torque shoulder from the loads encountered during use. This can be realized by making sure that all external forces are transferred between the members within the threaded area. One of the possibilities to obtain this goal is by limiting the gap size between the stab flanks which is present in standard trapezoidal connections. In this way, no axial play exists and axial forces can be better resisted. This approach usually results in the application of a crest-to-root gap instead of the standard stab-to-stab gap. Despite solving the problem regarding the resistance against compressive and tensile forces, it should be noted that when making up these kinds of connections, no radial but axial stresses are induced. Another consequence of using dovetail threads is that an opposite effect, compared to buttress threads, is induced. During make-up, the pin is pulled outwards while the box is pulled inwards, causing the box to be in hoop compression and the pin in hoop tension.

In order to maintain the ability of making-up threads without axial play, known as wedged threads [1.18], two different methods can be applied. The simplest method is to create a wedging effect between the load flanks and one or more torque shoulders. When applying this method, multiple torque shoulders [1.69,70] are often provided since working loads are often not desirable on the shoulder containing the main sealing surface. Another possibility, which is gaining importance during recent years, is the application of different pitch lengths for the thread helixes containing the load and stab flanks [1.71,72] as shown in Figure 1-15.D. When making up wedged threads, axial stresses are induced rather than hoop stresses which makes these types of threads beneficial when high pressure ratings have to be obtained.

With the introduction of modern production methods, it is possible to develop specialized threads such as the one shown in Figure 1-15.F. It is, for example, possible to split up the different flanks in two [1.73] or more [1.74] parts. These third generation threads, such as the Chevron type thread [1.75], are known as faceted threads and can often be found in patents of recent years [1.76-78]. They combine the positive effects of different flank angles used in

trapezoidal thread configurations. It should be mentioned that despite their regular appearance in patents, their effectiveness has not been proven yet and to date, their commercial availability is very limited to non-existent.

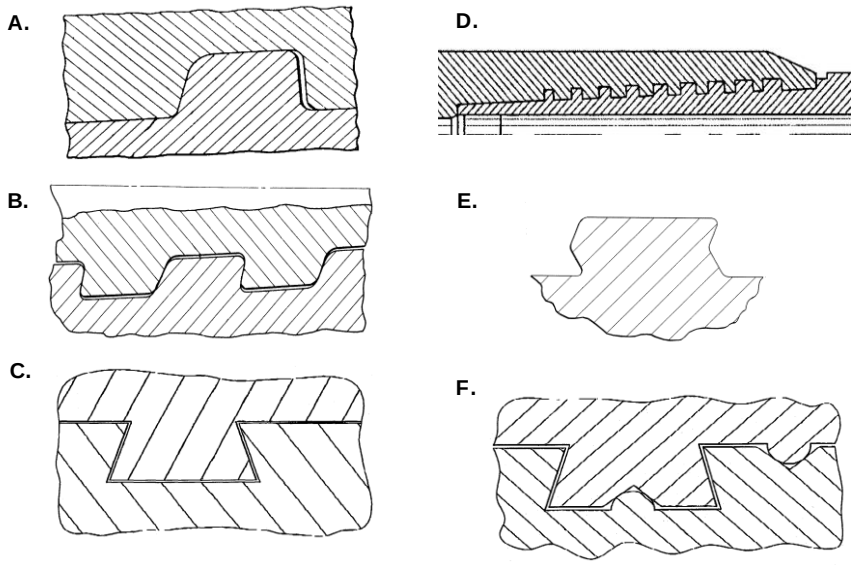

Figure 1-15: Examples of different thread types:
API buttress [1.34](A), modified buttress [1.64](B), dovetail [1.65](C), wedged [1.66](D), faceted [1.67](E) and specialized [1.68](F) threads.

In order to increase the stabbing depth and reduce the required amount of make-up turns, threads are sometimes used as two-step threads as applied in the Hydril-design (Figure 1-14.c). These threads are known as Hydril threads [1.79-82] when negative load flank angles are used. When positive load flank angles are used, it is referred to as modified Hydril threads [1.83].

Within this section, only a limited amount of possibilities have been described. Because of the huge amount of patents filed in recent years, the overview is limited to the easier, basic modifications which are often applied. In order to obtain a full overview of recent developments and more complicated modifications, it is advised to consult the patents filed under following CPC-classes:

- E21B17 : …; Casings; Tubings
- F16L15/001 : Screw-threaded joints with conical threads
- F16L15/06 : Screw-threaded joints characterized by thread shape

5 Objectives of the current research

5.1 Contributions to general knowledge

Within each chapter, the state-of-the-art of the related topic is covered. Based upon this publically available information, enhancements of and additions to current literature are made. Within this dissertation, four distinct contributions are made and are briefly mentioned below.

5.1.1 Expand range of experimental validation methods

Related to experimental validation techniques, the use of infrared monitoring is proposed as an additional validation tool. Up to date, this technique has never been used for threaded connections with the purpose of validating numerical predictions of its mechanical integrity.

In Chapter 3, preliminary tests are conducted and the applicability and potential of this technique is shown. Using thermography, estimations of variables which have never been accurately validated, such as contact pressures, can be made.

5.1.2 Comparison of a 2D with a 3D finite element model

While some numerical studies related to threaded connections have attempted to compare the use of 2D models with full 3D models, no one has ever tried to make this comparison for tapered standard buttress connections. Appendix A includes a numerical comparison of the make-up stage between a 2D axisymmetric and a full 3D model.

5.1.3 Prediction of make-up torque

One of the disadvantages of current models, both analytical and numerical, is the lack of knowledge about the required make-up and break-out torque. Make-up torque is often predicted using the applied thread compounds minimum and maximum friction values, resulting in a tremendous range of allowable torque values. Break-out torques are generally considered to be unknown until a certain amount of experiments are conducted for every type of connection.

Within the thesis, an effort is made to narrow down the possible make-up torque values by taking into account the contact pressure dependency of the thread compound on the coefficient of friction. The conventional and proposed methods are compared with an experimental make-up curve in Chapter 4. Since break-out torque values are believed to be more complex and unlikely to be predictable in combination with the limited experimental scope of this research, they are not considered.

5.1.4 Limitations and enhancements of 2D models

Despite popular belief in the accuracy of simplified 2D models, certain precautions have to be taken into account when trying to simulate the connection's behavior when loads exceed the material's yield limit.

Damage is typically not included in standard 2D models, resulting in the tendency to overestimate the integrity of the vanishing threads. This can lead to inaccurate and even wrong simulation results. Keeping these limitations in mind, improvements are suggested in Chapter 4.

5.2 Proposing an enhanced threaded connections

5.2.1 Technological enhancement

When trying to introduce a new or enhanced technology, the economical capabilities are of utmost importance. From an industrial point of view, technological advances in any sector have to deliver at least one of the following three criteria [1.11]:

- unlock difficult-to-access resources;
- improve exploration and production economics;
- reduce environmental impact.

It is the intention to provide a better understanding of the behavior of threaded-and-coupled connections used in the oil field. This knowledge can then be used to develop a new, enhanced connection which might potentially fulfil all three criteria. By better understanding the connection's behavior, it might be possible to reduce safety and design factors and remove excessive material. By reducing the amount of material, weight reduces and longer strings can be assembled. This allows unlocking deeper reservoirs. By applying changes to the geometry of the threads, it might be possible to increase the connection's rating, allowing to be used in wells containing higher pressures or increased temperatures. In addition, the speed of the make-up procedure might be increased which reduces the required rig time and significantly reduces production costs. Furthermore, a more predictable connection equals a more reliable connection. With increasing reliability, the chances of leaks reduce together with the risk of catastrophic environmental disasters.

5.2.2 Geometric improvements to meet industrial demand

While it is evident that the main objective of new connections is to be stronger and more reliable using the same or even lesser amount of material, one feature is of major importance: the difference in outer diameter at the transition where the coupling is located. In order to prevent being stuck downhole, flush connections are preferred since the outer diameter of the connection is equal to the outer diameter of the pipes it connects. However,

such connections do not have a 100% performance rating resulting in a joint weaker than the strength of the used pipes. An overview of the relation between excess outer diameter and mechanical efficiency (or performance rating) of contemporary connections is given in Figure 1-16. From this figure, it is clear that the intention of obtaining a flush-type connection which is as strong as the connected pipes is the final, yet currently unreached objective. Since having a threaded region implies a local reduction in wall thickness, it is very unlikely to ever obtain a connection with a 100% mechanical efficiency fitting the flush design. However, it might be possible to develop a near flush connection.

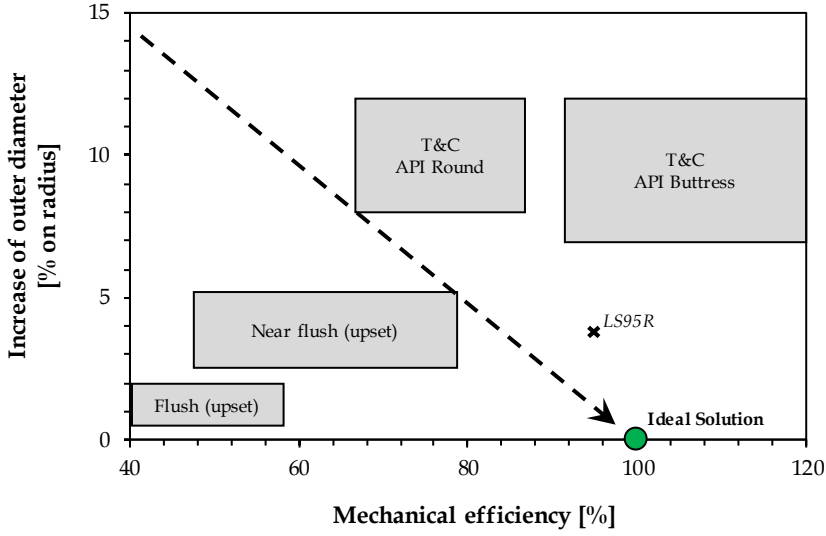

Figure 1-16: In order to achieve a 100% efficiency, an increased outer diameter is currently inevitable.

It is one of the objectives of this thesis to investigate the effects of geometric features on the connection's performance taking into account the intention of obtaining a 100% mechanical efficiency and to reduce the outer diameter of a T&C connection (see section 3.1). This research focusses on load cases consisting of a combined axial tension and internal pressure. Using these two load cases allows proposing a research method which can be expanded for external pressure and axial compression. Once this expansion is performed, connections subject to use at depths up to 700 meter can be investigated (see section 2). While bending will not be addressed within this thesis, it is believed that, with limited effort, this type of loading can be included as well by combining various 2D simulations containing compression and tension (thin walled) [1.84] or by using computationally costly 3D models (thick walled). This would allow the methodology to be used for connections reaching up to 1,200 meters deep. Once this depth is exceeded, failure mechanisms become

too complex due to the introduction of torsion, corrosion and extreme temperatures.

As part of the conducted research, a new 114 mm (4.5 inch) connection is designed with an intended mechanical efficiency of at least 95% and an increased outer diameter of 3.8% on the radius instead of the standard 7.8%. Referring to Figure 1-16, it can be seen that the mechanical efficiency of this connection is intended to be similar to an API buttress threaded coupling while its outer dimension is similar to a near flush connection.

In addition to be one step closer to the ideal solution, the connection has the potential to match the three criteria related to technological advances mentioned in section 5.2.1. By reducing the outer diameter and the threaded area, the amount of required material and overall weight of strings can be reduced. Thus, longer strings can be assembled, unlocking deeper, difficult-to-access reservoirs. By modifying the thread taper, deeper stabbing and a reduced number of make-up turns can be implemented. This reduces rig time and facilitates the assembling process, improving production economics. Additionally, the reduced outer diameter reduces the risk of getting stuck downhole. Finally, the reduced leak paths at the threads reduce the likelihood of leaks. In turn, this reduces the environmental impact of the drilling and producing of wells.

6 Overview of the dissertation

This dissertation is organized in seven chapters. The first chapter sketches the overall situation in which the oil industry operates. Attention is given to the availability of current oil reserves, the prospective for the coming decades and defines the requirements new technologies need to meet in order to be of economic value. Additionally, a short historical overview of the available types of connections is presented based on a patent review. Hereby, the focus is pointed on the invention of new design characteristics and the way inventors tried to deal with problems occurring in the field and advances in technology. The chapter is concluded with the announcement of a newly defined connection. The second chapter lists all definitions required to uniquely define every aspect of a threaded connection. Finally, an overview of the commonly adopted design process and the standardized procedures is provided which are used to test newly developed premium connections.

After providing a theoretical outline, the results of a limited experimental test program, intended to validate the developed numerical model, are discussed in chapter 3. Within this program, three different types of tests are conducted. The standardized procedures of each type of test are described and subsequently the available equipment, practical deviations in the applied approaches are justified. This chapter is concluded by discussing the obtained results and by comparing the various applied measurement techniques.

Chapters 4 and 5 contain the performed numerical work. The first gives an overview of the developed numerical models, both 2D and 3D. After defining performance parameters which will be used to quantify the effectiveness of various connections, a validation is performed by comparing both models and by using the experimental data obtained in chapter 3. The second stage of the numerical part contains a parametric study and is written down in chapter 5. In this chapter, the effects of changes to certain geometric features of the thread in combination with make-up and external tension and internal pressure are monitored, using the previously defined performance parameters. Based on these results, a new thread geometry is proposed and compared with the standard buttress connection and its successor, the SR23 connection.

The thesis' conclusions and suggested future work are formulated in the final chapter. In addition, some preliminary studies are added to assess the feasibility of the suggested work. The last section of this chapter also comprises the personal reflections of the author on the investigated research topic.

References

[1.1] BP, *Statistical Review Workbook 2014*, 2014

[1.2] Rahman, M., *Oil and gas: the engine of the world economy*, OPEC, 2004, accessed 12 November 2014 <www.opec.org>

[1.3] Sonowal, K., Bennetzen, B., Wong, P. and Isevcan, E., *Continuous improvements lead to Maersk Oil Qatar's longest horizontal well in the world*, 2009, accessed 12 November 2014 <http://www.drillingcontractor.org>

[1.4] Payne, M., Miller, M.A., and Suryanarayana, P.V., *New generation well design methods address deepwater HPHT design challenges*, Deep Offshore Technology, Espirito Santo, Brazil, November 8-10, 2005

[1.5] Sakhalin, *Sakhalin-1 Project Breaks Own Record for Drilling World's Longest Extended-Reach Well*, press release, 2012

[1.6] The Guardian, *Shell presses ahead with world's deepest offshore oil well*, 2013, accessed 12 November 2014 <www.theguardian.com>

[1.7] He, L.J., Hu, S.B., Yang, W.C., Wang, J.Y., Yang, S.C., Yuan, Y.S. and Cheng, Z.H., *Temperature Measurement in the Main Hole of the Chinese Continental Scientific Drilling*, Chinese Journal of Geophysics, 49(3), pp. 671-678, 2006

[1.8] Shadravan, A., and Mahmood, A., *HPHT 101-What Petroleum Engineers and Geoscientists Should Know About High Pressure High Temperature Wells Environment*, Energy Science and Technology, 4 (2), 2012, pp 36-60

[1.9] *The Black Gold Rush: Where's All the Oil?*, accessed 12 November 2014, <http://www.jonesoil.ie>

[1.10] World Energy Council, *2010 Survey of Energy Resources*, London, 2010

[1.11] Triepke, J., *Understand Oilfield Technology Lifecycles [OCTG Case Study]*, 2014, accessed 12 November 2014, <www.oilpro.com>

[1.12] BP, *BP Announces Oil Discovery in the Deepwater Gulf of Mexico*, press release, 2014, accessed 12 November 2014 <www.bp.com>

[1.13] United States *Environmental Protection Agency, Assessment of the Potential Impacts of Hydraulic Fracturing for Oil and Gas on Drinking Water Resources: Executive Summary*, EPA/600/R-15/047a, June 2015

[1.14] Energy Information Administration, *Average Depth of Crude Oil and Natural Gas Wells*, 2015

[1.15] Tenaris, *Why pipe matters in today's energy industry*, 2013

[1.16] *Tubing reference tables 2003*, World Oil, January 2003

[1.17] Tenaris Hydril, *Premium connections*, catalogue

[1.18] Hou, F.J. and Banker E.O., *Tubular connection with helically extending torque shoulder*, United States Patent, US2014/0145433 A1, 2014

[1.19] American Petroleum Institute, *Attachment 10 SRXX-BTC_5CA*, 2009

[1.20] API, *API 5B: Specification for threading, gauging, and thread inspection of casing, tubing and line pipe threads*, American Petroleum Institute, 1996

[1.21] Goulas, B., *A method of providing a solid gall preventer in a pin and box joint*, United States Patent, US 3831259A, 1974

[1.22] O'Neill, A., *Pipe Joints*, United States Patent, US 179815, 1876

[1.23] Allison, A.C., *Screw-Threaded Pipe Joint and Coupling*, United States Patent, US 214076, 1879

[1.24] Morse, J.O., *Wrought Iron coupling for Pipe Sections*, United States patent, US 263943, 1882

[1.25] Miscellaneous Publication 141, *Report of the National Screw Thread commission*, US Department of Commerce, Bureau of Standards, fourteenth edition, 1933

[1.26] Bole, W.A., *Pipe Coupling*, United States Patent, US 332184, 1885

[1.27] Evans, S., *Threaded oil well drill stem connection with the threads having included crest angle of 90 degrees*, United States Patent, US 2772899, 1956

[1.28] Montgomery, G.A., *Interior shoulder single piece tool joint*, United States Patent, US 1889870, 1932

[1.29] Montgomery, G.A., *Tubular Coupling*, United States Patent, US 1889867, 1932

[1.30] Reimschissel, C.A., *Tubular Joint Seal*, United States Patent, US 2181343, 1937

[1.31] Hoye, E.C., *Threaded Joint for Tubular Products*, United States Patent, US 2909380, 1958

[1.32] American Petroleum Institute, *WI 2317: Tech Report on LTC/BTC Performance Properties and Leak Resistance: Thread compounds - Rev SS-2006*, report, 2006

[1.33] Coberly C.J. and Wagner E.M., *Some Considerations in the Selection and Installation of Gravel Pack for Oil Wells*, august 1938

[1.34] Webb, S., *Sealed Threaded Pipe Joint*, United States Patent, US 2772102, 1956

[1.35] Breihan, J., Bailey, A.G., and Hegler, M., *Oilfield tubular connection with increased compression capacity*, United States Patent, US 7780202 B2, 2010

[1.36] Nishi, M., and Suzuki, T., *Screw joint for oil well piping*, United States Patent, US 6174000 B1, 2001

[1.37] Macarthur, M.D., *Tubing and tubing joint*, United States Patent, US 2532632 A, 1950

[1.38] Van Der Wissel, H.T., *Box-and-pin-type Threaded Joint having Different Pitches and Pitch Diameters*, United States Patent, US 3079181, 1956

[1.39] Franz, W.F., *Threaded Tubing Joint*, United States Patent, US 3109672, 1963

[1.40] Blose, T.L., *Threaded Tube Joint having a Metal-to-metal Seal*, United States Patent, US 3224799, 1965

[1.41] Maples, J.H., *Pipe Connection*, United States Patent, US4253687, 1981

[1.42] Hinderliter, F.J., *Rotary Tool Joint*, United States Patent, US2102072, 1935

[1.43] Singleton, J.C., *Well Casing Setting and Backing-off Coupling*, United States Patent, US2107716, 1937

[1.44] Archer, M.T., *Packed Tool Joint*, United States Patent, US2110825, 1938

[1.45] Knox, G.S., *Sealed Joint for Tubing*, United States Patent, US2907589, 1956

[1.46] Mac Arthur, M.D., *Synthetic Resin Seal Ring in tubing Joint for Plastic Coated Tubing*, United States Patent, US3100656, 1959

[1.47] Blount, F.E., *Liner-Carrying Well Pipe and Joint*, United States Patent, US3336054, 1965

[1.48] Hokanson, L.W., *Drill Rod Structure*, United States Patent, US3667784, 1970

[1.49] Stone, F., Redondo, B., and Stone, A.L., Well pipe joint, United States patent, US 2239942 A, 1941

[1.50] Maurer, W.C., *Connection for Pipe Joints*, United States Patent, US3822902, 1974

[1.51] Hinderliter, F.J., *Rotary tool Joint*, United States Patent, US2110127, 1938

[1.52] Riemschissel, R.A., *Tubular joint seal*, United States Patent, US 2181343, 1939

[1.53] Reeves, D.E., *Threaded Pipe Connection with Compressible Seal ring*, US4703959, 1987

[1.54] *Definition: conically or frustoconically shaped*, classification 96/261, internet <www.patentec.com>, accessed April 13, 2015

[1.55] Matsuki, M., *Threaded tube joint structure for casing, particularly oil well tubing*, United States Patent, US 3870351 A, 1975

[1.56] API, *Investigation of leak resistance of API 8-round connector: Final report for API PRAC project 84-53*, American Petroleum Institute, 1984

[1.57] Asbill, T., *Report DEA-5: Analysis and testing joint industry project on leak resistance of 7" LTC connections*, July 1984

[1.58] Moyer M.C., Day, J.B. and Hirshberg, A.J., *Torque position make-up of tubular connections*, United States Patent, US 4962579, 1990

[1.59] Bestoflife, *Best-O-Life 2000*, 1980's

[1.60] American petroleum Institute, *Seal Ring Specifications for API Connections*, 1982

[1.61] Beckert, H.J., and Blose, T.L., Threaded tube joint having a metal-to-metal seal, United States patent, US 3224799 A, 1965

[1.62] Blose, T.L., *Tubular connection*, United States Patent, US 3989284 A, 1976

[1.63] Kohyama, F., Inoue, Y., and Akase, S., *Threaded joint with high gas-leak-tightness for oil and gas well pipe*, United States Patent, US 4377302 A, 1983

[1.64] Patterson, B.R., and Schneider, W.P., *Tubular connections*, United States Patent, US 4508375 A, 1985

[1.65] Simpson, N.A.A., Harall, S.J., Metcalfe, P.D., et al., *Coupling tubulars*, United States Patent, US 20080007060 A1, 2008

[1.66] Mallis, D., Sivley, R., Reynolds, H., *Floating wedge thread for tubular connection*, United States Patent, US 20060145480 A1, 2006

[1.67] Leng, K.T., *Threaded pipe connection with a pressure energized flex-seal*, United States Patent, US 20130020072 A1, 2013

[1.68] Simpson, N.A.A., Harall, S.J., Metcalfe, P.D., et al., *Coupling tubulars*, United States Patent, US 20040017081 A1, 2004

[1.69] Blackburn, J.W., and Baron, B.E., *Threaded connection*, United States patent, US 4521042 A, 1985

[1.70] Mallis, D.L., and Reynolds, H.A., *Wedge thread with torque shoulder*, United States patent, US 7690696, 2010

[1.71] Watts, J., *Open type wedgethread connection*, United States Patent, US 20020074799 A1, 2002

[1.72] Ortloff, A.J., and Reeves, D.E., *Threaded pipe connection having wedge threads*, United States Patent, US 4703954 A, 1987

[1.73] Saunders, D.D., Kalsi, M.S. and Chen, G., *Tool joint*, United States Patent, US 4549754 A, 1985

[1.74] Sivley, R., *Threaded connection especially for radially plastically expandable conduit*, United States Patent, US 20050285398 A1, 2005

[1.75] Blose, T.L., *Tubular connection having a chevron wedge thread*, United States Patent, US 4600224 A, 1983

[1.76] Church, K.L., *Thread form for tubular connections*, United States Patent, US 20080277933 A1, 2008

[1.77] Church, K.L., *Hang-free thread design*, United States Patent, US 20060131882 A1, 2006

[1.78] Church, K.L., *Arrow-shaped thread form for tubular connections*, United States Patent, US 8267436 B2, 2012

[1.79] Blose, T.L., *Dovetail connection for pin and box joints*, United States Patent, US 4161332 A, 1979

[1.80] Blose, T.L., *Dovetail connection for pin and box joints*, United States Patent, US 4192533 A, 1980

[1.81] Maples, J.H., *Pipe connection*, United States Patent, US 4253687 A, 1981

[1.82] Mallis, D.L., and Ward, G.W., *Step-to-step wedge thread connection and related methods*, United States Patent, US 8496274 B2, 2013

[1.83] Blose, T.L., *Cylindrical threaded connection*, United States Patent, US 4244607 A, 1981

[1.84] Macdonald, K.A., and Deans, W.F., *Stress Analysis of Drillstrings Threaded Connections using the Finite Element Method*, Engineering Failure Analysis, 2(1), 1-30, 1995

Chapter 2

Design process

<< *This page intentionally left blank* >>

Table of Contents

1 Introduction

The second chapter of the thesis gives an overview of the design approach applied when developing threaded connections. Section 2 explains the difference between two fundamental approaches: uniaxial or biaxial on the one hand and the more recent triaxial approach at the other. Consecutively, the design methodology is elucidated in section 3. Within this section, all steps encountered are explained and relevant information is provided. Finally, a conclusion is formulated relating the design principles to the development of a new connection.

2 Uniaxial, biaxial or triaxial?

Before focusing on the comparison of the different design methodologies, it is important to clarify the meaning of uniaxial, biaxial and triaxial. This is required since a lot of confusion exists as a result of a misinterpretation originating in the late 1980s. In the peer reviewed paper by Kastor [2.1], the use of 'biaxial' and 'Barlow' was considered interchangeable. Within this paper, the term 'biaxial' did not refer to the stress state of the material in which only two of the three von Mises axes were used, but referred to the described design methodology taking into account a combination of internal pressure and axial tension. This also resulted in the use of 'biaxial' to describe the design methodology taking into account the triaxial von Mises criterion.

To avoid any misunderstandings, 'uniaxial' and 'biaxial' will refer to the methodology described in the API RP 5C3 [2.2], which neglects radial stresses, and the term 'triaxial' will refer to the ISO 13679 [2.3], which uses all three stress components of the material.

In essence, the Barlow equation is based on a one-dimensional expression to approximate the hoop stress which is in turn linked to the yield strength of the material and is given by Equation 2.1:

$$\sigma = \frac{p_i D_o}{2t} \qquad \text{(Eq. 2.1)}$$

In this formula, σ is the hoop stress in the pipe material, p_i represents the internal pressure, t the wall thickness and D_o the outer diameter. While this formula was initially considered to provide a good approximation for the burst pressure (in this specific case is σ the yield strength and p_i the burst pressure), two major remarks can be made. First of all, there is no distinction between a pipe with capped ends, a pipe with open ends or a pipe with tension end load [2.2]. Therefore, the effects of axial tension are not considered. Additionally, this formula is based on a simplification of the Lamé equations

and consequently, it is only valid for the case in which a wall thickness of zero is present. Therefore, it is less accurate than the Lamé approximation of yield used in the triaxial von Mises equivalent (VME) stress. The von Mises equivalent stress is given by:

$$\sigma = \sqrt{\sigma_a^2 + \sigma_h^2 + \sigma_r^2 - \sigma_a\sigma_h - \sigma_h\sigma_r - \sigma_r\sigma_a} \qquad \text{(Eq. 2.2)}$$

With (for the case of internal pressure):

$$\sigma_a = \frac{F_a}{\pi(D_o - t)} \qquad \text{(Eq. 2.3)}$$

$$\sigma_h = p_i \frac{{D_o}^2 + (D_o - 2t)^2}{{D_o}^2 - (D_o - 2t)^2} \qquad \text{(Eq. 2.4)}$$

$$\sigma_r = -p_i \qquad \text{(Eq. 2.5)}$$

Within these formulas, F_a is the axial force, σ_a is the axially induced stress, σ_h the hoop stress and σ_r the radial stress at the inner diameter.

Both design methodologies are graphically summarized in Figure 2-1. From this figure, it can be seen that a large overlap is present between both methods. This zone indicates the working loads the pipe can resist according to both the ISO 13679 and the API RP 5C3. Additionally, it can be seen that the triaxial method tends to increase the service area in three of the four quadrants. For the quadrant containing internal pressure and axial compression however, the interpolation of the burst pressure limit and the axial compression limit as described in the API RP 5C3 standard should not be used. While this interpolation is often assumed in literature, no information about allowable load combinations in this quadrant are defined (see further in Section 3.2.1.5). The reason for this absence is that the main failure mechanism as a result of axial, compressive forces is buckling and not plastic failure.

The relative difference between both approaches is shown in Figures 2-2 and 2-3. The first figure is created based upon the relative difference between the calculated burst pressures for all available API pipe dimensions ranging from 100 mm to 600 mm (approximately 4.5 inch and 24 inch). It can be seen that the Barlow approach provides burst pressures up to 15% higher than the ones obtained using the Lamé equations. For every family (pipes with the same outer diameter), increasing the wall thickness results in an increasing difference which results in an increasing non-conservative design. This

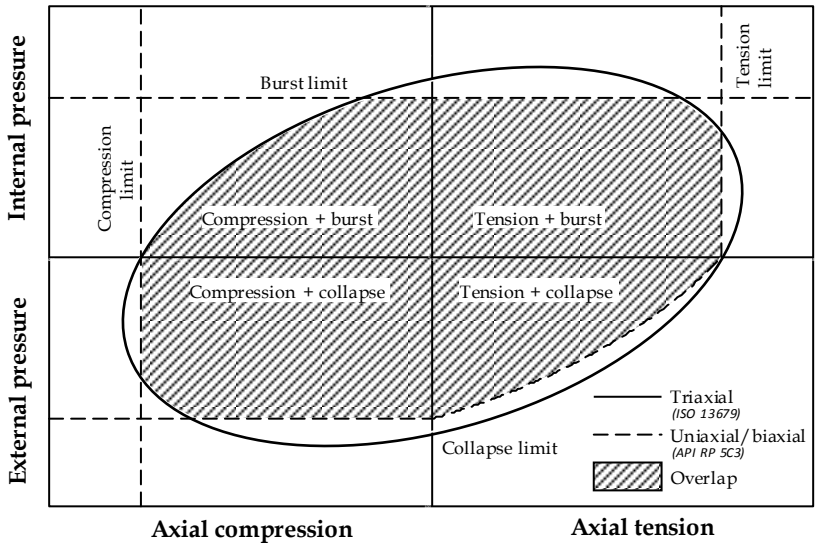

Figure 2-1: Schematic representation of the two possible design methodologies together with a set of consistent design factors for the pipe body

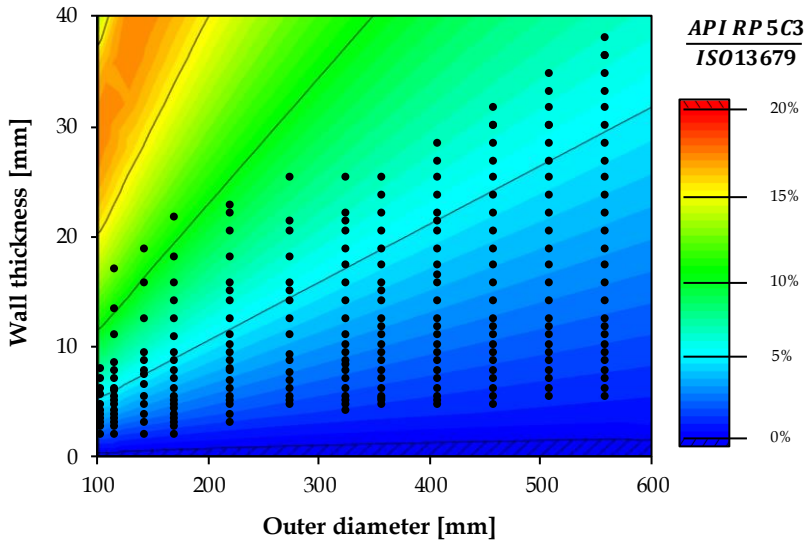

Figure 2-2: Overview of the available API pipes (*black dots*) and calculation of the difference between the burst pressure calculated by the Barlow equation and by the ISO 13679 standard

increasing trend can be visualized when considering the D/t ratios for all pipes as is shown in Figure 2-3. This trend proves to be independent of the various families and only depends on the wall thickness relative to the outer diameter.

An additional study calculating the maximum internal pressure for all load combinations containing internal pressure and axial tension reveals additional information related to the difference between both approaches. While Figure 2-3 suggests that both the von Mises equivalent stress (ISO 13679) and Barlow equation (API RP 5C3) provide approximately the same results for thin walled pipes (e.g. D/t = 80), Figure 2-4 suggests that the Barlow equation is highly conservative once axial loading is applied. This difference reaches its maximum value when the axial load is equal to about 55% of the yield strength of the material. In contrast, the Barlow equation can yield non-conservative predictions of burst pressure for thick-walled pipes (e.g. D/t = 8) when or low or high axial forces are combined with internal pressure.

Based on these observations, it is sound to assume that the triaxial design provides more accurate results, especially when using thick walled pipes. However, it is advised to only use the overlapping regions between both approaches, indicated by the dashed region in Figure 2-1 since these load combinations are covered by both approaches.

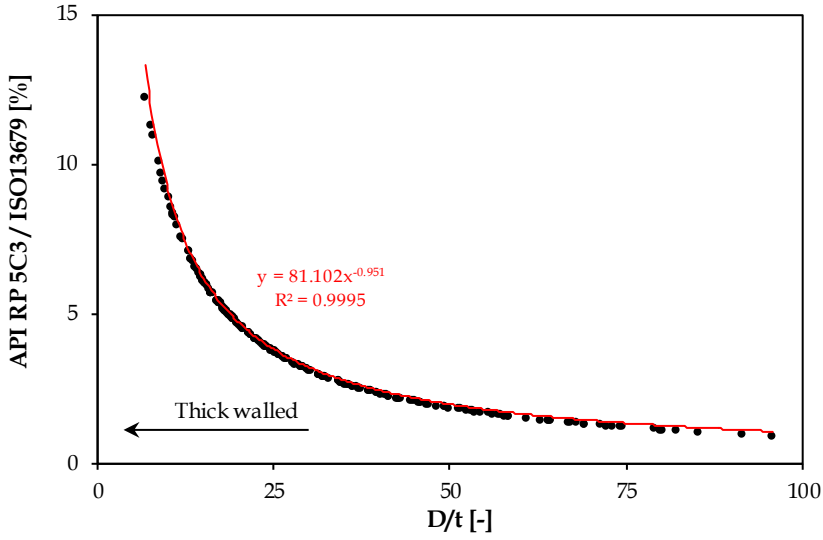

Figure 2-3: When plotting the difference of the calculated burst pressure in function of the D/t ratios of the API pipes shown in Figure 2-2, significant differences are observed when using thick walled pipes

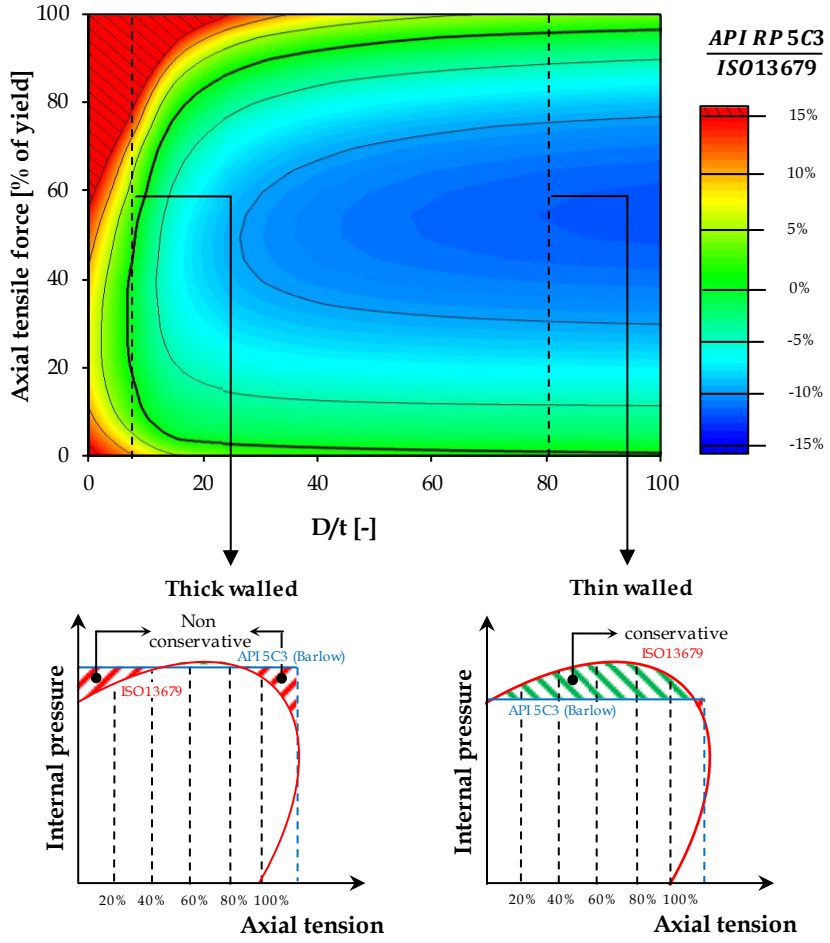

Figure 2-4: When calculating the advised maximum (internal) pressure combined with axial loading up to yield, the Barlow equation can be considered less conservative when using thick(er) walled pipes

3 Design methodology

When designing a threaded connection, a number of tasks [2.4] have to be taken into account:

- The string's mechanical integrity has to be ensured by providing a design that accounts for all the anticipated loads that can be encountered during its lifetime.
- The economic cost has to be kept to a minimum.

- Clear documentation indicating the usability of the connection has to be provided to prevent exceeding the design envelope by applying loads to the connection which were not anticipated during the design.

Related to the design process, various approaches can be applied. Probably the most common approach is the conventional design process in which the most demanding load cases are considered. Because of the over-conservative nature of this methodology, statistical approaches are often preferable. Within these approaches, the statistical distribution of all variables is considered, generally resulting in a more efficient design. Despite a variety of possible design approaches, four distinct phases can always be identified: boundary conditions, requirements, validation and completion. These stages are schematically shown in Figure 2-5 and are discussed below. It should be mentioned that the current thesis focusses on the transition and feedback between the second and third phase of the design process, being the requirements and validation, with in particular the numerical feedback. In the following chapters of this thesis, a methodology is proposed which allows making justifiable adjustments to the geometry of a threaded connection based on numerical results.

3.1 Boundary conditions

As a first step of the design process, the boundary conditions of the threaded connection need to be identified. These parameters can not be changed throughout the design process and are dependent on the intended application and on the characteristics of the pipes that need to be connected.

3.1.1 Intended application

For oilfield applications, a distinction is made between two major categories: tubing/casing and drill connections. The research described in this dissertation will focus on the first category, and more specifically on the casing connections which are the connections that remain in the well itself. Choosing this type of connection allows the study to focus on static loads. This is in contrast with risers or drill connections for which fatigue loads are a major concern. Additionaly, casing connections do not necessarily require the use of a torque shoulder and/or sealing surface.

3.1.2 Pipe parameters

Apart from the intended design, certain parameters are closely related to the geometry and grade of the pipes which have to be connected. An example of such a parameter is the outer diameter of the connection which has to be equal to the one of the pin(s) when a flush joint is requested. Furthermore, the pipes will also determine the rating, indicating the mechanical efficiency of the connection.

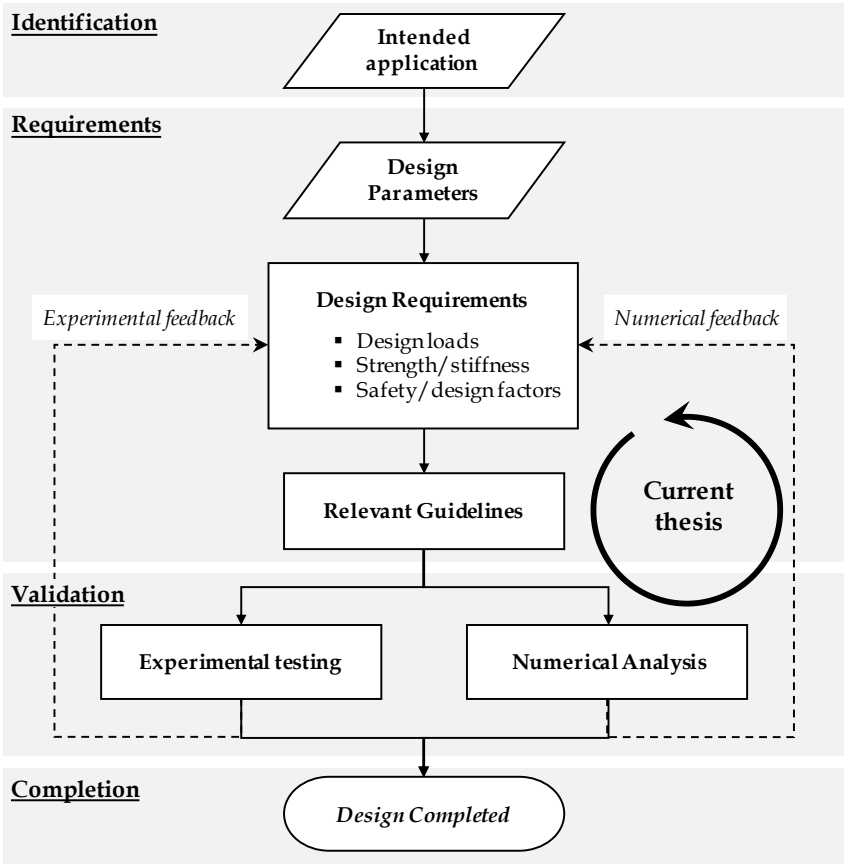

Figure 2-5: Schematic overview of the design process (adopted from [2.5])

3.2 Requirements

Once the boundary conditions are known, the requirements for the new connection have to be defined. These requirements can be divided in two major parts. On the one hand, guidelines are formulated in codes and standards (Section 3.2.1). These rules have to be taken into account and limit, together with the boundary conditions, the scope in which the design process can take place. On the other hand, requirements related to expected loads (Section 3.2.2), intended performance level (Section 3.2.3) and safety margins (Section 3.2.4) have to be defined.

3.2.1 Relevant guidelines

User experience throughout the years is written down in codes and standards in order to increase safety in the field. These should be used as

guidelines throughout the design process to ensure a reliable connection with repeatable and predictable performance.

International standards and recommended practices assure the structural reliability. However, the application of these documents related to the use of safety factors requires a sound engineering judgment for every application. Some cases are not considered in these documents, and as stated in the ISO 11960 [2.6] introduction:

"Users of this International Standard should be aware that further or differing requirements may be needed for individual applications".

A graphical representation describing the necessity of standards is given in Figure 2-6. In order to describe the performance of the product, in this case the threaded connection, three different parameters can be used: material performance which is related to metallurgic research, structural performance based on mechanics and life expectancy based on predictions, testing and experience. In order to estimate these parameters, the working conditions consisting of multi-axial loads, thermal profiles, fluid dynamics, interaction between materials and fluids,… need to be evaluated and interpreted. The tools available for this are various standards and proprietary specifications.

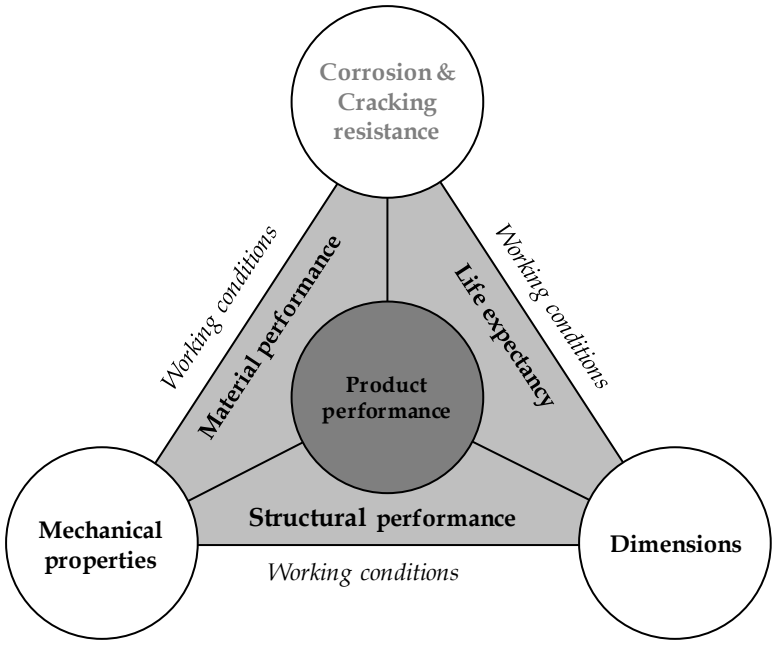

Figure 2-6: Graphical overview of the connection between boundary conditions (white) and product performance using standards (light grey) (Adopted from [2.7])

Using these documents, the required dimensions, mechanical properties and resistance to various failure mechanisms can be derived.

In general, a distinction can be made between two different kinds of guidelines: industrial and testing guidelines. While industrial guidelines are more of a predictive nature and tend to predict a connection's behavior by using experimentally validated formula, typically describing the structural performance, the testing guidelines are designed to provide a procedure for testing new connections and to estimate the material performance.

3.2.1.1 API 5CT (ISO 11960)

The standard *Petroleum and natural gas industries – Steel pipes for use as casing or tubing for wells* [2.8] provides valuable information about the required material properties such as tensile properties, impact toughness, hardness variation and resistance to sulfide stress cracking and how to obtain them (e.g. possible heat treatment operations, chemical composition, hardenability, grain size). Since it is possible that not all cases are covered by this standard and when risk concerns still arise, supplementary requirements and product level specifications to improve structural reliability can be applied. This can be done by determining additional mechanical properties, by conducting statistical testing and by developing NDT acceptance criteria. Many of these supplementary procedures get adopted in the standard. Example hereof is the SR12 addition containing information about the statistical analysis of impact testing or appendix H5 which takes into consideration the application of high strength steels.

3.2.1.2 API 5C1

The *Recommended practice for care and use of casing and tubing* [2.9] provides valuable information about how to join two pipes together, providing a detailed description on how to perform the stabbing and make-up operation. For API Round threads, tables are provided containing reference torque values which have to be obtained during make-up of both casing and tubing.

3.2.1.3 API 5C2

The *Bulletin on Performance Properties of Casing, Tubing and Drill Pipe* [2.10] contains tables with the minimal performance of couplings defined in the aforementioned standard API 5CT. The performance parameters listed consist of collapse resistance, pipe body yield, internal yield pressure and joint strength. While it was not the intention to serve as a guide manual, this standard could be used to reliably select an appropriate grade, size and weight to be used when the occurring forces are known. All data in this standard was later transferred into formulas which are written down in the research guideline API 5C3 and therefore, standard API 5C2 was discontinued in 1999.

3.2.1.4 API RP 5A3 (ISO 13678)

The *Recommended Practice on Thread Compounds for Casing, Tubing and Line Pipe* [2.11] focusses primarily on the characteristics of the thread compound applied on the threads when assembling a connection. The main focus is on the friction and sealing characteristics. In the appendices, various tests are described to evaluate the behavior of the thread compound such as a fluid sealing test. It is worth noting that the complexity of galling is observed in this standard. While extensive research has been done in the past in an effort to predict this failure mechanism [2.12], no industry consensus has yet been reached. Until today, the thread compound manufacturer remains responsible for the extreme contact pressure performance of his thread compound. The latest version of this standard [2.13] concludes that a reliable prediction is only possible by applying make-and-break tests as described in ISO 13679 (see Section 3.3.1).

3.2.1.5 API 5C3 (ISO 10400)

The *Technical Report on Equations and Calculations for Casing, Tubing, and Line Pipe Used as Casing or Tubing; and Performance Properties Tables for Casing and Tubing* [2.2] provides predictions about the performance of the connections by means of formulas for various failure modes such as burst, collapse, compression and axial strength. These estimations are determined by applying a classical, deterministic and continuum mechanics approach. This standard is typically used for pipes and standard connections and estimates performance limits for a number of load cases. These load cases are illustrated in Figure 2-7. It is important to point out that annex F of the standard API 5C3 offers insights in the development of a probabilistic approach to estimate the collapse performance properties taking into account the statistical variability of product parameters.

3.2.1.6 API 5C5 (ISO 13679)

The *Recommended Practice on Procedures for Testing Casing and Tubing Connections for Petroleum and natural gas industries – Procedures for testing casing and tubing connections* [2.3] can be considered to be the replacement of the API 5C3 when trying to certify proprietary premium connections. Within this standard, all failure modes discussed in the API 5C3 are incorporated and additional experimental procedures are defined to evaluate a wide range of possible load combinations consisting of axial tension/compression and internal/external pressure, ensuring rigid and reliable connections. Figure 2-8 provides an overview of all tested load combinations. The ellipse represents all load combinations resulting in an equivalent von Mises stress equal to the material's yield stress. A variety of load combinations, consisting of combinations of internal/external pressure and axial tension/compression (indicated by the squares in Figure 2-8), is tested by applying a cyclic load path.

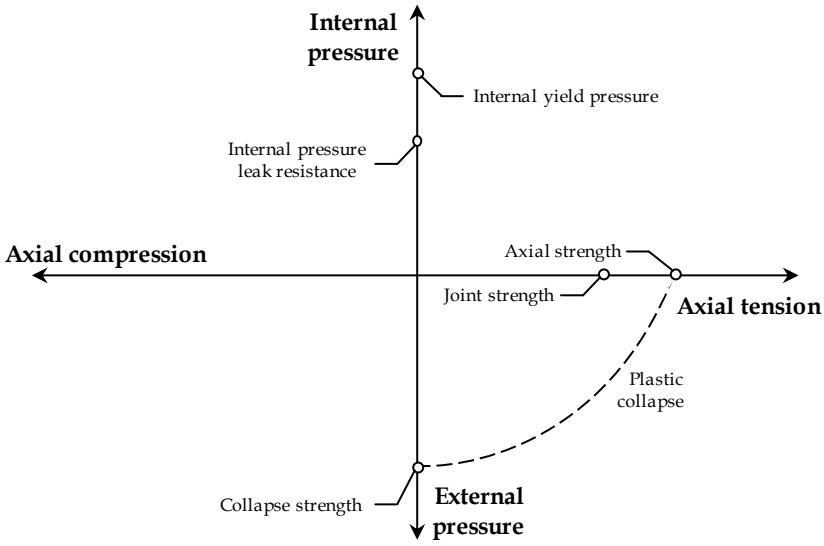

Figure 2-7: Indication of the limits defined in the API 5C3

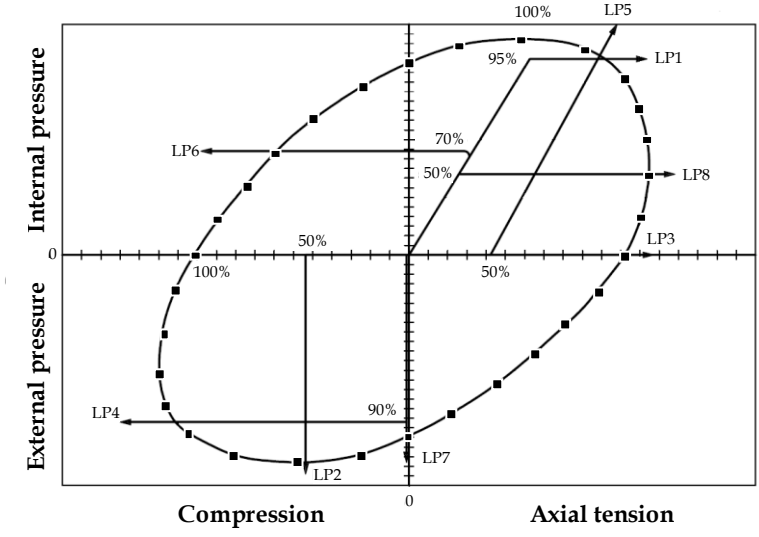

Figure 2-8: Schematic overview of the tested load combinations according to the ISO 13679 standard (adopted from [2.6])

After this procedure, various different limit load paths (LPx) are applied up to failure in an effort to gather additional information related to the failure conditions. It should be mentioned that a different specimen is used for every limit load path (see further in section 3.3.1).

When comparing the approach described in the API 5C3 (Figure 2-7) with the one provided in ISO 13679 (Figure 2-8), it is immediately visible that the latter standard provides a more extensive test schedule. While the API 5C3 only provides estimates for burst, collapse and axial tension, the ISO 13679 requires the actual testing of combined load combinations and different failure tests. However, despite a more extensive testing schedule, the ISO 13679 should not be considered the actual successor of the API 5C3. While the last version of the API 5C3 contains a statistical approach, the ISO 13679 does not. This is a huge limitation, especially when considering that a lot of design methodologies such as *Reliability Based Design (RBD)* or *Quantitative Risk Analysis (QRA)* are based on statistical approaches. An addition to allow these design methods may (and is likely to) be added in the future.

3.2.2 Design loads

Within the framework of this thesis, external torsion, bending and temperature are not considered and only pressure loads and axial loads are considered. The investigation of these load combinations is usually sufficient for casing connections up to a depth of 700m [2.15].

External pressure loads on casing and tubing strings are mainly produced by cement and fluids outside the casing and can be modeled by pressure distributions depending on the type of fluid. Alternatively, when these pressurizing fluids are located within the string, an internal pressure is present. In turn, axial loads are usually mechanical loads associated with the casing hanging weight (self-weight), shock loads during running and loads induced during the installation of the string. Additional examples of these loads are often wellbore deviation, bending loads in dogleg regions (in case of directional drilling) and buoyancy effects as the result of the used drilling mud.

3.2.3 Performance rating

The objective of threaded couplings designed nowadays is to acquire a 100% mechanically efficient connection. This is considered a connection which is equally strong as the pipe body of the connected pins. However, in addition to the mechanical joint efficiency and sealing characteristics, other requirements have to be considered as well. First of all, the designed connection has to be manufactured and inspected in an economical way. Once the connection is correctly produced, it has to be installed in the field where ease of use (e.g. deep initial stabbing) and limited installation time is required [2.16]. With the current environmental concerns, the use of thread compounds

is a major issue. In order to be able to make-up and break-out the connections, the coefficient of friction has to be low and predictable. However, historically used thread compounds containing lead are no longer allowed nowadays [2.17]. A current tendency observed in this field is the development of dopefree connections [2.18]. A limited elaboration about this type of connections will be given in chapter 7. In addition to the man-made regulations, environmental limitations are posed by the conditions of the well such as increased temperatures and an acid environment. Related to the latter, the connection has often to be enhanced by applying coatings and adapting the applied materials in an effort to counter possible corrosion damage.

3.2.4 Safety and design factors

While it is the intention to provide a reliable string at a minimum cost, failures can still occur. Most documented failures are known as *off-design failures* and occur because the string was exposed to loads exceeding the design envelope. In contrast, *on-design failures* are rather rare. This implies however, that the string designs are mostly conservative. If a failure occurs, it is often at the threaded connections that are being used to assemble the strings [2.19]. This implies that either field make-up practices are not adequate, or that the connection design basis is not consistent with the pipe body design basis. Therefore, the performance of the threaded connections is always compared with the pipe body performance, which is defined as the *rating* of the connection. In order to have a string that will fail in the pipe body rather than the threaded connection, connections with a mechanical efficiency rating exceeding 100% have to be used.

During the design process, a distinction between load, design and safety factors has to be made. The loads are the forces acting on a certain connection. These include axial tension, axial compression, internal pressure, external pressure, bending and torsion. The *safety factor* equals the pipe resistance divided by the applied (or expected) load. The *design factor* is the minimum acceptable safety factor in any case, related to the expected acting loads. The relationship between design and safety factor can be expressed by the following formula:

$$DF = SF + LF \qquad \text{(Eq. 2.6)}$$

In which DF is the actual design factor, SF is the safety factor and LF the load factor which is the additional safety margin based on the uncertainty of the expected loads. This means that when a connection is designed with a design factor of 3 and a safety factor of 2.5 to withstand a tensile load of 100kN, the connection is designed not to fail when tensile loads up to 300kN are applied. This exceeds the mandatory acceptable load of 250kN (determined by

the safety factor) by 50kN. The actual design factor, typically ranging between 1.0 and 1.75, is based on various parameters such as the expected loads, the used connections and the applied calculation method [2.20]. This factor is often based on the ability of the engineer to estimate the magnitude of the expected working loads. When a higher level of uncertainty is present, the design factor has to be higher. The minimum allowed safety factor in excess of the design factor is defined in case certified API connections and pipes are being used. These factors are listed in Table 2-1 [2.21]. From this table, it is observed that the safety factors for the connections and pipe body may be different. This is because the connection jump-out and failure criteria for API casing connections such as the Buttress connections specified in API Bull 5C3 [2.2] are based on ultimate tensile strength (UTS) while the pipe body axial failure criterion is based on specified minimum yield strength (SMYS). The 1.6 design factor for axial tension was originally derived using the UTS/SMYS ratio of the API grade N-80 (UTS = 552 MPa (*80 ksi*); SMYS = 689 MPa *(100 ksi)*), which is approximately 1.25 and was frequently used when these safety factors were introduced in the 1950's. By multiplying the 1.3 pipe body safety factor with the 1.25 ratio, a rounded safety factor of 1.6 was obtained. This approach indicates that the defined safety factors in the default standards are not intended to be used with high strength steels which typically have a lower UTS/SMYS ratio than the N-80 steel. For this reason, modern proprietary connections, which are connections related to a specific company, often use different safety factors which are experimentally validated. One of the examples are the high strength TN HC products of Tenaris as illustrated in Figure 2-9 [2.22]. Since the steels of this high collapse (HC) product range exceed the steel grades defined in the API 5CT, the API defined safety factors for collapse are not accurate.

Table 2-1: API defined safety factors

Load Case	***Safety factor***
Uniaxial tension	1.3 *(pipe)* or 1.6 *(connection)*
Uniaxial compression	1.2
Burst	1.25 or 1.1 *(depending on pressure)*
Collapse	1.1
Triaxial design	1.25

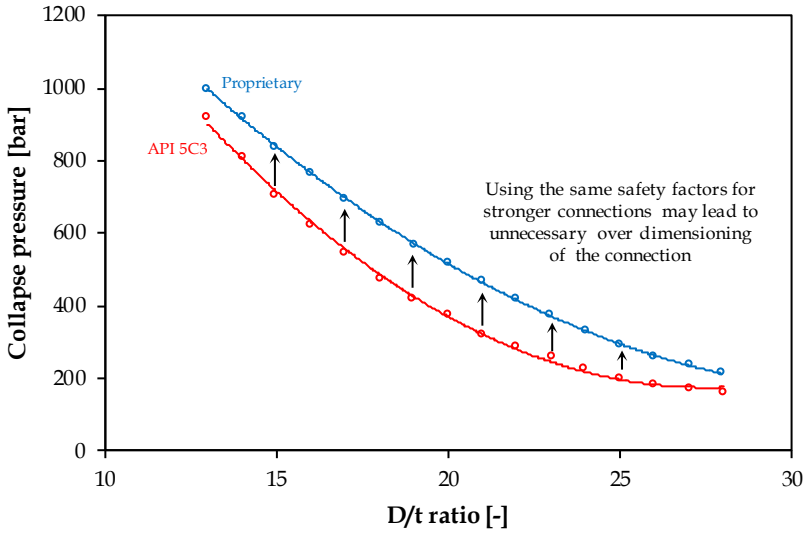

Figure 2-9: Difference between the API defined collapse resistance and actual collapse resistance of stronger, proprietary steel grades.

It can be concluded that by using design and safety factors, a certain amount of conservatism is introduced when developing connections. This amount of conservatism even increases when modern day steels are being used in combination with API defined safety factors. This causes over dimensioning and results in an increased cost. In order to keep this over dimensioning to a minimum, it is of utmost importance to have a proper understanding of the behavior of the connection. When it is possible to predict how the connection will react when exposed to certain loads, it is possible to reduce the design and safety factors. This reduction will eventually be translated in a more efficient use of materials and in an overall reduction of the cost of the well.

3.3 Connection validation

Before introducing a newly developed connection on the industrial market, an extensive validation has to be performed. Since it is often too expensive to test the connection for every dimension (outer diameter and wall thickness) and material, a combined procedure using experiments and numerical simulations is permitted.

3.3.1 Experimental validation

In the past, the standard API 5C3 was used to calculate the limit loads of connections which were then tested experimentally. Nowadays, the more

recent standard ISO 13679 describes the preferred procedures and is mandatory when testing proprietary premium connections.

A schematic overview of the testing procedures is shown in Figure 2-10. Each specimen must be prepared with a required thread-seal interference, such as high-low, low-high, high-high, low-low. To achieve these situations, thread taper combinations known as pin fast-box slow, pin slow-box fast, and pin nominal-box nominal are often used to evaluate the change of the actual interference of thread and seal [2.23]. The procedure makes a distinction between four classes called CAL I through IV that are determined based on their intended use. CAL I is the only class which is solely used for liquid service and testing is performed at room temperature without external pressure and the application of bending loads is optional. CAL II adds thermal cycling with a cumulative exposure to nitrogen gas of 5 hours at an elevated temperature of 135 °C. A more severe class, CAL III, which is used for gas and liquid service, includes external pressure in the cyclic testing. Finally, the CAL IV connections which are used for the most severe applications such as the use in *high pressure high temperature* (HPHT) wells, include bending and thermal/pressure-tension cycling with a cumulative exposure of about 50 hours to gas at 180 °C. The prescribed procedure in the 2002 standard includes the use of eight sets of specimen. Each of these specimens are subjected to three different types of tests: a *make-and-break test* (MBT, blue), a *test load envelope* (TLE, green) and a *limit load test* (LLT, purple).

During the MBT, the connection is repeatedly made-up to test its galling resistance and required torque specifications. Different make-up positions are tested and during the final make-up, the maximum allowed torque is applied for further testing. Depending on the required CAL classification, the connection is subjected to a thermal cycle to dry out the thread compound which is required for a reliable and consistent assembly before applying the TLE. The TLE consists of a cyclic load path in which various load combinations are applied, illustrated by the squares in Figure 2-8. Depending on the series being performed, load combinations from different quadrants of the von Mises ellipse are tested. Once all load combinations are applied without failure of the connection or pipe body, a final LLT is conducted. For each specimen, a different failure path is defined in an effort to cover as many different failure modes as possible.

The brief overview given above suggests that, despite using a limited amount of specimens, the procedures require an extensive and expensive experimental setup. These expenses are even higher for new products because various members of the connection family need to be tested. As a result of the huge costs, amount of specimens required and complexity of the procedure to validate a connection design, more recent versions of this standard (starting with the new release in 2010) reduced the number of specimens required for the full validation from eight to five as indicated in Table 2-2 [2.25]. It is

important to mention that, despite the reduced number of required specimens, the total amount of time required for testing CAL IV connections with the new procedure suggested in DIS 13679 is increased by a factor of three up to 120 days due to the changes made to the thermal cycles.

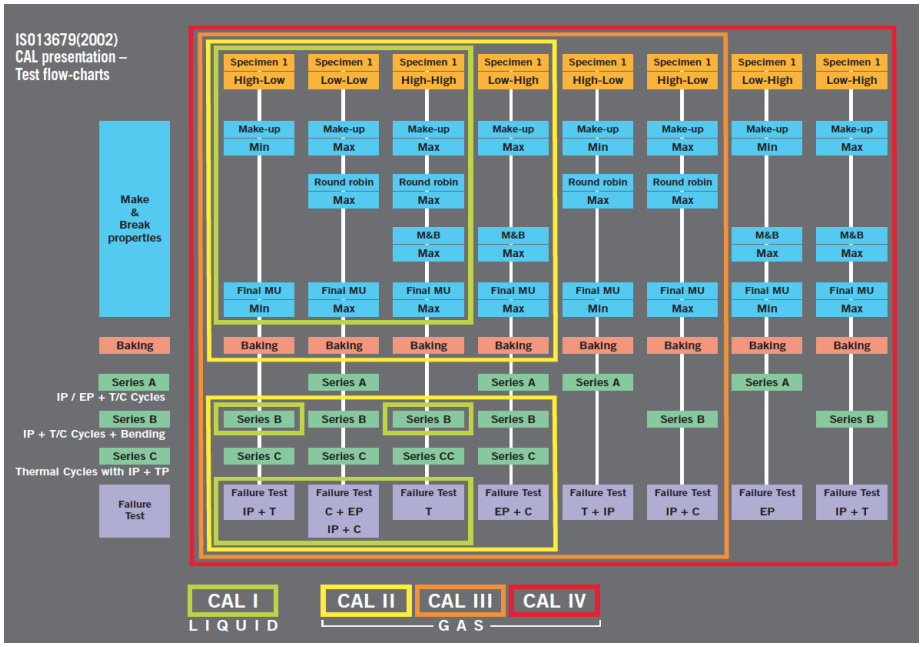

Figure 2-10: Graphical representation of the test procedure in accordance with ISO 13679 [2.24]

Table 2-2: Overview of the difference between the old (2002) and new (2015) version of the ISO 13679

	ISO 13679:2002								*ISO 13679:2010 (DIS)*				
Specimen	*1*	*2*	*3*	*4*	*5*	*6*	*7*	*8*	*1*	*2*	*3*	*4*	*5*
Make/Break	✓	✓	✓	✓	✓	✓	✓	✓	✓	✓	✓	✓	✓
*TLE** [series]*		A		A	A		A		B	B	B	B	
	B	B	B	B		B		B	C	C	C*	C*	
	C	C	C	C					A	A*	A*	A*	
*Limit Load *** [LP]*	1	2	3	4	5	6	7	8	3	2*	1*	6*	5

* Only CAL IV
** See Figure 2-10
*** See Figure 2-8

3.3.2 Numerical validation

As mentioned in section 3.3.1, the prescribed experimental procedure for testing connections is very expensive and therefore, it is economically impossible to test every possible connection size and material for every connection design. In an effort to lower the total testing costs, a combined numerical and experimental approach has been proposed [2.26,27]. Figure 2-11 represents an overview of an entire family belonging to a certain connection design. Within this family, connections for pipes with an outer diameter from 127 mm (5 inch) to 179 mm (7 ¾ inch) are available and D/t ratios of approximately 5 through 10 are covered. In total, the family consists of 28 different members. Since testing 28 connections in accordance with the ISO 13679 standard would cost a large amount of time (over a month of testing per connection and even longer using the new, proposed standard) and results in a huge cost, it is possible to only test the extremities of the design. In practice, this means that for every pipe outer diameter, the lower and upper D/t ratio has to be tested experimentally. This significantly reduces the total amount of physical connections subjected to the standardized testing procedure to 10. However, reducing the number of connections subject to experimental testing does not imply that the other configurations do not require any form of investigation. A numerical analysis is required to demonstrate that the behavior of the simulated connections is similar to the behavior of the experimentally tested connections. Criteria which can be used for such a comparison are for example the magnitude of plastic deformation, location of maximum stresses, … as a result of a various combinations of loads.

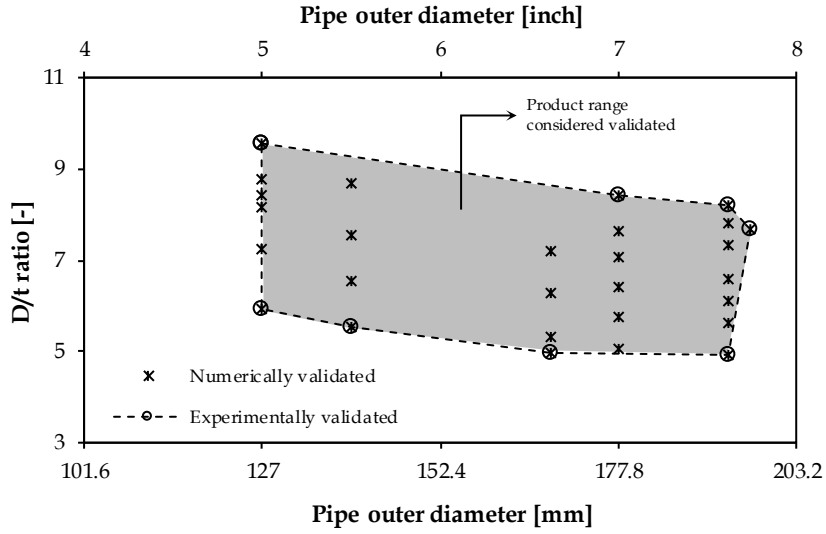

Figure 2-11: Validation procedure for a new connection family (adopted from [2.27])

3.4 Completion

Once all required experimental tests and numerical simulations are conducted and the results are favorable, the newly designed connection can be distributed after official certification.

4 Conclusions

Throughout this chapter, the main steps required during any design process were presented. Comparing the uniaxial/biaxial with the triaxial approach, it was concluded that the latter approach is generally preferred and will be used for the development of an enhanced connection later in the thesis (see Chapter 6).

The important parameters required to be known at the start of the design process are the type (Threaded-and-Coupled), purpose (casing/tubing), size (4.5 inch) and wall thickness (7 mm). In addition to the geometric variables, an additional estimation of the expected working conditions and intended rating is desirable. Since the intended connection should be possible to operate up to depths of 700 m, axial tension and compression in addition to internal and external pressure can be expected.

Once the geometry of the entire connection, including threads, is uniquely defined, an experimental validation is required. When the same geometry is tested for various sizes, the additional use of numerical validation allows a reduced experimental testing program. Within this thesis, the experimental testing will be based upon the methodology used for the CAL I connections as specified in the ISO13679:2002 and will be limited to the case of internal pressure combined with axial tension. While the experimental testing will not be performed on the developed connection, the data will be used for the validation of the numerical modelling approach. Within this thesis, the validation of the connection up to applied load combinations of 95% of its yield strength will be numerically validated.

References

[2.1] Kastor R.L., *Triaxial Casing Design for Burst*, SPE/IADC Drilling Conference, 9-12 February, Dallas, TX, USA, 1986, SPE-14727

[2.2] American Petroleum Institute, *API RP 5C3:Petroleum and natural gas industries - Formulae and calculation for casing, tubing, drill pipe and line pipe properties*, First edition, 1993

[2.3] ISO specification 13679, *Petroleum and Natural Gas Industries – Procedures for Testing Casing and Tubing Connections*, European Committee for Standardization, 2006

[2.4] Norsok, *D-010: Well integrity in drilling and well operations*, standards Norway, 2004

[2.5] Aadnoy, B.S., Aasen, J.A. and Pollard, M., *Casing design – review of design methodology*, Rock-well consultants, 2003

[2.6] ISO specification 11960, *Petroleum and Natural Gas Industries – Steel pipes for use as casing or tubing for wells*, European Committee for Standardization, 2014

[2.7] Daguerre, F., Merliahmad, M. and Tivelli, M., *International standards and recommended practise for assuring structural reliability on OCTG products*, Tenaris University, DMF, 4th Petroleum Forum, Presentation, 2010

[2.8] American Petroleum Institute, *API Spec. 5CT/ISO 11960: Casing and Tubing (U.S. Customary Units)*, seventh edition, 2002, Washington, DC

[2.9] American Petroleum Institute, *API RP 5C1: Recommended practice for care and use of casing and tubing*, eighteenth edition, 1999, Washington, DC

[2.10] American Petroleum Institute, *API Bull 5C2: Bulletin on performance properties of casing, tubing and drill pipe*, twenty-first edition, 1999

[2.11] American Petroleum Institute, *API RP 5A3/ISO 13678: Thread Compounds for Casing, Tubing, and Line Pipe*, second edition, 2003, Washington, DC

[2.12] American Petroleum Institute, *API prac Project 88, 89, 91-51, Investigation of Pipe Thread compounds Section 5, "Galling Test"*, 1992

[2.13] American Petroleum Institute, *API RP 5C3/ISO 13678:2012: Evaluation and testing of thread Compounds for use with Casing, Tubing, Line Pipe and drill stem elements*, third edition, 2012, Washington, DC

[2.14] NACE, *MR0175/ISO 15156, Petroleum and Natural Gas Industries – Materials for Use in H2S Containing Environments in Oil and Gas Production*, first edition. 2001. Houston, Texas

[2.15] Tenaris, *Why pipe matters in today's energy industry*, 2013

[2.16] Tenaris, Hydril, *Dopeless technology*, brochure, 2012

[2.17] Stringfellow, W.D. and Jacobs, N.L., *Environmentally acceptable drill pipe thread compound*, PennWell Conferences and Exhibitions Co., 1992

[2.18] Castineiras, T., *Dopeless pipe connections yield benefits*, Journal of petroleum technology, 2008

[2.19] Klimack, B.K., *Rotatable and bendable casing connections*, WIPO Patent, WO2013075228A1, 2013

[2.20] Energy resources conservation board, *Directive 10: Minimum casing design characteristics*, 2009, internet: https://www.aer.ca, accessed on 03/04/2015

[2.21] Hansen, B., *Production casing design consideration*, Devon Energy Corporation, 2006

[2.22] Tenaris, *Steel grades: high collapse*, internet: http://www.tenaris.com, accessed on 03/04/2015

[2.23] JFE-steel, *Premium Joint, "JFEBEAR" for OCTG*, TECHNICAL REPORT No. 7, 2006

[2.24] Vallourec, *Premium connection testing*, Connection: the vallourec opil & gas online magazine, 2012, internet: http://www.connection-mag.com, accessed 03/04/2015

[2.25] C-Fer, Vallourec and Stress engineering services, *Laboratory experience with high temperature external pressure connection testing*, API conference, 2011, presentation, internet: http://mycommittees.api.org, accessed 03/04/2015

[2.26] Powers, J.P., Baker, D.A. and Chelf, M.S., *Application of connection productline evaluation*, Proceedings of the IADC/SPE Drilling conference, IADC/SPE 112639, 2008

[2.27] Bradley, A. B., Nagasaku, S., and Verger, E., *Premium Connection Design, Testing, and Installation for HPHT Sour Wells*, Society of Petroleum Engineers, 2005, doi:10.2118/97585-MS

Chapter 3

Experimental testing

Table of Contents

1 Introduction

This chapter comprises the test procedures and results of the tests carried out for the validation of the numerical model discussed in Chapter 4. In Section 2, the standardized procedure used to certify newly designed premium threaded connections for liquid service is described in detail. Section 3 reveals the types of tests that were performed during this research. Next, specimen geometry (Section 4), equipment (Section 5) and instrumentation (Section 6) are discussed. Finally, in Section 7, an elaborate discussion of the obtained results is given. During this discussion, different measuring methods are compared with each other, and hypotheses explaining the observed behavior of the couplings are suggested. These hypotheses will be further explained and investigated in Chapter 4, where the numerical results are discussed.

2 CAL I testing

2.1 Overview

An overview of the ISO13679:2002 standard describing the testing procedures for premium threaded connections was given in Chapter 2. While this standard is intended for premium connections, the described approaches will serve as a basis for investigating the (modified) Buttress connections. For sake of simplicity and safety, the applied tests for the shoulderless, standard threaded specimen used in this study (see section 4.1) are based on the CAL I procedure. This procedure is considered for connections with the least severe, liquid applications. CAL I connections are subjected to cyclical test loads, including internal pressure using a liquid test fluid, axial tension and compression. Subjecting the specimen to bending loads is optional and external pressures, baking and thermal cycling tests are not taken into account at all. CAL I testing takes place at ambient temperature and only requires three specimens to complete the procedure. These specimens (indicated by the standard as S1, S3 and S6 [3.1]) are selected based on the geometry of their tapers. S1 and S6 are composed of a pin with a slow taper and a box with a fast taper, S3 is assembled using two members with both nominal tapers.

The three specimens used for the CAL I procedure are subjected to the following tests:

S1: MU - FMU – Series B – Failure 1
S3: MU - RRG - MBG – FMU – Series B – Failure 3
S6: MU - RRG – FMU – Series B – Failure 2

With:

Failure 1: Failure test using internal pressure and axial tension
Failure 2: Failure test using internal pressure and axial compression

Failure 3: Failure test using axial tension
FMU: Final make-up (field end)
MU: Make-up (mill end)
MBG: Make-up/break-out test for galling resistance (field end)
RRG: Round robin make-up/break-out test for galling resistance (field end)
Series B: Test load envelope with test series B

The objectives of the CAL I testing procedure, consisting of three types of tests, are illustrated in Table 3-1. Generally, the objective of the test load (TLE) is considered the primary objective of the entire test when the CAL I procedure is followed.

2.2 CAL I procedures

2.2.1 Make-up tests

The make-up tests comprise the MU, MBG and FMU parts mentioned in section 2.1. The standard procedure for the make-up/break-out states that for each make-up a dry and clean connection ought to be used. Before assembling, a thread compound, of which type and amount together with the allowable tolerances are provided by the manufacturer, is applied. Subsequently, the pipe and box are connected with each other and the torque-turn diagram is measured during the process. A make-up condition is considered successful when 95% or more of the maximum torque is reached for a high specified torque and when 105% or lower of the minimum torque is reached for a low specified torque. The reference torque levels are specified by the manufacturer. For testing purposes, the testing requires suggested minimum and maximum values for both the thread compound and make-up torque depending on the test, as is indicated in Table 3-2. During make-up, it is important to maintain a rotational make-up speed no less than 90% of the maximum recommended rotational speed in order to be realistic. While damage is more likely to occur

Table 3-1: Objectives of the CAL I testing procedure

Specimen	Make-up	Test load (TLE)	Limit load
S1	Thread galling	Minimum leak integrity	High internal pressure with tension increasing to failure
S3	Maximum box hoop stress	Leak resistance at maximum make-up tightness	Tension to failure
S6	Maximum pin axial stress	Leak resistance at maximum make-up tightness	Internal pressure with compression increasing to failure

Table 3-2: Overview of make-up conditions

Specimen #	Thread Compound			Torque		
	MU	*MBG*	*FMU*	*MU*	*MBG*	*FMU*
	A end	*B end*		*A end*	*B end*	
S1	H	-	H	L	-	L
S3	H	L	H	H	H	H
S6	H	L	H	H	H	H
Used abbreviations						
H	Manufacturer's recommended maximum value					
L	Manufacturer's recommended minimum value					
NOTE	Integral joints are considered B end threads					

using high rotational speeds (e.g. due to misalignment, cross threading, wobbling of the connection, …), it is the objective to test the most critical situations. Furthermore, in order to simulate field conditions as best as possible, a vertical make-up position should be used.

A T&C connection exists of two ends: A and B (see Figure 3-1). The A-end is the mill end while the B-end is the field end. Since A-end joints are not intended to be broken out in the field and remain assembled throughout their lifetime, the torque applied is normally higher than the torque applied at the field end. For the B end of the connection, a make-up/break-out test using the least specified amount of thread compound is required for two of the three specimens (S3 and S6) to test the retorque characteristics of the connection. In addition, specimen S3 requires a detailed galling investigation. This includes cleaning the connection after break-out and photographing both pin and box to inspect for signs of galling. Differences in the geometry between the first and last break-out are traced as well.

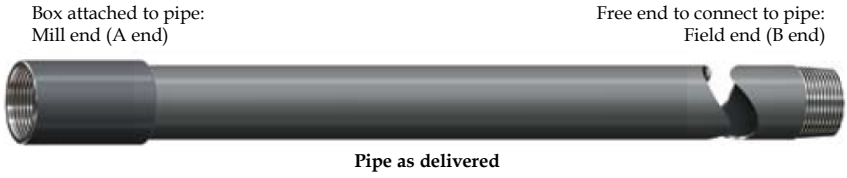

Figure 3-1: Indication of mill end (A) and field end (B) of the delivered pipe which already contains a box

2.2.2 Test load envelope tests

A second type of test is the *Test Load Envelope* or *TLE* test. The combined load testing for CAL I specimens is the main objective of the procedure and is

limited to applying a combination of internal pressure and axial tension/compression, known as test series B.

In order to determine the load combinations, the minimum allowable yield strength of the mother pipe, the minimum allowable wall thickness and the specified outer diameter are used. The load combinations are then calculated based on the von Mises Equivalent (VME) stress and a certain percentage of the yield strength of the coupling. The equations are given in appendix B of the standard [3.1]. In Figure 3-2, a test load envelope is illustrated. Within this figure, *A* represents the combinations possible to obtain a 100% VME stress of the pipe body yield envelope while *B* shows a 95% VME pipe body yield envelope. The load combinations corresponding to an ellipse are then applied counter clockwise (combinations 1 through 9), starting with pure tension, repeated clockwise (9 through 1) and once again counter clockwise (1 through 9) as illustrated in Figure 3-2. When leakage is detected, the pressure load step is held constant for one hour in order to determine the leak rate. Once a leak rate of 1mm³/sec is reached, the connection is considered to have failed.

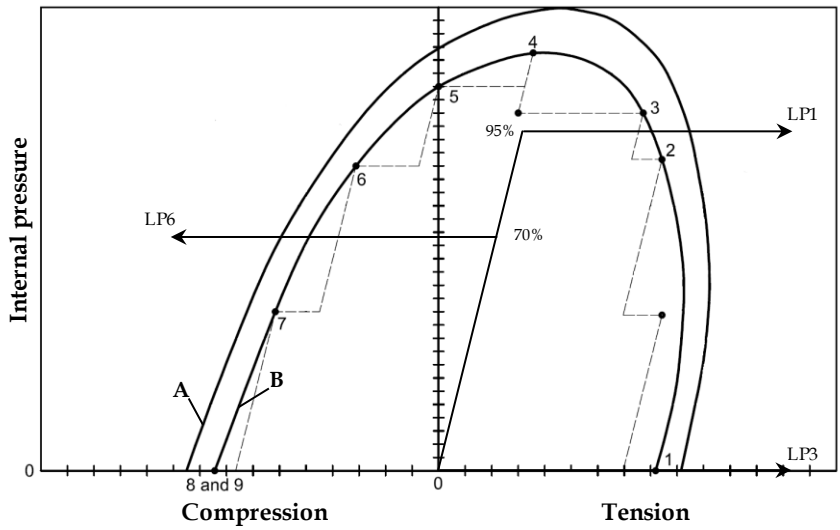

Figure 3-2: Overview of a test load envelope and limit loads

2.2.3 Limit load tests

Once the test load envelope procedure is conducted completely, a limit load test is performed. During this test, a specimen is tested up to failure by applying a combination of internal pressure and tension (S1), only tension (S3) or a combined internal pressure and compression (S6). The corresponding load paths are indicated in Figure 3-2 as LP1, LP3 and LP6 respectively. When a combination of axial tensile load and internal pressure is applied, the internal pressure is increased to 95% of its maximum internal pressure when no axial

load is applied for S1 and up to 70% of its maximum when a compressive load is applied until failure (S6). The connection is considered to have failed once:

- the critical leak rate of 1 mm^3/sec is reached;
- the increase or decrease of the specimen length exceeds 3%;
- the volume of the specimen changes with more than 6%.

3 Validation experiments

3.1 Make-up tests (MU)

3.1.1 Purpose

The intention of the make-up tests is to measure various parameters that will later be used to validate the numerical model (see Chapter 4). During the tests, it is important to measure various parameters which can be used for either direct validation of the numerical model or for indirectly supporting hypotheses regarding the connection's behavior. The outputs suitable for direct validation are the applied rotation, the induced torque and the strains at the outside of the box. The indirectly applicable data are the temperatures measured at the outside of the box.

3.1.2 Setup

An experimental setup was developed to assemble threaded connections using a torque unit (see section 5.1). It is schematically illustrated in Figure 3-3. The box of the assembly is fixed at one end while the pin is being rotated.

During the testing, the resulting torque is measured at the box end. At one side of the assembly, a speckle pattern is applied to part of the box surface and will be used to extract the strains by using Digital Image Correlation (DIC) (see further in Section 6). To obtain a second reading of the strains, twelve biaxial strain gauges are evenly divided over three sections and are equally distributed over the circumference of the box at the threaded region which is in contact when pin and box are assembled (see section 6.2).

On the opposite side, part of the box surface is painted with a black emissivity spray to ensure a constant emissivity value of 0.97. The temperature of this area is then measured using a thermographic camera (see section 6.5). In addition, the temperature is measured at two additional places using thermocouples (see section 6.4).

3.1.3 Procedure

Before joining the two members together, a thread compound conform to the API RP 5A3 standard [3.2], named *API Modified* (see section 4.4), is

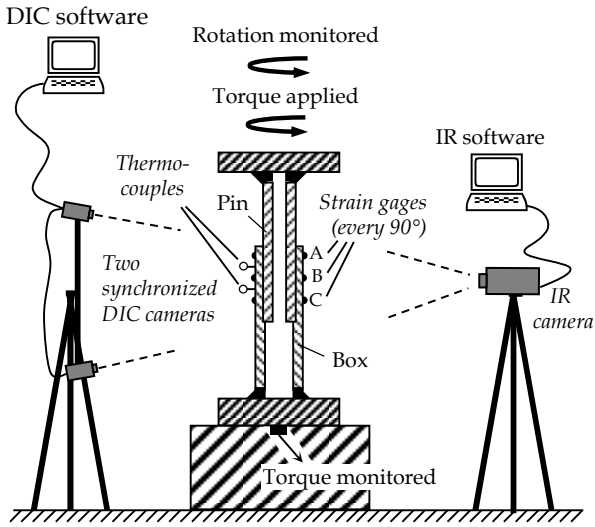

Figure 3-3: Make-up setup

manually applied at both the pin and box part of the coupling. During this process, the entire threaded surface is covered with dope. Once the thread compound is applied and both parts are aligned, the connection is manually assembled until a position prior to its hand tight position is reached. This way, the full torque-turn diagram can be monitored. Finally, the test is conducted using a torque unit to complete the make-up using a rotational speed of approximately 0.1 rpm.

The main differences when compared to the standardized procedure, summarized in section 2.2.1, are the unspecified amount of thread compound and the reduced rotational speed. Since the specimens are custom made, no suggested amount of dope is prescribed and therefore, just enough thread compound to cover the entire threaded area of both pin and box is used without monitoring the exact weight. It is assumed that excessive thread compound will be pushed out of the connection instead of creating pressure pockets since no torque shoulder or sealing surface is present. Similar to the case of the thread compound, no guidelines are provided related to make-up speeds. The applied make-up speed is mainly limited by the manual setup. These differences are acceptable since the objective of the tests is not to certify a connection, but to validate a numerical model. Furthermore, no distinction is made between the types of thread interference as a result of taper mismatch. While taper mismatch may be effecting the results significantly, these effects can be approximated using techniques described in Chapter 4.

3.2 Test load envelope (TLE)

3.2.1 Purpose

During the TLE tests, various combinations of internal pressure and axial tension are applied. These tests are a reproduction of a limited amount of real working conditions under ideal circumstances.

It is the intention of these tests to validate certain parameters such as the leak resistance, which is assumed to be 275 bars when using the *API modified* thread compound in combination with the standard API Buttress threads, and the mechanical behavior when external loads are applied. In addition, similar measurements as described in section 3.1.2 are conducted. The strains and temperature measured will be used to validate a finite element model (see Chapter 4).

3.2.2 Setup

The instrumentation used for the TLE tests is similar to the instrumentation used in the make-up setup. The redundant use of two different methods to measure strains and temperature is applied at the outer surface of the box. Tests are performed using a 1000 kN tensile test rig (see section 5.2). In order to apply internal pressure, the connection with the test rig is fitted with the possibility of connecting an external pressure pump (see section 5.3) at the bottom while the pressure is measured at the top as is illustrated in Figure 3-4.

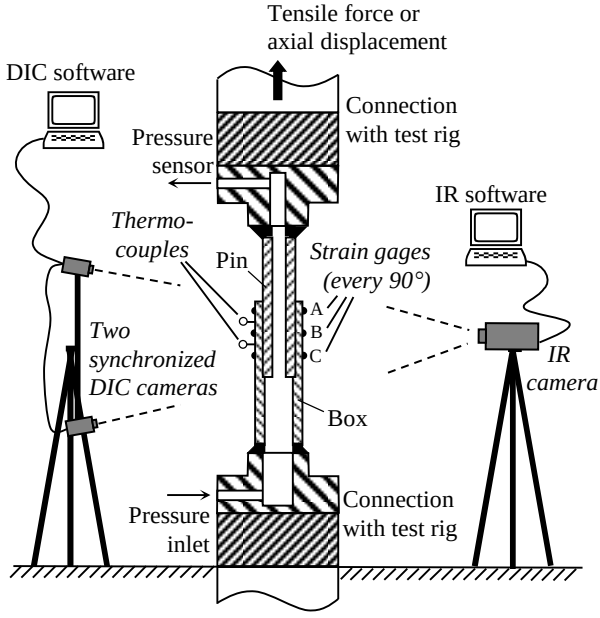

Figure 3-4: TLE and limit load test setup

3.2.3 Procedure

It is the intention of the TLE test to evaluate various cases of combined loading. However, due to the unknown internal pressure at which the connection will leak, standard procedures as described by the ISO 13679 were not adopted. While it is common practice to test all combinations having the same percentage VME of the pipe body yield limit, the internal pressure was gradually increased and for every pressure step, the axial tensile loading was increased from 0 to 70% of its pipe body yield strength (approximately 300 MPa in this case) as indicated in Figure 3-5. This procedure was continued until excessive leakage was observed, causing the internal pressure to decrease abruptly over 50%.

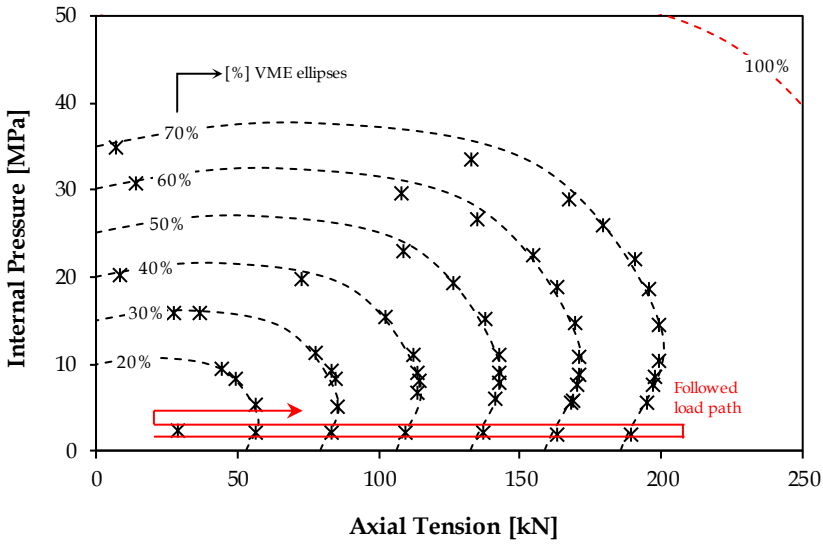

Figure 3-5: Overview of the tested load combinations and indication of the modified load path followed.

3.3 Limit load tests (LL)

3.3.1 Purpose

After conducting the TLE tests, leakage occurs and the connection cannot be pressurized anymore. For this reason, it is not possible to conduct a limit load test based on a combination of axial load and high internal pressure as is required for the S1 and S6 specimens. Therefore, an axial limit load test is conducted with the aim of revealing the weakest location in the threaded connection. In addition, this test reveals valuable information about the failure mechanism.

3.3.2 Setup

The tensile failure test is in practice an extension of the TLE tests in which axial tension is applied without internal pressure until the specimen fully breaks. For this reason, the same setup used for the TLE tests (see section 3.2.2) is adopted.

3.3.3 Procedure

The procedure for the tensile failure test can best be compared with an axial tensile test. During this test, an axial displacement using steps of 0.5 mm at a tensile rate of 0.02 mm/sec is applied until failure. After every step, a DIC (Digital Image Correlation) and IR (Infrared) picture are taken before proceeding to the next. In contrast with the standard, the test was not stopped at 3% total elongation, but continued until the specimen fully broke.

4 Test specimen

4.1 Geometry

The experiments are conducted on 52 mm (2 inch) diameter pins with a wall thickness of 6.95 mm. Because of the small outer diameter of the specimen, the threaded pipes are not commercially available and custom manufacturing of a standard Buttress thread as defined by API 5B [3.4] was necessary. The dimensions deviating from the API standard used to define the geometry can be found in Figure 3-6.

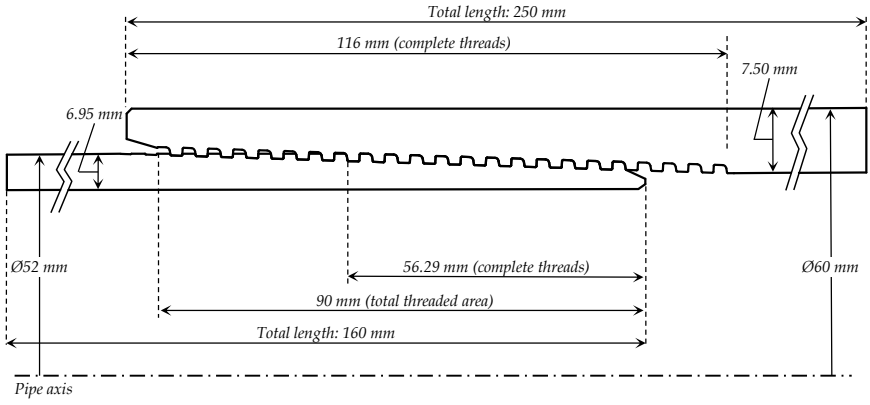

Figure 3-6: Overview of the specimen geometry. Only the thread profile is in accordance with the API 5B [3.4].

4.2 Measured data

In order to explain the observed behavior during the tests, various geometrical parameters of both pin and box are measured. The thread profile is measured with an accuracy of 0.01 mm for the lengths and 0.01 degree for the angles using a *Nikon profile projector type 6CT2*. The outer diameter and wall thickness were obtained using a regular caliper. In order to get a reliable value, five measurements at different locations are taken and averaged. An overview of the average value of the measured parameters can be found in Table 3-3. It should be mentioned that, while the five measurements of the majority of the parameters resulted in a limited scatter, the thread height of the pin differed significantly. This is caused by a slight offset of the tapered pitch diameter, causing a reduced cut of the threads resulting in a partly uncut crest section of the thread.

Table 3-3: Theoretically defined (API 5B) and experimentally measured data of various geometric parameters

Parameter	*Theoretical*		*Measured*		
	Min	*Max*	*Set 1*	*Set 3*	*Set 5*
Box – Thread Height [mm]	1.549	1.600	*1.54*	*1.46*	1.56
Box – Thread Pitch [mm]	5.029	5.131	5.08	5.09	5.08
Box – Load Angle [degrees]	2.000	4.000	2.71	3.31	3.27
Box – Stab Angle [degrees]	9.000	11.000	9.78	9.55	9.82
Box – Taper Angle [degrees]	3.433	3.833	3.69	3.45	*3.36*
Box – Outer diameter [mm]	59.97	60.03	60.00	60.00	60.02
Pin – Thread Height [mm]	1.549	1.600	1.56	*variable*	*variable*
Pin – Thread Pitch [mm]	5.029	5.131	5.09	5.09	5.09
Pin – Load Angle [degrees]	2.000	4.000	2.55	3.00	2.92
Pin – Stab Angle [degrees]	9.000	11.000	10.17	*8.87*	9.86
Pin – Taper Angle [degrees]	3.491	3.776	*3.22*	*3.45*	3.65
Pin – Outer Diameter [mm]	51.97	52.03	51.94	51.88	51.97
Pin – Wall Thickness [mm]	6.08	6.95	6.19	6.64	6.18

4.3 Material

Figure 3-7 shows the materials used for both pin and box are grade B plain carbon steels, as defined by the API 5L [3.5], with a yield strength of respectively 370MPa and 300MPa. The ultimate strength is 620MPa with an elongation of 14.2% for the pin and 547MPa with an elongation of 16.5% for the box.

4.4 Thread compound

4.4.1 Benefits

An *API modified* thread compound was used during the experiments. Despite the growing tendency of using dopefree connections (see Section 7),

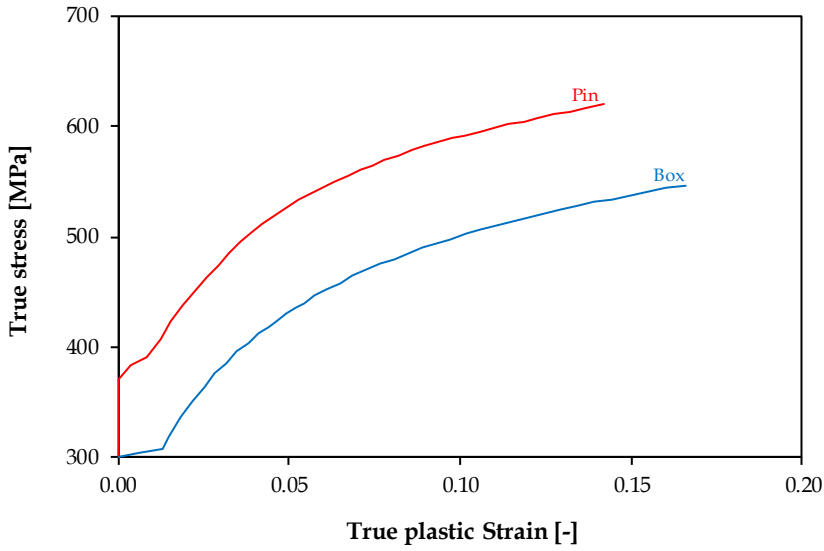

Figure 3-7: Stress strain curve of the Grade B materials up to necking

lead-free thread compounds are still used when a solid coating designed for friction reduction is not applied on the threaded area.

Thread compounds are used for a variety of reasons. First of all, applying dope on the threaded area provides a reduced, consistent and predictable coefficient of friction. Using the *API modified* thread compound reduces the coefficient of friction to a value between 0.02 and 0.08 (for more details, see Chapter 4). By reducing the coefficient of friction, the frictional forces and accompanying make-up torque are reduced. This reduction is translated in a reduction of frictional heat and also causes a reduction of the risk of galling which is defined as the transfer of material between pin and box, causing sticking when making up the connection.

Finally, when no sealing surface is present, the solid particles in the thread compound will migrate through the voids in the helical thread. Once the compound is dried out, these particles are stuck and clog any possible leak path up to a certain amount of pressure. When using an API Modified compound, the connection is assumed to be leak tight up to 275 bars with a maximum gap size of 150 µm [3.7].

4.4.2 Frictional force multiplier

Thread compounds are known to reduce the coefficient of friction, which in turn leads to lower frictional forces. This reduction is translated into a lower torque level required to obtain a certain make-up position.

Apart from the coefficient of friction, the geometry of the threaded area also has a tremendous effect on the frictional forces. When considering the geometry of a Buttress thread, an axial clearance of approximately 150 µm can be observed when taking into account the allowable tolerances. This gap has detrimental effects on the leak tightness of the coupling. However, the axial movement enabled by this clearance makes sure a crest/root contact is present over the entire threaded area. The location of the contacting flanks is important because the connection types without a torque shoulder rely on a radial clamping force to ensure their rigidness. The amount of clamping force highly depends on the make-up position combined with the angle of the contacting flanks.

Using vector analysis (see Figure 3-8) assuming that a root-crest contact exists and that $\overrightarrow{F_R}$ (force on the root) and $\overrightarrow{F_C}$ (force on the crest) are equal (since both lengths are equal and the distribution of the clamping force is assumed to be uniform over the threaded area), it can be shown that the frictional force (F_F) is proportional to the clamping force ($F_{C,R}$) using a frictional force multiplier *k* corresponding to following formula:

$$F_F = \mu F_{C,R} k \qquad \text{(Eq. 3.1)}$$

This can be written as:

$$F_F = \mu (F_C + F_R) k \qquad \text{(Eq. 3.2)}$$

With:

$$k = \frac{cos\alpha \ + \ cos\beta}{(tan\alpha \ + \ tan\beta)\ cos\alpha\ cos\beta} \qquad \text{(Eq. 3.3)}$$

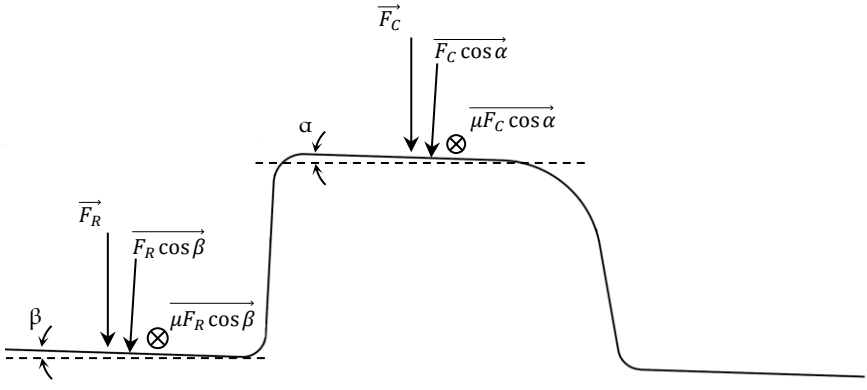

Figure 3-8: Vector analysis of trapezoidal threads

The results of this equation, similar to the ones found by Watts [3.8], are illustrated in Figure 3-9 as a function of the first (ω) and second (ϕ) contacting flank angles. These flank angles are measured starting from the line perpendicular to the pipe axis. From this figure, it is apparent that wedging the threads (contact between the load and stab flanks) of API Line Pipe or API Round connections (ω = 30°, ϕ = 30°) will result in a required torque with a frictional force multiplier of 2. For the wedged Buttress thread (ω = 10°, ϕ = 3°), the *k*-factor would be 8.8 which causes very high torque requirements, demanding excessive torque units, in order to obtain the desired radial interference. By maintaining the gap at the stab flanks (as is the case for API Buttress threads), the contact occurs at the crests/roots and the *k*-factor is reduced to 1 (ω = 88.2°, ϕ = 88.2°). The grey area indicates the combinations of load and stab flank angles for which a radial force cannot be generated when making up the connection. Therefore, several thread forms such as dovetail threads with a uniform pitch length cannot be used to generate an initial radial interference.

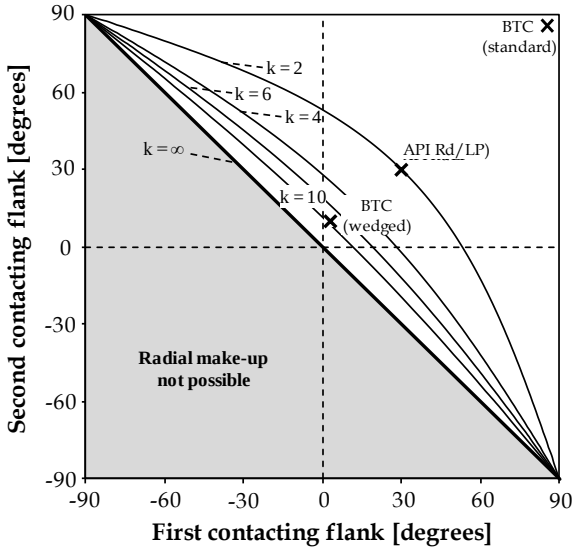

Figure 3-9: Frictional force multiplier in function of the angles of the contacting flanks

5 Equipment

5.1 Torque unit

In order to make up a connection with a predefined make-up torque or up to a certain make-up position, a setup enabling relative rotational movement

is required. A refurbished torque unit with a torque capacity of up to 2500 Nm, depicted in Figure 3-10, is used for this purpose.

By turning the hand wheel (2), a larger worm gear (3) is driven and a rotational movement is applied to the pin member specimen (1). The angular position of the gear is measured using an absolute encoder (see section 6.1). The other member of the assembly, the box, is clamped at the opposite site of the test rig to a linear guiding system (6). This axial movement is required to take into account the relative axial displacement during make-up. The resulting torque is measured by connecting the box to a lever (5) which is further connected to a load cell (4) which is connected to the frame.

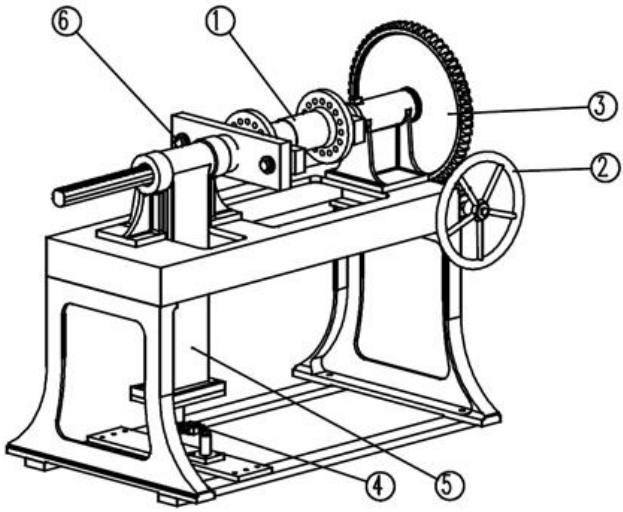

Figure 3-10: Used torque unit

5.2 Tensile test rig

In addition to make-up torque, axial tension needs to be applied when performing a TLE or limit load test. After make-up, the specimen is mounted in a universal 1000 kN tensile test rig. Axial loads of up to 1000 kN can be applied, using a force or displacement controlled input. The former is typically used when performing a TLE test while the latter is preferred when performing a fracture tensile test.

5.3 Pressure pump

In addition to the possibility of applying an axial load, connection points are provided in the mounting blocks of the specimen to connect an external membrane pump with a maximum capacity of 800 bars using water as a pressurizing fluid.

6 Measurement techniques

6.1 Make-up torque and rotation

In order to enable the creation of the torque-turn diagram (see section 7.1.1), two sensors are attached to measure the applied rotation and the resulting torque. The rotation of the main gear is measured using a Kübler absolute encoder T8.5862.1224.2004 which is able to measure the rotational position with a 0.044 degrees tolerance. At the other end of the specimen, a 5 kN Sensy-loadcell type 2712 is placed at a distance of one meter from the axis of the specimen. This allows measuring a resulting torque of up to 5 kNm with an accuracy of 5 Nm.

6.2 Strain gauges

The strains at the outside of the box, required for validation purposes, are measured with two different methods. The first technique uses twelve biaxial FCA-3-11 –type strain gauges (*SG*) with an accuracy of 0.0005 %. These strain gauges are equally distributed over three different sections A, B and C and are spaced 90 degrees apart (see Figure 3-11). The location of the three sections is based on the estimated relative position of the pin related to the box. Section A is defined as the section near the last engaged thread of the pin at the end of the box. Section C is placed in such a way that it is assumed to be located near

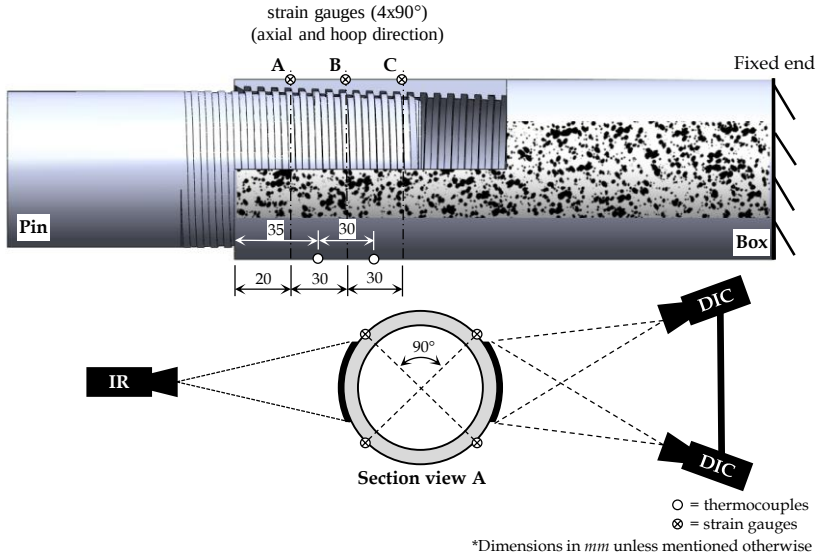

Figure 3-11: Indication of the locations of the strain (SG + DIC) and temperature (TC + IR) measurement techniques

the center of the box above the location of the pin tip at the opposite end of the threaded area (see Figure 3-11). Finally, section B is placed in between A and C and should approximate the location where the vanishing threads transform into complete threads. The location of the three sections does not require to be placed with pinpoint accuracy since the relative position of pin and box after make-up is unknown.

6.3 Digital Image Correlation

In recent years, the use of Digital Image Correlation (*DIC*), a contactless, optical method to measure strain is widely used. In order to gain more global information about the mechanical behavior of the connection, DIC is applied at one side of the coupling in addition to the previously mentioned strain gauges. Accurate DIC calculations require the application of a non-uniform high-contrast speckle pattern on the specimen's area of interest, i.e. the outer surface of the box. This pattern was achieved by projecting black spray droplets upon a uniform, dry white bottom layer of paint. The DIC algorithm calculates the displacement field that produces the highest correlation between images of a deformed specimen surface and a reference image of the undeformed specimen. Hereto, a sum of squared differences is calculated and iteratively minimized at every investigated point, comparing the grey values in a subset around the point in the reference image with its corresponding values in the deformed image. Using a stereovision system consisting of two cameras, three dimensional displacements are obtained. From this displacement field, surface strains can be obtained by means of differentiation. The images in this record were obtained from a stand-alone system containing two synchronized monochromatic 14 bit cameras, with a resolution of 2452 by 2054 pixels (provided by Limess GmbH). The DIC analysis was then performed using the VIC3D software of Correlated Solutions Inc. The speckling procedure was optimized in order to obtain speckles of approximately 0.1 by 0.1 mm in size, corresponding to a speckle size of 3 by 3 pixels as advised by Sutton et al. [3.9].

6.4 Thermocouples

Special attention is given to the temperature of the specimen when loads are applied. By monitoring the temperature at the outer surface, heat sources at visually inaccessible locations can be identified and estimated. Generally, heat is generated by friction and/or deformation [3.10]. Therefore, the temperature distribution of the connection is considered as an additional parameter that allows indirect validation of the numerical model. Two different methods are used. A first method is the use of two K-type thermocouples (*TC*) located above the threaded area as illustrated in Figure 3-11. These calibrated thermocouples are primarily used as control parameters for the infrared (IR) monitoring technique described below.

6.5 Infrared monitoring

In analogy with the DIC approach for measuring strains, a more advanced and optical method for measuring the temperature field of the entire visible area is considered. This technique is frequently used to investigate fatigue failure (dynamic loads) [3.11-13], but only limited results have been published for quasi-static loads. Based on studies of welded joints performed by Kutin et al. [3.14,15], it was shown that the intensity of the measured temperature can directly be correlated to the amount of applied tensile load and accurately reveals the areas containing plastic deformation. The use of infrared monitoring combined for threaded connections has not been frequently reported. The only documented study containing this approach was conducted during make-up, where the temperature increase is initiated by the frictional energy [3.16]. However, due to the limited amount of pixels present in the area of interest, the resolution of the area of interest used in that study is considered too low to make quantifiable claims about the location and magnitude of the mechanisms responsible for the temperature increase within the connection. Results of the effects of external, quasi-static loads on the temperature distribution in threaded connections have not been published yet.

The implementation of infrared thermography (*IR*) is performed by using an infrared camera type Infratec 8340. This thermographic camera measures in the mid-wave infrared band (2.5 μm) and its thermal sensitivity (Noise-Equivalent Temperature Difference - NETD) is smaller than 25 mK. Furthermore, a resolution of approximately 7 pixels/mm is used and the rate at which the pictures are taken does not affect the results. A more detailed description of the applied technique can be found in [3.17]. In order to increase emission and reduce reflection causing noise, the area of interest on the box is painted with a black emissivity spray. This way, a constant emissivity value of about 0.97 can be obtained.

7 Results

7.1 Make-up tests

7.1.1 Torque-turn diagram

A typical torque-turn diagram for tapered threaded connections without torque shoulder or sealing surface can be found in Figure 3-12. Three different regions can be observed. At first, a running-in zone can be observed. In this region, a limited amount of torque is to be applied because of initial taper mismatch and/or geometric deviations and due to compression of the applied thread compound. The excess dope between the thread flanks is pushed out and migrates through the available gaps. In case migration of the thread compound is obstructed, local pressure build-up at the threads occurs, causing

anomalies in the torque-turn diagram and resulting in an unreliable performance of the made-up connection. In contrast with API LinePipe, local plastic deformation of the threads of an API Buttress connection is very limited during the first make-up run and has no significant effect on the torque-turn diagram. The second region is the so-called elastic region. This region can be defined as the allowed make-up region and the torque to turn ratio is considered constant. Apart from local plastic deformation near the vanishing threads, no excess plasticity is observed. It should be mentioned that a certain minimum amount of torque is required to prevent *downhole make-up* (tightening of the connections during working conditions) or to prevent the connection from falling apart when in service. This determines a lower torque limit and therefore, the lower part of this elastic region is not useful. A third and last region is characterized by a reduced torque over rotation ratio, resulting in an upper torque limit. Within this region, global plasticity occurs throughout the connection and reusability and structural integrity become questionable. A method to determine an appropriate lower and upper torque limit is further explained in Section 2.1 of Chapter 5.

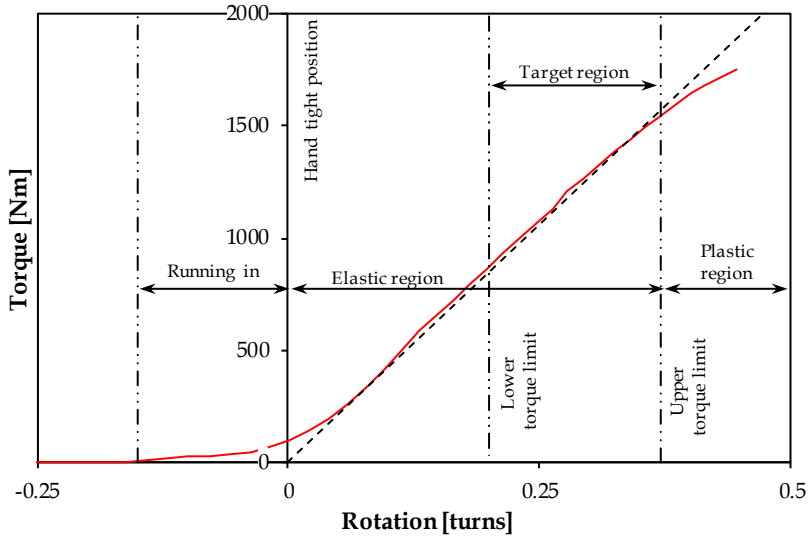

Figure 3-12: Measured torque-turn diagram with indication of the most important zones

7.1.2 Axial and hoop strains

Figure 3-13 and Figure 3-14 respectively show the hoop and axial strains measured at the outer surface of the box using DIC. For the DIC measurements, images were taken every 2 rotational degrees. During post processing, the strains are extracted over 19 different paths over the circumference as

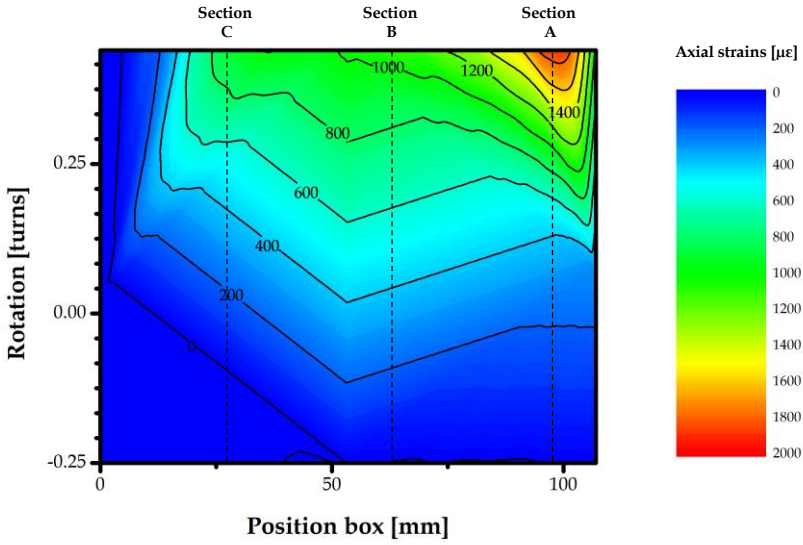

Figure 3-13: Hoop strains during make up.
A rotation of 0 turns represents the hand tight position

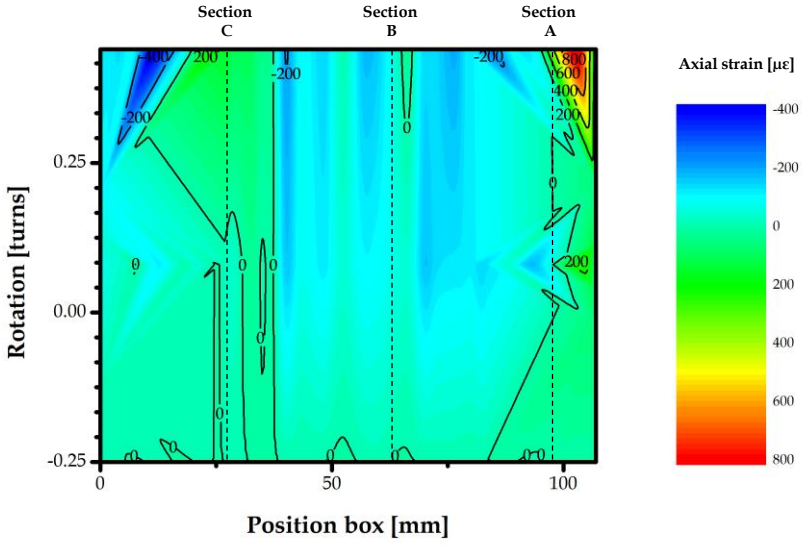

Figure 3-14: Axial strains during make up.
A rotation of 0 turns represents the hand tight position

illustrated in Figure 3-15. Using this figure, it can be seen that most of the box is under tensile hoop strain as a result of the applied make-up. During the make-up, the box is expanded while the pin is compressed as the result of the tapered thread profile. An increased amount of tensile hoop strains can be observed near the tip of the box as a result of a small initial taper mismatch of 0.07 degrees. Because the taper of the pin is slightly larger compared to the taper of the box at this location, additional tensile hoop strains are generated, deviating from the expected, more uniform strain distribution in axial direction (see further in Chapter 4). While an overall axial compression is visible and expected as the result of positive hoop strains, a distinct zone with axial tension is visible near the pin tip resulting from local bending. This bending is caused by the absence of contact at the tip of the box resulting from the thread taper in combination with make-up (see Figure 3-16). This leads to an absence of outwards forces and some sort of elastic springback phenomenon occurs.

In addition to the DIC measurements, twelve biaxial strain gauges were applied. The measured hoop strains using both DIC and strain gauges are shown in Figure 3-17 for the three sections illustrated in Figure 3-11. The results of the strain gauges are obtained by continuously monitoring the strains throughout the entire experiment with a sampling rate of 10Hz. The full lines indicate the minimum and maximum values measured by the four strain gauges within the same section. The dashed line represents the average values of all four strain gauges within the same section. A similar method of representation is used for the DIC results after averaging the calculated strains

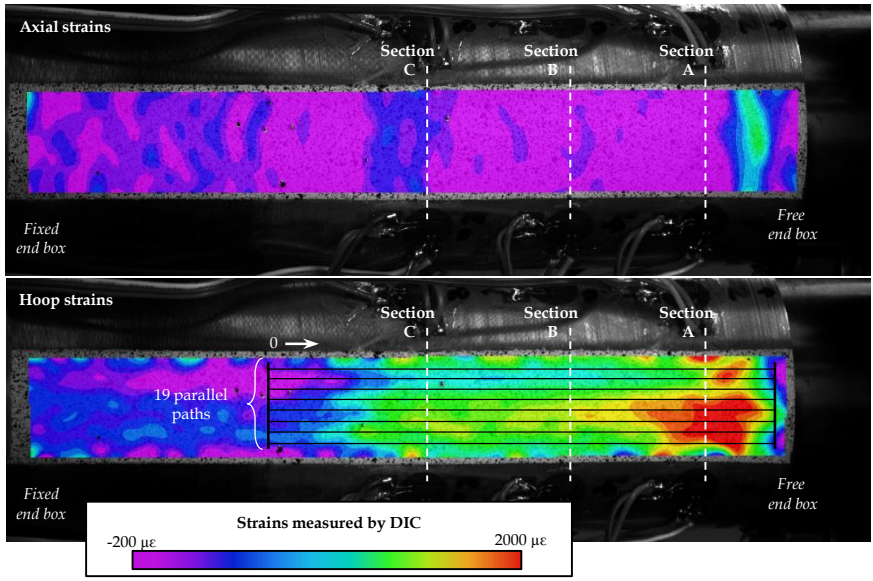

Figure 3-15: DIC results after applying a make-up of 0.4 powerturns

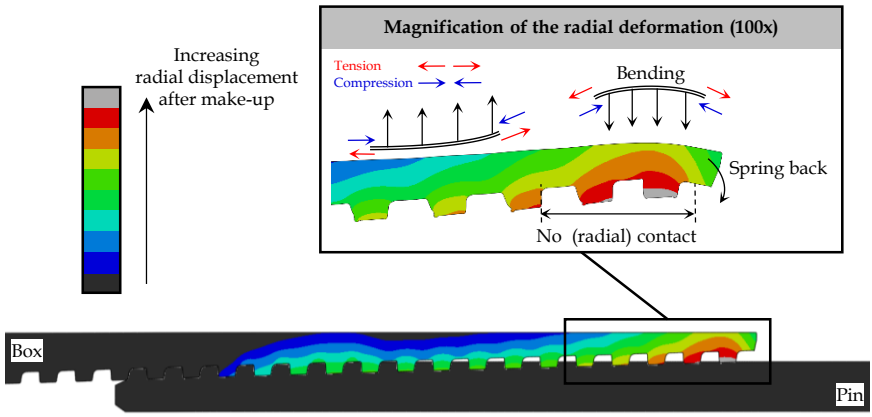

Figure 3-16: Tendency of spring back near the box tip after loss of radial contact (see Chapter 4 for more details about the numerical model)

over a 5 mm length centered near the strain gauges for all axial paths. When comparing both measurement techniques, it can be observed that for sections B and C the results are almost identical. For section A, which is located near the tip of the box where the highest strains are expected, the strain gauges tend to provide slightly higher hoop strains compared to the DIC measurements when exceeding 0.625 powerturns. This is likely to be caused by a limited amount of misalignment between pin and box. While the strain gauges are positioned over the entire circumference, leveling out the effects of misallignment, the DIC measurement focusses on a limited area. This way, the effects of misalignment will be more pronounced in the results of the latter approach. This assumption is supported by the increasing difference between the individual strain gauges within the same section at the higher make-up levels. While some of the strain gauges remain within the elastic area, plastic deformation appears to occur in others.

7.1.3 Temperature

Since it is not possible to measure contact pressure within the contact itself, an indirect method is applied to gather indicative information. It is hypothesized that thermal imaging of the connection will offer valuable insights. Temperature increase in the connection can be caused by: deformation of the material and friction originating from the relative sliding of the thread surfaces of pin and box. In both cases, the generated energy is transformed into heat and becomes visible at the outer surface of the box due to thermal conduction throughout the material.

Figure 3-18 shows the tip of the box after applying a 1750 Nm make-up torque, which corresponds to 0.4 powerturns. In order to determine the increased temperature distribution, the data of 16 axial, parallel paths which

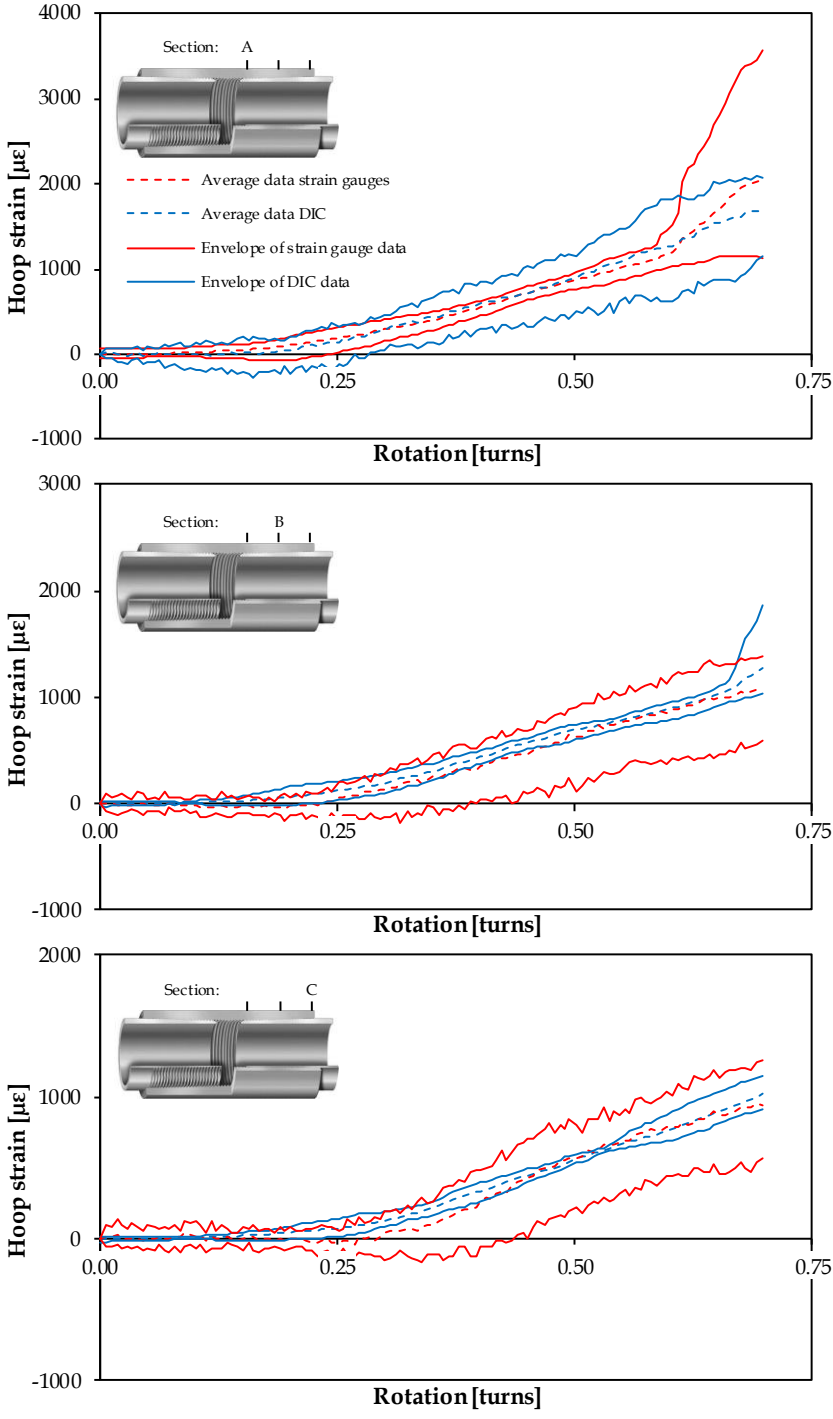

Figure 3-17: Comparison of the hoop strains measured with DIC with the ones measured using strain gauges

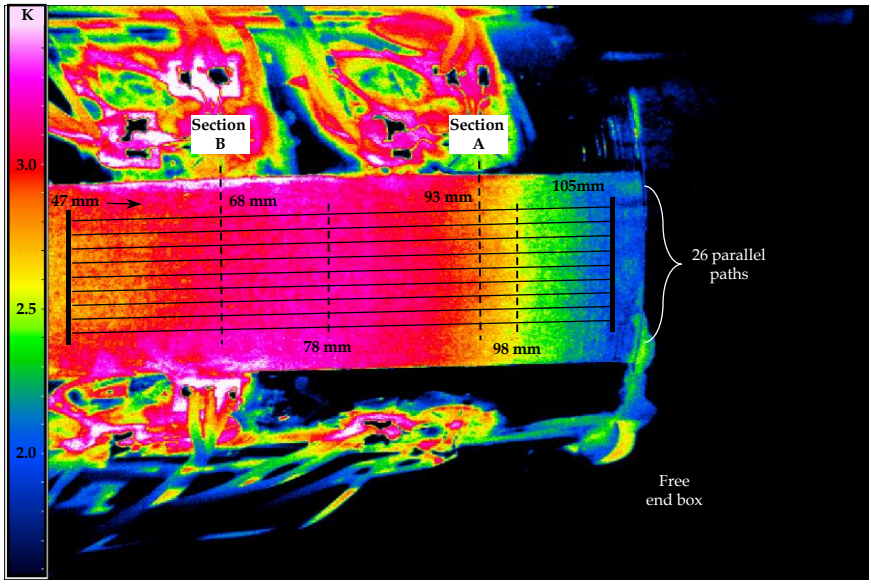

Figure 3-18: IR result at 0.4 power turns (145 degrees) make-up (1750Nm)

are evenly distributed over the entire area of interest are taken into account. After averaging the results in the same section, a reliable axial temperature distribution is obtained for the given assembly. The results in function of rotation and location along the thread are illustrated in Figure 3-19. This figure indicates that make-up induces the highest temperature increase at about 75 mm on the outer surface of the box. The cause for this increase is either plastic deformation or frictional energy. When comparing the measured temperature distribution (Figure 3-19) with the DIC strain distribution at the outer surface of the box (Figure 3-13 and Figure 3-14), it is clear that the location of maximum temperature and maximum plastic deformation at the outer surface of the box do not coincide. Therefore, the increase in temperature is unlikely to be explained by solely assuming plastic deformation of the box. This means that at this point, no complete conclusions can be drawn based on only the visible results obtained by the thermography. In an effort to resolve this issue, numerical modelling (Chapter 4) and an estimation of the frictional energy and its effect on the temperature distribution (Chapter 7) is required.

Furthermore, a discontinuity is visible at about 0.3 powerturns. At this position, the experiment was halted due to a small technical error.

7.2 Test load envelope experiments

A TLE test with the load combination described in Table 3-4 was conducted in accordance with the procedure described in section 3.2.3. Before being subjected to the combined internal pressure and axial tensile test, the specimen

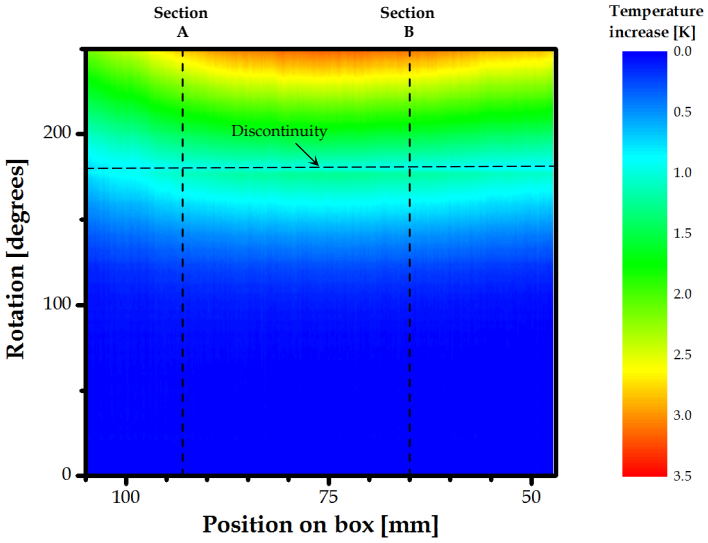

Figure 3-19: Temperature increase during make-up

was made-up twice. After breaking out the connection assembled with a 962 Nm torque (well within the elastic make-up region), a 1643 Nm make-up torque was applied since this value marks the start of the plastic make-up region and is therefore the upper torque limit. Next, the connection was dried out for twenty days at room temperature.

Additional TLE tests were carried out on different assembled connections without being dried out. It is concluded from the results that when the connection is not dried out, the thread compound is still partly liquid and the critical pressure the connection is able to withstand is considerably lower. Because the Pin5/Box5 set (see Table 3-3) was able to resist a significant part of the 70% Test Load Envelope, which is the test load envelope that contains combinations of internal pressure and axial tensile loads up to 70% of the capacity of the pipe body, this specimen is used for further investigation (the axial limit load test) to gather more significant information which can be used for the validation of the numerical model (see Chapter 4).

7.2.1 Strain gauge measurements

The strain gauge measurements are illustrated in Figure 3-20 for both the axial and hoop strains for all combinations with an internal pressure up to 360 bars and an axial tensile force up to 200 kN. These results were obtained starting from measured data points (see Table 3-4) and interpolated combinations were calculated using a thin plate spline (TPS) smoothing algorithm [3.18].

Table 3-4: Overview of the load combinations introduced during the performed TLE test (see Figure 3-5)

TLE Point	*Tension* [kN]	*Internal pressure* [bar]	*TLE Point*	*Tension* [kN]	*Internal pressure* [bar]
1	28.5	22	**28**	77.7	118
2	56.2	22	**29**	112.0	118
3	83.0	22	**30**	142.3	118
4	109.7	22	**31**	171.1	118
5	136.3	22	**32**	199.3	118
6	162.9	22	**33**	27.3	162
7	189.4	22	**34**	36.3	162
8	56.4	55	**35**	102.0	162
9	85.5	52	**36**	137.9	162
10	96.0	65	**37**	169.5	162
11	113.8	65	**38**	199.4	162
12	141.3	65	**39**	8.1	206
13	168.5	62	**40**	72.8	206
14	168.2	62	**41**	126.3	206
15	195.1	85	**42**	163.3	206
16	49.5	85	**43**	196.0	206
17	84.3	85	**44**	108.8	239
18	114.1	85	**45**	154.4	239
19	142.4	85	**46**	190.7	239
20	170.1	85	**47**	134.7	281
21	197.4	95	**48**	179.4	281
22	44.0	95	**49**	13.9	310
23	83.1	95	**50**	107.9	310
24	113.8	95	**51**	167.3	310
25	142.7	95	**52**	6.8	356
26	170.6	95	**53**	133.0	356
27	198.1	22	**54**	0	390
			55	0	452

Based on these results, several conclusions can be drawn. First of all, an increase in axial tensile load results in an increase in axial strains at all sections. However, the influence of an increase in internal pressure is not straightforward. When the internal pressure is increased, the axial strain decreases in section A while the axial strain increases in sections B and C, without any increase of the applied axial load. Taking into account the Poisson effect, which causes the connection to contract with increasing internal pressure, the behavior of section A can be understood. However, in order to explain the behavior of sections B and C, special attention has to be given to the effect of the internal pressure on the end caps of the connection. The axial load induced by the internal pressure can be calculated as follows:

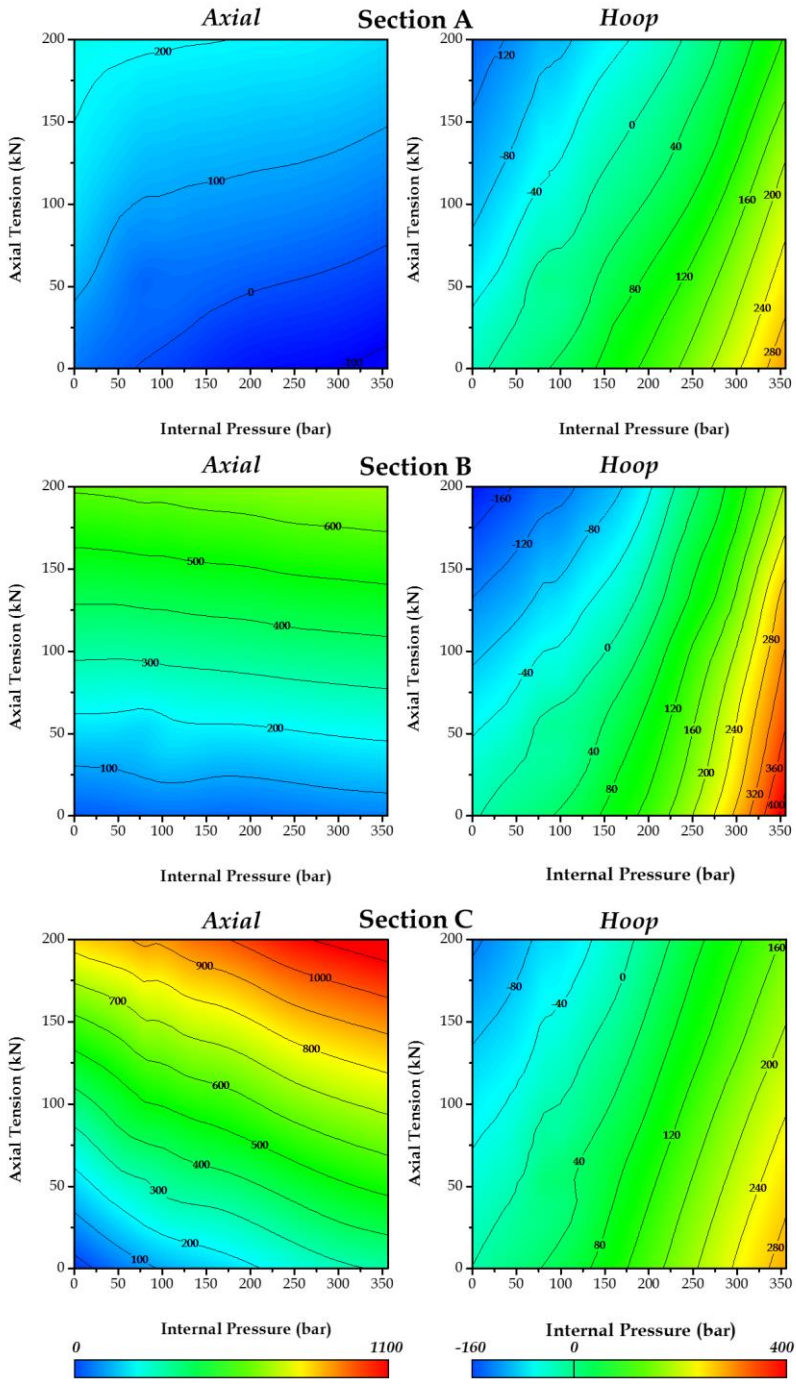

Figure 3-20: Axial and hoop strains [με] of the connecting box measured by strain gauges

$$F_a = p_i \frac{{D_i}^2}{4} \pi \qquad \text{(Eq. 3.4)}$$

Within this formula, F_a is the resulting axial load, p_i the internal pressure and D_i the pipe inner diameter.

When considering section C, which is assumed to be in front of the threaded area of the pin, the situation in which only an internal pressure of 325 bars is applied corresponds with an axial strain of about 300 με, as can be seen in Figure 3-20. According to the test results, this amount of strain is also reached when a pure axial tensile force of about 80 kN is applied. When inserting the inner diameter of the box in Equation 3.4, an induced axial force of 50 kN is calculated. This estimation is 37% short of the measured value. In order to take into account this significant mismatch, following hypothesis might be considered. For the load cases containing low internal pressures (< 100 bar), a discontinuity in the linear tendency of the strains is visible. Since section C is located near the tip of the pin, complex strain distributions may be present and it is possible that the connection slightly shifts towards a new equilibrium. This also means that the geometry in section C slightly differs between the load case containing low pressures, and the load cases containing high pressures. This assumption may invalidate the reasoning that, within this experiment, the strains measured at low internal pressures can be related to the strains measured at high pressures. When interpolating the linear trend of the high pressure load cases towards the low pressure load cases, an axial force of approximately 60 kN can be found, which is acceptable taking into account the complexity of the experiment.

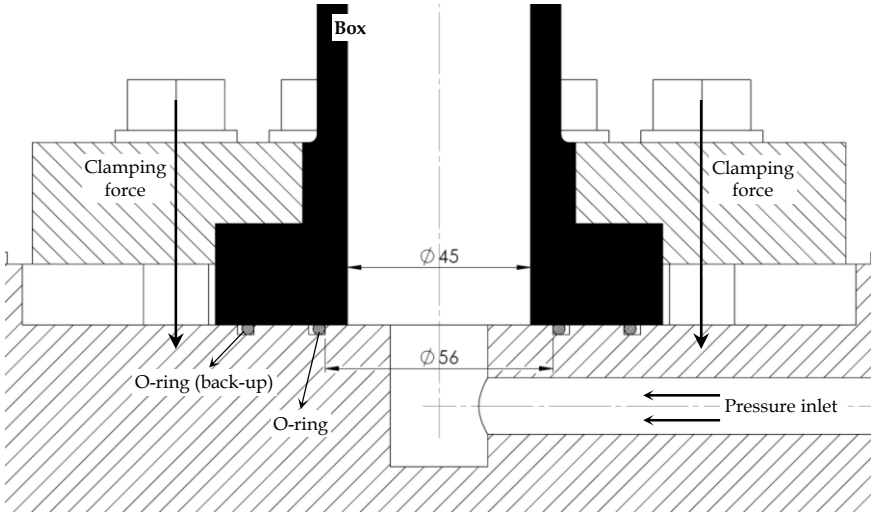

Figure 3-21: Connection of the box to the test rig includes two O-rings

It should be noted that this tensile force is not transferred to the tip of the box because of the threads in between as is illustrated in Figure 3-22. Since section A is situated near this position, only a very limited amount of axial force is present in this region (as can be seen when considering the effect of the axial tensile force on the axial strains in Figure 3-20). The axial strains in this section are mainly affected by the combined effects of internal pressure and the accompanying Poisson effect.

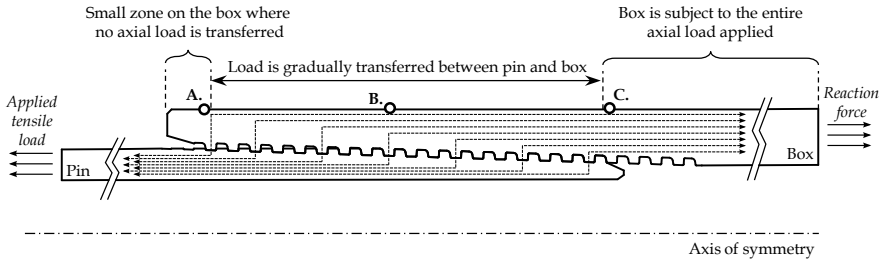

Figure 3-22: Schematic overview of the load transfer between pin and box

7.2.2 DIC measurements

In addition to the use of strain gauges, DIC measurement of axial and hoop strains is performed. Based hereon, the strains of 16 different paths parallel to the pipe axis are extracted and averaged to reduce noise. Subsequently, the values of the different sections in which the strain gauges are located are extracted and plotted in Figure 3-23. From this figure it is apparent that, despite an obvious trend, no straightforward relations can be observed concerning the influence of internal pressure and/or axial tension on the axial and hoop strains. This is a direct result of the limited accuracy of the DIC approach when trying to measure elastic deformations. The accuracy of DIC is considered to be about ± 0.01% strain in optimal conditions, which is equivalent to 100 με. This value is considerably higher than the one of the strain gauges (5 με).

Figure 3-24 gives an overview of the differences between the strains calculated using the DIC system and the strains measured by the strain gauges. In order to make a consistent comparison for both low strain levels and high strain levels, the absolute value of the differences are normalized using the elastic strain limit of the box material. This elastic strain limit is 1428 με and is calculated using the equation 3.5.

$$\varepsilon_{el} = \frac{\sigma_{YS}}{E} \qquad \text{(Eq. 3.5)}$$

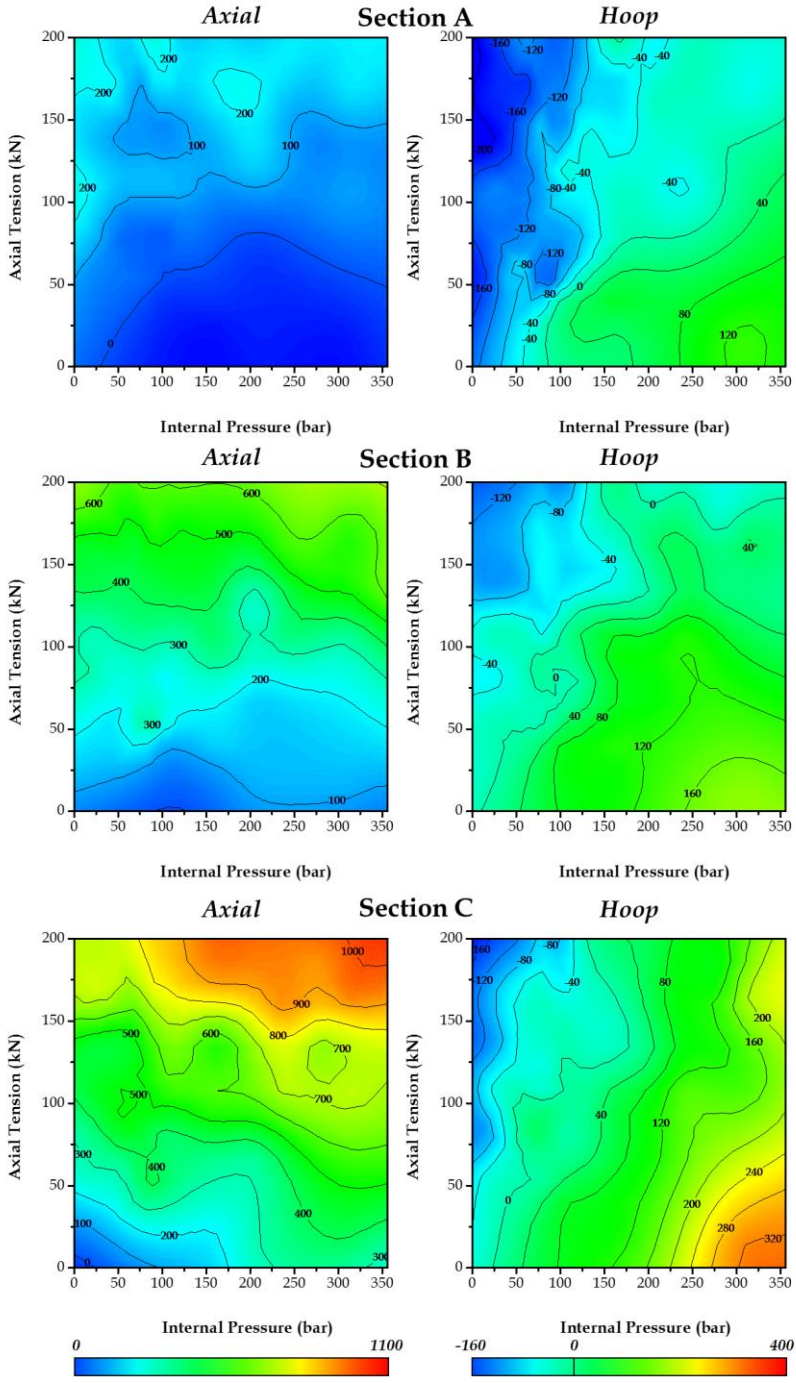

Figure 3-23: Axial and hoop strains [με] of the connecting box measured by DIC

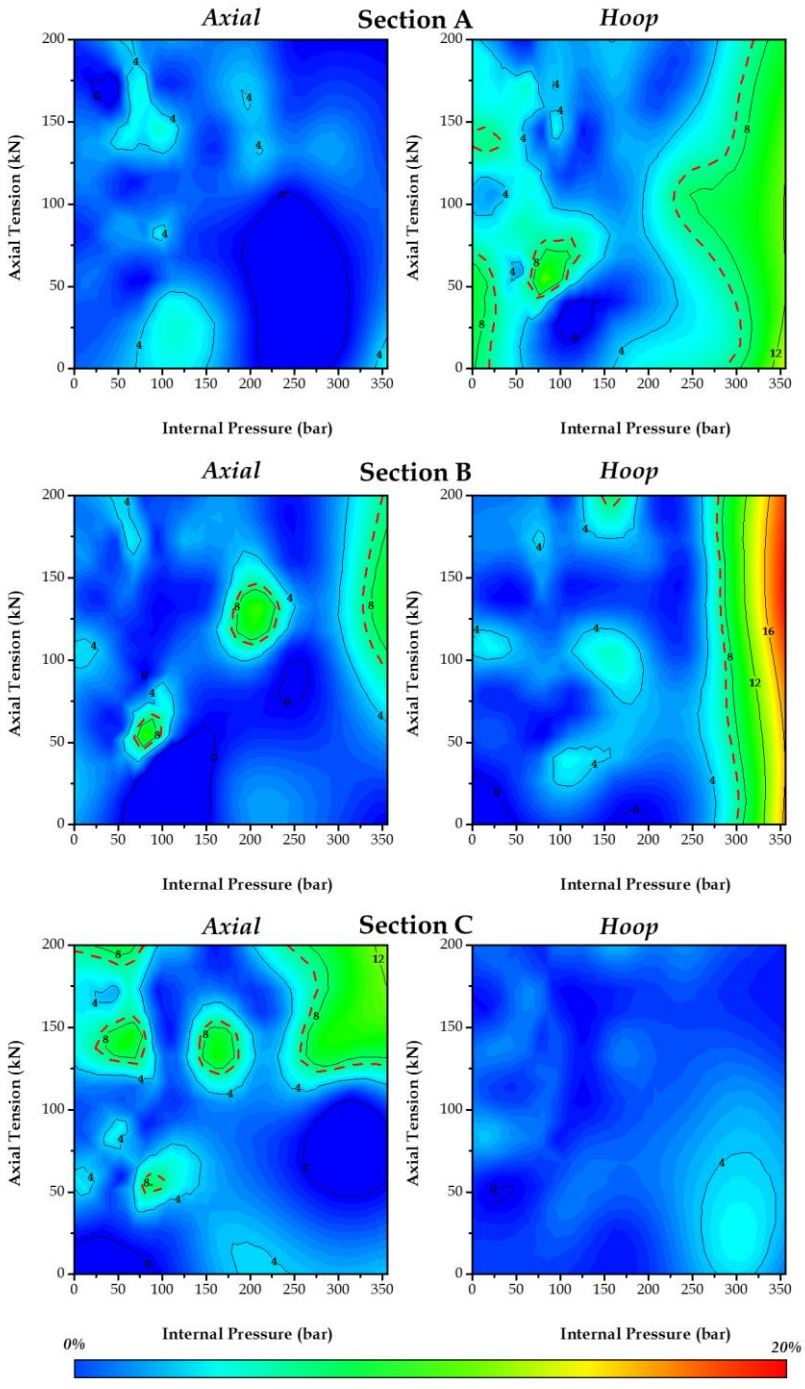

Figure 3-24: Difference between axial and hoop strains measured with DIC and strain gauges relative to the maximum elastic strain

By using the normalized strains, a better understanding is provided related to the reliability of the results. If percentage differences based on DIC or strain gauge values alone are used, the differences will be very high when low elastic strains are measured. In contrast, when taking the absolute differences, the opposite would be true. Since the critical value of measured strain used to switch from the one criterion (percentage differences) to the other (absolute differences) is unknown and would be arbitrary, it is opted to use the normalized strain approach, which is valid over the entire range of measurements. Using this criteria, it can be concluded that when taking into account the uncertainty of 100 με, which corresponds with 7% and is indicated in the figure with a red dashed line, the vast majority of the results obtained by DIC match the results obtained by the strain gauges.

Based hereon, two distinct observations can be made. At first, when considering the hoop strains, the reliability of the DIC measurements decreases when internal pressure increases, especially when exceeding 300 bars in sections A and B. The reason for this increasing unreliability can be related to the calculated coordinate system used to process the DIC results. Since it is very hard to assign an accurate cylindrical coordinate system to the post processing software in which the axes correspond with the geometry of the heavily curved specimen, it is possible that a minor misalignment (both a translation and a rotation) is introduced as the results of allowable tolerances on the geometry and inaccuracies from the measurement itself. Additionally, as a result of this misalignment (out-of-center), the assumed and actual radius of the specimen could vary. This means that the data extracted from paths further away from the cameras could provide less accurate data. Secondly, the axial strains for sections B and C appear to be less accurate when higher tensile loads are applied. This is possibly caused by a slight mismatch between the area of the strain measurements using strain gauges and the one using DIC. Within the section C, strains are relatively large and the slightest axial misalignment of the addressed area can result in a large deviation.

7.2.3 Temperature

The monitoring of the temperature proved useful during make-up testing to provide evidence of mechanisms occurring away from the visible surface of the connection (see section 7.1). For the TLE test however, temperature changes remain very limited because of the relatively small loads applied. Since the tests are performed well within the elastic region, little temperature changes are detectable. Apart from a slight temperature decrease illustrated in Figure 3-25 which is characteristic for an elastically deformed specimen [3.19], no conclusive evidence of the magnitude of the deformation by monitoring the heat is detectable due to excessive scatter.

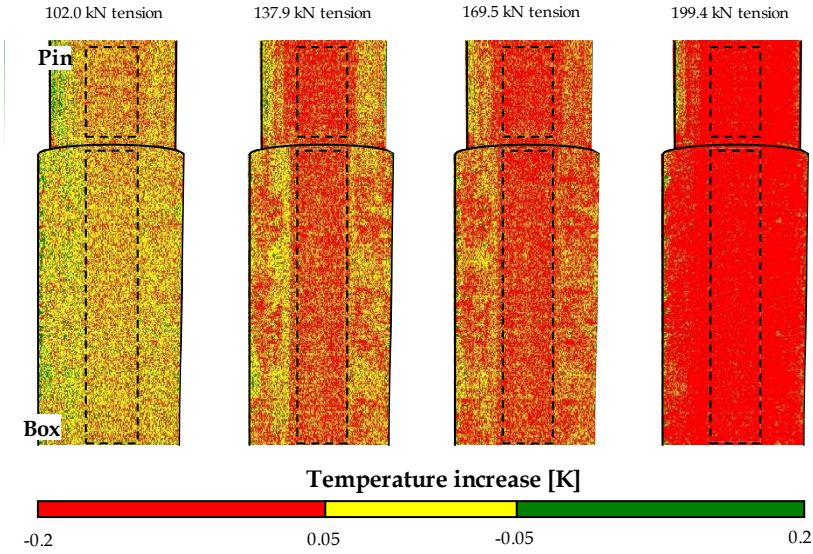

Figure 3-25: Distribution of temperature changes for an internal pressure of 162 bars and varying axial tensile load

7.3 Limit load tests

A limit load test applying axial tension (LP3) was conducted on the Pin5/Box5-specimen. Before applying the tensile load, the specimen was made-up to 961 Nm and after a break-out, it was reassembled to 1643 Nm, causing limited local plastic deformation. The latter make-up torque corresponds to a powertight make-up of about 0.4 turns. Thereafter, the connection was subjected to a TLE test. After applying a tensile load of 198.8 kN combined with an internal pressure of approximately 90 bars, the specimen showed excessive leaking and the test was terminated.

7.3.1 Force-displacement curve

During the limit load test, the axial force is measured and represented against the piston displacement of the test rig as shown in Figure 3-26. Based on this curve, five different regions, delimited by the dotted lines, can be distinguished. After removing initial play, a first region (I) is defined up to an axial displacement of 1.7 mm. This section is considered to be the elastic behavior of the connection and is characterized by a linear relationship between the displacement and the applied load up to 293 kN. Following, a second zone (II) can be observed in which the relationship between displacement and applied force is no longer linear and cannot be explained by only considering the material characteristics. Due to local jump out of the connection near the last engaged threads with limited height, the most critical section of the assembly moves from the box to the pin (see section 8 of Chapter

4 for more details). Once a stable critical section in the connection is reached at 6.63 mm displacement, the force-displacement diagram is determined by the material characteristics of the pin throughout region III. Once the maximum tensile load is reached at 443 kN, necking occurs at the pin (in this case) and region IV is initiated. When a total axial displacement of 21.9 mm is reached, the connection separates when (in this case) the pin breaks (V).

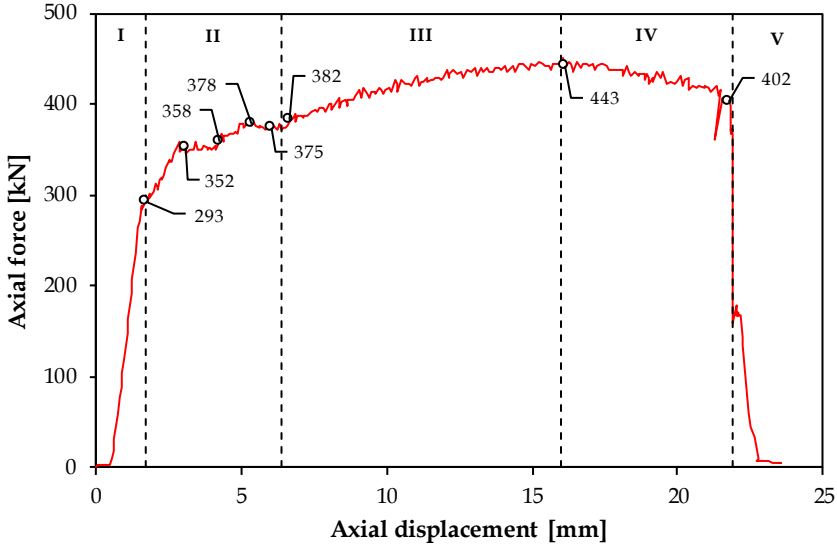

Figure 3-26: Experimental force-displacement curve with indication of the various transition points

7.3.2 Strain gauge measurements

In order to better understand the behavior of the connection, strain gauge measurements are conducted on the outer surface of the box in three different sections, corresponding to a section near the vanishing threads (section *A*), near the middle of the thread (section *B*) and near the location of the pin tip (section *C*). The results for both axial and hoop strains at four different locations in each section, evenly distributed over the circumference, are given in Figure 3-27 and Figure 3-28 respectively. The different zones which were defined by analyzing the force-displacement diagram of Figure 3-26 are indicated by vertical dotted lines. It should be noted that three out of four strain gauges located in section *C* loosened when axial displacements of respectively 2.35 mm, 5.17 mm and 5.24 mm were reached.

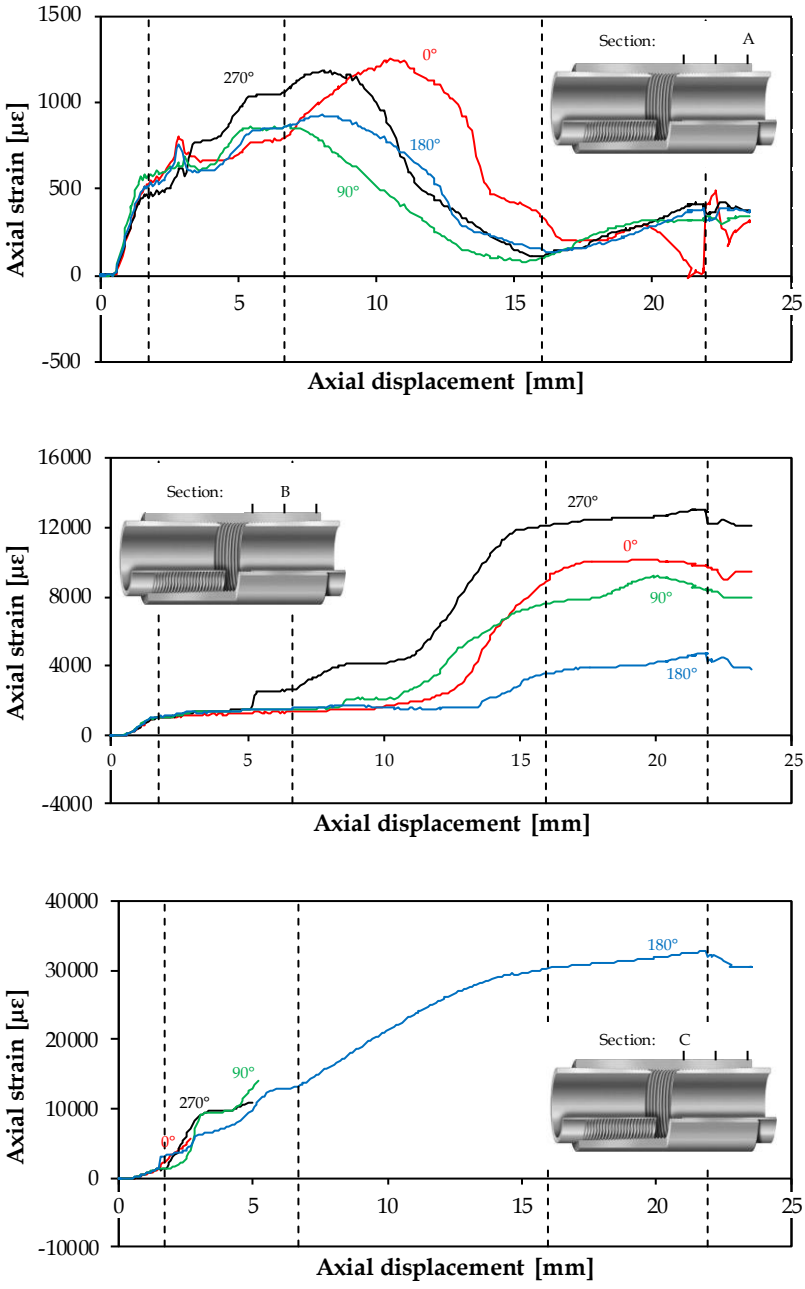

Figure 3-27: Axial strains measured by strain gauges throughout the limit load test

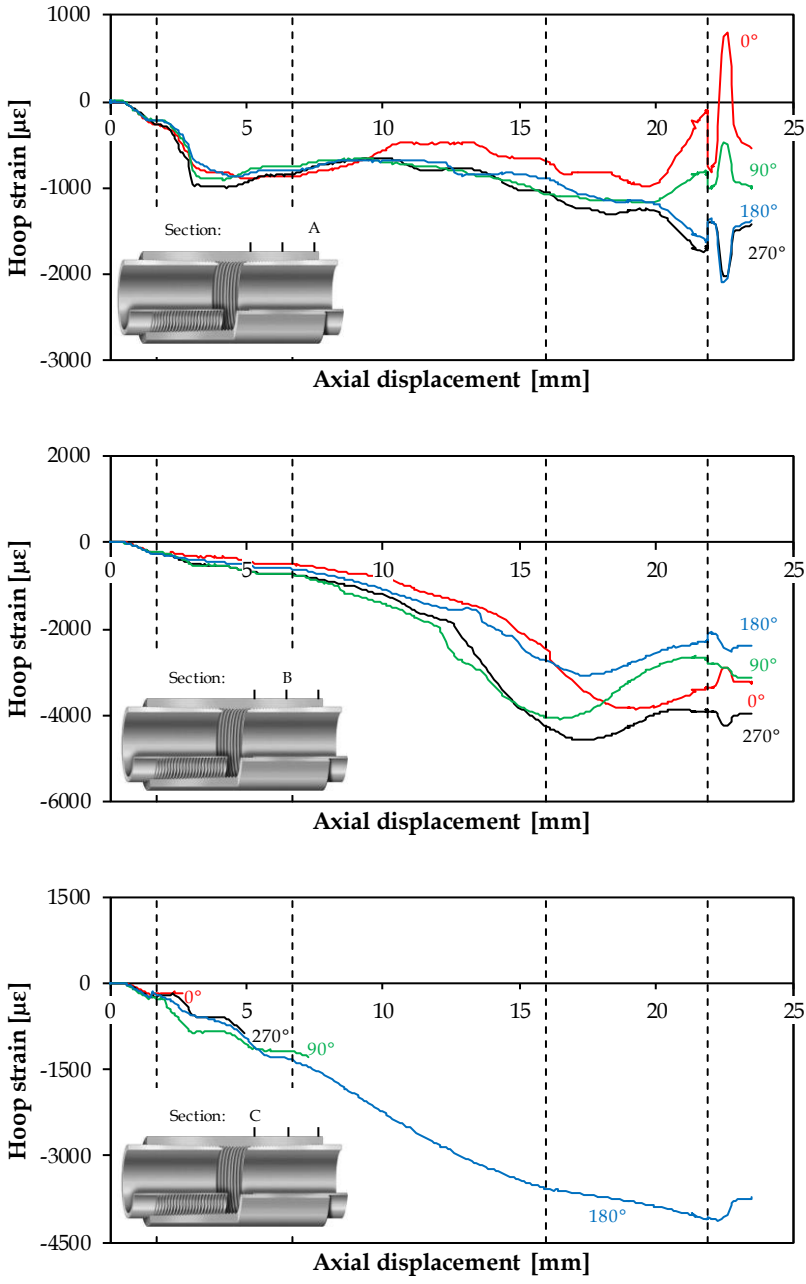

Figure 3-28: Hoop strains measured by strain gauges throughout the limit load test

When applying an increasing axial tensile force, it is expected to cause increasing axial tension in all sections where the strains are measured. However, when assessing the strains measured in section *A*, it is visible that the strains decrease in zone *III* and fluctuations are noticeable in zone *II*. This behavior can be explained when assuming a gradual, local jump out at the end of the vanishing threads. When the load flanks of the threads are not in contact anymore, the applied tensile forces are not carried by the material in section *A* since the threads slide over each other. Up to necking of the pin, the load carrying capacity of the vanishing threads diminishes, explaining the gradual decrease of axial strains in section *A*, while the axial strains in section *B* increase. However, once the pin starts to neck and ovalization occurs, the threads in section *A* re-engage and a limited amount of tensile load is transferred, causing a slight increase in axial stress. Evidence of the ovalization can be seen when comparing the hoop strains over the circumference within the various sections. In section *A*, it can be observed that at about 20 mm axial displacement, the hoop strain in the strain gauges located at 90° and 270° decrease while at 0° and 180° the strains increase.

7.3.3 DIC measurements

Using the force-displacement diagram shown in Figure 3-26, eight different points were highlighted, indicating five distinct zones. The axial strains, measured using DIC, over the length of the box for all these points are shown in Figure 3-29 in which the zero location is assumed to be the location of the pin. Using this figure, it is clear that most deformation of the box occurs in the region ahead of the pin tip. Furthermore, various zones (IIb, IIe and IV) contain very little strain increases while the axial displacement still increases. This suggests that plastic deformation occurs within the connection, at the pin.

Zone I: Elastic deformation

At first, the play is removed and the elastic deformation of the assembly results in a small increase of the axial strains in the investigated surface. Most of the increases are located at about 14 mm ahead of the pin tip.

Zone II: Start plastic deformation: yielding and jump-out

As shown in Figure 3-26, zone *II* can be subdivided into five different parts. Once the connection has reached its elastic limit, the section most susceptible to plastic deformation starts to deform. In the case shown in Figure 3-29, a section at the box, between -10 and -40 mm, proves to be most critical and strain hardening results in strengthening of this section (zone *IIa*).

While the box section ahead of the pin tip is deforming by the applied axial displacement, the most critical section of the pin, which is currently stronger than the most critical section of the box, is deforming as well. Once the applied axial displacement is sufficient, the last engaged (vanishing) threads fail as a result of shear damage or plastic deformation. This causes localized jump-out

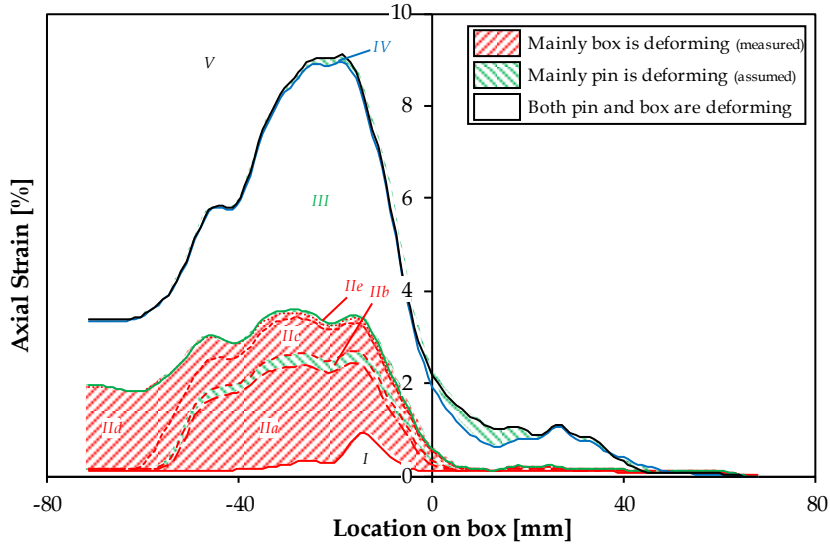

Figure 3-29: Evolution of axial strains over the outer surface of the box. The location at 0 mm is considered the location where the pin starts. Most deformations are located in front of the pin tip.

and causes the critical section of the pin to change towards the thinner pin tip and redistributing the axial load over less threads. During this process, axial displacement requires almost no additional tensile load and therefore, the axial strains visible at the box in zone *IIb* remain quasi constant. This phenomenon can also be backed by monitoring the relative displacement of the pin relative to the box as is shown in Figure 3-30. In this graph, it can be seen that the pin suddenly moves about half a millimeter without a significant increase of applied tensile load (see Figure 3-26).

After the initial shear failure at the incomplete threads, shearing at the pin threads continues throughout the helix of the thread, explaining the continued increase in relative displacement between pin and box visible in zone *IIc*. In addition to the local plastic deformation in the pin, also the box continues its deformation, which was already initiated in zone *IIa*.

Once the next critical section of the pin is stabilized, relative displacement between both members stops and the strain hardening of the box continues throughout zone *IId*.

At a certain point, the most critical section of the connection, being the pin in this case, begins to deform severely (zone *IIe*). Initially, this local deformation is limited to the Lüder's phenomena of the pin material. This results in constant axial strains throughout the box and a very limited relative displacement.

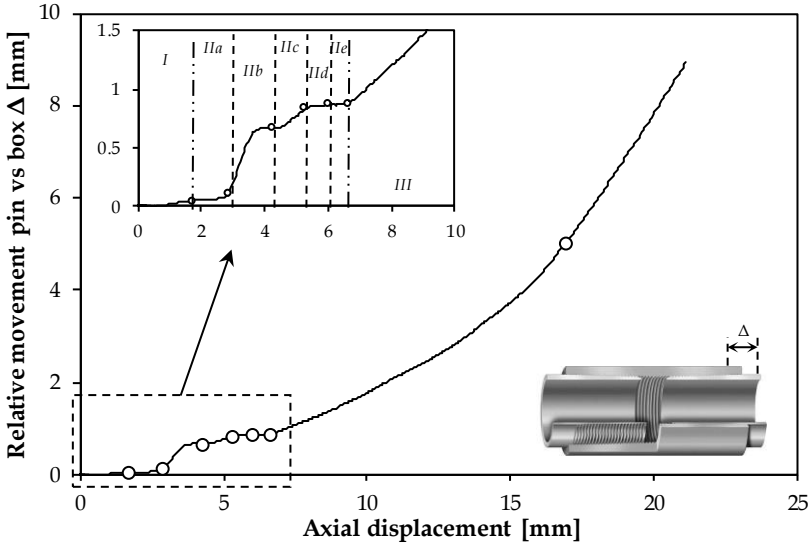

Figure 3-30: Relative displacement between pin and box

Zone III: Plastic deformation

When applying further axial displacement, the pin deforms plastically in its most critical section and zone *III* is initiated. Since both pin and box have similar strengths, both members deform plastically. The deformation of the box can be seen using DIC, while the plastic deformation of the pin can be assumed since the relative displacement between pin and box increases significantly.

Zone IV + V: Necking and Fracture

Once a critical axial displacement is reached (approximately 16 mm), the pin starts to neck, initiating zone *IV*, and finally breaks (zone *V*).

7.3.4 Comparison of strains

A comparison of the strains obtained during the limit load test using digital image correlation on the one hand and strain gauges on the other hand is shown in Figure 3-31 using the averaged results. Evaluating the axial strain, both measurement techniques show similar results. Apart from some exceptions at the lower displacement levels, the results measured by the strain gauges are situated within 10% of the DIC results. For the larger strains, as is the case for section A, the deviation between both measurements is less than 5%. This indicates that when applying an axial displacement, the effects of axial misalignment are limited.

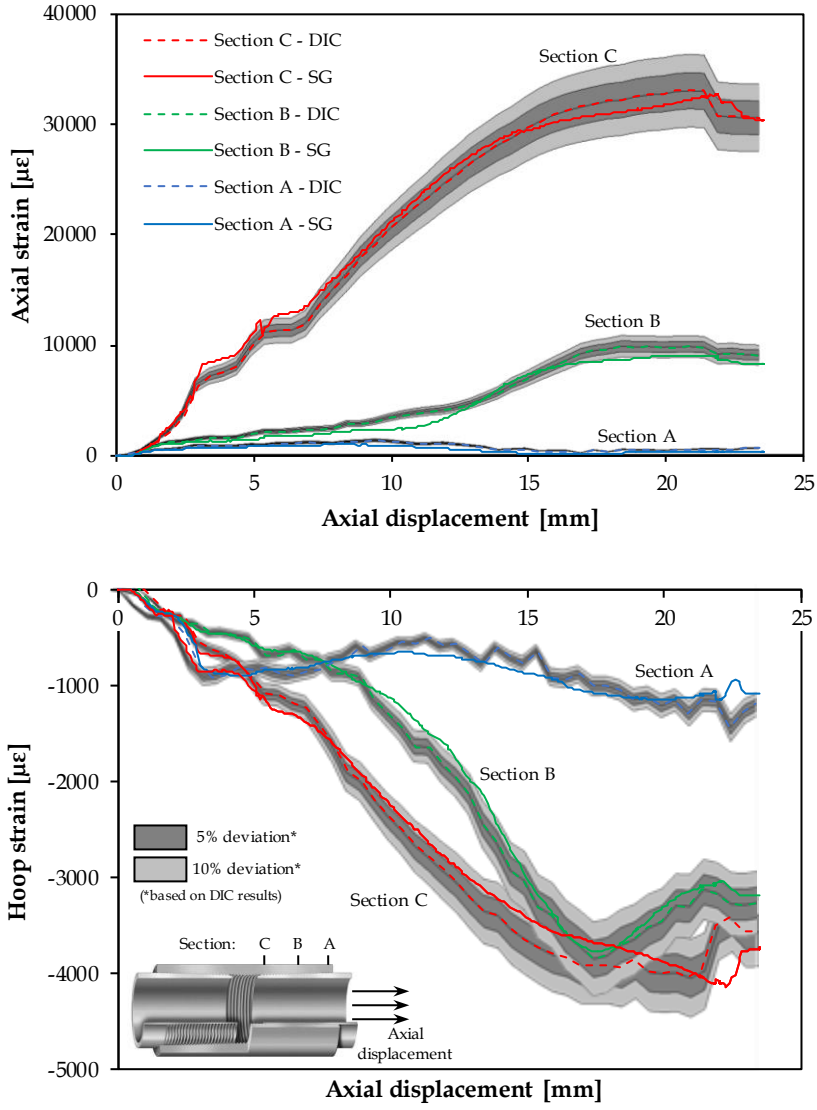

Figure 3-31: Axial (top) and hoop (bottom) strains measured using Digital Image Correlation (DIC) and strain gauges (SG).

Despite a similar global behavior, the comparison of the hoop strains indicates larger deviations, especially for section A. While the tendencies of the hoop strains are similar for both the DIC and strain gauge results, the relative differences are in excess of 10%. Two major parameters contributing to these large deviations have already been mentioned before. First of all, the magnitude of strains are much smaller than observed in the axial direction. This means that while the absolute deviation may be similar or even less as

was the case for the axial strains, the percentage difference may be much higher. A second and probably the most important parameter is the difficulty related to the determination of accurate hoop strains. As was already mentioned in section 7.2.2, calculating the hoop strains based on the obtained DIC pictures is difficult in case of heavily curved surfaces.

7.3.5 Temperature

The results of the infrared measurements are shown in Figure 3-32 and Figure 3-33. The first figure shows the averaged, relative temperature distribution at the outside of the box for zones defined using Figure 3-26. In analogy with the DIC measurements, the behavior of the temperature increase can be explained using the aforementioned hypotheses. The start of zone *I* is considered to be the reference picture. Additionally, the subsequent figures of Figure 3-33 show the different, visually identifiable stages throughout the limit load test using the IR pictures.

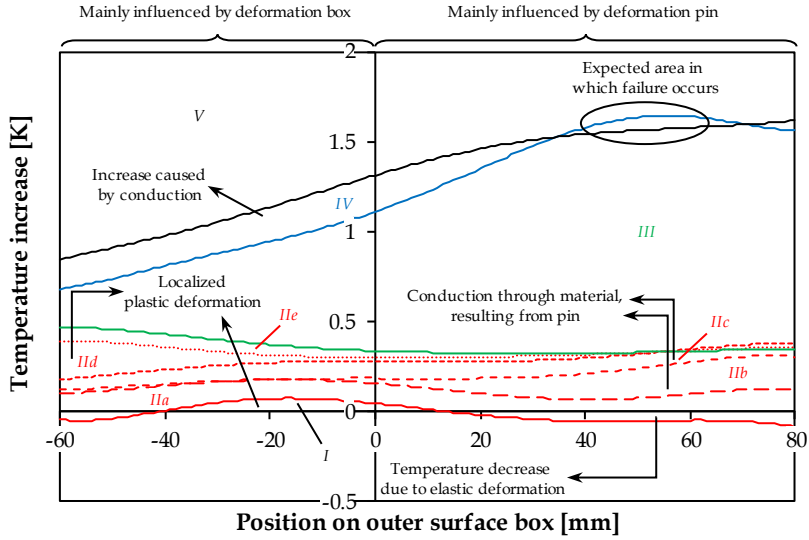

Figure 3-32: Extracted data based on the IR measurements shown in Figure 3-33

Zone I: Elastic deformation

When an axial displacement up to the yield strength of the connection (start zone *IIa*) is applied, a temperature decrease of about 0.05 °C resulting from the elastic deformation is visible. This reduction is visible at almost the entire surface of the box, except for the location between -40 mm and 20 mm. This location is considered the area ahead of the pin tip and is, when all threads are engaged, the critical section in which plastic deformation tends to occur.

This location was also identified by examining the axial strains using DIC (see Figure 3-29).

Zone II: Start plastic deformation: yielding and jump-out

Zone *IIa*, in which the yield strength of the connection is exceeded, is characterized by a quasi uniform temperature increase of about 0.1 °C. Part of this increase in temperature is caused by further plastic deformation of the box

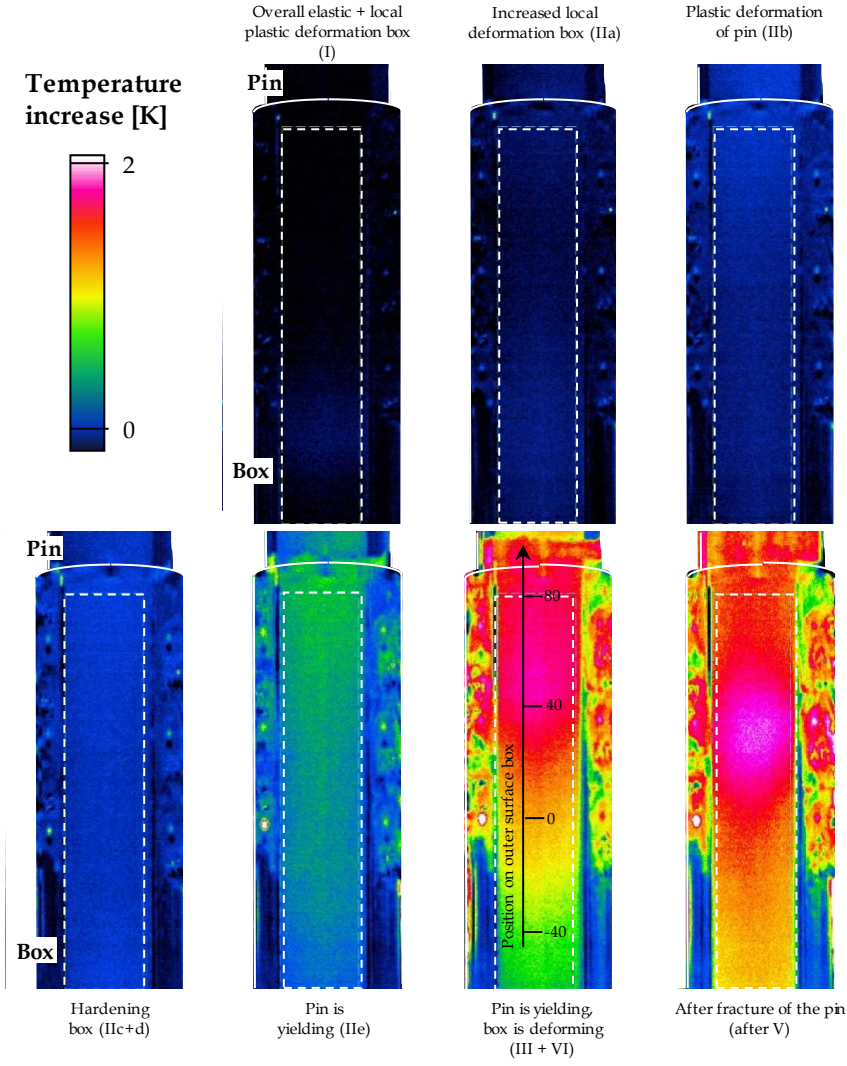

Figure 3-33: Different stages of the limit load test as observed by infrared measurements

ahead of the pin tip. While a temperature decrease would be expected over the threaded area since no plastic deformation was observed by DIC, the opposite can be seen. This temperature increase is caused by the plastic deformation at the vanishing threads which will eventually lead to the local jump-out revealed using the DIC data.

When local jump-out occurs (zone *IIb*), temperature increases up to 0.18 °C are observed in the threaded area while the temperature at the box body remains constant. The majority of the observed heat is caused by the plastic deformation of the vanishing threads of the pin.

Once the gradual stripping of the vanishing threads has come to a halt, zone *IIc* is reached and plastic deformation at the box results in a temperature increase in front of the pin tip. Further conduction of heat rather than deformation is responsible for the increase in the threaded area.

When zone *IId* is reached, the plastic deformation is localized at the box, causing temperature increases of up to 0.22 °C. This mechanism continues until the strain hardening causes the box to strengthen and the pin starts to deform plastically, indicating zone *IIe*.

Within this zone, the temperature at the tip of the box (between 50 mm and 80 mm), stops to increase and even tends to decrease as the result of cooling effects caused by the surrounding air. In addition, this is likely an indication that the box is no longer into contact at this position, resulting in an insulating air barrier which effectively stops heat conduction from the pin. At this point, the heat generated as a result of deformation at the pin did not have enough time yet to migrate towards the visible surface through conduction.

Zone III: Plastic deformation

At the initiation of zone *III*, the weakest vanishing threads have failed and a stable, critical section at the pin is reached, leading to a more stable behavior. This critical location is located near the last engaged thread of the pin, causing temperature increases around 60 mm at the surface of the box by means of thermal conduction of the plastic deformation energy.

Zone IV + V: Necking and Fracture

While the axial displacement increases, limited plastic deformation at the box increases ahead of the pin tip. This deformation in addition with thermal conductivity is responsible for the temperature increase within this area. In the threaded area however, the main deformation is located near the LET of the pin, which is the weakest link in the joint. The heat transfers through the material as a result of conduction and a peak value is observed near the location of 50 mm. This location is in contrast with the local peak observed by the DIC measurements at the outside of the box. However, the overall location of this peak approximates the location where the pin will break after necking

(zone *V*). The mismatch between DIC and IR measurements is further considered in Section 3 of Chapter 7.

8 Conclusions

Within this chapter, an experimental approach to validate a numerical model is suggested based upon the CAL I procedures described in the ISO 13679 standard. This approach consists of a make-up test, a test load envelope using load combinations containing axial tension and internal pressure and a limit load test.

From the make-up tests, it was shown that the characteristic torque-turn diagram consists of three regions: the running in, the elastic and the plastic region. When making up a connection, the target make-up region should be chosen in the upper part of the elastic region.

In order to take into account the unknown leak resistance of standard connections, a load path differing from the standard is suggested for the TLE test. This way, more load combinations can be tested and more data can be extracted.

When conducting a limit load test by applying axial tension, monitoring the force-displacement curve has proven to be valuable. While many details need to be investigated using additional data, a distinction of several zones within this curve could yield valuable insights about the connection's behavior such as occurrence of yield, stabilization of the critical section and local jump-out.

In an effort to gather the maximum amount of information possible, strain and temperature measurements at the outside of the box were conducted for all tests. It is advised to measure both axial and hoop strains using digital image correlation (DIC) and strain gauges (SG) to get a better understanding of the occurring deformations. The accuracy of DIC proved to be sufficient to measure the hoop strains during make-up and the axial strains during the axial limit load test. However, the strains induced during the TLE test require to be monitored by the more local, yet more accurate strain gauges. In addition, valuable information related to inaccessible locations can be assessed by measuring the temperature distribution using infrared monitoring (IR). Using the visible thermal energy, mechanisms such as subsurface plastic deformations and increasing contact pressures can possibly be visualized.

References

[3.1] ISO specification 13679, *Petroleum and Natural Gas Industries – Procedures for Testing Casing and Tubing Connections*, European Committee for Standardization, 2006

[3.2] American Petroleum Institute, *API RP 5A3: recommended practice on thread compounds for casing, tubing, line pipe, and drill stem elements*, third edition, 2011

[3.3] Jet-lube inc., *API-Modified: High pressure thread compound*, MSDS datasheet, 2008

[3.4] American Petroleum Institute, *API 5B: Specification for threading, gauging and thread inspection of casing, tubing and line pipe threads*, fifteenth edition, 2008

[3.5] American Petroleum Institute, *API 5L: Specification for line pipe*, forty-fifth edition, 2013

[3.6] Teodoriu C., *Rotary-shouldered connections make-up torque calculation considering the effect of contact pressure on thread compound's friction coefficient*, Oil Gas: European Magazine, 2009, 35, 172–178

[3.7] Watts, J.D., and Ramos, B. W., *Wedgethread pipe connection*, United States patent, US 6682101 B2, 2004

[3.8] Watts, J. D., *High strength, low torque threaded tubular connection*, United States Patent, US 5427418, 1995

[3.9] Sutton, M.A., Orteu J-J., and Schreier, H.W., *Image correlation for shape, motion and deformation measurements: basic concepts, theory and applications*, New York: Springer, 2009

[3.10] Assanelli, A.P., and Dvorkin, E.N., *Finite element models of OCTG threaded connections*, Computers & Structures, 4, 47, 725-734, 1993

[3.11] Yan, Z., Zhang, H., Wang, W., et al., *Temperature evolution and fatigue life evaluation of AZ31B magnesium alloy based on infrared thermography*, Transactions of Nonferrous Metals Society of China, 23(7), pp 1942-1948, 2013

[3.12] Liu, J., Gao, X., Zhang, L., et al., *On the Use of Infrared Thermography for Analysis of Fatigue Damage in Ti6Al4V-Welded Joints*, Journal of materials engineering and performance, 23(8), pp 2965-2972, 2014

[3.13] Iziumova, A. and Plekhov, O., *Calculation of the energy J-integral in plastic zone ahead of a crack tip by infrared scanning*, Fatigue & fracture of engineering matrials & structures, 37(12), pp. 1330-1337, 2014

[3.14] Kutin, M., Ristic, S., Pruvlovic, R., et al., *Application of thermography during tensile testing of butt welded joints*, FME transactions, 133-138 (39), 2011

[3.15] Kutin, M., Ristic, S., Burzic, Z., et al., *Testing the tensile features of steel specimens by thermography and conventional methods*, Scientific technical review, 66-70 (60), 2010

[3.16] Guangjie, Y., Zhenqiang, Y., Qinghua, W., et al., *Numerical and experimental distribution of temperature and stress field in API round threaded connection*, Engineering Failure Analysis, 13, 1275-1284, 2006

[3.17] Parkus, H., *Thermoelasticity*, second edition , Springer Verlag, 1976

[3.18] Donato, G., and Belongie, S., *Approximation Methods for Thin Plate Spline Mappings and Principal Warps*, 2002

[3.19] Pandey, K.N., and Chand, S., *Deformation based temperature rise: a review*, International journal of pressure vessels and piping, 80, 673-687, 2003

Chapter 4

Numerical model: ThreadGenBT

Table of Contents

1 Introduction

This chapter includes all information about the developed finite element model which will further (chapter 5) be used to investigate the effect of small geometric changes on the performance of the connection. Section 2 gives a brief overview of the state-of-the-art related to the used numerical modelling approaches, both two dimensional and three dimensional. Up to date, a lot of work has been reported using two dimensional axi-symmetric models which are popular due to the limited calculation power which is required. The development of such a model is thoroughly described in Section 3. In addition, a full three dimensional model is described in Appendix A and is used to simulate the make-up stage and allows to investigate the effect of the thread helix and the required make-up torque. Following the outline of the numerical models, the outputs used to investigate the mechanical behavior of the connections are given in Section 4 and Section 5. Once all definitions and tools are explained, the applicability and methodology of the developed model and its outputs is outlined in Section 6. Subsequently, the aforementioned models are validated in Section 7 by comparing the 2D model with the experimentally acquired data of Chapter 3. Additionally, a preliminary study is reported in Appendix B and focusses on an approach to locate the most critical section (i.e. failure location) when tensile loads exceeding the API-defined tensile strength are applied. The suggested methodology adapts the contact surface based on the plastic deformation of the critical section of each thread. By comparing the numerical results with the experimentally determined fracture location, the feasibility of the approach is assessed. Finally, conclusions are drawn in Section 8.

2 Use of numerical modelling

2.1 Two dimensional axi-symmetric models

In an effort to study threaded connections, a combination of the experimental approach at one side and the numerical approach at the other is the required method. When modelling threaded connections using finite element methods, two distinct methodologies can be used. On the one hand, it is possible to model the entire three dimensional connection and calculate the assembly process starting from a hand tight position, in which a neutral stress state is assumed. The time and effort required to analyse a three dimensional model is not efficient due to increased difficulties related to the creation of the models and due to the long calculation times. For this reason, a two dimensional axi-symmetric model is often preferred. By using a 2D model, it is possible to increase the level of detail within a section of the connection due to a significant reduction of elements and calculation times. The use of these 2D axi-symmetric models has been proven by means of experimental validation [4.1] to provide sufficiently adequate results for the industry and is

generally accepted for various kinds of simulations such as fatigue, static loads and temperature [4.2-5]. For this reason, a lot of studies using 2D axi-symmetric models have already been performed on API round [4.6-8] and API Line Pipe [4.9] connections.

For tapered, trapezoidal threads used in connections without a shoulder, very limited accessible literature is available. This is possibly directly related to industrial demands at the time. When numerical tools became widely accepted in the 1980s, the more advanced premium connections rather than standard connections happened to be the primary industrial focus. The earliest documented simulation of an API buttress connection was published in 1993 by Assanelli et al. [4.10]. However, despite the mentioning of a buttress thread, no validation of any kind is provided for this thread type. In addition, very limited results of simulations of the API buttress connection are shown and the numerical methods used to model make-up are not revealed. While Assanelli et al. only considered plasticity, Kawashima [4.11] studied the effects of vanishing threads and concluded that utilizing the vanishing threads is necessary to prevent jump-out. In addition, a criterion is proposed in which it is suggested to consider that an incomplete thread fails once the tear resistance at its root is less than the tensile strength of the material. A comparison between the jump-out behavior of API round threads and API buttress threads, by creating plots containing the axial tensile force in function of average tensile strain in the connection, is published by Xie [4.12]. It is concluded that, in contrast with API round connections, the API buttress connections do not show any sign of jump-out. Despite this expected conclusion, the paper does not provide any details about whether or not (part of) the vanishing threads are likely to fail or have actually failed.

2.2 Three dimensional models

Despite the advantages of using the simplified two dimensional models, it is not possible to include the effects of the 3D helix shape of the thread because the helical structure is by definition neglected in the 2D model. Therefore, a numerical study comparing the 2D and 3D model is required. Unfortunately, very limited information about such a comparison is present in literature. An attempt to compare hybrid models of a shouldered connection with 2D axi-symmetric and full 3D models containing a thread helix was made in 1994 by Bahai et al. [4.13]. In this comparison, the similarities related to load distribution were partially validated. However, due to the use of a very coarse mesh, no conclusive evidence for the effect of the neglected thread helix could be derived. In analogy, further research was attempted to investigate the validity of these axi-symmetric models by Chen et al. [4.14] who conducted a study in which a three dimensional UNF (*Fine UNified screw thread*) and UNC-type (*Coarse UNified screw thread*) bolted lap joint under axial tension was compared with a 2D-axi-symmetric model by using the load distribution as a comparative parameter. Within this study, almost no differences were

observed when an external tensile load was applied, but it should be noted that these types of threads are not tapered and no initial make-up was applied. Shahani et al. [4.15] made a similar study using a 5 inch IEU (*Internal and External Upset*) shouldered and tapered drill pipe subjected to a 30 kNm make-up torque. Based on their results, stress concentrations calculated with the 3D model containing the thread helix appeared to be six times less than the ones obtained by the 2D-axi-symmetric model. Because of the presence of a torque shoulder, as was the case in the studies conducted by Zhong [4.5] and Sches [4.16], no large amounts of rotational displacement were required when simulating the assembly during make-up and therefore, this study cannot be used as a reference for shoulderless connections.

In an attempt to quantify the influence of the thread helix and the make-up torque, a full 3D model able to simulate the make-up stage is designed and described in Appendix A. In essence, this model only differs from the two dimensional approach by including a thread helix and therefore, such a comparison is possible. Due to the excessive amount of computational resources required, it is practically not possible to combine this model with a parametric modelling approach.

3 2D axi-symmetric model

Figure 4-1 illustrates a two dimensional, elastic-plastic axi-symmetric model that is created in Abaqus™/Implicit to simulate the quasi-static state of the connection after initial make-up followed by external loads including axial tension/compression, internal pressure and external pressure. In order to induce an initial stress state as the result of a make-up procedure, an initial radial overlap is applied. This overlap is calculated using the following equation:

$$\delta = n_N \, p \, tan(\varepsilon) \qquad \text{(Eq. 4.1)}$$

Within this equation, δ is the radial overlap (in mm), n_N the number of make-up turns, p the pitch of the thread (in mm) and ε the taper angle.

Figure 4-2 gives an overview of the structure of the Python based software ThreadGenBT, which was developed within this research. Microsoft Excel is used as a user-interface to input all the geometrical data, material properties and load conditions and to compile these variables into an input file. Once the input file is generated, a Python script is used to create the model in the finite element software Abaqus™. Once the numerical model is created, the preprocessing is concluded and Abaqus™ is used to calculate the mechanical behavior of the connection with the defined loads. Once the calculations are

concluded, the post processing criteria as defined in section 5 are calculated and extracted to text files and/or graphs.

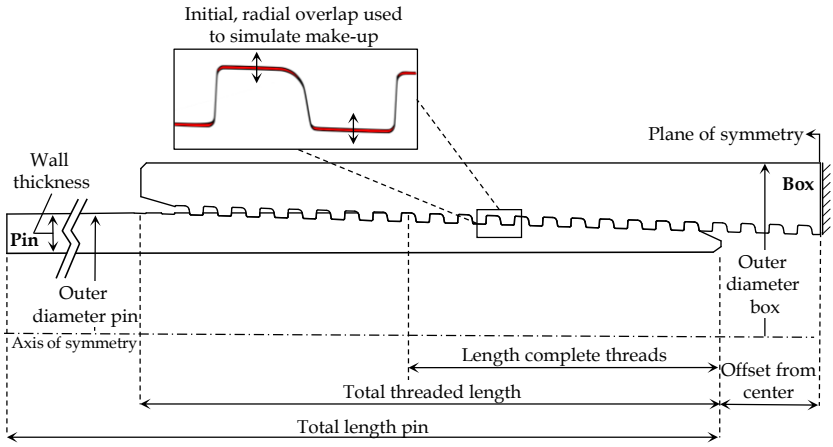

Figure 4-1: 2D axi-symmetric model

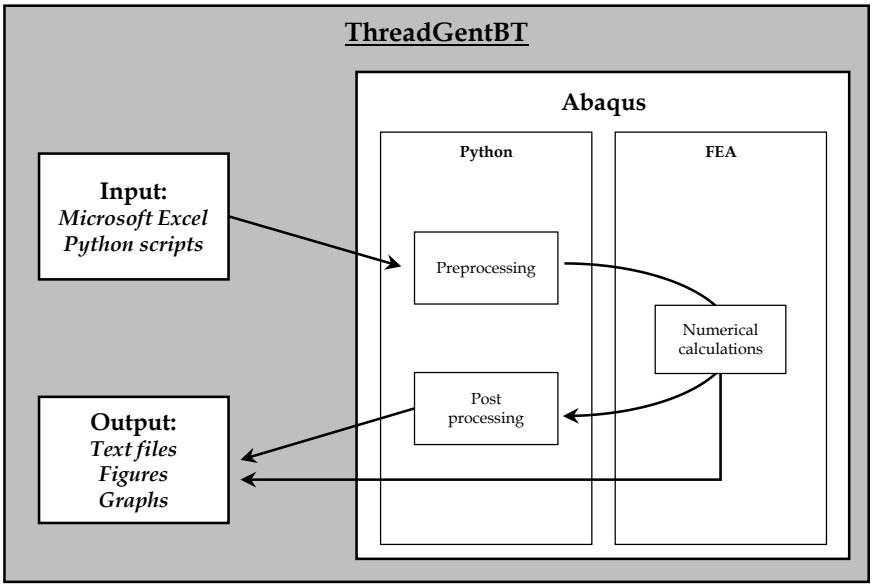

Figure 4-2: Overview of the ThreadGenBT software

3.1 Boundary conditions

The used model, schematically shown in Figure 4-1, was initially designed to model threaded and coupled (T&C) type connections. However, when changing the symmetrical boundary condition at the mid-plane of the box into a boundary condition limiting all movement except the radial direction, then this model can be used to simulate integral connections.

3.2 Contact definitions

The contact behavior between pin and box is defined as a node-to-surface contact and is calculated using the default hard contact in normal direction combined with a frictionless, penalty method to automatically resolve the initial overlap. It was opted to replace a surface-to-surface contact as was the case for the 3D model (see Appendix A) as the result of an enhanced calculation efficiency without the loss of accuracy. After the make-up stage, a coefficient of friction is added based on the calculated contact pressure along the threaded region (see section 3.4.5). This coefficient of friction is usually around 0.05.

Various methods can be applied to resolve the initial overlap. Figure 4-3 illustrates the obtained Abaqus™ internal variable *CTRQ*, which is a value representing a friction independent torque using the contact pressure, for three different methods. A first method takes into account the contact type. Within this method, a surface-to-surface and node-to-surface contact algorithm are compared [4.21]. Another method is to define an estimation of the maximum initial amount of overlap defined in the model. Within this part of the study, the direction in which to resolve this overlap was not defined. Finally, the last method combines a given amount of overlap with a direction in which to resolve this overlap to facilitate the numerical calculations. The latter method is often not possible due to the geometry of the connection (e.g. when negative flank angles are being used on the trapezoidal thread). After comparing the results of this study, shown in Figure 4-3, only minor differences are observed. Therefore, a node-to-surface approach combined with automatically resolving the initial overlap is preferred, resulting in faster and more stable performance of the numerical calculations without losing significant accuracy of the results.

To investigate the effects of initial friction during resolving the initial overlap to simulate make-up, four different make-up positions are simulated using five different coefficients of friction as can be seen in Figure 4-4. From this figure it is clearly visible that the total torque is linear with the initially applied coefficient of friction. This indicates that the contact pressures during make-up are independent of the coefficient of friction. This means that, in order to speed up calculation times, a frictionless contact can be applied during make-up where the initial overlap is resolved.

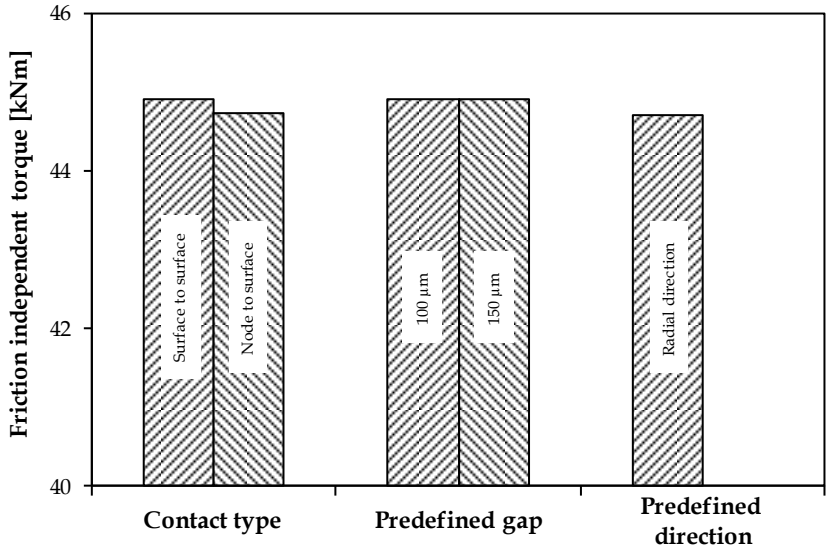

Figure 4-3: Comparison of the effect of different, standard available contact algorithms in Abaqus on the friction independent torque.

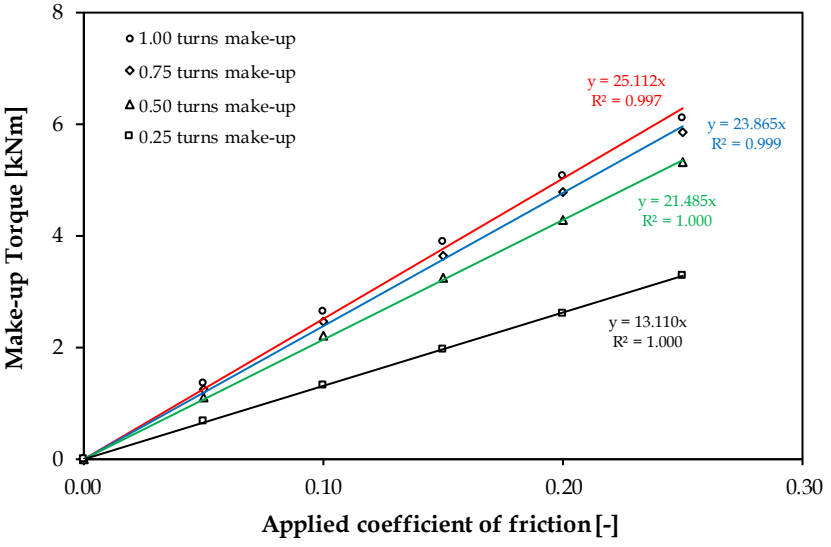

Figure 4-4: Torque can be calculated by multiplying the coefficient of friction with the CTRQ value of frictionless make-up

3.3 Mesh convergence

3.3.1 Applied Mesh

The applied mesh consists of solid, axi-symmetric trapezoidal (CAX4) and triangular (CAX3) elements. Their size depends on their vicinity to the threaded contact area. The elements closest to the contact area are smaller than the elements in the bulk material. The various sizes are dependent on the performed mesh convergence study and are determined based on the parameters that are to be extracted at the locations. In the contact area, a 2 to 3 ratio of pin-to-box nodes is applied since this ratio provides the best results [4.22].

3.3.2 Mesh convergence using stresses / strains

In an effort to reduce the required calculation times, a stress-based convergence study was performed on the bulk material and is illustrated in Figure 4-6. Based on this study, a mesh size of 1 mm for the bulk material proved to be sufficient to provide reliable results. No significant effect on calculation times was observed. A similar study was performed to determine the optimal, workable mesh size for the zone II which is required for a smooth transition towards the contact zone (zone I). Since no noticeable differences could be observed, the mesh size of this zone depends on zone I, for which the mesh size has been based on a convergence study of the contact pressure (see section 3.3.3). Using the stresses as a convergence criterion, a mesh size of 50µm proved sufficient.

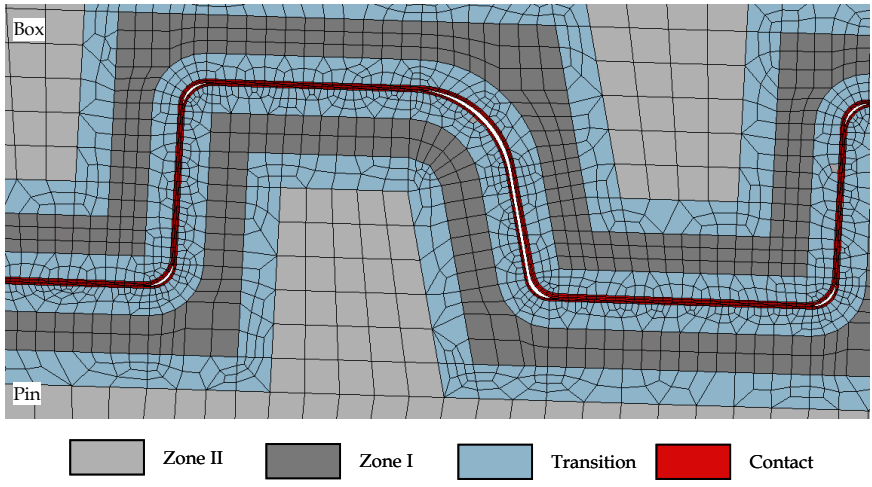

Figure 4-5: Example of the applied 2D axi-symmetric mesh with indication of the different zones

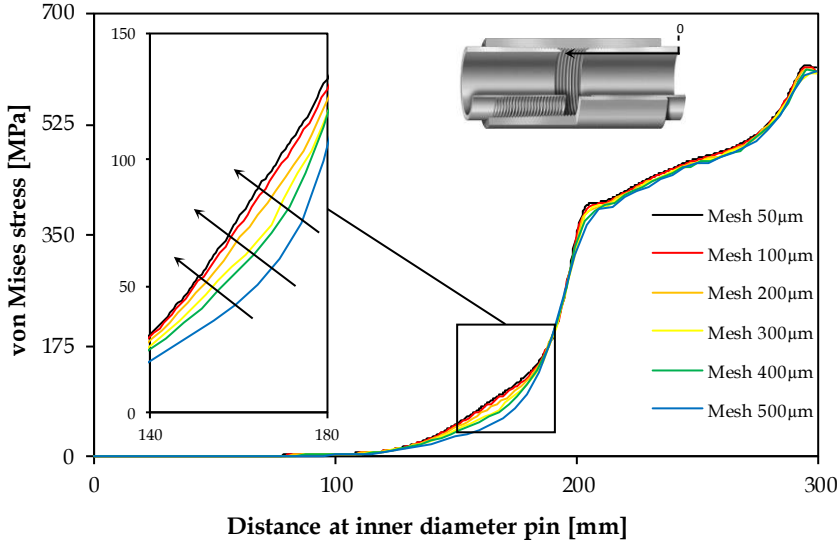

Figure 4-6: Stress based mesh convergence study at the inner surface of the pin shows that using a 50 µm mesh size is sufficient

3.3.3 Mesh convergence using contact pressure

It is observed from Figure 4-8 that contact pressure spikes exist at the extents of the flanks. The reason for these spikes is related to the geometric transition from a straight contact edge to a radius, causing a discontinuity in the contact length which leads to contact stress concentrations at both ends of the contact surface [4.23]. This difficulty was expected based on the analytical solution of a regular shrink fit connection [4.24]. At the curvature discontinuity point, where the fillet is merged to the flat portion, the pressure distribution features local infinity derivative [4.25]. Corner contact singularities are common and their presence is often not intuitive [4.26]. In literature related to fretting fatigue, the infinite contact pressure is often resolved by an asymptotic approach using stress intensity factors [4.27] or a multi-axial fatigue approach where the stresses are considered at a specified length away from the actual contact [4.28-32]. Using the asymptotic approach, the contact pressure distribution can be estimated using two different asymptotes [4.33,34] as shown in Figure 4-7. Without going into detail, the contact area can be divided in two regions: one containing stick, and the other slip. For each of these areas, an asymptote can be fitted locally, in the regions $0<x/d<<<1$ (first asymptote) and $x/d>>>1$ (second asymptote), by using two scaling factors as indicated in the figure. Considering K_N^* the normal force and d^* the projected length of the radius in contact, the transition area can be defined by [4.35]:

$$p(x) = 3\frac{K_N^*}{4\sqrt{d^{*3}}}\left[2\sqrt{xd^*} + (x - d^*)ln\left|\frac{d^* - x}{d^* + x}\right|\right] \qquad \text{(Eq. 4.2)}$$

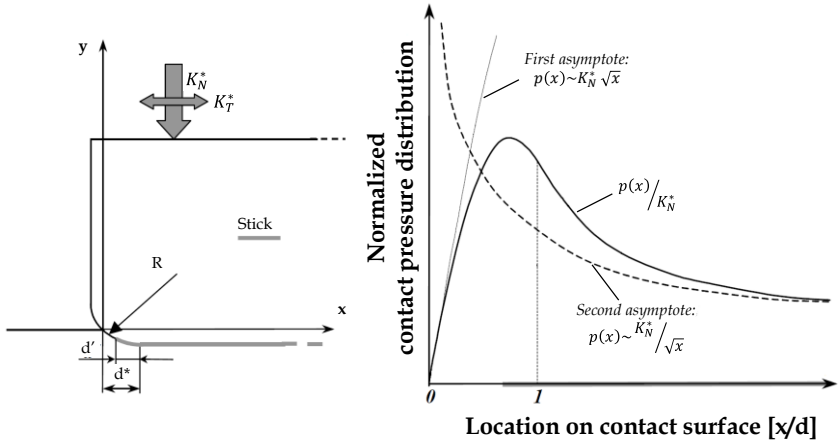

Figure 4-7: Estimation of the contact pressure distribution in case of a geometric discontinuity using two asymptotes. (Adopted from [4.35])

In addition to the existence of the contact pressure spikes, the contact pressures (*CPRESS*) do not converge when the mesh is refined. Despite the known existence of these $\left(1/\sqrt{x}\right)$-singularities [4.36-38], the inability of Abaqus to converge after resolving initial overlap with respect to mesh refinement was unanticipated. These problems are related to the inability of Abaqus in predicting the high pressure gradients that exist near the geometric discontinuity. When reducing the mesh size, the shape of the pressure spikes (illustrated in Figure 4-8) appears to approximate the theoretical pressure distribution shape shown in Figure 4-7 as the second asymptote. This tendency was also found in reference [4.39]. However, when the mesh is refined, the pressure spikes grow and the solution is also more oscillatory because a polynomial interpolation for the pressure distribution is trying to capture a spike. By increasing the number of nodes within this region, more terms containing unknown values for displacements and contact pressures are added to the equation and oscillations are expected. This behavior is described in more detail by G. Strang [4.40,41] and can be compared with the Gibbs phenomenon. This phenomenon is the manner in which a continuously differentiable periodic function behaves at a jump discontinuity and is shown in Figure 4-9. From this figure, it can be seen that an overshoot exists at the location of the discontinuity, which is comparable with the behavior of the numerically calculated contact pressure.

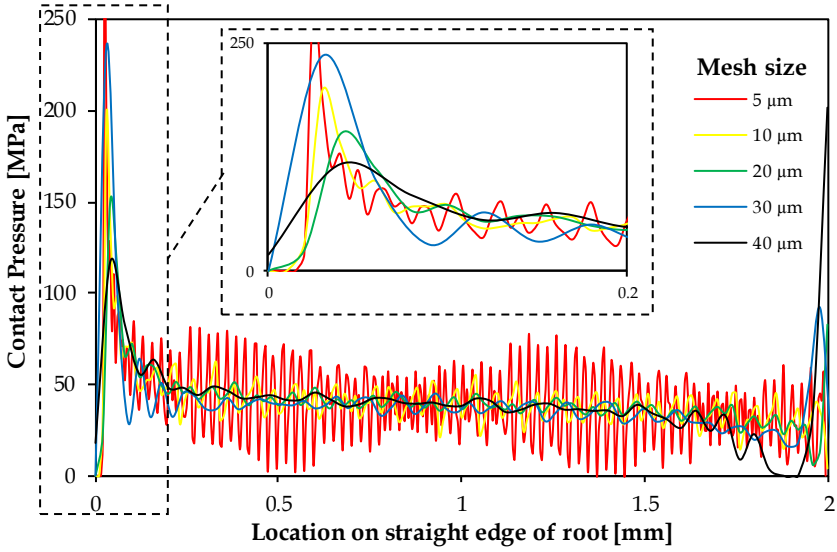

Figure 4-8: Indication of contact pressure distribution and pressure spikes relative to mesh size for a 4.5″ BTC connection with 0.5 turns make-up.

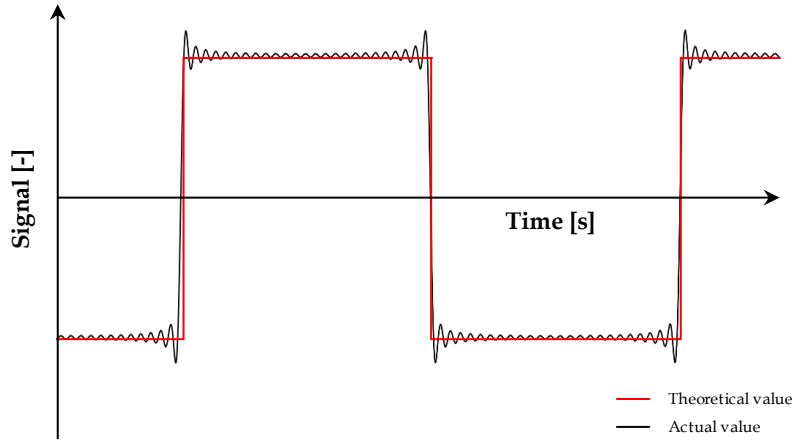

Figure 4-9: Schematic illustration of the Gibbs phenomenon

In order to quantify the reliability of the calculated contact pressure, the contact pressure accuracy (CPRESSERI) is extracted from the numerical model. It should be noted that this variable cannot be used to calculate actual contact pressure but it gives an indication of the reliability of the calculated contact areas. When high values are reached, either the solution at that location is potentially inaccurate, the mesh is too coarse or a stress singularity exists nearby. The CPRESSERI variable is normalized with the average contact pressure of the flank. This average is calculated after eliminating the extremes

of the contact area containing the pressure spikes, reducing the contact length by 10% at both ends. It should be mentioned that the normalization is required since otherwise, nodes with low contact pressures will automatically be considered unreliable. As a criterion, up to a 10% normalized contact pressure indication is allowed before omitting the results for further use [4.42]. The results representative for the accuracy and reliability of the contact pressure of the model are given in Figure 4-10 for various mesh sizes. At this point, no consensus is reached on how to interpret the occurring contact pressure peaks. In order to calculate the second asymptote shown in Figure 4-7, a sufficiently small mesh is required to capture the shape of the spike. Yet, a sufficiently large mesh size is required to capture the contact pressure away from the discontinuity. In addition, the location of this pressure spike is dependent on the slip/stick behavior of the contact and the physical meaning of the maximum contact pressure is unknown. Since the complexity and origin of this phenomenon are situated outside the scope of this research, the pressure spikes are not further considered within this thesis. Similar to previous work by Van Wittenberghe [4.43], the extents of the flanks containing the pressure spikes are not considered. This assumption is based upon the observation that these spikes have limited effects on the calculated torque values due to their limited size and tendencies of galling are not explicitly considered within this study. Therefore, not the maximum contact pressure, but the average contact pressure will be used for future calculations.

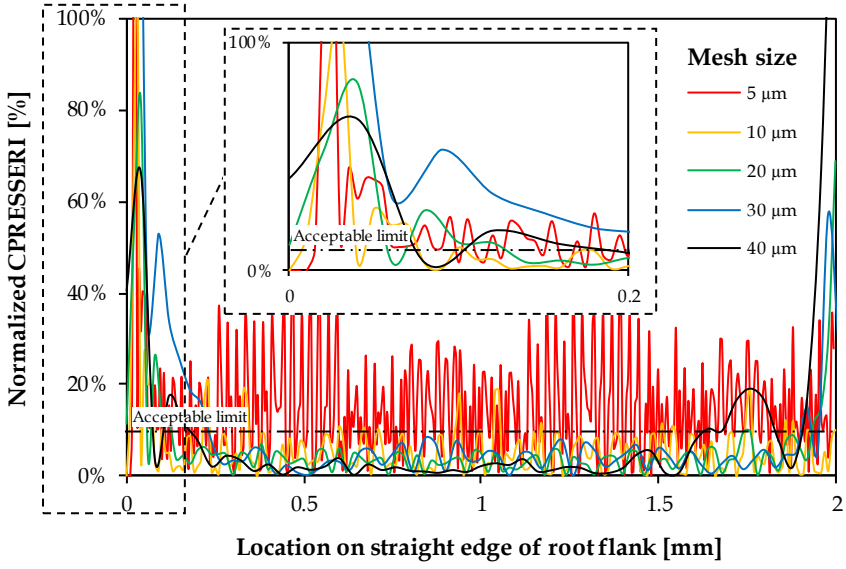

Figure 4-10: Normalized CPRESSERI for various mesh sizes.

3.4 Hypotheses

3.4.1 Mill end versus field end

In order to minimize rig time, T&C-type connections used in the fields are already attached to the pipe at one side in the mill. This side is therefore called the mill end. Because this connection should remain throughout its lifetime, the torque applied is usually higher than the torque used at the other end, the field end as shown in Figure 4-11. Depending on size, material, torque tolerances and geometry, this difference can exceed 50% for connections such as VAM TOP HT [4.44]. Because of this difference in make-up conditions, it is required to investigate if the make-up torque applied at the mill end has any effect on the stress state of the field end.

In order to investigate these effects, a connection without mid-plane is simulated. Instead of the symmetrical boundary conditions at the center of the connection, both sides are fully modelled. The worst case condition is simulated by applying various make-up conditions (see Figure 4-11) at one end, while no make-up is applied at the opposite end.

When one end of the connection has a lower make-up torque, stresses in the center appear to be slightly smaller, adding a limited amount of conservatism to the method using mid-plane symmetry. However, no changes are noticeable in the threaded part.

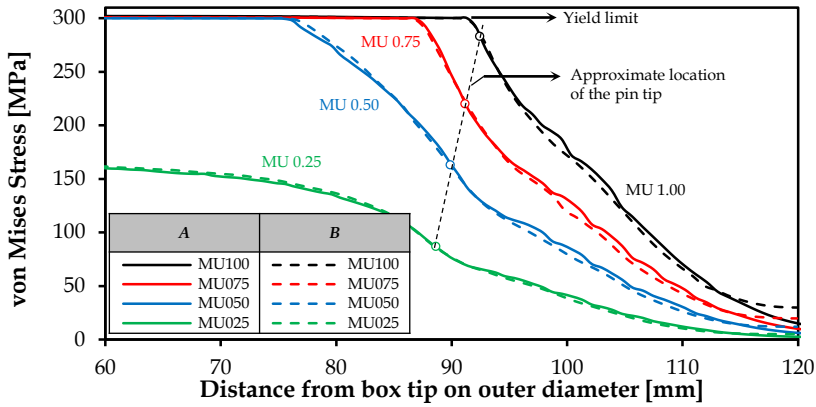

Make-up	A	B
Field end	See legend	See legend
Mill end	No make-up	See legend

Figure 4-11: Comparison of the von Mises stresses at the outside of the box using symmetric (dotted line) and asymmetric (full line) make-up for four different make-up positions: 0.25, 0.50, 0.75 and 1 turn.

3.4.2 Axial symmetry

By assuming axi-symmetric conditions, the size of the model is reduced significantly and a finer mesh can be applied while maintaining acceptable calculation times. By assuming axial symmetry, the thread helix of the connection is neglected. This imposes a reduced total surface area of the various flanks as illustrated in Figure 4-12.

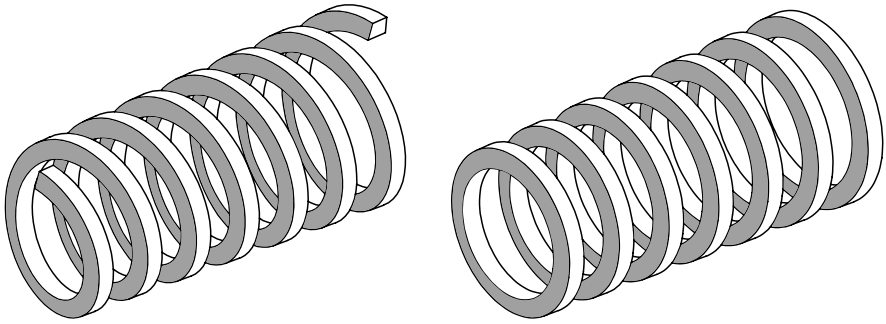

Figure 4-12: Helical area vs axi-symmetric area for 7 windings

The resulting area differences for all flanks using a standard Buttress thread [4.17] for up to 25 windings are illustrated in Figure 4-13. A limited, yet conservative difference of less than 0.2% can be observed in all cases. It can be stated that the use of an axi-symmetric model instead of including the full helical structure has a negligible effect on the magnitude of the total contact surface of the threads.

3.4.3 No geometric tolerances

In order to be able to manufacture the threaded connections, tolerances for the threads are specified in the standard [4.17] and are listed in Table 4-1. In addition to the threads, also the unthreaded pipe and coupling are subject to tolerances listed in API 5B [4.17] and are in turn summarized in Table 4-1. Because of increasing difficulties associated with statistical use of geometric tolerances in both the creation of the model as well as the interpretation of the obtained results, the nominal values of the dimensions modified by the average value of the tolerances are used. The study of the effects of geometric tolerances is currently outside the aim of the conducted research due to its complexity and since this will primarily affect sealing characteristics and not the overall stress/strain state of the connection, there is a need for extensive experimental testing. A suggested approach to incorporate this in further research is suggested in chapter 7.

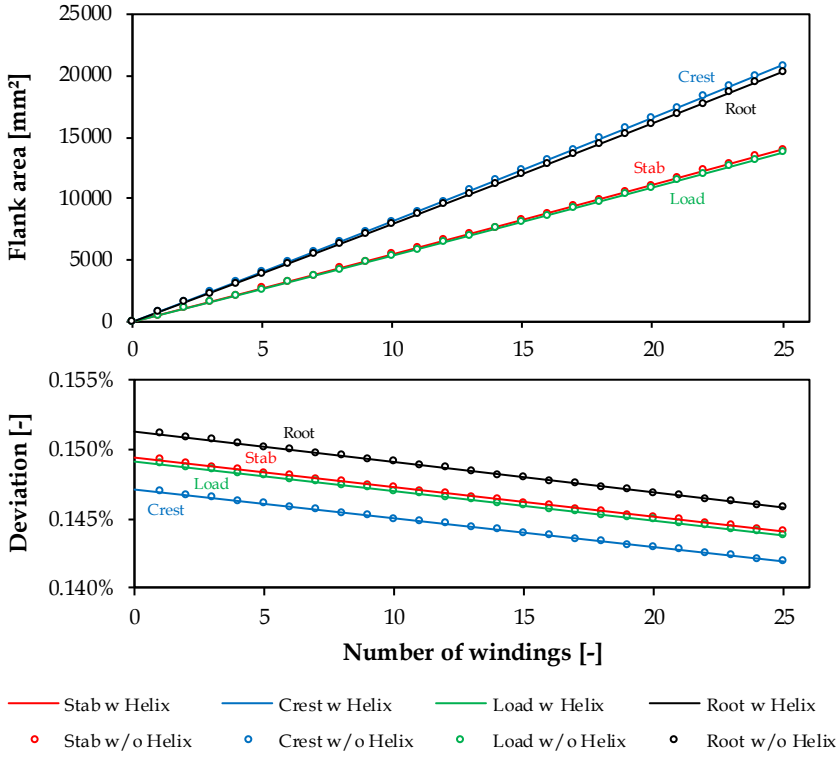

Figure 4-13: Influence of the helix on the flank area.

Table 4-1: Tolerances on buttress thread

Parameter	*Tolerance*	
	Min	*Max*
Taper coupling: per m on diameter [mm]	-2.286	+4.115
Taper coupling: 0.0625 m/m on diameter [mm]	-0.064	+0.114
Taper pipe: per m on diameter [mm]	-1.372	+3.200
Taper pin: 0.0625 m/m on diameter [mm]	-0.038	+0.089
Pipe (imperfect threads): per m on diameter [mm]	-1.372	+4.115
Pipe (imperfect threads): 0.0625 m/m on diameter [mm]	-0.114	+0.343
Lead: per mm [mm]	-0.002	+0.002
Lead: cumulative [mm]	-0.102	+0.102
Thread height [mm]	-0.025	+0.025
Included angle [degrees]	-1	+1
External thread length (L4) [mm]	N/A	N/A
Length pin tip to triangle stamp (A1) [mm]	-0.787	+0.787
Chamfer at pipe and coupling end [degrees]	-5	+5

3.4.4 Material properties

The material properties used in the FE-model are assumed homogeneous throughout the entire connection. The characteristics of different materials including Grade B, J55, TN80 and P110 are experimentally obtained by performing tensile tests on specimens taken from pipes. Their engineering stress-strain (s-e) curves have been converted into true stress (σ) and true strain (ε) values using the well-known relations ε = ln(1 + e) and σ = s(1 + e). The obtained curves are then averaged and discretized as illustrated in Figure 4-14. Since these relations lose validity beyond localized necking, true stress-strain values in the post-necking region were obtained from extrapolation as defined by Ling [4.45]:

$$\sigma = \sigma_m \left[\alpha(1 + \epsilon - \epsilon_m) + (1 - \alpha)\left(\frac{\varepsilon}{\epsilon_m}\right)\right] \qquad \text{(Eq. 4.3)}$$

Where σ_m is the engineering yield stress, ϵ_m the engineering yield strain and α is a parameter which allows for a power law extrapolation (α = 0), a linear extrapolation (α = 1), or cases in between (0 < α < 1). Figure 4-14 shows true stress-strain curves and includes the post-necking stress-strain behavior for three different cases: α = 0.0 (power law extrapolation), α = 0.5 (intermediate extrapolation) and α = 1.0 (linear extrapolation). For this purpose, an alpha value of 0.5 was used (see further section 7.3.1).

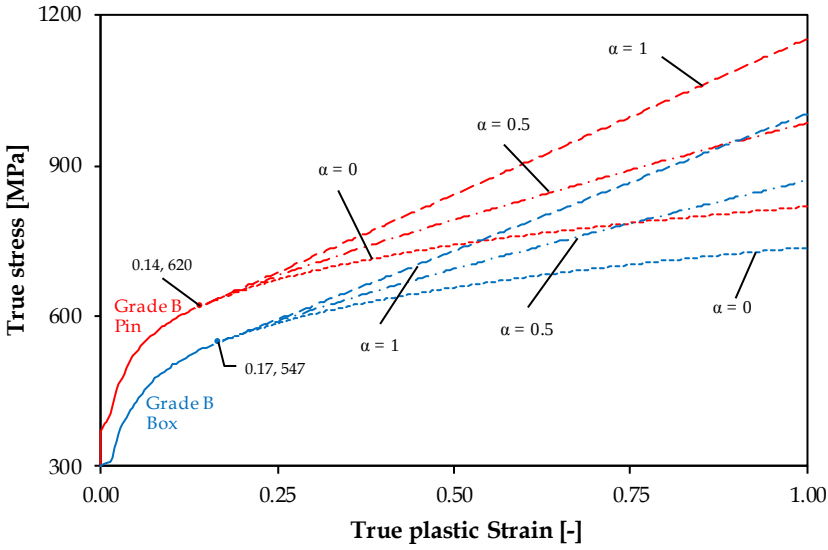

Figure 4-14: The stress-strain characteristics for both pin and box, including different extrapolation exponents

3.4.5 Use of friction

Thread compounds are usually applied to the threaded region of the couplings to reduce friction. In general, the behavior of thread compounds consisting of lubricant and solid particles can be explained by considering the situation in which two plates contain a certain amount of thread compound between them as is illustrated at the top, right side of Figure 4-15 [4.46]. A contact pressure is created by applying a certain normal load (N) to the plates. When the normal force is very low (Figure 4-15.A), very little, unnoticeable friction (F_f) is caused when the plates undergo a relative displacement because the solid, metallic particles (MP) are able to move freely in the lubricant components (LC). When the normal force is increased (Figure 4-15.B), the solid particles start to touch and roll over each other, generating friction up to measurable values. When even higher normal forces are applied, the solid particles start to deform plastically in the shape of flakes, forming layers. From that moment on, friction exists between the layers and is proportional with the applied load.

The frictional behavior of the used *API Modified* thread compound is given by equation 4.4 and is illustrated in the left part of Figure 4-15. This formula takes into account the contact pressure dependency of the thread compound as was obtained by an API test program [4.48].

$$\begin{aligned}\mu = & -9.86\,10^{-16}\,p_c^6 + 1.36\,10^{-12}p_c^5 - 7.30\,10^{-10}\,p_c^4 \\ & + 1.91\,10^{-7}\,p_c^3 - 2.38\,10^{-5}\,p_c^2 \\ & + 1.21\,10^{-3}\,p_c + 3.03\,10^{-2}\end{aligned} \qquad \text{(Eq. 4.4)}$$

From this figure, a local maximum situated around a contact pressure of approximately 40 MPa can be observed after which a local minimum around 135 MPa appears. The reason for the drop of the coefficient of friction is not fully described, but the following hypothesis can be drawn [4.46]. It is plausible to assume that at the end of stage B, the solid particles are sufficiently pressed against each other in order to not roll over each other. Solid layers (SL) of particles are formed in which the particles can initially still move, but are not able to jump over each other. At this point, (part of) the solid particles start to function as micro roller bearings. Once a high enough contact force is reached, causing sufficient contact pressure (135 MPa in this case), to freeze the particles within their formed matrices, their only degree of freedom is the ability to rotate and as a result the particles act as roller bearings. Once exceeding this contact pressure, the particles start to deform plastically or start to fracture and become abrasive.

As previously mentioned, the initial make-up situation is calculated by resolving an initial radial overlap and is considered to be a geometric action which is independent of the coefficient of friction (see section 3.2). Once the make-up conditions are known, an element dependent coefficient of friction

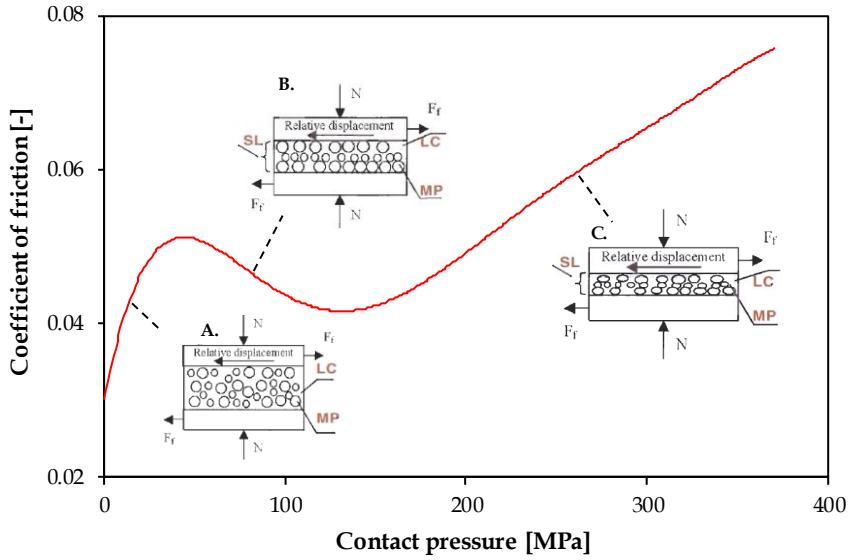

Figure 4-15: Contact pressure dependency of the coefficient of friction of *API modified* thread compound.
The compound's behavior is schematically illustrated.

can be assigned depending on its contact pressure to calculate the frictional torque by using equation 4.5.

$$T_F = \sum_{i=0}^{i} 2\pi * \mu_i * CP_i * l_i * r_i^2 \qquad \text{(Eq. 4.5)}$$

In this formula, i represents the number of elements, CP the contact pressure of the element, l the contact length, r the location from the pipe axis and μ the coefficient of friction which is dependent on the calculated contact pressure.

Since it is practically not possible to assign an element-dependent coefficient of friction to every single element, a uniform coefficient of friction is calculated to match the global frictional torque calculated using a pressure dependent friction coefficient. The average coefficient of friction can be determined using formula 4.14 where μ_g is the global coefficient of friction, T_F the frictional torque calculated using equation 4.5 and $CTRQ$ the numerical make-up value independent of the coefficient of friction (see section 4.2).

$$\mu_g = \frac{T_F}{CTRQ} \qquad \text{(Eq. 4.6)}$$

Figure 4-16 illustrates the torque-turn diagrams (see section 4.2) for the experimentally used connections based on the minimum and maximum defined value inherent to the used thread compound [4.47] together with the situation in which a variable coefficient of friction for each element was applied using a post processing *Python* script. Based on these results, the calculated, uniform coefficient of friction was found to be approximately 0.053 for this particular connection. When the geometry of the model changes, this value is likely to change as well. It is worth noting that the uniform coefficient of friction is quasi-independent of the applied make-up torque, as can be seen in Figure 4-17.

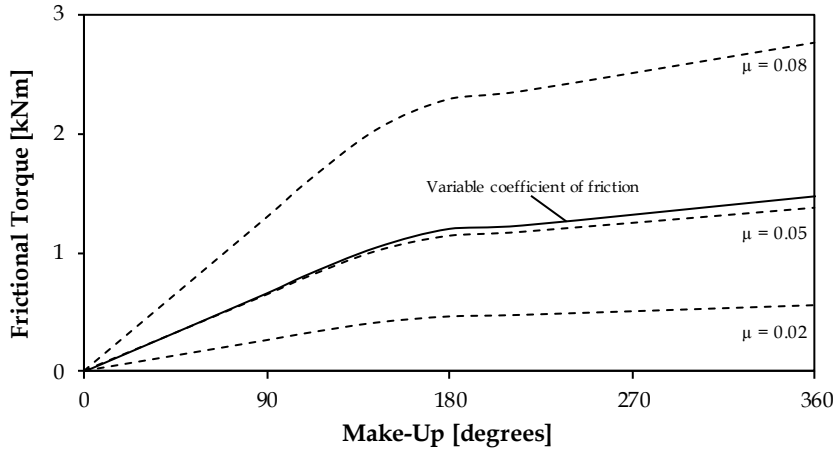

Figure 4-16: Comparison of the results using a variable coefficient of friction per element and a uniform coefficient of friction

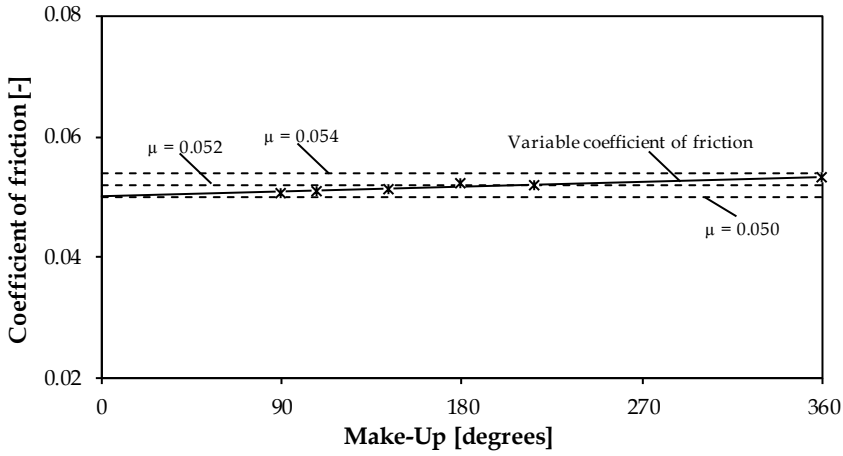

Figure 4-17: Comparison between the use of a variable and uniform coefficient of friction

4 Direct outputs

4.1 Stresses and strains

Two of the directly available output values of the numerical model are the occurring stresses and strains. The primary objective of extracting the strains is to directly compare them with the experimental results for validation purposes. When assessing the effect of the load conditions on the behavior of the connection, evaluating the stresses is often preferred over the strains. This way, possible locations with stress concentrations are better visualized. In contrast, the use of strains is often preferred when comparing numerical and experimental data since stresses cannot be measured directly.

4.2 Torque-turn diagram

As mentioned in Chapter 3, the torque turn diagram shows the relationship between the relative rotational displacement of pin and box past its hand tight position and the required torque.

In a 2D axi-symmetric model, the friction independent approximation of the maximum resisting torque a press fit connection can resist is used when predicting the torque required to obtain a certain make-up state. This torque is calculated based upon the contact pressure and is given in equation 4.15.

$$CTRQ = \iint r^2 \, p_c \, ds \, d\theta \qquad \text{(Eq. 4.15)}$$

When a constant coefficient of friction is assumed, the maximum torque can be calculated using the following equation:

$$T_{CTRQ} = \mu \, CTRQ \qquad \text{(Eq. 4.16)}$$

It should be noted that only the CTRQ-value obtained after fully resolving the overlap can be used for further reference. When a torque-turn diagram needs to be generated by using a two dimensional model, each make-up position requires its own simulation with the appropriate amount of initial overlap. Different uniform friction levels can be considered by simply substituting the appropriate coefficient of friction in equation 4.16.

5 Indirect outputs

In order to assess the performance of various threaded connections when in service, three distinct performance criteria are defined. Based on these criteria,

connections can be compared to each other when certain work conditions apply.

5.1 Plasticity criterion

5.1.1 Background

As a first performance criterion, the extent of plasticity in the connection is being assessed. Initially, plastic deformation was often used to create a reliable thread seal for low pressure equipment [4.49]. However, for heavy duty connections, this sealing mechanism is no longer used. Plastic deformation, especially at the torque shoulder if one is present, is avoided because of the accompanying extreme contact pressures significantly increasing the risk of galling [4.34-36]. In addition, plastic deformation along the threads can trap the used thread compound leading to pressure pockets in the connection, rendering the assembly unfit for duty. Sometimes, special features such as buffer zones are added to the connection to avoid plastic deformation when, for example, using two stepped thread designs [4.53] (see Chapter 1).

Generally, it can be stated that when a connection is subject to reuse, global plastic deformation has to be avoided. When plasticity is induced, the threaded area may become overly deformed or even damaged and a break out and subsequent make up might become impossible.

5.1.2 Practical implementation

In Figure 4-18, an example of a regular plasticity curve, presenting the total amount of plastic energy in function of the make-up position, is added to a torque-turn diagram for a threaded connection without torque shoulder and sealing surface. From this graph, two linear areas and one transition area can be seen. When a low amount of make-up turns is applied, a linear tendency between plastic energy and make-up position, characterized by a negligible slope (zone A), can be observed. Within this range, an unavoidable but limited amount of plasticity occurs at the end of the vanishing threads. These effects are very local and the connection is still considered to be usable. For the high make-up turns (Figure 4-18, zone C), the plastic energy increases drastically and indicates the start of global plastic deformation. Between the mainly elastic (zone A) and global plastic (zone C) areas which can both be approximated by a linear relationship, there is a transition area (zone B). Within this area, the local plastically deformed areas at the roots of the vanishing threads grow, but the plastic strains remain limited.

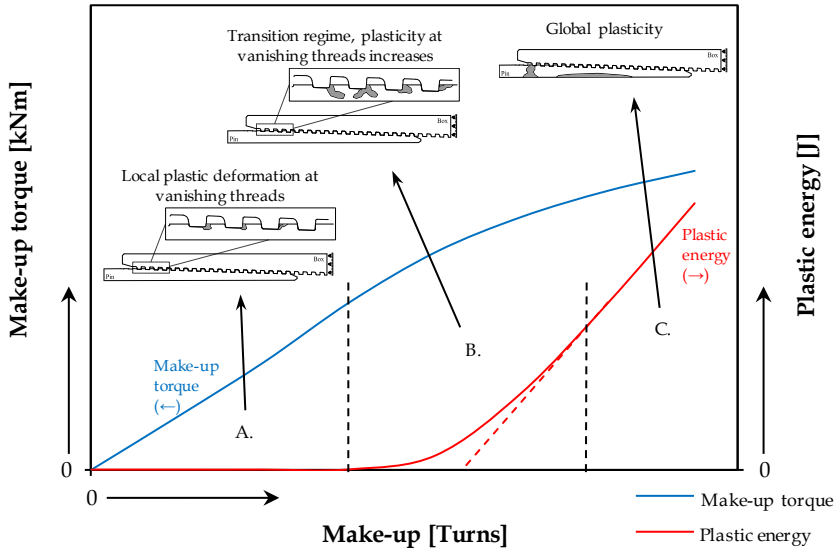

Figure 4-18: Schematic overview of a plasticity curve plotted together with the torque turn diagram. The various plasticity regimes are indicated as local (A), transition (B) and global (C).

5.2 Leakage criterion

5.2.1 Background

A second important criterion to investigate is the leak tightness of the connection. Nowadays, a lot of effort is done to design *zero leakage* connections. It should be noted that *zero leakage* is an ill-defined concept. If zero leakage is assumed to be no leakage at all, the intention of creating such a connection while avoiding plastic deformation is contradictory since it is not possible to do this without inducing plastic deformation or polymeric seals which have a very limited area of application [4.54]. Therefore, it makes no sense to focus on *zero leakage* or *no leakage* connections [4.55] and a concept of 'leak tightness' should be defined based on a threshold value for stable leak rates. Examples of such leak rates are 1.4 mm^3/sec adopted by NASA for fuel connections [4.56] or 1.0 mm^3/sec defined in the ISO standard for the testing of premium threaded connections [4.57]. It should be noted that the defined threshold leak rates are depending on the application, fluid, pressure and temperature [4.58-60].

Based on the above approach using a threshold leak rate, only a binary GO or NO GO comparison can be made. In order to differentiate between connections which did not seem to leak, additional parameters need to be addressed. When a sealing surface is present, it is a usual approach to consider the contact pressure (p_c) and contact length (Γ) over these surfaces. Sometimes,

these two parameters are joined together and are defined as a seal index (SI) [4.61] which is given by:

$$SI = \int_{\Gamma} p_c \, d\Gamma \qquad \text{(Eq. 4.17)}$$

An example of an analysis using such a seal index can be found in Figure 4-19. This picture shows the investigated load cases on the left and the calculated seal index on the right. The sealing capabilities of the connection are believed to be better for the load cases containing a high seal index.

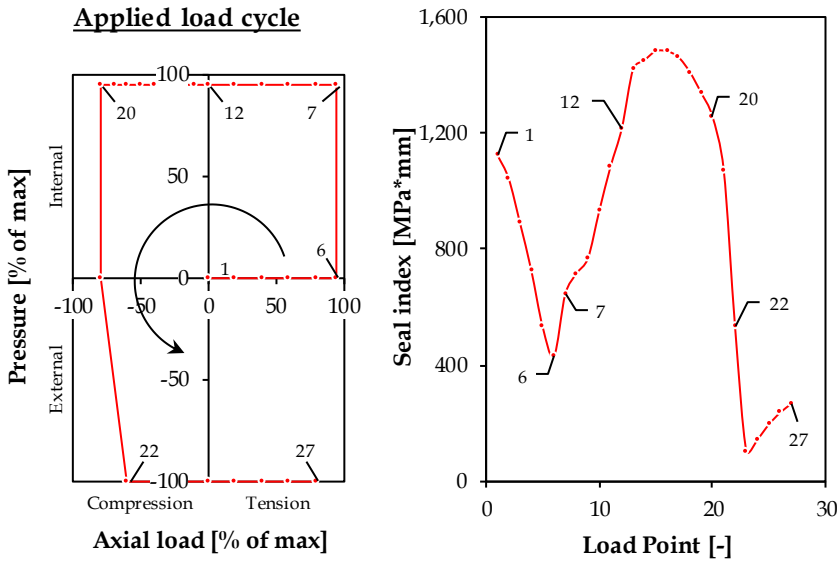

Figure 4-19: Example of the use of a seal index. Generally, the higher the index, the better the connection for the given purpose. (Adopted from [4.61])

Since this research focusses on standard trapezoidal threaded connections, no sealing surfaces are present. Therefore, in contrast with the work of Asbill et al. [4.62], relating the reliability of the thread seal to a parameter combining contact pressure and contact length is not considered to be useful because a gap exists between the threads. The necessity of this gap was previously explained in Section 4.4.2 of Chapter 3. In this type of connections, a geometrically imposed leak path is already present and is sealed with the used thread compound. The effectiveness of the used thread compound, containing solid particles of a certain size, depends on the gap size between the threads. For the used thread compound, a maximum gap size of 150 µm was stated in

[4.63] for pressures up to 275 bars. When the gap size is kept below this limit, the particles in the thread compound are not able to be squeezed out, providing an effective thread seal.

When considering leakage through the threaded area, two possible leak trajectories can occur. First of all, the pressure can migrate through the thread helix. When the gap size is sufficiently large, excessive pressure pushes the thread compound out of the connection and a leak path is formed [4.64]. Usually, more than two thread turns are required to provide a reliable seal [4.65]. Another possible leak mechanism is called cross leakage [4.66]. In this case, the pressure is able to shift between two different flank helixes by migrating over a certain flank in a particular section. For example: the pressure is able to escape from the root helix into the crest helix by creating a small leak channel over the stab flank. Therefore, it is highly advisable to assume a leak tight barrier only when all four flank openings are below the critical gap size of 150 μm. Additionally, the smaller the gap size, the better the assumed sealing characteristics since the gaps get easier clogged by the solid particles.

Despite the apparently straightforward approach when considering these requirements, the applicability of this criterion remains unclear. A distinction should be made between make-up and in-service conditions when taking into account the critical gap size. During make-up, the liquid phase is still present in the thread compound. This allows the particles to easily reorganize. When in service, the thread compound is often dried out which causes a restricted movement of the solid particles. When the solid particles are unable to move and reorganize when loads are applied, cracks can occur in the thread compound leading to a leak path. The distinction between the case of make-up and in-service conditions is not explicitly made in literature and therefore, it is opted to conduct the leak path criteria twice. Once after make-up and once after applying external loads in which the relative change in gap size is considered.

5.2.2 Practical implementation

In order to extract this indirect output, another built-in variable called '*COPEN*' is used to investigate whether or not the clearance between the thread flanks is below the critical limit of 150 μm. This variable represents the shortest distance between the point at which it is calculated to the nearest contact surface of the other member (pin or box). Since the slightest gap size is enough for a pressurized connection to start leaking, the maximum value over every flank is considered. These values are extracted for all four thread flanks and plotted in function of thread number and load. They can be assumed to be a continuous function because of the helical shape of the thread. Since the vanishing threads are not considered to have leak tight characteristics, they are not considered.

5.3 Distributed load criterion

5.3.1 Background

The load distribution in a threaded coupling is often used as an approach to visualize the effectiveness of the threads. By assessing this parameter, insights are provided on how the load is distributed over the threaded surface. In ideal conditions, every thread carries the same amount of load. A detailed analytical theory for predicting the distribution of load in non-tapered threads of a bolt taking into account radial expansion of the nut was published by Sopwith [4.67]. Stoeckly and Macke [4.68] expanded Sopwith's theoretical work to include the analysis of a tapered thread on either bolt or nut. The effect of this taper introduces an initial axial recession at the thread roots which must be incorporated into the equation. The reason that one element of the connection was tapered and the other parallel, was to redistribute the load within the connection, by essentially creating a variable pitch along the taper. Additional research was conducted on the effects of yielding in the threads [4.69], concluding that when yielding occurs, the relative amount of the applied load transferred through the thread decreases [4.70], which is visible in the load distribution curve. This observation can be used as the basis of a criterion to detect overstressed threads in the connection.

In order to find a suitable variable to express the load distribution over the threads, it is opted to make a distinction between an axial and a radial load distribution. During make-up and internal/external pressure, the radial load distribution is predominant while when applying axial tension or compression, the axial load distribution is of main importance.

5.3.2 Practical implementation

In order to quantify the axial and radial load distribution, two different approaches are applied. Contact pressure is used for the radial load distribution while axial stresses are used for the axial load distribution. The main reason for calculating the load distribution using different methods is due to the previously mentioned convergence problems when assuming contact pressure (see section 3.3.3). Due to singularities inherent to the contact pressure, the use of this variable is avoided whenever possible, as is the case for the axial load distribution.

To calculate the axial load distribution, the pin member of the threaded connection is divided in n axial sections as indicated in Figure 4-20 and the total axial force transferred from the pin to the box between two subsequent sections is calculated by integrating the longitudinal stresses over the appropriate sections as is also proposed in references [4.71] and [4.72]. For the connection, the total applied axial force is equal to the summation of the forces transmitted between pin and box at each thread:

$$F_{a,a} = \sum_{i=1}^{n-1} \left| F_{a,S_i} - F_{a,S_{i+1}} \right| \qquad \text{(Eq. 4.18)}$$

The load transferred from pin to box through the contact at the thread flanks can be estimated by:

$$F_{a,i} = \left| F_{a,S_i} - F_{a,S_{i+1}} \right| \qquad \text{(Eq. 4.19)}$$

By combining equation 4.18 and equation 4.19, the relative load carried by thread *LET-i* can be calculated as follows:

$$F_{ar,i} = \frac{F_{a,i}}{F_{a,a}} \qquad \text{(Eq. 4.20)}$$

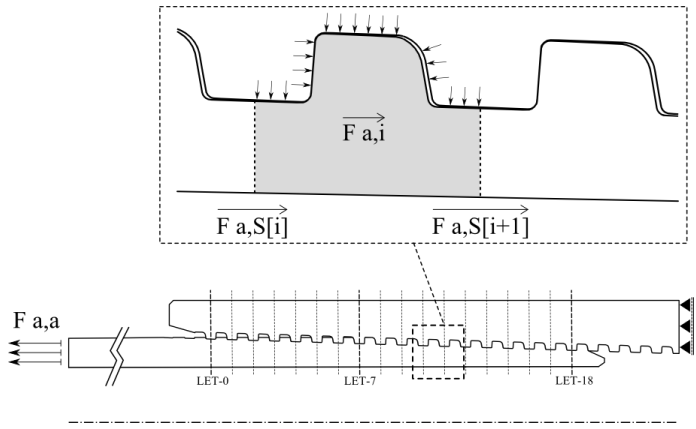

Figure 4-20: Division of the threaded connection in axial sections

In contrast, the radial load distribution is still calculated relying on the contact pressures. Herein, the summation of the radial component of the contact pressure multiplied by its element size is calculated for all elements of every thread. Consecutively, the radial load per thread relative to the total radial force acting on the assembly is calculated and visualized in a graph.

As a final note, it is pointed out that when using 2D axi-symmetric models, the forces calculated using the obtained stresses and length of the section are expressed in *force per unit of length*. In order to calculate the actual force acting in the various sections, an integration over the circumference is required.

6 Use of the numerical model

A flowchart explaining the working procedure of ThreadGenBT is shown in Figure 4-21. In order to assess the performance of a connection, an estimation of the minimum and maximum amount of initial make-up is required. This is done by performing two series of simulations. First of all, only make-up is simulated ranging from 0 to 3 powerturns with an increment of 0.2 turns (*A*). Once this series is done, the plastic energy is plotted in function of make-up (*B*) and the maximum make-up position when no external loads are applied is calculated (*C*). A detailed explanation how this position is determined can be found in Chapter 5. The upper limit obtained by these

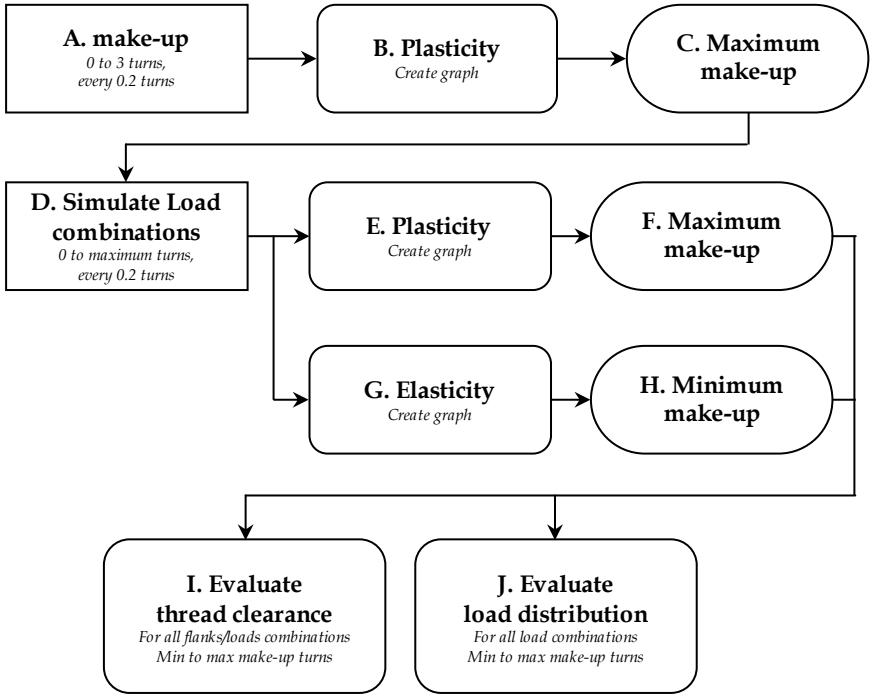

Figure 4-21: Graphical overview of the working method using ThreadGenBT

simulations is an overestimation since additional working loads will be applied to the connection. Therefore, an increased number of simulations (*D*) are performed using make-up combined with various load paths. These load paths consist of a combination of internal pressure and axial tension up to a Von Mises equivalent stress corresponding to a certain percentage of the yield strength, depending on the intended performance rating of the connection. Using various load paths, new maximum make-up positions are calculated based on the plastic energy (*E*) and the minimum value is considered to be the

maximum make-up position (*F*). In addition, a certain amount of torque is required to ensure a rigid connection and to prevent downhole make-up or break-out. This minimum value (*H*) is based upon a similar methodology as the maximum position (see Chapter 5), but instead of the plastic energy, the elastic energy is used (*G*). Using the minimum and maximum values, a range is defined in which an acceptable amount of make-up is considered. This range is similar as the one indicated by the stamped triangle on standard buttress connections.

Once the reusability, indicated by limiting the plastic deformation, of the connection is assured by limiting the make-up position, the sealing capabilities of the connection can be estimated (*I*). In order to do this, the gap size between the flanks after make-up is plotted and evaluated for the complete threads only because the vanishing threads will not be able to create a reliable seal. For every considered connection, the absolute gap size is considered after various cases of make-up. When all four flank openings of a thread are below the critical value and this for five consecutive threads, the connection is considered to be leak tight up to 275 bars internal pressure after make-up. Because of externally applied load combinations consisting of axial tension and internal pressure, the changes of the flank openings, defined as relative gap sizes, are monitored. Based hereon, straightforward conclusions cannot be made. It is assumed that smaller changes in the previously defined sealing area are more favorable. However, the extent and whether or not a critical relative gap size exists, is yet to be examined.

In addition to the assessment of the sealing area, the relative change in gap size as the result of external loading after make-up can also be used to assess the ability of the thread to take up the working loads. When no change in gap size can be observed it can be concluded that working conditions have no effect on the examined section of the thread. This behavior can also be assessed by considering the load distribution (*J*). When no loads are acting on a thread, the load distribution on this thread will be zero and the gap size at the flanks will not change.

7 Validation

Before using the numerical models for predicting trends and suggesting changes to existing geometries in order to enhance a connection's performance, a numerical and experimental validation is required to justify the hypotheses (see section 3.4) and use of boundary conditions (see section 0). An experimental validation is required to ensure the model is reliable. In analogy with the comparison of strain gauge and DIC results in Chapter 3, the results of the 2D axi-symmetric model are compared to the experimental results of make-up, TLE and limit load test.

7.1 Make-up

7.1.1 Torque-turn diagram

The experimentally measured torque turn diagram together with the numerical predictions can be found in Figure 4-22. During the experiments, an API Modified thread compound was used and according to the API standard [4.74], this thread compound has a coefficient of friction between 0.02 and 0.08. Using both minimum and maximum values, the required make-up torque can be estimated based on the frictional torque and the deformation torque using a fixed coefficient of friction.

The coefficient of friction is characterized by a large variability which makes it nearly impossible to predict the magnitude of the actual make-up torque. A contact pressure dependent coefficient friction is assumed as mentioned before. During the post processing of the results obtained by the numerical model, a contact pressure dependent coefficient of friction is assigned to each element within the contact area based on its contact pressure value. The required torque is recalculated based on equation 4.22 and the result is plotted in Figure 4-22. From this figure, it can be observed that the calculated torque matches the experimentally obtained make-up torque once 500 kNm is exceeded. Prior to this value, a running in stage as was previously explained in Chapter 3 is present.

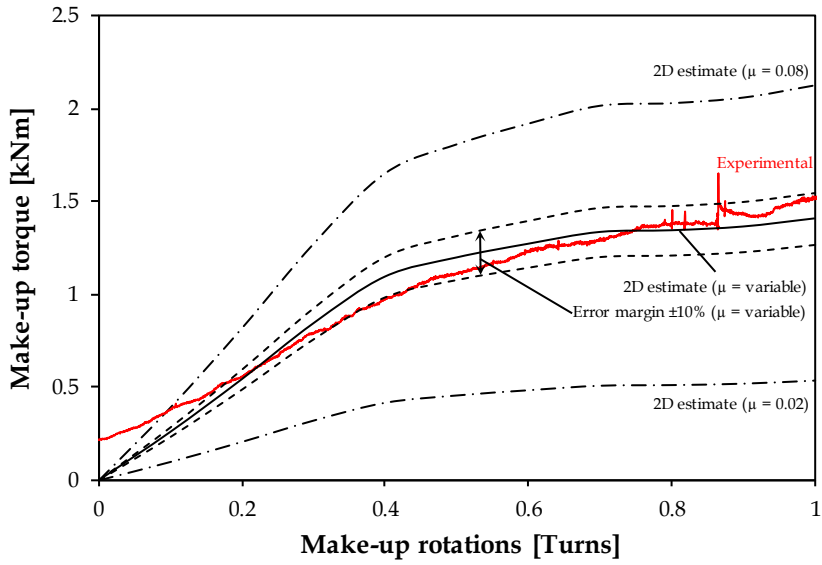

Figure 4-22: Comparison of the measured torque with the numerically predicted torque using a variable and constant coefficient of friction

7.1.2 Comparison of surface strains

A comparison between the strains predicted by FEA and the experimentally measured strains is illustrated in Figure 4-23 where *n* represents the number of make-up turns. Overall, an overestimation of the strains by the FE simulations is visible. The reason for this overestimation is caused by two

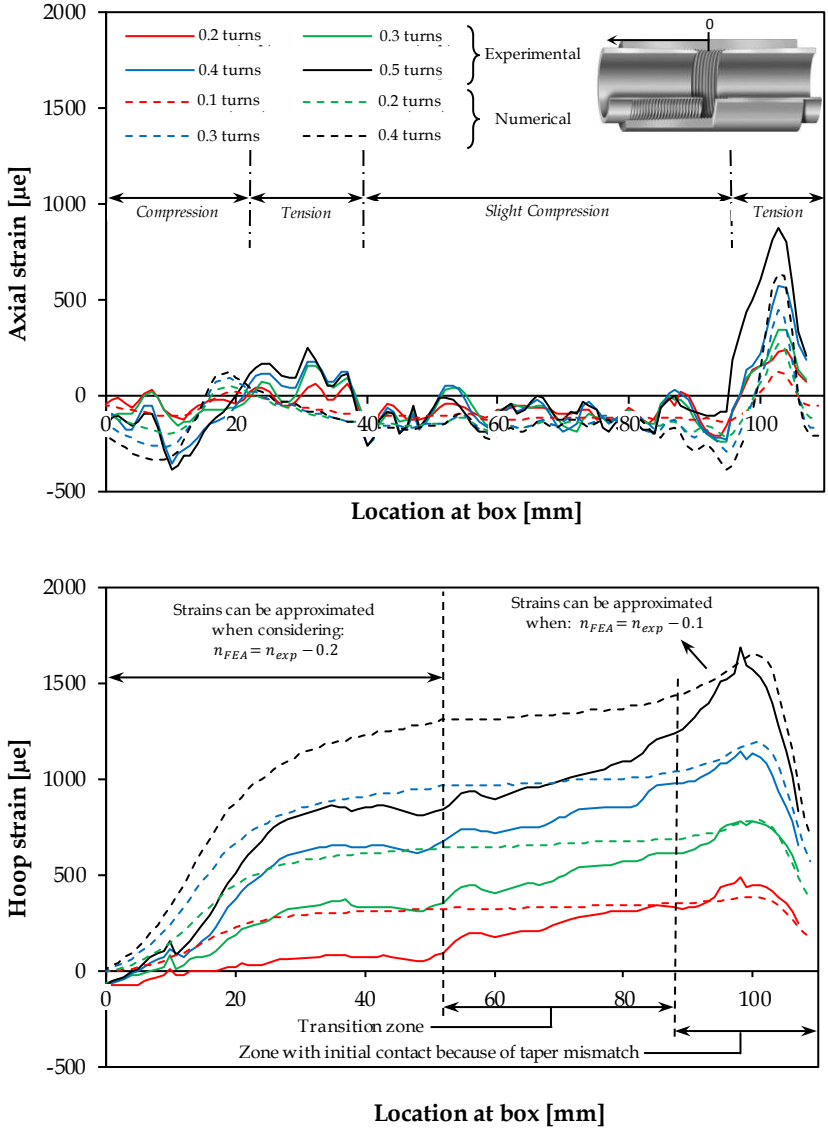

Figure 4-23: Comparison of numerically predicted with experimentally measured (using DIC) strains.

parameters: the location of the hand tight position and the occurrence of localized taper mismatch. According to the standard, the amount of powertight make-up turns is defined starting from the handtight plane. This is a virtual plane in which the torque required for the assembly starts to increase. During the experimental assembly, the thread compound used to lower the coefficient of friction is being compressed before the threads are fully engaged. Since this compound is not taken into account during the FE simulations, the strains obtained by simulating a certain number of make-up turns are slightly higher than in reality. In this case, the offset between the numerical and experimental handtight plane appeared to be approximately 0.1 turns. Apart from the absence of thread compound, the effect of taper mismatch is visible as well. It can be seen that higher strains were generally predicted at the outer surface of the box. Due to the initial taper mismatch, initial contact is established near the tip of the box (slow box combined with a fast pin). When assembling tapered connections, taper mismatch is very likely to happen. Despite being common, this is a very complex matter since this mismatch is not uniform over the entire threaded connection. Since make-up is modelled using a uniform overlap rather than a sequence of individual tapers, a realistic taper mismatch cannot be modelled using the developed model. Due to this limitation, only the assumed numerical overlap at the location of initial contact is a correct assumption for a given make-up position. For the other part of the threaded contact, the used overlap is an overestimation compared to the reality and causes an overestimation of the occurring hoop strains. From the figure, it is visible that the overestimation of overlap is roughly one tenth of a turn near the beginning of the threaded contact area (between a distance of 20 mm and 50 mm on the box outer surface). In between, the overestimation gradually decreases. It should be noted that realistically modelling taper mismatch using 2D axi-symmetric is nearly impossible because of the uncertain and variable amount of overlap that should be used over the entire section.

7.1.3 Contact pressure

It was pointed out in Chapter 3 that the primary source of heat was caused by frictional energy since the region containing the maximum temperature increase did not coincide with the region containing the maximum deformation.

The frictional force at every location along the contact can be calculated using the following equation:

$$F_f = 2\pi \sum_{i=0}^{n} r_i \, \mu_i \, p_{c,i} \, s_i \qquad \text{(Eq 4.23)}$$

Within this formula, the coefficient of friction is contact pressure dependent and can vary for every element. The experimentally determined thermal data after make-up is shown in Figure 4-24 together with the average contact pressures at the root flanks calculated by the numerical model. The average contact pressure was determined by dividing the total contact force per length by the contact length. When the contact force was determined, the pressure spikes in the first and last element of the contact (see section 3.3.3) were omitted from the equation. From this figure, it is observed that the region of maximum average contact pressures corresponds with the area of maximum temperature increase. Despite the matching of the overall region, the maximum of both areas do not correspond. In an effort to resolve this issue, a preliminary, thermal study is discussed in Chapter 7.

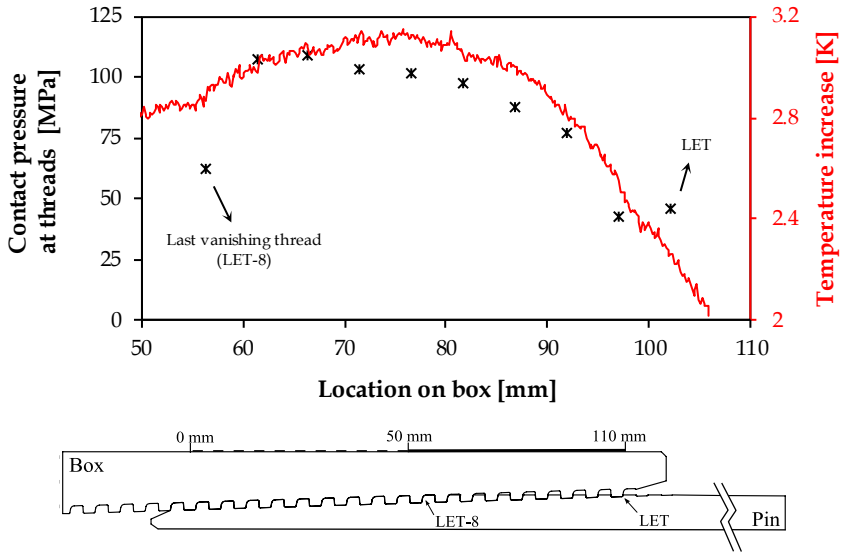

Figure 4-24: Measured temperature increase and numerically determined average contact pressures near the vanishing threads

7.2 Test load envelope

7.2.1 Strains

It was concluded in Chapter 3 that the data obtained by digital image correlation was less accurate compared to the data obtained using strain gauges because of the combination of the relatively high tolerance of DIC compared to the strain gauges and only limited, elastic strains were induced during TLE testing. For this reason, only the strain gauge data is compared with the numerically obtained strain values. The strains predicted by the finite element model for the various locations of the strain gauges applied to the

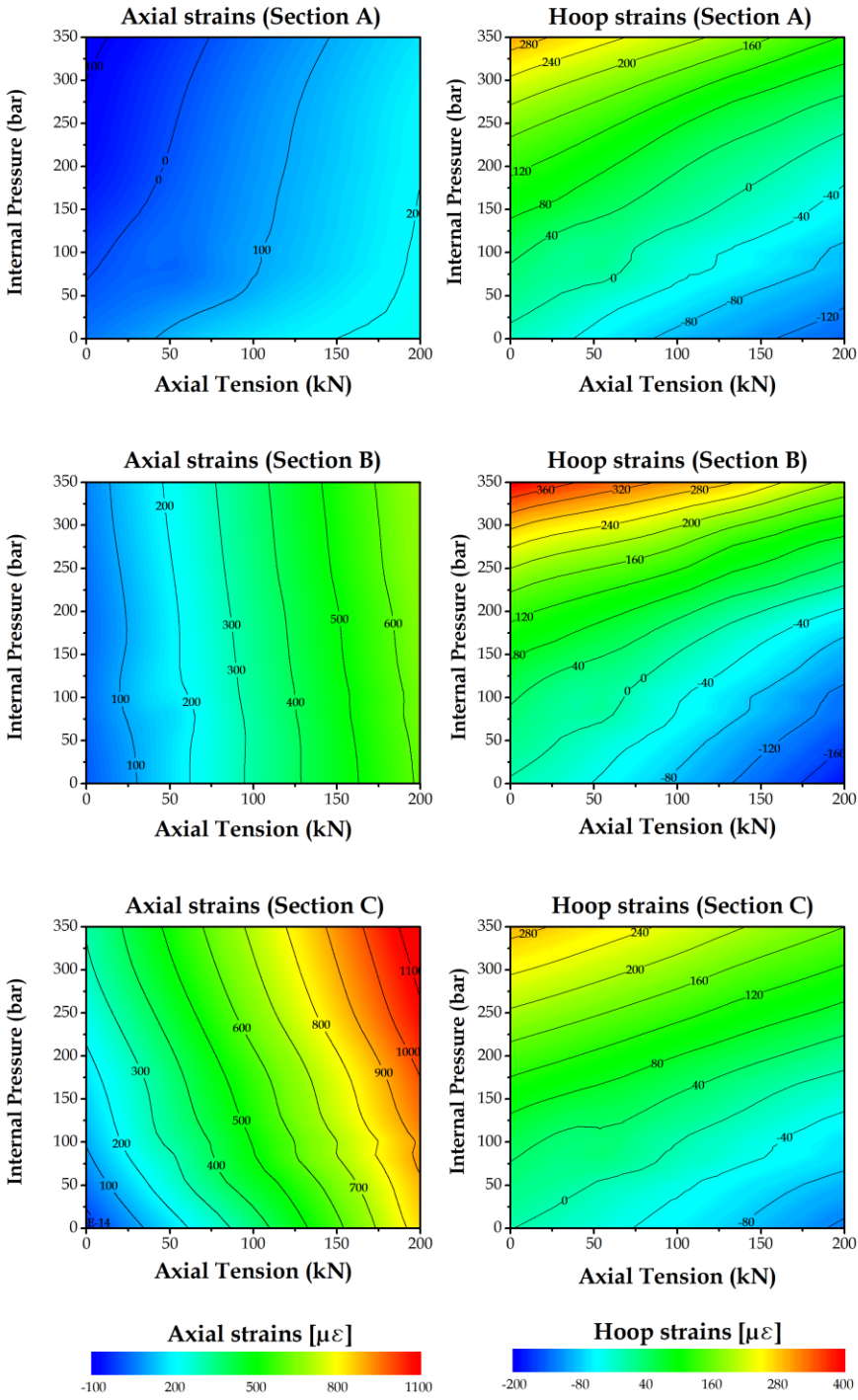

Figure 4-25: Results of axial and hoop strains using FEA

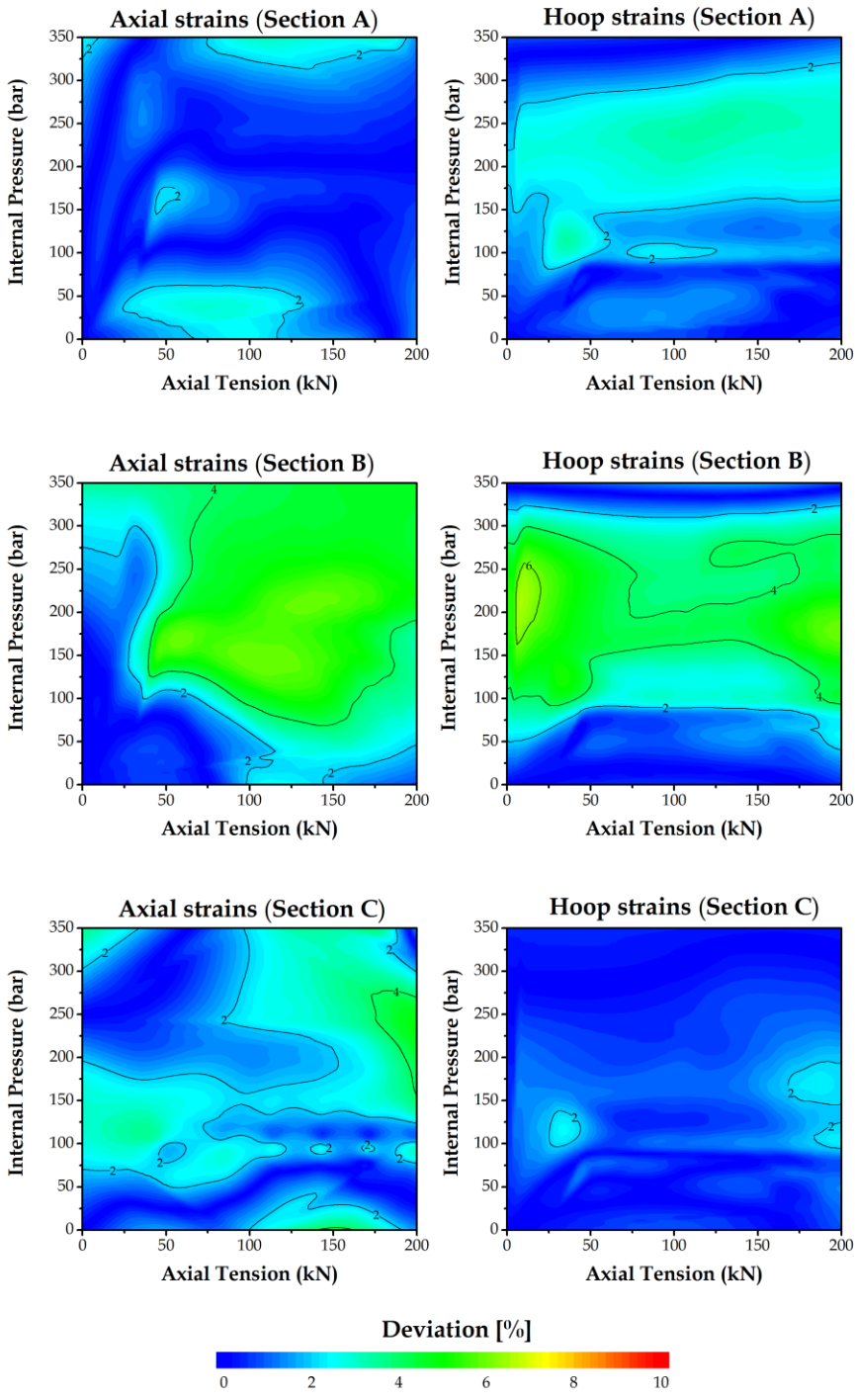

Figure 4-26: Deviation [%] between FEA and measured strain gauge data.

tested connection are given in Figure 4-25. These results were obtained by running five simulations using different load paths after applying a 0.7 turns make-up. The simulated load paths are schematically illustrated in the diagram containing the results for the axial strains of section A in Figure 4-25. The data was further interpolated using the thin plate spline technique in order to determine a best estimate of the situations with other combinations of internal pressure and axial tension. Axial strain increases when axial loading is increased and a slight increase is also noticeable when internal pressure increases. The latter can be explained by the fact that the internal pressure on the end caps induces a significant axial load, up to about 80kN when 350 bar is applied (see Chapter 3). Therefore, the axial tensile force applied in the numerical model was calculated according to the equation below.

$$F_{FEA} = F_{EXP} + p * \frac{ID^2}{4}\pi \qquad \text{(Eq. 4.24)}$$

Overall, a good correspondence between numerical and experimental results can be observed as illustrated in Figure 4-26. Using the normalized strains (see Chapter 3), deviations less than 7% or 105 με are observed. Taking into account commonly used design factors ranging up to 30% (see Chapter 2), deviations in the location of the strain gages, uncertainties of the model,… these deviations are considered acceptable.

Furthermore, the results obtained during this study suggest that the proposed methodology to link the experimentally measured make-up to the numerically predicted make-up is plausible and that the suggested approach can be used to conduct representative numerical research including make-up.

7.3 Tensile limit load test

7.3.1 Force versus displacement curve

Using the finite element model, the force-displacement curve of the tensile fracture test can be recreated. The results have been obtained using a reduced contact approach (see Appendix B). When comparing both curves, three differences have to be addressed. First of all, there is a small mismatch in the initial slope between the numerical prediction and the experimental when axial displacement starts. The reduced slope measured during the experiment is probably caused by the existence of initial play between the thread flanks which is gradually resolved. A second difference which is observed from the simulation results is the absence of the irregular shape observed in the experimental curve between axial displacements of 2 mm and 6 mm. This is caused by the contact definition which is being used and further addressed in Appendix B. A last difference is the increasing difference between the curves starting at an axial displacement equal to 11 mm. The maximum force that can

be resisted by the connection is only an approximation because the maximum strains which are experimentally determined are exceeded and damage is not included in the material properties. From an axial displacement of 11 mm onwards, the quantitative accuracy of the model cannot be guaranteed.

As mentioned previously in section 3.4.4, it is decided to use the material characteristic alpha to be 0.5 based on this force displacement curve. When a too low value is taken (alpha = 0), the pin is too weak and fails too early (around 16mm axial displacement in this case). In contrast, when the value is taken too high, the simulations do not converge. Worth mentioning is that the maximum force the connection can withstand is not affected by this value.

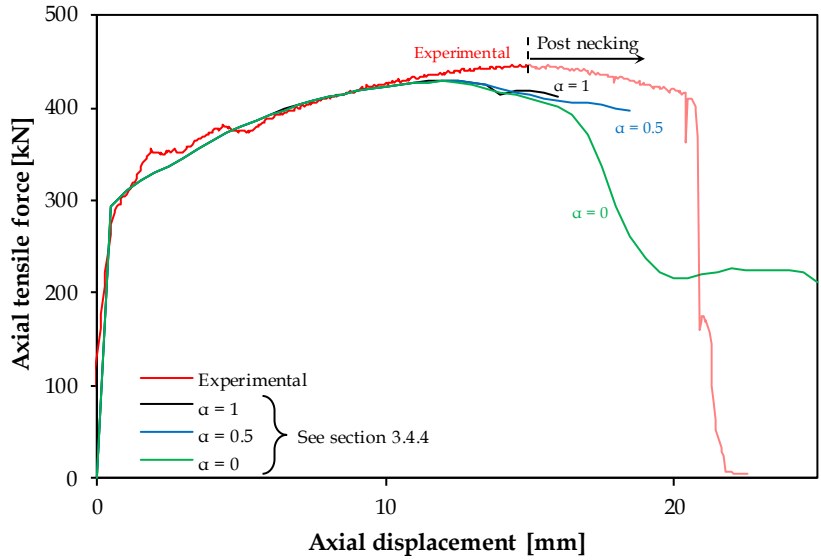

Figure 4-27: Numerically predicted and experimentally determined force-displacement diagram for a tensile limit load test

7.3.2 Comparison of strains

A failure test is in this thesis defined as a tensile test till mechanical failure. Applying axial loads leading to failure requires the introduction of criteria within the material definitions. Since these criteria are not within the scope of this research, the entire fracture test cannot be simulated at this point. Local failure or excessive plasticity leading to localized jump-out at the vanishing threads can be estimated by modifying the contact area of the threaded coupling (see Appendix B for more details). Based on the latter approach, the axial strains are recalculated and together with the experimentally determined results of the external axial strains at the box are illustrated in Figure 4-28. Within this figure, the axial strains are limited to the region directly in front of and behind the pin tip. The reason for this is that the axial strains between 60 mm and 120 mm (see Figure 4-28) are very limited due to localized jump-out.

Following the numerical results combined with knowledge of the failure surface, it is found that most of the vanishing threads show signs of local jump out as the result of excessive plastic deformation (see Chapter 3). This results in a quasi-independent behavior when axial loads are applied since the critical section of the box is located directly at the pin tip and almost no load transfer takes place through the vanishing threads. In order to compare both sets of data, the absolute differences between the axial strains are normalized by the experimentally determined fracture strain of the material of the box which is 14.38%. These results can be found in Figure 4-29. Based on these results, four zones with considerably higher deviations (above 5%) are detectable. While the deviations from zones I and II are considered acceptable as a result of unknown or incomplete variables such as local material characteristics, the ones observed in zones III and IV are considered substantial. The third zone, located above the first engaged thread, starts when the numerical calculation predicts necking of the box. Since the zone where necking (characterized by the location of maximum axial strain) occurs is very limited, the slightest axial deviation causes an increased deviation. Based on the results in Figure 4-28, the decrease in axial strains seems to be less steep in reality compared to the strains predicted. A possible reason for this offset is that the numerical strains reach their experimental strain limit in the box material (15.47% strain) at the inner surface near the threads. Similar to this assumption, the deviations of zone IV can be explained. Once an axial displacement of 11% is reached, the pin material reaches its experimentally determined maximum stress over the entire pin section. When higher displacements are applied, theoretically

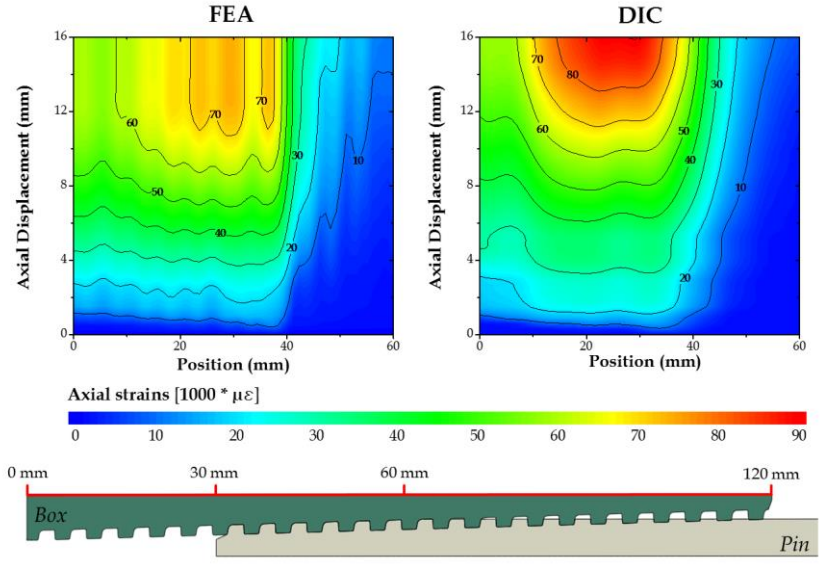

Figure 4-28: Axial strains obtained using FEA and DIC.

determined values are used and these assumptions (see section 3.4.4) are reflected in the strains measured in the critical section of the box. Overall, taking into account the reasons for the zones incorporating deviations higher than 5%, it can be concluded that the developed model can be used to cautiously predict the overall behavior of the connection although the model was originally not designed to simulate excessive plastic deformations and/or fracture loads.

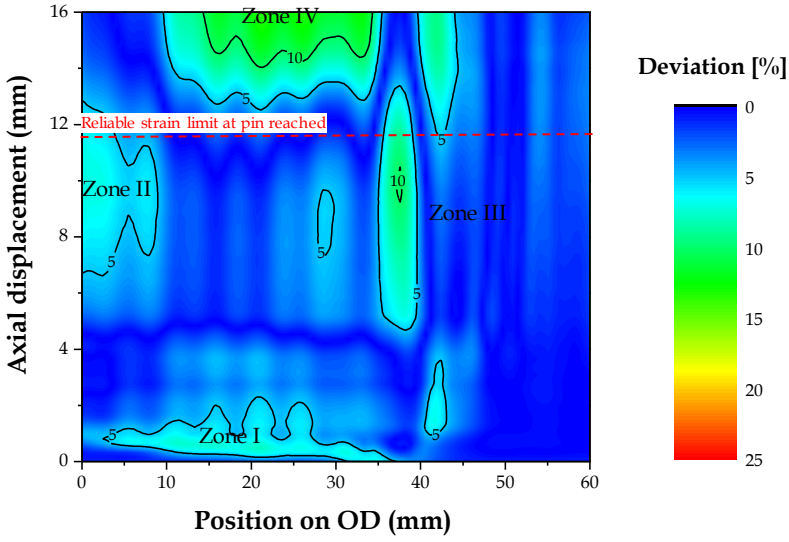

Figure 4-29: Deviation between DIC and FEA normalized by the fracture strain.

7.3.3 Indirect validation using thermal energy

In contrast to the make-up stage, energy is induced by plastic deformation rather than friction during the limit load test. This assumption can be investigated by linking the plastic energy of the connection to the observed thermal measurements at the outer surface of the box. In Figure 4-30, the top part represents the temperature as observed at the outside of the box while the lower part represents a section view of the plastic energy density in the connection. Assuming that higher plastic energy density results in a higher temperature increase at the outer surface on the box explains the location of the maximum temperature observed. This critical section is located directly above the point where the pin starts to neck.

It should be mentioned that a lot of heat appears to be transferred through a non-contacting area near the tip of the box. This is not entirely true since the simulation only shows the situation at a certain point. The unzipping of the

threads is preceded by shear failure and plastic deformation of the incomplete threads, causing surfaces for the generation and transfer of heat. Because of the use of a reduced contact surface, the plastic deformation at the majority of the vanishing threads cannot be observed in this figure.

An effort to provide better insights in the temperature distribution, generation and evolution can be found in Chapter 7.

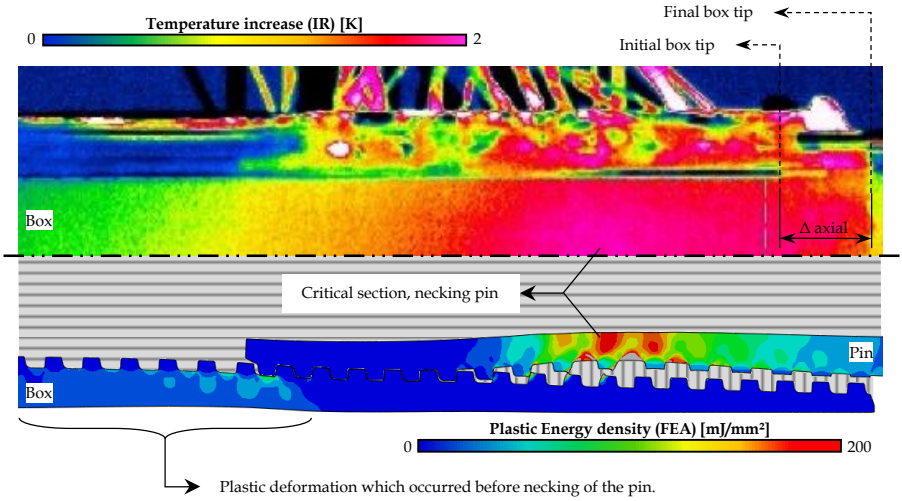

Figure 4-30: Measured temperature in combination with the numerical plastic energy density after necking of the pin

8 Conclusions

Within this chapter, an overview was provided focusing on the possibilities using numerical finite element models. Based on a comparison between a realistic but coarse meshed 3D model (see Appendix A), including the thread helix, and a densely meshed 2D axi-symmetric approximation of the same connections, the latter approach proved to be sufficient when examining threaded connections. The 2D modelling methodology was validated using the experimental results obtained in Chapter 3 and considered reliable. When loads exceeding the yield strength are applied, local failure of threads should be considered (see Appendix B)

Even when no helix is included, it was shown to be possible to estimate the required amount of make-up torque by combining the contact pressure, the contact pressure dependent coefficient of friction of the applied thread compound and the internal energy of the connection.

With the objective of comparing the behavior of threaded connections subjected to initial make-up and combined workloads, three output

parameters are defined and will be used to investigate new and existing connections:

- Total amount of plastic energy
- Thread clearance along the thread flanks
- Axial and radial load distribution

References

[4.1] Asbill, W.T., Pattillo, P.D. and Rogers, W.M., *Investigation of API 8 Round Casing Connection Performance – Part I: Introduction and Method of Analysis*, Journal of Energy Resources Technology, 106(1), pp. 130-136, 1984

[4.2] Kristens, A.S., Toor, K., and Solem, S., *Finite Element Analysis of Jar Connections: Modeling considerations*, Special Issue for the 18th TH Nordic Seminar on Computational Mechanics, 2005

[4.3] Yuan, G., Yao, Z., Wang, Q., and Tang, Z., *Numerical and Experimental Distribution of Temperature and Stress Fields in API Round Threaded Connections*, Engineering Failure Analysis, 13(8), pp. 1275-1284, 2006

[4.4] Dvorkin, E.N., and Toscano, R.G., *Finite element Models in the Steel Industry: Part II: Analysis of Tubular Products Performance*, Computers & Structures, 81(8), pp. 575-594, 2003

[4.5] Zhong, A., *Thread Connection Response to Critical Pressure*, Abaqus Users' Conference, Paris, france, pp. 690-706, 2007

[4.6] Yuan, G., Yao, Z., Han, J. and Wang, Q., *Stress distribution of oil tubing thread connection during make and break process*, Engineering Failure Analysis, 11(4), pp. 537–545, 2004

[4.7] Chen, S., Li, Q., Zhang, Y. and An, Q., *Finite element analysis of tooth load distribution on P-110S conic threaded connections*, International Journal of Pressure Vessels and Piping, 88(2-3), pp. 88–93, 2011

[4.8] Assanelli, A.P., Xu, Q., Benedetto, F., Johnson, D.H. and Dvorkin, E.N., *Numerical/Experimental Analysis of an API 8-Round Connection*, Journal of Energy Resources Technology, 119(2), pp. 81-88, 1997

[4.9] Van Wittenberghe, J., De Baets, P. and De Waele, W., *Nonlinear Contact Analysis of Different API Line Pipe Coupling Modifications*, Journal of Pressure Vessel Technology, 132(5), 2010

[4.10] Assanelli, A.P. and Dvorkin, E.N., *Finite element models of OCTG threaded connections*, Computers & Structures, 47(4–5), pp. 725–734, 1993

[4.11] Kawashima, H., *Effect of incomplete threads on the jump-out tensile failure of premium connections for oil and gas wells*, JSME International journal, series I, 33(1), 1990

[4.12] Xie, J., and Tao, G., *Analysis of casing connections subjected to thermal cycle loading*, Simulia customer conference, 2001

[4.13] Bahai, H., and Esat I.I., *A hybrid model for analysis of complex stress distribution in threaded connectors*, Computers & Structures, 52(1), pp. 79–93, 1994

[4.14] Chen, J., and Shih, Y., *A Study of the Helical Effect on the Thread Connection by Three Dimensional Finite Element Analysis*, Journal of Nuclear Engineering and Design, 191, pp. 109-116, 1999

[4.15] Shahani, A. R., and Sharifi, S. M. H., *Contact Stress Analysis and Calculation of Stress Concentration factors at the Tool Joint of a Drill Pipe*, Materials and Design, 30, pp. 3615-3621, 2009

[4.16] Sches, C., Desdoit, E. and Massaglia, J., *Fatigue resistant Threaded and Coupled Connectors for Deepwater Riser Systems: Design and Performance Evaluation by Analysis and Full Scale Tests*, Proceedings of the 27th International Conference on Offshore Mechanics and Arctic Engineering - 2008, 5, pp. 407-420, 2008

[4.17] API specification 5B, *Specification for Threading, Gauging, and Thread Inspection of Casing, Tubing and Line Pipe Threads*, American Petroleum Institute, 1996

[4.18] Rivero, G.J., Dunn, T.E., and Parker, C.W., *Position make-up indicator system*, United States Patent, US 20120210552 A1, 2012

[4.19] Chen, J., and Shih, Y., *A Study of the Helical Effect on the Thread Connection by Three Dimensional Finite Element Analysis*, Nuclear Engineering and Design, 191, pp. 109-116, 1999

[4.20] Jaurrieta, M. A., *Explicit FE Simulations of Large-scale Tests on Beam-to-RHS Column Connections*, Tubular Structures X: Proceedings of the 10th International Symposium, pp. 511-518, 2003

[4.21] Abaqus 6.12, *Abaqus Manual, 38.1.1 Contact formulations in Abaqus/Standard*, 2012

[4.22] King, S., and Richards, T., *Solving contact problems with abaqus*, DS UK Ltd. Coventry, 2013

[4.23] Norton, R.L., *Machine design an integrated approach*, 2nd edition, pp. 573-578, 2000

[4.24] Santus, C., *Fretting fatigue of aluminum alloy in contact with steel in oil drill pipe connections, modeling to interpret test results*, International Journal of Fatigue, 30, 4, pp 677-688, 2008

[4.25] Beghini, M., and Santus, C., *Analysis of plane contact with discontinuous curvature*, Meccanica, 42, pp 95-106, 2007

[4.26] www.3ds.com, Dassault Systèmes, Confidential Information, 18/03/2013 ref.: 20100928MKT038

[4.27] Dini, D., and Hills, D.A., *Bounded asymptotic solutions for incomplete contacts in partial slip*, International journal of solids and structures, 41, pp 7049-7062, 2004

[4.28] Araújo, J.A., and Nowell, D., *The effect of rapidly varying contact stress fields on fretting fatigue*, International journal of fatigue, 24, pp 763-775, 2004

[4.29] Araújo, J.A., Susmel, L., Taylor, D., et al., *On the use of the theory of critical distances and the modified Wöhler curve method to estimate fretting fatigue strength of cylindrical contacts*, International journal of fatigue, 29, pp 95-107, 2007

[4.30] Ding, J., Sum, W.S., Sabesan, R., et al., *Fretting fatigue predictions in a complex coupling*, International journal of fatigue, 29, 7, pp. 1229-1244, 2007

[4.31] Taylor, D., *Geometrical effects in fatigue: a unifying theoretical model*, International journal of fatigue, 21, pp. 413-420, 1999;

[4.32] Taylor, D., and Wang, G., *The validation of some methods of notch fatigue analysis*, Fatigue and fracture of engineering materials and structures, 23, pp. 387-394, 2000

[4.33] Nowell, D., Dini, D., and Hills, D.A., Recent developments in the understanding of fretting fatigue, Engineering fracture mechanics, 73, pp. 207-222, 2007

[4.34] Hills, D., and Dini, D., *A new method for the quantification of nucleation of fretting fatigue cracks using asymptotic contact solutions*, Tribology international, 39, pp. 1114-1122, 2006

[4.35] Hills, D., and Dini, D., *The use of asymptotic solutions in fretting fatigue*, ECF15, 2004

[4.36] Dundurs, J., and Lee, M.S., *Stress concentration at a sharp edge in contact problems*, Journal of elasticity, 2, 2, 1972

[4.37] Charchman, C., Mugadu, A., and Hills, D.A., *Asymptotic results for slipping complete frictional contacts*, European Journal of Mechanics - A/Solids, 22, 6, pp. 793-800, 2003

[4.38] Giannakopoulos, A.E., Lendley, T.C., and Suresh, S., *Aspect of equivalence between contact mechanics and fracture mechanics: theoretical connections and a life-prediction methodology for fretting-fatigue*, Acta materialia, 46, 9, pp. 2955-2968, 1998

[4.39] Jagadish, R., *A Computational Investigation of Contact Pressure for a Non-pneumatic Wheel with a Meta-material Shear Band*, doctoral thesis, 2010

[4.40] Strang, G., and Fix, G.J., *An Analysis of the Finite Element Method*, Prentice-Hall, Inc., 1973

[4.41] Strang. G., *Introduction to Applied Mathematics*, Wellesley-Cambridge Press, 1986

[4.42] Simulia, *Error indicator output*, Abaqus Analysis User's Guide, 2013

[4.43] Van Wittenberghe, J., *Experimental analysis and modelling of the fatigue behaviour of threaded pipe connections*, doctoral thesis, 2011

[4.44] VAM-USA, *VAM TOP make-up Specifications*, internet: <http://www.vam-usa.com>, accessed 11/12/2014

[4.45] Ling Y. *Uniaxial true stress-strain after necking*, AMP Journal of technology, 5, 1996

[4.46] Teodoriu, C., *Rotary-Shouldered Connections Make-up Torque Calculation Considering the Effect of Contact Pressure on Thread Compound's Friction Coefficient*, OIL GAS European Magazine, 4, pp. 172-178, 2009

[4.47] American Petroleum Institute, *API RP 5A3: recommended practice on thread compounds for casing, tubing, line pipe, and drill stem elements*, third edition, 2011

[4.48] American Petroleum Institute, *Test data from API E&P SC5 Work Item 1033 – "Thread Compound Research"*

[4.49] Miller, R.A.Jr. and Thornton, D.M., *Port Thread*, United States patent, US4033615, 1977

[4.50] Sugino, M. and Yamamoto, M., *Threaded Connection Tubular Goods*, United States patent, US6045165, 2000

[4.51] DeLange, R.W., Evans, M.E., Costa, D.S. and Eason, R., *Threaded Connection with High Compressive Rating*, United States Patent, US6581980B1, 2003

[4.52] Yamamoto, M. and Sugino, M., *Threaded Connection for Oil Country Tubular Goods and its Method of Manufacturing*, United States Patent, US6237967, 2001

[4.53] Gillot, L., Verger, E. and Tartar, O., *Threaded Element on a Component with Opposed Threading Portions and Corresponding Tubular Threaded Connection*, United States Patent, US8220844, 2012

[4.54] Milberger, L.J. and Radi, A., *Evolution of Metal Seal Principles and Their Application in Subsea Drilling and Production*, Offshore Technology Conference, OTC 6994, 1992

[4.55] National Aeronautics and Space Administration, *Design Criteria for Zero-Leakage Connectors for Launch Vehicles. Vol2, Leakage Flow*, NASA NAS 8-4012, 1963

[4.56] National Aeronautics and Space Administration, *Advance Valve Technology*, NASA SP-5019, 1965

[4.57] ISO specification 13679, *Petroleum and Natural Gas Industries – Procedures for Testing Casing and Tubing Connections*, European Committee for Standardization, 2006

[4.58] Rathburn, F.O., *Experimental Leakage Rate Experiments*, Advanced Technology Laboratories, General Electric Company

[4.59] Weiner, R.S., *Basic Criteria and Definitions for Zero Leakage Fluid, Technical Report No. 32-926*, Jet Propulsion Laboratory, 1966

[4.60] Lvovsky, O. and Grayson, C., *Aerospace Payloads Leak Test Methodology*, ARES Corporation, 2010

[4.61] TCPO, *TP-CQ Premium Connection*, Datasheet, internet: <http://www.tpcointernational.com>, accessed 11/12/2014

[4.62] Asbill, W.T., Pattillo, P.D. and Rogers, W.M., *Investigation of API 8 Round Casing Connection Performance – Part III: Sealability and Torque*, Journal of Energy Resources Technology 106(1), 144-152, 1984

[4.63] Watts, J.D. and Ramos, B.W., *Wedgethread Pipe connection*, United States Patent, US 6682101B2, 2004

[4.64] Kielminski, W., *Pipe coupling connection sealing apparatus*, United States Patent, US4579831, 1987

[4.65] Reynolds, H., *Downhole threaded connection with scalloped wedge threads*, United States Patent, US7717478B2, 2010

[4.66] Frame, W.M., *Leak-resisting pipe thread*, United States Patent, US2177100A, 1938

[4.67] Sopwith, D.G., *The Distribution of Load in Screw Threads*, Proceedings of the Institution of Mechanical Engineers, 159(1), pp. 373-383, 1948

[4.68] Stoeckly, E. E., and Macke, H. J., *Effect of Taper on Screw-Thread Load Distribution*, Transactions of ASME, 74, pp. 103-112, 1952

[4.69] Wang, W., *Determination of load distribution in a threaded connector with yielding threads*, Mechanism and Machine Theory, 31(2), pp. 229-244, 1996

[4.70] Liao, R., Sun, Y., and Zhang, W., *Nonlinear Analysis of Axial-load and Stress Distribution for Threaded Connection*, Chinese Journal of Mechanical Engineering, 22(6), pp. 869-875, 2009

[4.71] Bahai, H., *A parametric model for axial and bending stress concentration factors in API drillstring threaded connectors*, International Journal of Pressure Vessels and Piping, 78(7), pp. 495–505, 2001

[4.72] Xu, H., Shi, T., Zhang, Z., et al., *Loading and contact stress analysis on the thread teeth in tubing and casing premium threaded connections*,

Mathematical problems in engineering, http://dx.doi.org/10.1155/2014/287076, 2014

[4.73] Assanelli, A. P., and Dvorkin, E. N., *Finite Element Models of OCTG Threaded Connections*, Computers & Structures, 47(4), pp.725-734, 1993

[4.74] American Petroleum Institute, *API RP 5A3: Recommended Practice on Thread Compounds for Casing, Tubing, and Line Pipe*, American Petroleum Institute, 1st edition, 1996

Chapter 5

Parametric study using ThreadGenBT

<< *This page intentionally left blank* >>

Table of Contents

1 Introduction

The parametric study described in this chapter is based on an extensive study using finite elements. In Section 2, the effects of make-up are analyzed and a minimum and maximum make-up position are suggested which will be taken into account when studying the effects of additional parameters in the following sections and the next chapter. While this section also gives a clear overview of the capabilities of ThreadGenBT using a load flank angle modification, Section 3 investigates the effect of the global parameters. These parameters are defined as the parameters defining the overall shape of the connection, excluding the thread geometry.

For every geometry, four different load paths are applied in order to cover the extremes of the first quadrant of the VME ellipse (see Chapters 3 and 4). The performance parameters defined in Chapter 4 are quantified for all load paths up to the connection's yield strength using increments of 10%. In addition, the results for a combined load equal to 95% of the pipe body strength are discussed. In total, around 1600 simulations were performed to gather all data required for this parametric study.

2 Principles of make-up

As mentioned in previous chapters, an initial preload, defined as make-up, is applied when tapered threaded specimens are being assembled. Since the behavior of the connection is highly dependent on this preload, a thorough understanding of this make-up stage is desirable. In essence, make-up can be compared with a press fit of a gear on a shaft. When assembling a tapered connection, the box is radially pushed outwards, while an opposite force acts on the pin as is indicated in Figure 5–1. This way, the pin comprises negative hoop strains while the box is subjected to positive hoop strains.

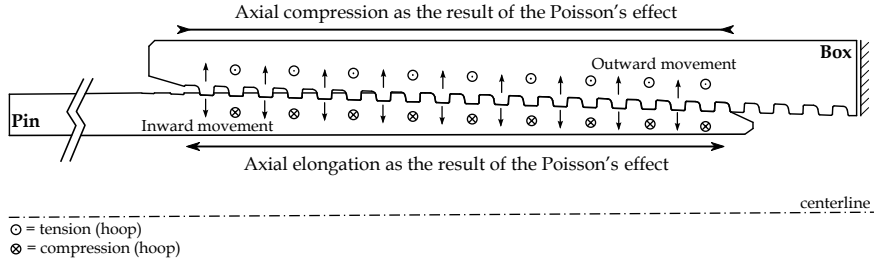

Figure 5–1: Schematic overview of the effect of make-up on the hoop, radial and axial strain distribution in the connection.

2.1 Plasticity

In order to determine an upper and lower limit defining the optimal make-up range, it is suggested to use the total energy outputs of the numerical model. Both the model's plastic and elastic energy are plotted in Figure 5–2 together with an approximation of the friction independent holding torque (CTRQ). Within this figure, a distinction is made between three different regions. The middle region represents the advised make-up range, marked 'Make-up target', while the other two zones represent inappropriate make-up positions for distinct reasons. The zone containing the lower torque values represents the make-up conditions in which excessive axial play is still present, easily allowing relative axial movement leading to leakage. The zone containing the higher values is unfit because of excessive plasticity, limiting the ability of reusing the connection components.

The upper limit is established using the plastic energy curve. This curve can be divided into two different regimes with a transition area in between as mentioned in Chapter 4. After calculating where the linear approximation representing global plasticity intersects the X-axis, an upper limit of approximately 1.77 turns can be found. This position also matches the condition where the elastic energy is starting to saturate after applying a similar approach. Using this elastic energy curve, an S-shaped curve can be recognized. This shape indicates that there is no linear relation between applied make-up and resulting elastic energy. While this is evident for the cases exceeding the upper limit due to the introduction of global plasticity, this is anticipated for the lower make-up positions when assuming similar conditions as when applying a press fit. The reason for this deviation is the existence of initial play. In order to ensure a crest-root contact along the thread, axial play between stab and/or load flanks is required. During make-up, not only a radial expansion is induced, but also a relative axial shift as the result of axial changes caused by the Poisson's effect (see Figure 5–1). This mechanism is further explained in section 2.3 but for now, it is assumed that the location where the linear approximation of the middle part of the elastic strain curve intersects the X-axis indicates the lower limit of the desired make-up region. For the example used, a lower limit of 0.57 turns can be found. This point also marks the onset of local plasticity at the vanishing threads, which is considered inevitable and is indicated by a slight increase of plastic energy. Referring to Figure 5–2, it can be seen that the suggested make-up region is reduced using an additional shift of the suggested upper torque limit. This shift takes into account the additional energy induced by the working loads. When a connection is stressed to its limits during make-up, it is impossible to resist any external forces without deforming plastically. It should be mentioned that the limits obtained by using linear trends as mentioned above should be handled with care. While the defined limits can be explained using numerical data, the results of this approach are not exact and a certain margin

of safety should be considered when applied on actual connections. Therefore, the exact make-up target should be chosen to be near the middle of this interval, or at least including a sufficiently high margin of safety which is established using experimental data. In addition, it is important to mention that while the upper limit is obligatory, the lower limit is optional. This limit does not represent an actual lower limit related to use in the field, but shows the minimum position at which the actual play is removed. It is possible that for practical use, a certain torque value requiring a make-up position exceeding the suggested lower limit is required to prevent disassembly of the string during installation.

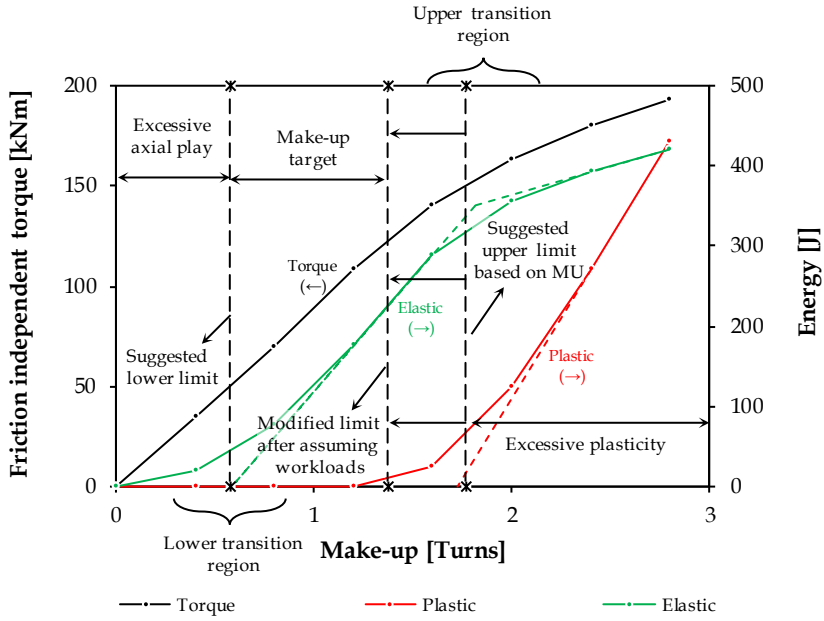

Figure 5–2: Holding torque together with both elastic and plastic deformation energy for make-up positions up to 2.8 power turns for a 114.3 mm (4.5 inch), grade B connection.

2.2 Load distributions

An important parameter which is commonly investigated in threaded connections is the load distribution over the engaged threads. When considering the load distribution in trapezoidal threaded connections, it is important to make a distinction between the axial and radial load distributions. By applying a certain amount of initial make-up and load combinations, these distributions are altered.

The objective of applying power turns to a connection is to hold the joint together using an induced radial force. The radial load distribution, given in

Figure 5–3, provides insights in the distribution of this clamping load. From this graph, it can be observed that a fairly even distribution with a slight increase near the vanishing threads is obtained for all make-up positions. In all cases, three threads (LET(-1), LET-9 and LET-19) show significant increases. The increased values at the first and last threads are typical for tapered connections, comparable to the pressure spikes observed near the extremes of the contact flanks mentioned in Chapter 4. The middle thread (LET-9) represents the transition from complete to vanishing threads and is subject to an elevated radial force as a result of its unique, incomplete thread form which causes contact to exist on the root-, partial crest- and load flanks. In addition, the peak pressures along the surface near the transition from contact to no contact are included as well, causing a peak in the average contact pressure for the crest flank as is visible in Figure 5–4. The shift of maximum carried load at the beginning of the thread, from LET-1 for lower make-up positions to LET-0 for higher make-up positions, is caused by the additional thread in contact as a result of adding additional make-up rotations. While for low make-up positions only 18 threads are in contact, positions exceeding 1 make-up turn add an additional thread to their contact surface. Within this example, the threaded pin area consists of only 19 threads, representing the maximum possible number of engaged threads. When increasing the amount of applied make-up, a small overall relief of the complete threads is seen, with a significant decrease at the second engaged thread (LET-18). The reason for this decrease is explained later.

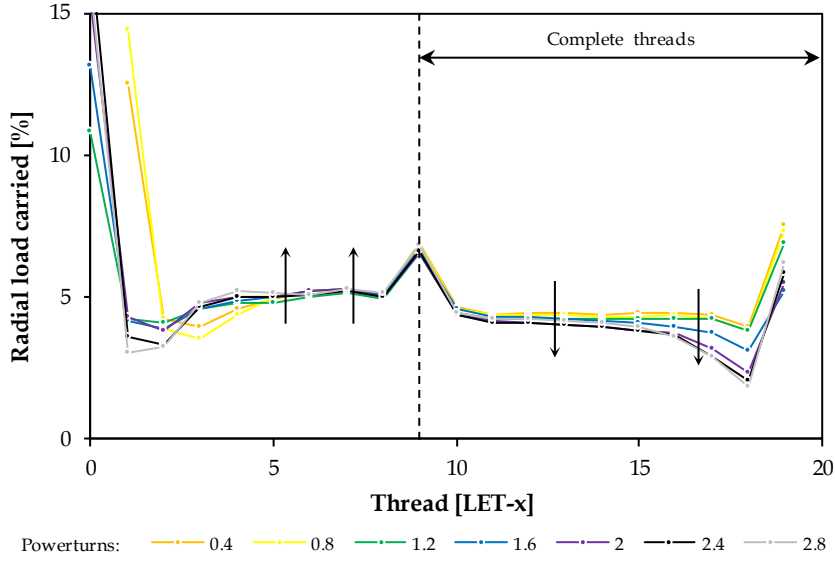

Figure 5–3: Radial load distribution for various make-up positions.

As expected, Figure 5–4 shows that the average contact pressure, defined as the contact force per length divided by the flank length, increases with increasing make-up turns for most of the threads. However, there is no linear relationship between make-up turns and contact pressure. Once the plasticity limit of 1.6 turns is reached, the incremental increase of contact pressure tends to reduce. While it is evident that an asymptotic limit for the average

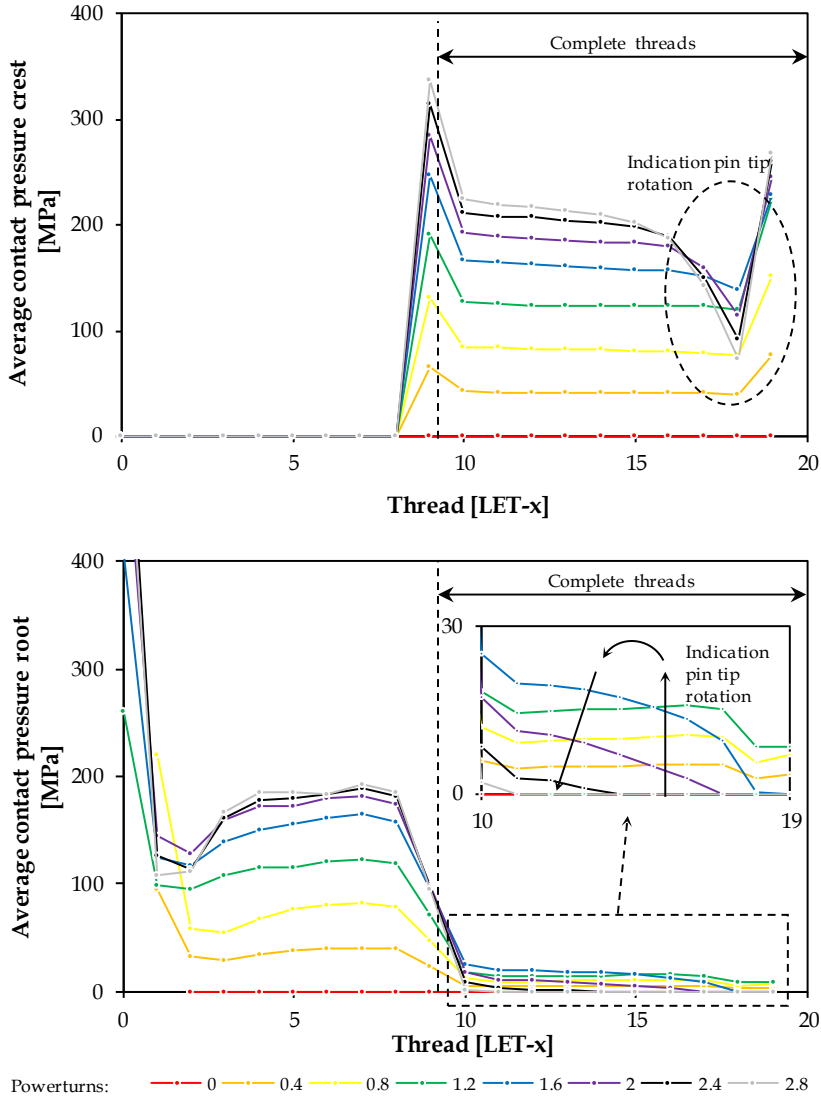

Figure 5–4: Average contact pressure on the crest and root flanks for make-up positions ranging from 0 to 2.8 power turns.

contact pressure exists, this does not explain why the average contact pressure decreases within the complete threads region near thread LET-18. This abnormality is caused by a rotation of the pin tip, which will be described in detail later. As a result of this rotation, both the contact pressure at the roots and crests in the affected area are reduced, eventually initiating separation. Within this region, contact pressures on the stab flanks show a significant increase (not shown in the figure).

Due to the stress state of the connection during make-up, it is not possible to make claims based on the axial load distribution using the axial stresses in the various sections as suggested in Chapter 4 when axial loads are applied. When the pin is radially shrunk due to the applied make-up, an axial elongation is initiated as a result of the Poisson's effect as was previously illustrated in Figure 5–1. However, this elongation does not induce any stresses when no boundaries limiting this displacement are encountered. While for low make-up levels such as 0.8 turns this movement is only restrained by the slight taper, causing low compressive stresses, high make up levels such as 2.8 power turns cause high compressive stresses in the pin tip due to the closed stab clearance while the majority of the axial strains in this member are still positive. For this reason, the average movement of the various thread sections is used to gather information about the behavior and deformation the pin, rather than the stresses.

Figure 5–5 gives an overview of the averaged, relative displacement of all sections associated with the threads (from LET through LET-19) at the middle of the root flanks. The dashed lines represent the various sections, while the full black lines represent the various make-up positions and a representation of the overall shape of the pin is provided. A fairly even elongation, quantified by considering the displacement of two succeeding sections, of the entire pin can be observed, regardless of the applied amount of make-up. This was to be expected based on the uniform radial load distribution mentioned earlier. Using the applied amount of make-up, two distinct regions can be observed which are separated by the line representing the condition of 1.6 make-up turns. This boundary approximates the previously found upper limit of the targeted make-up range. Prior to the 1.6 turns make-up position, the pin is stretched and pushed inwards. Since the section of the pin tip is smaller than the corresponding section of the engaged box, the pin is forced towards the pipe axis. Near the last engaged threads, a small negative axial displacement is observed. This displacement is caused by the contacting load flanks and indicates the likely occurrence of elastic deformation and even some, very limited, plastic deformation near these flanks. Once the upper torque limit is exceeded, drastic changes related to sectional displacement and deformation are observed. From the behavior of the first engaged thread, it can be observed that no significant axial movement is noticeable. This is caused by the closure of the gap located at the stab flank at the tip of the pin. Once 1.6 make-up turns

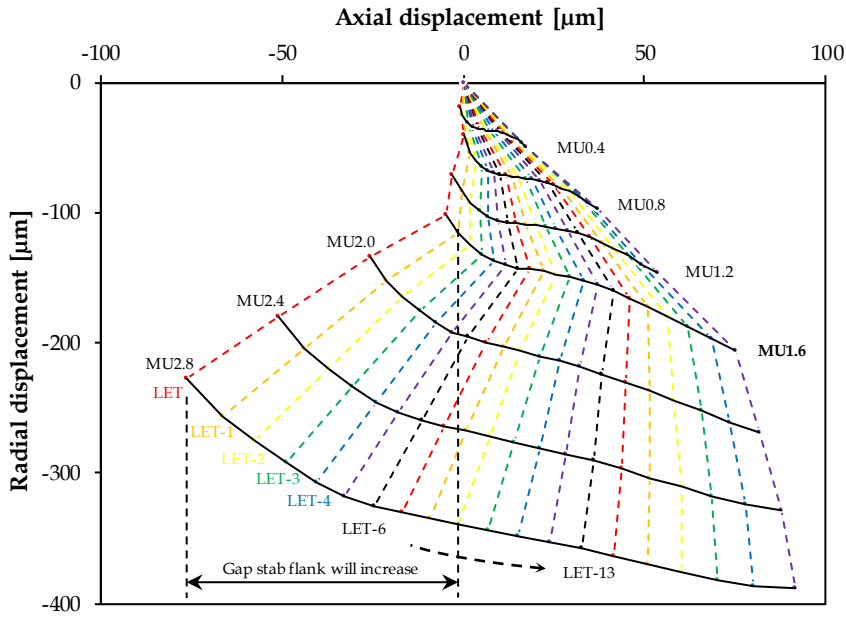

Figure 5–5: Average axial and radial displacements of the various axial sections, measured at the center of the root flank of the corresponding thread (see Figure 5–6).

are reached, the stab flanks make contact and the threads become locked, resisting the axial movement induced by the Poisson's effect. Consecutively, increasing axial compressive stresses are induced throughout the pin. As a result, additional elongation is forced at the opposite end. Since the load flanks of the vanishing threads are not fully formed, plastic deformation and even potential failure are initiated and cause the threads to lose engagement. Resulting from this local jump-out, the gap size at the stab flanks will further increase. An additional, subtle change can be observed near the pin tip at the first engaged thread (LET-19). The relative radial displacements compared to the following thread (LET-18) reduce. This indicates a local rotation of the pin tip, shown in Figure 5–6, as a direct result of the stab flank angle and the locking of the threads as is further explained in section 2.3.

When an external, axial tensile load is applied, the axial load distribution can be calculated using the method defined in Chapter 4. Figure 5–7 indicates that by increasing the level of make-up, a rotation of the load distribution can be found. This rotation takes place around the approximate location where the transition from vanishing threads to complete threads occurs. This means that by increasing make-up, the applied tensile load can be transferred from complete threads to vanishing threads. When sufficient make-up is applied, parts of the complete threads are not subjected to the applied axial tensile load,

creating a zone within the threaded area which is independent of the externally applied loads. This way, no excessive relative movement is present, resulting in a potentially suitable location for creating a reliable thread seal (see Chapter 1). Despite this advantage, additional make-up also increases the loads near the vanishing threads. This means that the maximum load in the vanishing threads increases together with the likeliness of local failure herein. In this case, the reliable applicability of the finite element methodology can only be assured when careful and sound judgment is incorporated and additional considerations may be required such as the ones previously described in section 9 of Chapter 4.

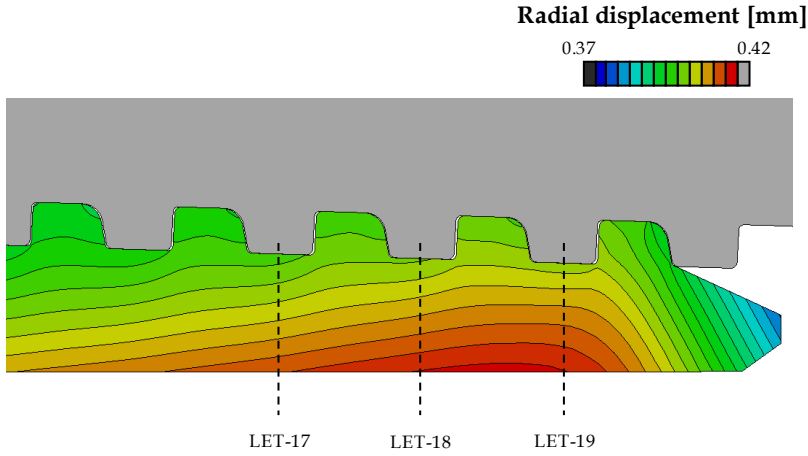

Figure 5–6: Rotation at pin tip as a result of contact at the stab flank.

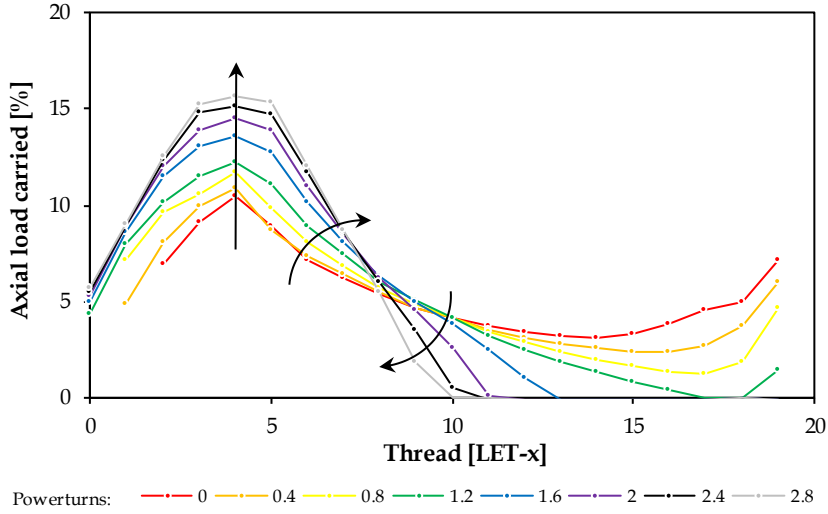

Figure 5–7: Axial load distribution after applying 95% pipe body load.

2.3 Gap size

It was mentioned earlier, in section 2.1, that the lower limit of the targeted make-up range does not allow axial play. In order to elaborate on this statement, it is required to consider the load flank and stab flank clearance of the three first and the three last engaged threads. These gap sizes are illustrated in Figure 5–8 and Figure 5–9 respectively. In addition to these two variables, the combined gap sizes are shown as well. The gap size per flank is calculated using the average value of the closest distance between every node from the appropriate pin-flank to the opposite, corresponding flank located on the box. The combined gap sizes per thread are then calculated using the mathematical summation of both values calculated at the load and stab gaps of every thread. While this value does not offer the exact axial gap size since the direction in which the flank clearance is defined slightly differs for the various flanks, it is considered to be a good approximation and sufficiently accurate for the objective of this study.

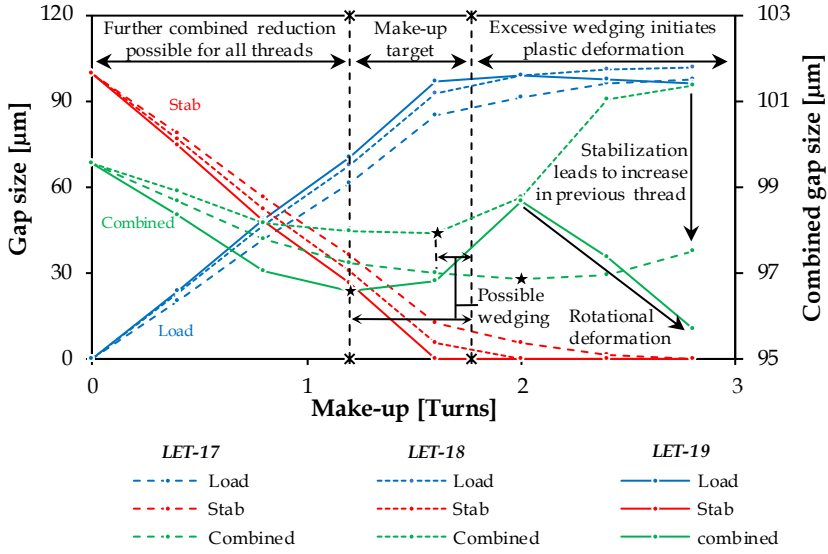

Figure 5–8: Overview of the gap sizes at the load flank, stab flanks and combined (load + stab flank gaps) of the first three threads.

Figure 5–8 represents the three threads located at the tip of the pin: the first engaged thread or LET-19 (densely dotted line), the LET-18 (full line) and the LET-17 (sparsely dotted line). For every thread, the average flank clearances at the load (blue) and stab (red) flank are given together with the combined values (green). In addition to the relationship between gap size and make-up turns, the defined torque regions (see section 2.1) are indicated as a reference. Using the average gap sizes between the various flanks, it can be observed that the clearances between the load flanks increase with increasing amount of

powerturns while the stab flanks show an opposite behavior. It is also noted that the magnitude of relative gap size decreases for both the load and stab flank when threads farther from the pin tip are considered. Due to the Poisson's ratio, this change is not linear with the distance between the considered thread and the pin tip. In general, a first, rapid change is observed up to about 1.6 make-up turns. From that position onwards, a reduced increase up to a certain value is noticed. This transition point is located within the aimed make-up zone and is caused by the closure of the gap size near the stab flank on the first thread. Once the clearance at this location disappears, the threads become wedged between the stab flank of the first engaged thread and the load flank of the last engaged thread. This means that further make-up without plastic deformation is hard to obtain. When applying further make-up, the pin is pushed inwards and elongates in axial direction due to its Poisson's ratio. Initially, a limited amount of elastic strain can be induced, but soon plasticity occurs at the pin tip, causing the total plastic energy to increase significantly (see Figure 5–2). This mechanism is also observed at the threads following the first engaged thread when make-up is increased. A similar tendency can be seen when assessing the combined gap sizes at the various threads. When monitoring the LET-18 and LET-17 threads, it can be seen that the combined clearance tends to stabilize once about 2.4 make-up turns are reached. From that point on, a slight increase caused by plastic deformation is visible. Once this position is reached, the axial clearance between the load flanks of the subsequent thread is removed and a similar tendency is observed, starting with the increase of the combined gap size. This indicates that the load flank generates an increasing amount of contact pressure on its flank due to the axial elongation. Based on the obtained results, it can be seen that, starting at 2 make-up turns, the combined gap size of the first engaged thread decreases. This is related to a decreasing gap size near its stab flank and is caused by a rotational movement in the pin tip itself. Once additional make-up turns are applied, the stab flank acts as a counter surface. Since this flank is oriented in an angle of 10 degrees, a force is generated towards the axis of the connection. This causes the pin tip to bend as was previously illustrated in Figure 5–6.

Finally, it can be observed that the minima of the combined gap sizes for all flanks, indicated by the black stars, occur just before the load flank closes. This difference is likely to be caused by the fact that the average opening between the flanks is considered, including the positions near the thread radii which are usually slightly larger. This deviation is less than 1µm and is not significant. The aim of this study is to provide numerical indications that when making up the connection to a position within the predetermined range, the overall axial play can be removed from the connection without introducing a significant amount of global, plastic deformation.

The existence of a wedging phenomenon can further be proven using the combined stab and load flank gap sizes of the last engaged threads. These

parameters are shown in blue and green in Figure 5–9 for the LET, LET-1 and LET-2. The various threads are represented by respectively the densely dotted, full and sparsely dotted lines. In this graph, it is observed that the load flanks maintain contact at all times. The combined gap size equals 100 µm when no make-up is applied. This value is inherent to the nominal geometry of the thread form as defined by the standard and can also be found in Figure 5–8 for the case without make-up. When make-up is applied, limited to no changes are observed until the target make-up zone is reached. Once this zone is exceeded, a steeper increase is noticeable. Since the load flanks remain in contact, the only alternative explanation is that the gap size increases and exceeds its nominal value. The magnitude of this relative increase exceeds 10 µm and is, given the elasticity limit of the material (0.27%), likely to be caused by plastic deformation at the thread roots. The existence of these plastic zones becomes visible when analyzing numerical simulations and will eventually lead to local shear or jump out which is further described in Section 3.2.2.1.

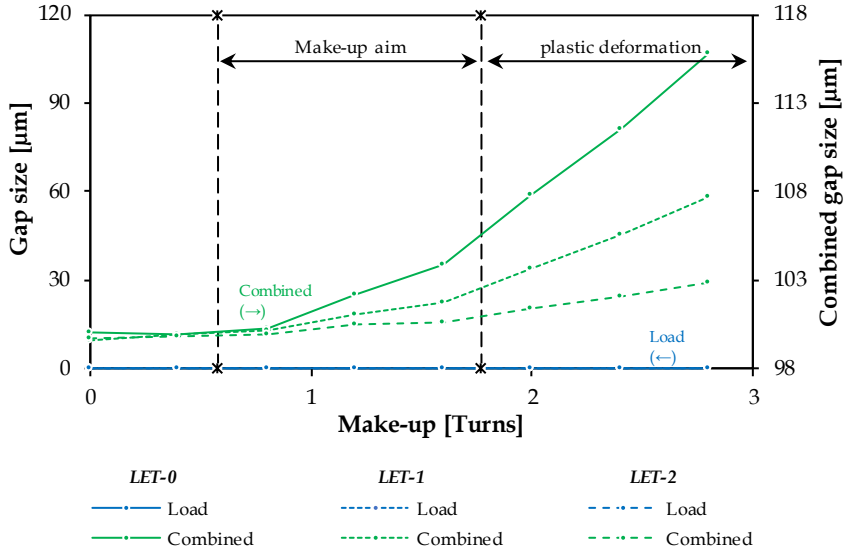

Figure 5–9: Local plastic deformation at the roots near the load flanks of the last vanishing threads cause gap sizes near the stab flanks to increase.

3 Effect of geometrical and material parameters

3.1 Outline of the parametric study

The main objective of the developed program is to determine and quantify the effects of various geometric changes made to trapezoidal threaded connections in a time efficient manner. It is the intention to provide these tendencies without having to manually post-process and examine every

simulation or load combination. Since connections are not being used without initial make-up, it is decided to examine the effects of the investigated parameters in combination with their maximum make-up position using the methodology previously explained in Section 7 of Chapter 4. This position is considered to be the most critical condition, with respect to plasticity, in which the connection can be used when internal pressure and axial tension are applied.

The performed study consists of three major parts, each representing a different performance output as previously defined in Section 6 of Chapter 4:

- Plasticity
- Load distribution
- Flank clearance or flank gap size

Since 'plasticity' is used to determine the maximum make-up position, a distinction is made between the case of only make-up (see Section 3.2.1) and the case of make-up in combination with working loads. These loads consist of a combination of axial tension and internal pressure (see Section 3.2.2). The other two performance outputs are then evaluated using the most critical load path, based upon the occurring plasticity, combined with the connection's maximum make-up position.

The study performed in this section focusses on various connection parameters regarding material properties and geometry. Since it is the objective of this thesis to use the gathered results to suggest a new geometry for a coupling that is able to connect a set of predefined pipes, only a limited number of geometrical and material properties are considered. In total, five different parameters are individually investigated:

- Load flank angle
- Wall thickness of the box
- Taper angle of the thread
- Material grade of both pin and box
- Material grade of the box without changing the material of the pin

While this list may appear very limited, the information gathered from these limited parameters is sufficient for proposing a design which is believed to yield an enhanced performance over the standard buttress connection.

It should be noted that connections have several other geometric features such as the chamfers on pin and box. While these features are believed to have some effect regarding resistance to fatigue loads [5.1], their effect on static loads is considered to be marginal and are therefore not taken in consideration in this study. Additional features such as grooves [5.2] or special nose designs [5.3] are not investigated since they are not present in the standard buttress connections as defined by the API 5B [5.4].

3.1.1 Load flank angle

The main objective of investigating the load flank angle is to determine whether or not the modification of flank angles has any significant effects on the global behavior of the connection using the aforementioned performance criteria. If limited to no significant effects are noticeable, changing the other flank angles is believed to be of even less importance. The choice of considering the load flank angle is based upon the observation that this is the only contacting flank of major importance when applying axial tension and that this is often the only flank angle which is explicitly mentioned in the majority of filed patents.

A total of seven different flank angles are considered, ranging from a negative -20° (negative flank angles which are characteristic for the hooked threads) to a positive +10°. The intermediate, simulated values are -10°, -5°, -3°, +3° and +5°.

3.1.2 Wall thickness

The relative difference between the wall thicknesses of the pin and the box evaluates possibilities of reducing the outer diameter of the box (see Section 5.2.2 of Chapter 1). In order to investigate the effects of changes to the wall thickness on the connection's rating, a *wall thickness ratio* is defined. This ratio is based on the wall thickness of both pin and box. Since the wall thickness of the box and pin are not constant throughout the threaded region as a result of the tapered thread design, a criteria uniquely defining these parameters is required. The wall thickness of the pin (wt_p) is defined as the nominal wall thickness of the pipe body, while the wall thickness of the box (wt_b) is defined as the thickness of the section above the first engaged thread in the middle of the box crest when assembled in hand tight position, as indicated in Figure 5–10. These sections represent an approximation of the critical section when assuming that no separation (local jump-out or fracture) along the vanishing threads occurs. Using these values, the *wall thickness ratio* (R_{wt}) is defined as follows:

$$R_{wt} = \frac{wt_b}{wt_p} \qquad \text{(Eq. 5.3)}$$

During this investigation, four different pin wall thicknesses are taken into account: 7 mm, 9 mm, 11 mm and 13 mm. Combining these values with a uniform box design results in wall thickness ratios equal to 1.24, 1.05, 0.86 and 0.67 respectively.

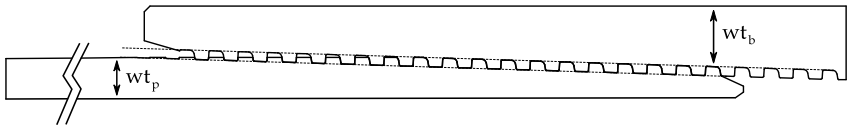

Figure 5–10: Graphical representation of the locations where the wall thickness for both pin and box is measured.

3.1.3 Taper angle

The *make-up loss* of the assembly, being the length of the pipe which is lost as a result of the overlapping threaded area, can be reduced by changing the thread taper. In contrast with the previously mentioned parameters, the results are much harder to interpret. The reason for this added complexity is related to the fact that by changing the angle of the threads, the length of the threaded area changes. This also implies that the ratio between the incomplete (vanishing) and the complete thread length changes. Additionally, the thread depth which affects the thickness and stiffness of the tip of both pin and box is altered when comparing taper angle modifications. In order to make a manageable comparison, an additional boundary condition is implemented to uniquely define the geometry. Therefore, it is decided that the thread length of the complete threads remains constant as visualized in Figure 5–11.

3.1.4 Material of pin and box

Referring to the API 5L standard [5.5], only the minimum yield strength of steel grades is defined. By changing the material grade of the entire assembly, effects of yield strengths exceeding the standardized values on the connection's behavior can be estimated. Additionally, a connection family (see Figure 2-11 in Chapter 2) usually consists of a certain geometric design applied to different sizes (outer diameter and wall thickness) and possible materials. By considering four different materials: GradeB, J55, TN80 and P110, which have a yield strength of respectively 300 MPa, 432 MPa, 578 MPa, and 802 MPa and are shown in Figure 5–12, the material-dependency can be evaluated. Since plastic deformation is avoided, the post-yield behavior of the material is of less importance during this study.

In order to translate the simulated materials in a more applicable parameter using the yield strength of the material (σ_{YS}), a yield ratio is defined. By using a normalized parameter, it is easier to determine whether or not it is beneficial to increase or decrease the material strength of the assembly for a given situation, while using the same geometry. Since a coupling design connecting two TN80 pipes will be developed (see Chapter 6), the yield strength of the TN80 material is used as a reference. The *yield ratio* (R_Y) is given by the following equation:

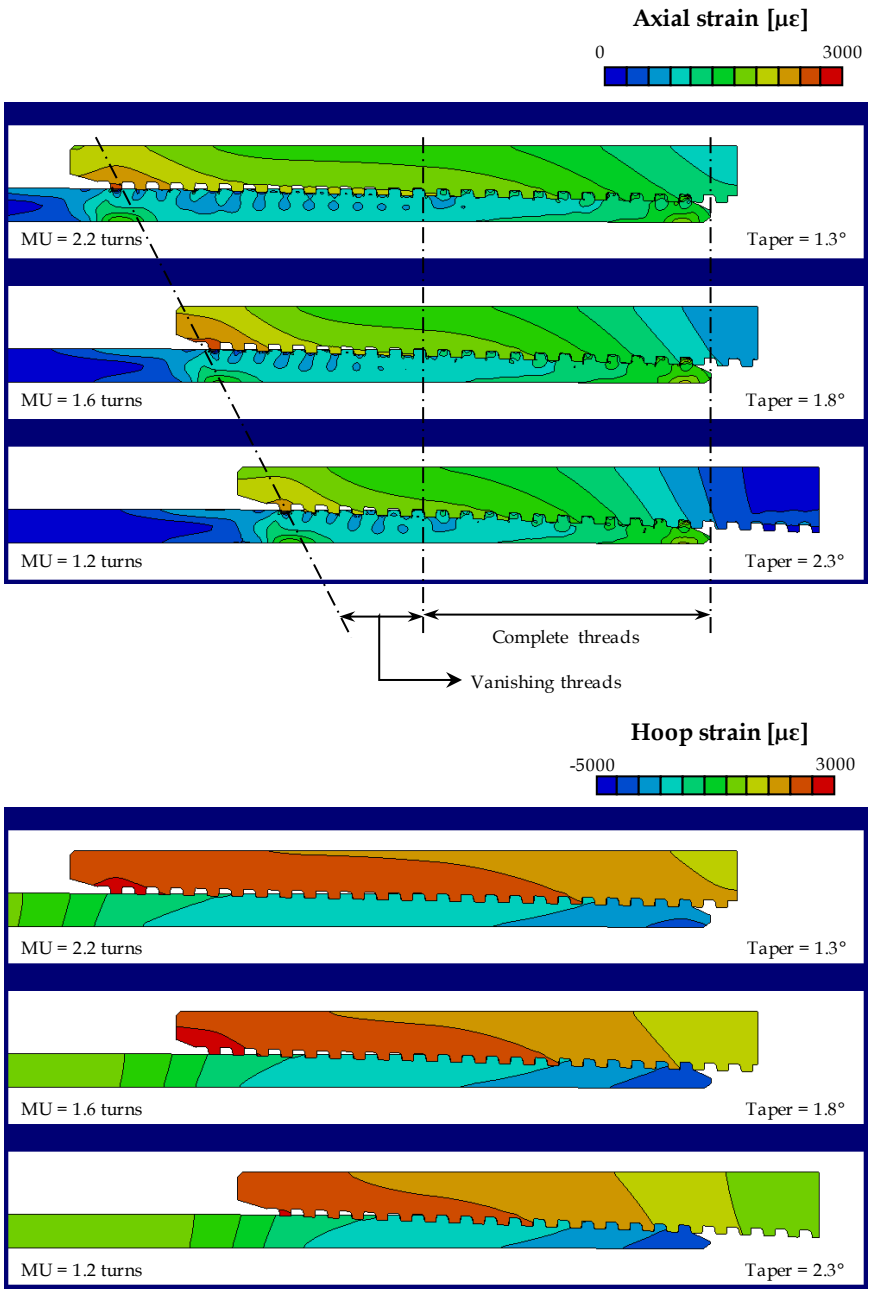

Figure 5–11: Overview of the geometry of the various taper angle modifications and representation of hoop and axial strains after a make-up in which a 0.25 mm radial overlap is resolved (See also Section 3.2.2.3).

$$R_Y = \frac{\sigma_{YS}}{578\ MPa} \qquad \text{(Eq. 5.1)}$$

This results in ratios of 0.52, 0.71, 1.00 and 1.39 for respectively a GradeB, J55, TN80 and P110 material.

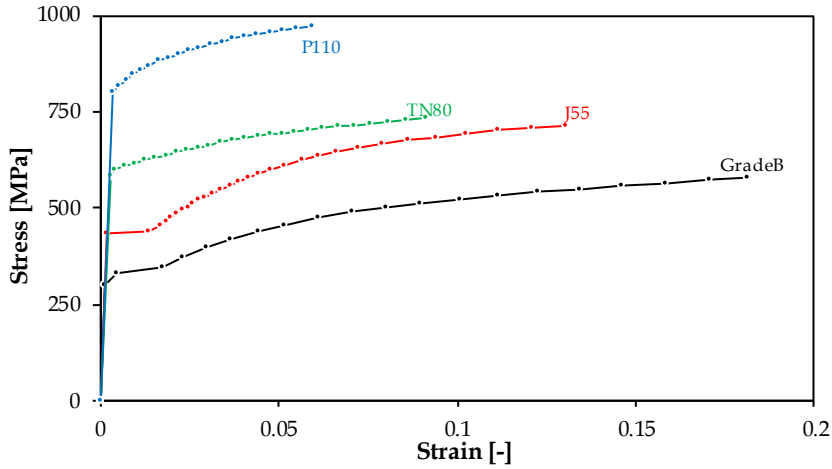

Figure 5–12: Stress-strain curves of the applied materials as used in the FEA simulations.

3.1.5 Material box only

Finally, in an effort to determine the effect of a strength mismatch between the yield strength of the box material ($\sigma_{YS,b}$) relative to the yield strength of the pin material ($\sigma_{YS,b}$), four different steels are being simulated for the box while maintaining a TN80 steel for the pin. The tested combinations using GradeB, J55, TN80 and P110 steel grades represent relative yield ratios of respectively 0.52, 0.71, 1.00 and 1.39. Herein, the *relative yield ratio* (R_{rY}) is defined as follows:

$$R_{rY} = \frac{\sigma_{YS,b}}{\sigma_{YS,p}} \qquad \text{(Eq. 5.2)}$$

3.2 Plasticity

3.2.1 Maximum make-up without working loads

One of the main objectives of examining the overall plasticity is the determination of the maximum make-up position. The total amount of plastic energy in the connection for make-up positions ranging from handtight to three powerturns and for various changing parameters (see earlier) are shown

in Figure 5–14. After applying the methodology described in section 2.1 of this chapter, the maximum make-up positions are calculated and are indicated by the red lines.

3.2.1.1 Load flank angle

It can be seen in Figure 5–14 that load flank angle modification has no significant effect on the maximum make-up position. For all load flank angles, the maximum make-up position is approximately 1.7 turns. This can easily be explained by considering the principles of make-up (see earlier in Section 2). Since the threads are not wedged (see Section 4.4.2 of Chapter 3), contact is primarily present between the root and crest flanks rather than the load and/or stab flanks.

3.2.1.2 Wall thickness

Similar to the load flank angle, limited variations are observed for the various wall thicknesses exceeding the 0.85 ratio. However, when reducing the wall thickness of the box relative to the pin, a significantly higher amount of plastic deformation is induced. Considering that a wall thickness ratio of approximately 0.67 corresponds to the standard connection, it can be concluded that for these connections the deformation of the box is larger than the deformation of the stiffer pin and that the box is already stretched to its limits, reducing its capabilities of resisting high internal pressures. The same amount of overlap can, for example when a wall thickness ratio of 1.24 is applied, be resolved with less plastic deformation. This will also result in lower contact pressures along the threaded area and a reduced make-up torque as is shown in Figure 5–13.

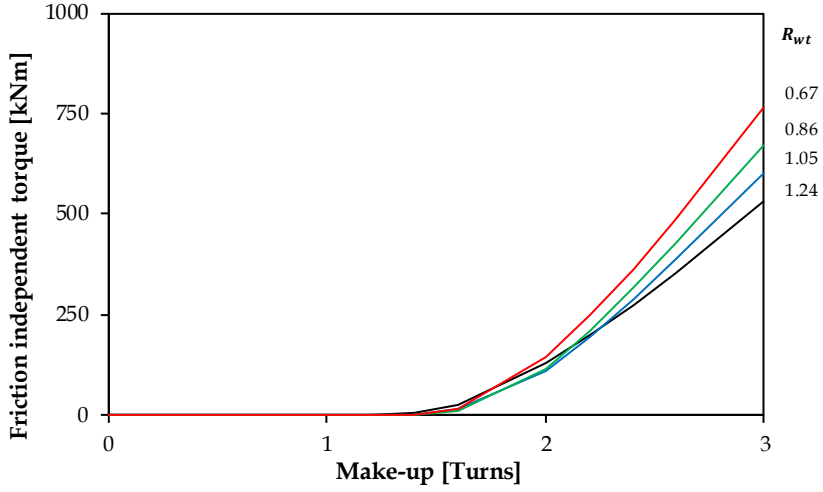

Figure 5–13: Effect of wall thickness on the calculated, friction independent make-up torque.

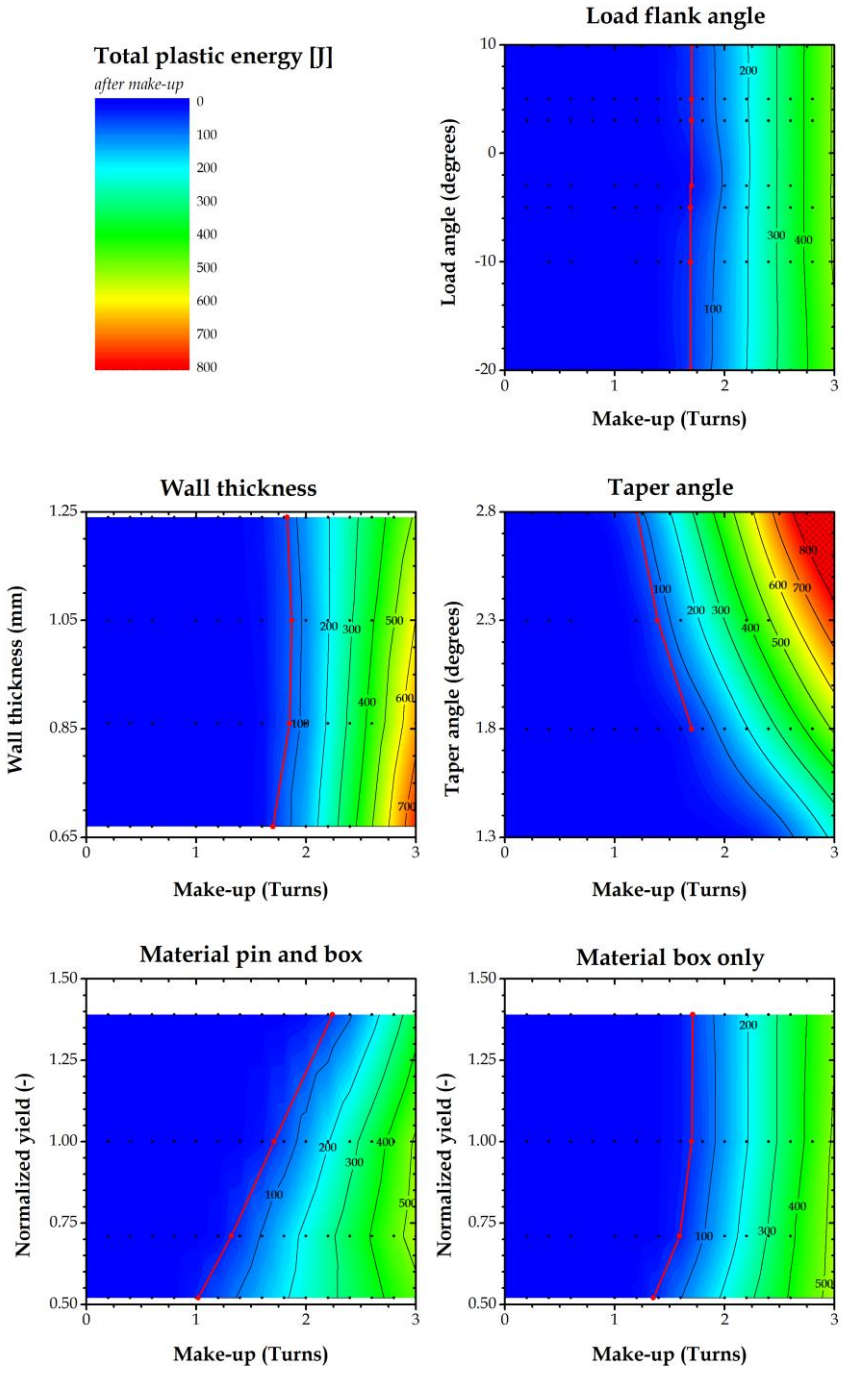

Figure 5–14: Effect of parameter modification on the plasticity of the connection after applying make-up.

3.2.1.3 Taper angle

In contrast to both the load flank angle and the wall thickness, changing the taper angle appears to have considerable effects on the maximum make-up position. Before going into detail, it should be mentioned that for a taper angle of 1.3°, no maximum make-up position could be calculated as result of the lack of plasticity induced when applying up to three powerturns. For the other angles, the maximum position decreases with increasing taper angle. However, a major issue related to the interpretation of the make-up positions must be considered. Previously, it was assumed that the number of make-up turns was representative for the amount of radial clearance. This is not the case when modifying the taper angle. This also implies that when comparing different connections with each other, not the number of make-up turns, but the amount of radial overlap could provide more straightforward results. The relation between radial overlap (δ) and taper angle (ϵ) is given below by following equation:

$$\delta = \tan(\epsilon) * p * MU \qquad \text{(Eq. 5.4)}$$

Within this equation, p is the pitch length in mm, MU the number of powerturns and δ the radial overlap in mm. By considering the amount of radial overlap that needs to be resolved as illustrated in Figure 5–15, different conclusions can be drawn. When the taper angle is increased, the amount of maximum radial interference is slightly increased. Thus, despite a reduced number of make-up turns, a slightly higher amount of radial clearance can be resolved. This behavior can easily be explained by assessing the reduced number of incomplete threads with increasing taper angle since this portion of the thread is most susceptible to plastic deformation.

A similar conclusion can be drawn using the torque-turn diagram shown in Figure 5–16. Within this diagram, a taper of 0.8 was added for reference purposes. While the torque-turn diagrams corresponding to the two smallest tapers are mainly linear over their entire length, the curves corresponding to the other sizes clearly show a transition point at an initial overlap of approximately 0.28 mm. The increased torque can be explained using Figure 5–17 in which the average contact pressures on both root and crest flank are shown. The stab and load flanks are omitted from the results since the contact pressures on these flanks are very limited to non-existent. For the crest flanks, shown in the top part of the picture, little differences are observed for the various taper sizes apart from a small decrease with increasing taper along the complete threads. For the vanishing threads, no contact pressures are present due to the cut-off thread height. In contrast, the root flanks of the vanishing threads are found to be the main reason for the torque difference. Considering that the area under the curves is representative for the amount of frictional energy, hence required torque, it is evident that the connection with the most

loaded, vanishing threads requires more energy to assemble since a larger part of the box and pin needs to be expanded and shrunk respectively. Finally it should be noted that the extreme high average contact pressures that are visible near the last engaged thread should be handled with care and are caused by a combination of limited contact length and singularities in the distribution of the contact pressure (see Chapter 4).

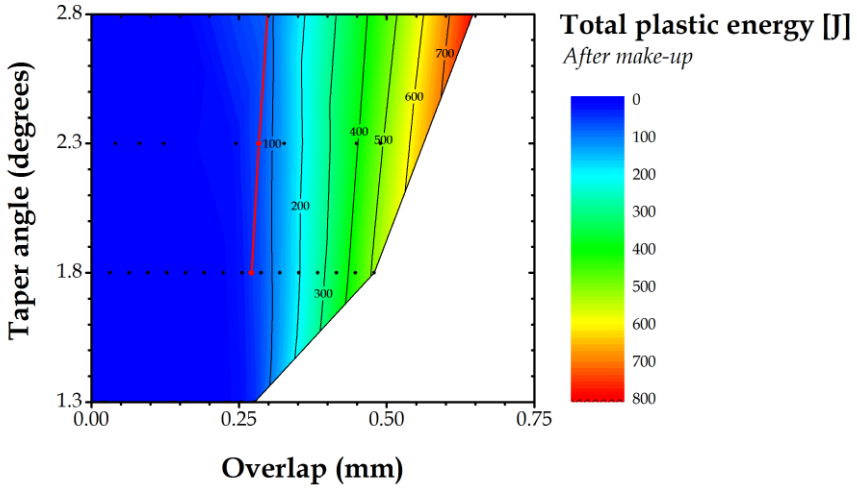

Figure 5–15: Effect of taper angle on the plastic deformation in function of radial overlap.

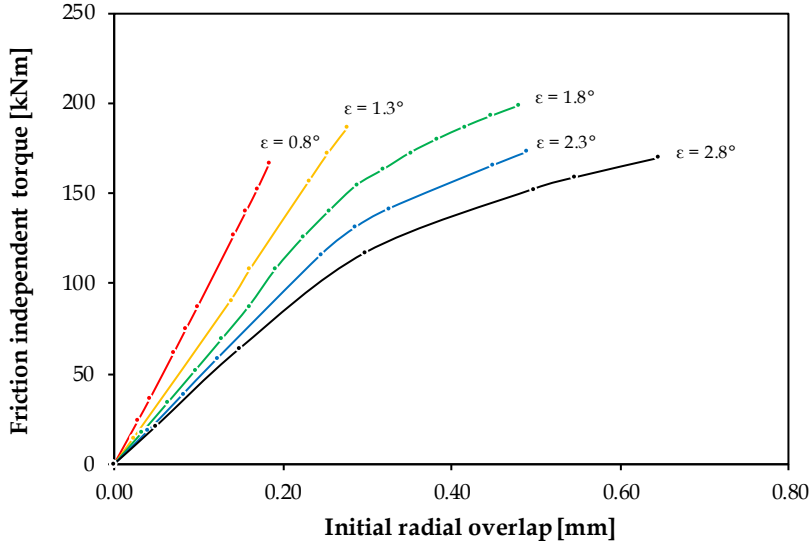

Figure 5–16 Approximation of the friction-independent holding torque after make-up.

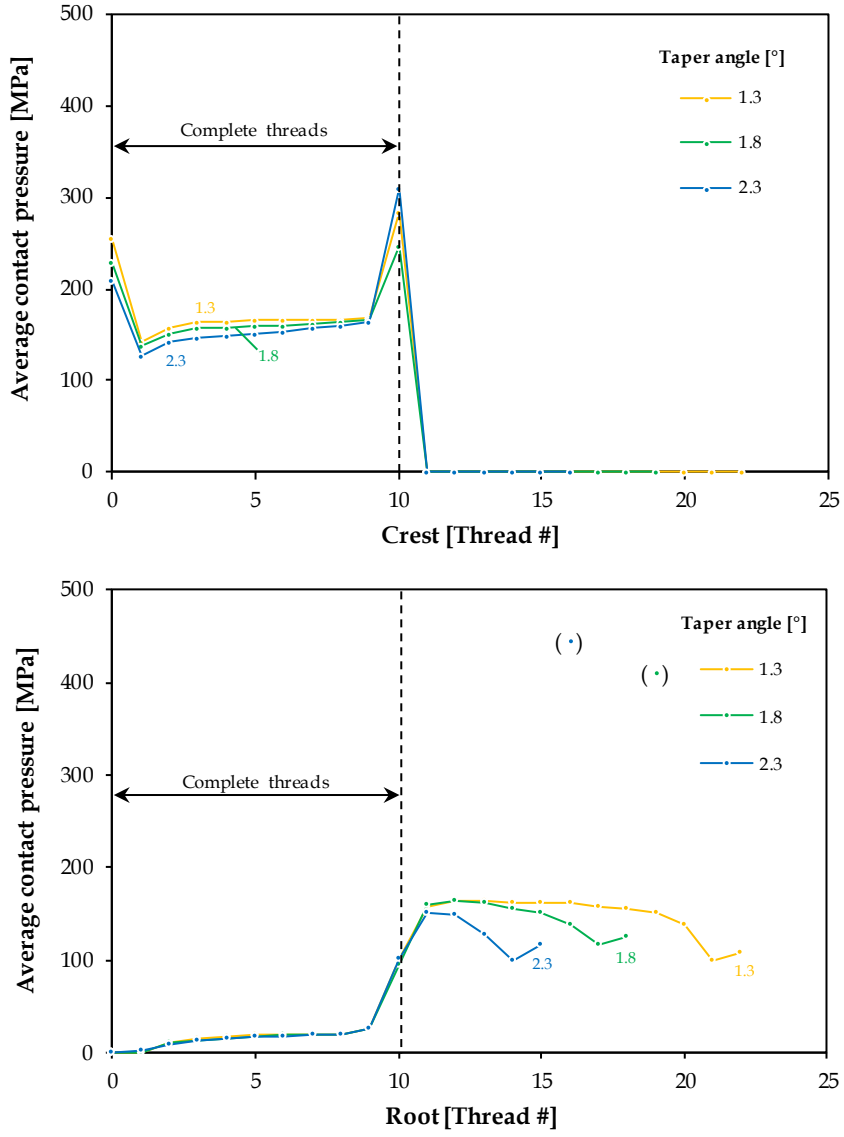

Figure 5–17: Average contact pressure at the crest and root for various taper angles.

3.2.1.4 Material parameters

In addition to geometrical parameters, also the material characteristics have a distinct influence on the maximum make-up position. When the steel grade of both the pin and the box is increased, the maximum make-up position is increased as well due to the increased yield strength. This increased yield strength allows larger elastic deformations. When only increasing the steel

grade of the box, the maximum make-up position can also be increased. However, once the pin starts to deform plastically, increasing the strength of the box does not offer any advantages since the pin has become the limiting part of the assembly.

3.2.2 Maximum make-up with working loads

In the previous section, the maximum make-up position was determined based on the plasticity of the connection after make-up. While this approach is suitable, it is not applicable in reality since it does not take into account the working conditions. In essence, every connection can resist a '*certain amount of elasticity*', depending on its yield strength. Once this amount is reached by means of elastic deformations as a result of applied loads such as make-up and working loads, the connection starts to deform plastically. Therefore, it is not advised to apply the maximum make-up calculated without considering the working conditions. Such an approach will most likely result in overstressing the connection.

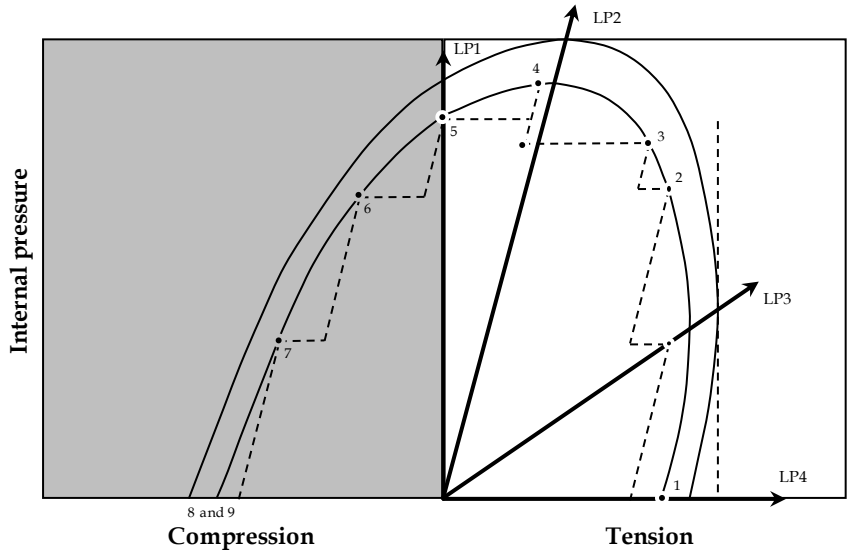

Figure 5–18: Overview of the simulated load paths plotted on the ISO13679 defined VME.

In an effort to determine the maximum applicable make-up position, four different load paths (LP), visualized in Figure 5–18, are considered in addition to initial make-up:

- LP1: Maximum internal pressure without axial tension
- LP2: Maximum internal pressure with axial tension
- LP3: Maximum axial tension with internal pressure
- LP4: Maximum axial tension without internal pressure

These load paths represent the extents of the von Mises ellipse as defined in the ISO 13679 standard [5.6] and are considered to be the most demanding conditions. For every investigated parameter and load path, 16 different simulations are performed to incorporate the effect of the initial make-up, which ranges from 0 to 3 powerturns and are calculated using increments of 0.2 turns.

3.2.2.1 Changing the load flank angle

As an example, Figure 5–19 shows the results for all investigated load flank angle geometries taking into account only make-up (red) and make-up combined with the four different load paths. From this figure, it is visible that the amount of plastic deformation is similar for all different load flank angles subject to the same load path. While the maximum make-up position during make-up was determined to be about 1.7 turns, this limit should be lowered to approximately 1.34 turns when additional working loads are considered. For the investigated cases, LP3, which consists of maximum axial tension and a limited amount of internal pressure, appears to be the most critical load combination. For all further studies, only a table conform Table 5-1 which consolidates the maximum make-up positions will be provided to increase readability of the results.

Table 5-1: Effect of load flank angle modification on the maximum make-up position taking into account a 95% rating.

Load flank angle [degrees]	*MU [turns]*	*LP1 [turns]*	*LP2 [turns]*	*LP3 [turns]*	*LP4 [turns]*	*Limit [turns]*
-20	1.69	1.45	1.48	1.34	1.45	1.34
-10	1.69	1.48	1.52	1.37	1.48	1.37
-5	1.69	1.48	1.51	1.37	1.48	1.37
-3	1.70	1.48	1.50	1.37	1.48	1.37
3	1.70	1.47	1.51	1.37	1.47	1.37
5	1.70	1.47	1.51	1.37	1.47	1.37
10	1.70	1.49	1.53	1.37	1.49	1.37

Since make-up influences the connection's behavior significantly, the maximum make-up position that ensures a 95% von Mises envelope will be used for further investigation. The decision to consider a 95% envelope rather than the 100% envelope is due to the plasticity effects occurring when applying loads equal to or near the yield strength of the connection.

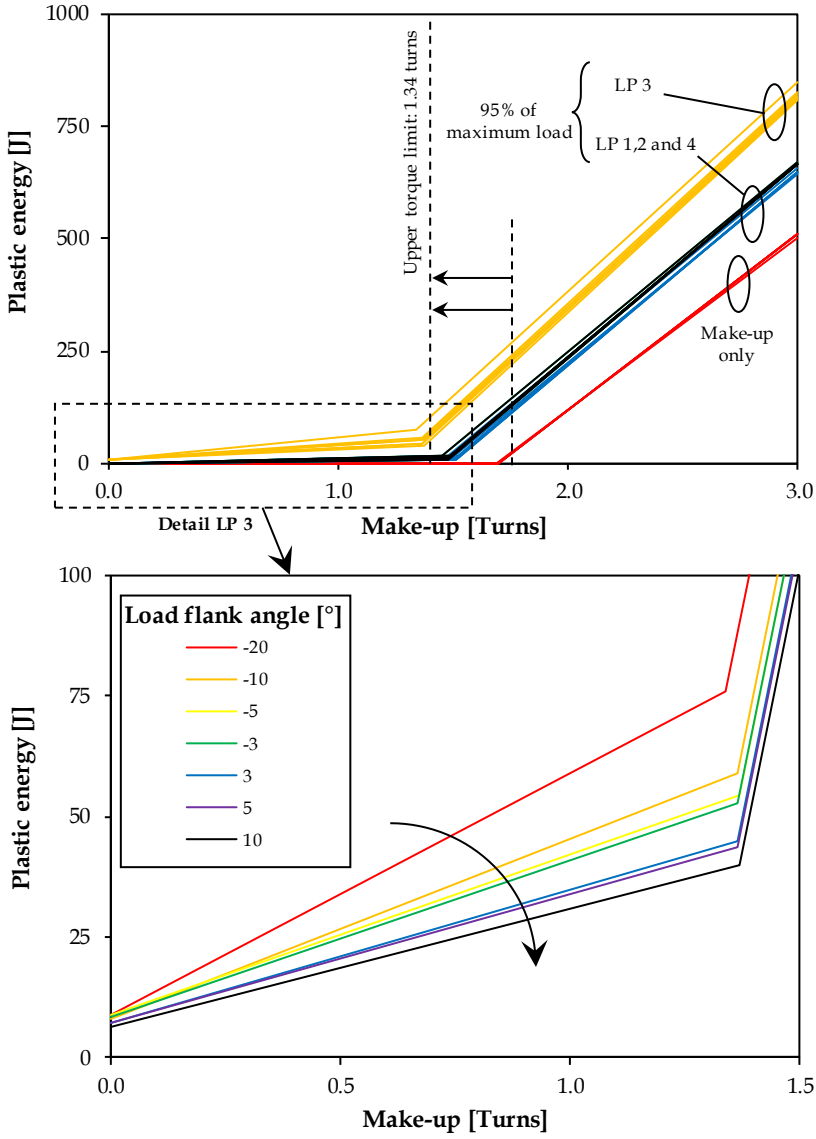

Figure 5–19: Determination of the torque limits of the connection.

In an effort to provide additional information regarding the effect of the load flank angle modifications on the plasticity, the data gathered after applying the most critical load path (LP4) is shown in detail in the lower part of Figure 5–19. From this graph, the linear approximations representing the mainly elastic and global plastic trends are visible. Although containing mainly elastic deformations, a significant amount of plastic energy is already noticeable for lower make-up positions when applying the workloads in accordance with LP3 (maximum axial tension combined with internal

pressure). This limited plastic deformation is located near the thread roots of the last engaged threads. The internal pressure tends to keep a root-to-crest contact while the considerable amount of axial tension forces the connection to deform in the areas near the root/load radii as a result of stress concentrations. In this respect, Figure 5–20 visualizes that using a negative load flank angle tends to induce shear failure, while using a positive load flank angle appears to encourage plastic deformation and sliding. This means that for a hooked thread profile, shear fracture is more likely to be initiated rather than jump-out.

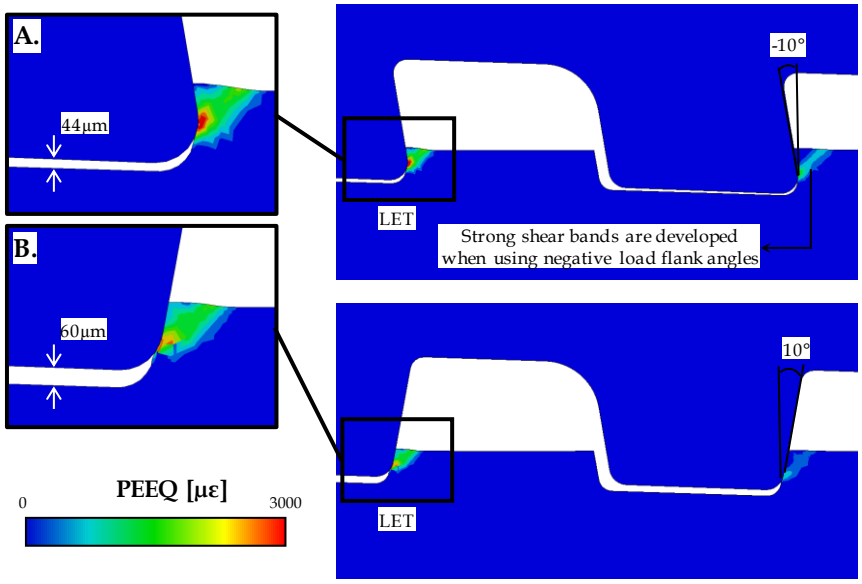

Figure 5–20: When applying an axial tensile load, hooked threads (A) generate higher PEEQ values in the shear planes while positive load angles (B) tend to crush the material, leading to lower intensity stresses and a larger area containing plastic deformation.

The aforementioned results can practically be applied when designing a connection able to resist working loads up to an equivalent force of 95% of its yield limit. However, when working loads are known to be less, for example only 80% of the yield strength, higher make-up levels can be applied since less deformation is expected. Using the same methodology, make-up positions allowing ratings from 0% (only make-up) up to 100% (the equivalent yield limit of the connection) can be calculated for all cases. These results are shown in Figure 5–21. Using these graphs, it is possible to read the maximum make-up position when a certain rating is required. In this case, positive load flank angles do not appear to have significant influence while excessive negative load angles appear to slightly limit the maximal torque position as a result of the increased plastic deformation near the thread roots.

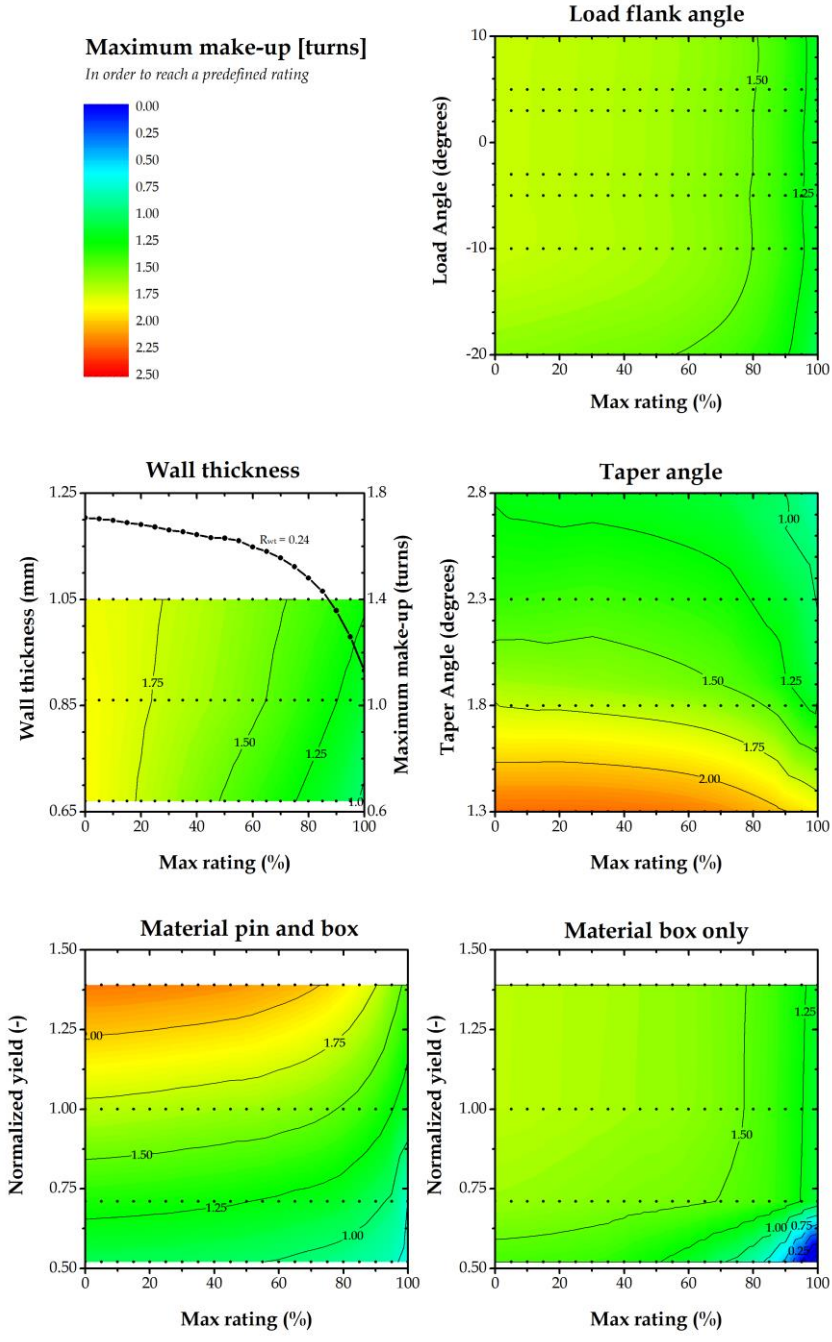

Figure 5–21: Maximum allowed make-up in order to reach a predefined rating, taking into account the worst case of the four examined working load combinations.

In addition to a maximum make-up position, the minimum make-up position (see before, section 2.1) was found to be around 0.55 turns and appears to be independent of the applied load flank angle. This results in an allowable make-up range of about 0.2 turns when a connection is required to withstand up to 95% of the pipe body yield limit.

3.2.2.2 Changing the wall thickness

In analogy with Table 5-1 for the load flank angle, Table 5-2 shows the maximum make-up positions for different wall thicknesses after applying make-up and various load combinations at 95% of its yield strength. Using this table, it can be seen that LP3 (maximum axial tension with internal pressure) is the most critical load path for the connection containing a 1.24 ratio, while internal pressure (LP1) appears to be the limiting load for the other cases.

Table 5-2: Effect of wall thickness modification on the maximum make-up position taking into account a 95% rating.

R_{wt} [-]	*MU [turns]*	*LP1 [turns]*	*LP2 [turns]*	*LP3 [turns]*	*LP4 [turns]*	*Limit [turns]*
1.24	1.70	1.47	1.51	1.37	1.47	1.37
1.05	1.85	1.33	1.40	1.42	1.37	1.33
0.86	1.87	1.19	1.35	1.51	1.31	1.19
0.67	1.83	1.06	1.23	1.28	1.36	1.06

The maximum make-up position taking into account the most critical load path to obtain a connection with ratings from 0% to 100% is shown in Figure 5–21. When assessing these results, a significant difference related to the behavior of the maximum make-up position in function of the connection's rating is observed between a wall thickness ratio of 1.24 and the other ratios. This is caused by a change related to the most critical load combination. While axial tension (LP3) is more critical than internal pressure when using a wall thickness ratio of 1.24, the opposite (LP1) is true for the other ratios. Since the results for the case of R_{wt} = 1.24 are dependent on a different load path than the other cases, it cannot be interpolated with the other results. Therefore, this exception is displayed as a line in addition to the contour plot containing the wall thickness ratios of 0.67 through 1.05. As a result of the different critical load combinations, using a wall thickness ratio of 1.24 allows higher make-up levels, especially where lower performance ratings (up to 50%) are required. For the other cases, a slightly higher amount of powerturns is allowed when using an increasing wall thickness ratio.

3.2.2.3 *Changing the taper angle*

Table 5-3 and Table 5-4 show respectively the maximum make-up position and matching radial overlap when changing the taper angle of the connection. The results presented in Table 5-4, using radial overlap, are used for comparison. When taking a closer look at the table, it can be seen that for the larger tapers (1.8° through 2.8°), all maximum initial overlap values are approximately 0.28 mm. For the smallest taper however, no value was found. This occurred because the total amount of plasticity was not sufficiently large when applying a maximum of 3 make-up turns. Therefore, this value was omitted from the investigation. Another option would have been to simulate additional make-up positions exceeding 3 turns. Additionally, it is observed that this wide range of possible make-up positions reported in Table 5-3 results in a narrow range between 0.18 mm and 0.23 mm radial overlap. Interesting to notice is that when using a steeper taper angle, more radial overlap can be induced in the connection. While the connection containing a taper angle of 2.8° can resolve a 0.23 mm radial overlap, using a taper of 1.3° will result in an overlap reduction of 20% or a 0.18 mm overlap.

Table 5-3: Effect of taper angle modification on the maximum make-up position taking into account a 95% rating expressed in number of turns.

Taper angle [degrees]	*MU [turns]*	*LP1 [turns]*	*LP2 [turns]*	*LP3 [turns]*	*LP4 [turns]*	*Limit [turns]*
1.3	N/A	1.91	1.92	1.67	1.56	1.56
1.8	1.70	1.47	1.51	1.37	1.47	1.37
2.3	1.39	1.18	1.20	1.13	1.08	1.08
2.8	1.20	1.03	1.04	1.00	0.92	0.92

Table 5-4: Effect of taper angle modification on the maximum make-up position taking into account a 95% rating expressed in radial overlap.

Taper angle [degrees]	*MU [mm]*	*LP1 [mm]*	*LP2 [mm]*	*LP3 [mm]*	*LP4 [mm]*	*Limit [mm]*
1.3	N/A	0.22	0.22	0.19	0.18	0.18
1.8	0.27	0.24	0.24	0.22	0.24	0.22
2.3	0.28	0.24	0.24	0.23	0.22	0.22
2.8	0.30	0.26	0.26	0.25	0.23	0.23

The reason why connections containing a steeper taper angle allow a lower amount of make-up turns can be understood when examining Figure 5–11.

Within this figure, three different connections containing a taper angle of respectively 1.3°, 1.8° and 2.3° are shown. The top part represents the maximum overall strains while the lower part illustrates the hoop strains. A radial overlap of 0.25 mm was resolved in an effort to generate the same strain state in all three cases. In order to obtain this amount of overlap, make-up positions of approximately 2.2, 1.6 and 1.2 make-up turns had to be simulated.

Before analyzing the trends based on the results obtained, it is important to point out that the effects on taper variations are strongly related to the way taper variation is defined. As already described above and visually illustrated in Figure 5–11, an additional boundary condition is required to uniquely define the thread geometry when changing the taper angle. Within this study, it was opted to maintain the thread length containing the full threads. This way, the connection contains approximately 10 complete threads and a variable amount of vanishing threads. The thickness of the pin tip cannot be chosen and is a direct result of this boundary condition.

When considering the overall impression of the results, the assumption that resolving a certain amount of overlap leads to a similar strain state in the connection for both the axial strains and the hoop strains appears to be valid. However, small differences can be observed. At first, the strains at the center of the box are smaller when the taper angle increases. This behavior can be explained by considering several causes. Since the thread length increases when the taper angle decreases combined with a higher number of make-up turns to reach the predefined amount of desirable overlap, the stabbing depth of low taper connections is deeper than when steep tapers are incorporated. This results in a smaller neutral zone at the center of the box where no direct interaction with the pin takes place. It is even possible that, when this zone is sufficiently small, significant interactions with the opposite side is noticeable as is the case for the 1.3° taper. These effects can be countered when redefining the size of the box to obtain a predefined neutral area at the center. In addition, steep tapers dictate smaller thicknesses at the pin tip. This translates in a reduced outward force of the box, reducing the strains in the center of the box. A second obvious difference between the simulated cases are the strain deviations near the last engaged thread. While these are very limited and no trends are observed related to the taper difference, the differences are caused by the varying geometry of the box end. Since the geometry and location of the drawn section changes, the chamfer changes as well, causing a local difference in stiffness of the box end.

3.2.2.4 Changing the steel grade of both pin and box

Table 5-5 gives an overview of the maximum make-up positions obtained based on the performed simulations and applied load paths. It is observed that large differences occur between the chosen materials. When a high yield limit is present, a higher *elastic energy reserve* is available. The elastic energy reserve

is introduced as a parameter representing the ability of a connection to deform elastically and is directly related to the yield strength of the material. When a high elastic energy reserve is present, the connection can typically deform more before permanent deformation occurs. Taking this into account, the relative order of the materials related to the maximum make-up turns makes sense. Additionally, it is observed that a linear relationship exists between the maximum amount of make-up turns and the yield strength of the applied material. Since the upper make-up limit is based on the introduction of global plastic deformation, this relationship was to be expected. An overview of the maximum allowed make-up position for the various cases including working conditions up to 95% of the yield strength of the pipe body is illustrated in Figure 5–21. From this figure, it is clear that by reducing the strength of the materials, the ability to apply high make-up positions decreases. A more subtle observation is that with reducing strength of material, the maximum amount of make-up turns appears to be less sensitive to increasing maximum loads.

Table 5-5: Effect of changing the steel grade of the entire connection on the maximum make-up position taking into account a 95% rating.

Yield ratio [-]	*MU [turns]*	*LP1 [turns]*	*LP2 [turns]*	*LP3 [turns]*	*LP4 [turns]*	*Limit [turns]*
0.52	1.02	0.88	0.90	0.79	0.73	0.73
0.71	1.32	1.12	1.14	1.04	1.37	1.04
1.00	1.71	1.48	1.52	1.37	1.19	1.19
1.39	2.24	1.97	2.02	1.71	2.21	1.71

3.2.2.5 Changing the steel grade of only the box

Finally, the maximum make-up positions when changing the box material can be found in Table 5-6. Based upon this table, it can be seen that using a 0.52 relative yield ratio between pin and box results in a make-up position which cannot be calculated after applying working loads equal to 95% of the pipe body strength. Due to the excessive difference of the yield strengths between both materials used in the joint, the box is the weakest member of the connection and the required pipe body rating cannot be reached.

One of the more important outputs of this study is shown in Figure 5–21. For the geometry of the standard coupling, it is made clear that the Grade B material (which corresponds with the relative yield ratio of 0.52) cannot be used for obtaining 100% pipe body performance, but can still be used when a rating equal to only 80% of the pipe body strength is required. In the latter case, the make-up during assembly should not exceed approximately 0.6 make-up turns. An assembly having a 100% pipe body resistance is already possible with a relative yield ratio of 0.71 combined with make-up positions not

exceeding 1.2 make-up turns. Higher relative yield ratios allow for higher make-up positions. In addition, it is interesting to notice that once a relative yield ratio of 1 is reached, all plasticity is located in the pin and increasing this ratio further will not affect the maximum allowed make-up positions. Important to note from these findings is that, since a relative yield ratio of 0.71 is still able to resist loads equal to 100% of the pipe body strength, the box is most likely over dimensioned.

Table 5-6: Effect of changing the steel grade of the box on the maximum make-up position taking into account a 95% rating.

Relative yield ratio [-]	*MU [turns]*	*LP1 [turns]*	*LP2 [turns]*	*LP3 [turns]*	*LP4 [turns]*	*Limit [turns]*
0.52	1.35	N/A	N/A	0.91	0.81	N/A
0.71	1.59	1.01	1.07	1.31	1.37	1.01
1.00	1.70	1.47	1.51	1.36	1.18	1.18
1.39	1.71	1.70	1.69	1.35	1.21	1.21

Regarding the determination whether the pin or box is the weakest member when external loads are applied in addition to initial make-up, Figure 5–22 offers valuable clues. Within this picture, the relative yield ratios of 0.71 and higher are shown. The simulation in which a Grade B box was used is removed from this plot since it is not possible to withstand the applied loads using this connection, as was already mentioned. For every material combination, the simplified plastic energy curve after applying a load equal to 95% of the pipe body strength is shown in function of the amount of make-up turns. A distinction is made between two different kinds of loads: internal pressure (full lines) and axial tension (dashed lines). From the figure, it can be seen that all curves representing the simulations in which an axial tensile load was applied are almost identical. This indicates that the behavior of the box under tension is similar for all cases and therefore, the box can be considered the strongest member of the connection. In contrast, differences can be seen for the case in which internal pressure is applied. From the box' point of view, it was already mentioned that internal pressure and make-up have similar effects. While increasing the strength of the material equals increasing the ability of the box to deform more elastically, it is obvious that higher yield ratios provide higher maximum torque levels for internal pressure. However, the slope of the curves is equal for all cases. This indicates that the response of the assembly as a result of the applied internal pressure is equal for all cases, suggesting that the box did not reach its limits and is able to resist the applied 95% pipe body load.

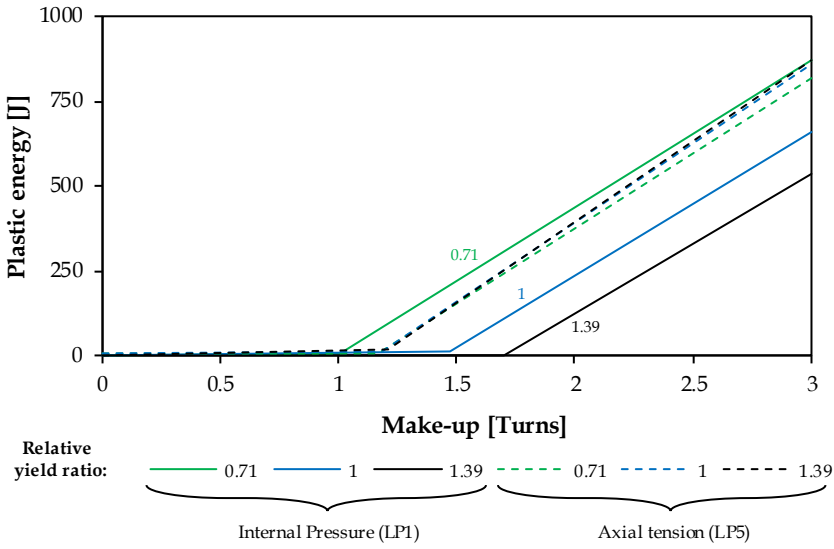

Figure 5–22: Determining the weakest member in the connection using the calculated plastic energy.

3.3 Load distribution

3.3.1 Radial load distribution

The result of parameter variation on the radial load distribution after applying maximum make-up is shown in Figure 5–23. Based on these results, none of the parameter modifications appear to have significant effects. The only observable changes are located near the last engaged thread. It should be noted that, depending on the amount of maximum make-up, this last engaged thread can vary. When, for example, thicker pins are used, a higher amount of make-up turns can be applied. This explains why not all the color plots contain data for all the threads. Higher make-up positions result in an increased number of threads in contact. The only exception is the case in which the thread taper is modified. Here, the number of vanishing threads is primarily dependent on the taper angle. Apart from the total number of engaged threads, the location of the transition zone where complete threads end and vanishing threads start remains constant at around thread 11.

3.3.2 Axial load distribution

After taking into account various make-up positions, the axial load distribution is investigated when the connection is subject to 95% of the maximum axial tension and the results are shown in Figure 5–24.

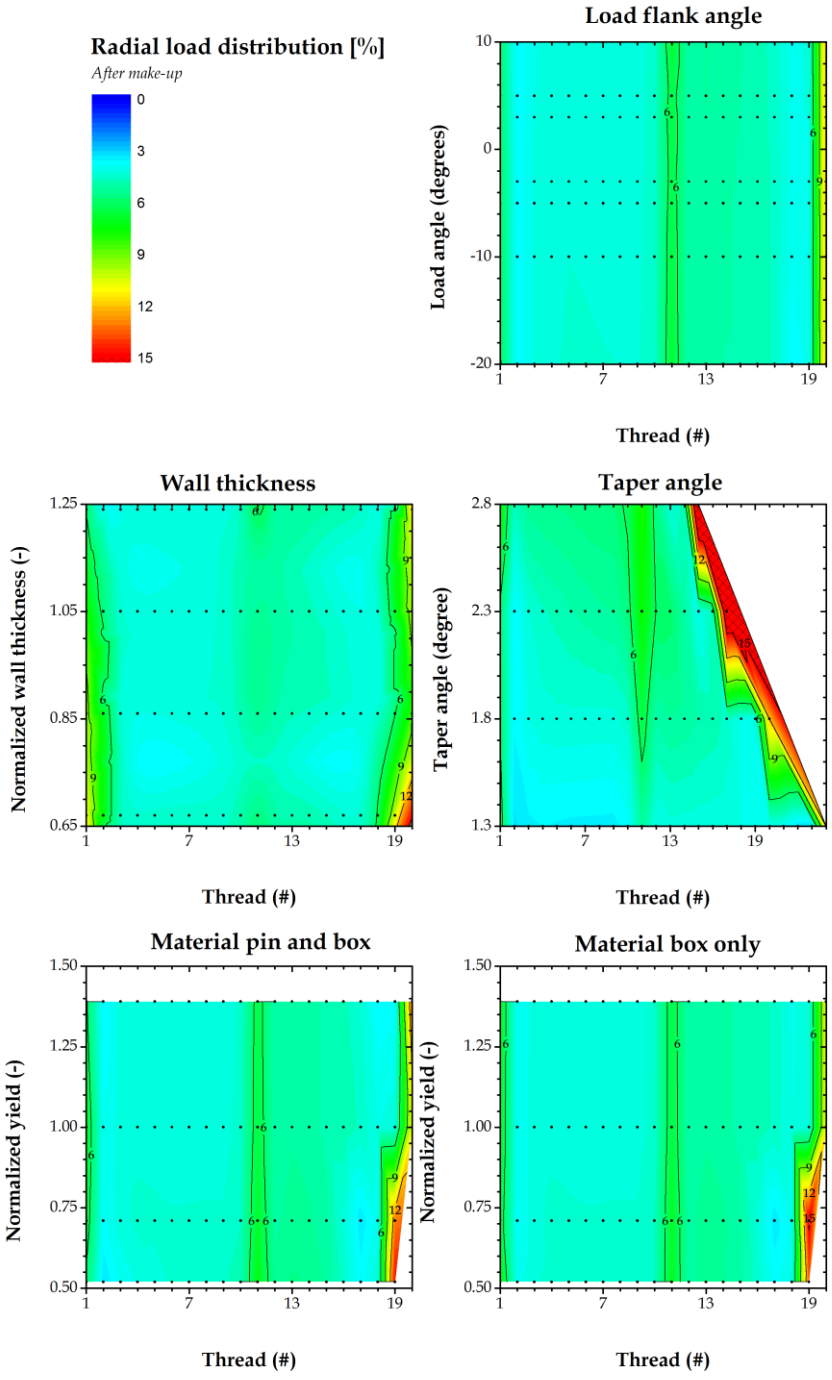

Figure 5–23: Effect of changing parameters on the radial load distribution after initial make-up.

When considering the effect of load flank angle, two major observations can be made. First of all, all angles show a slightly negative load distribution near the pin tip (thread 1 through 4 or 5). While this may be unexpected since an axial tensile load is applied, this anomaly is caused by initial compressive, axial stresses as a result of the initial make-up. Secondly, a maximum is visible near thread 16. The magnitude of this maximum increases with increasing load flank angle. This can be explained by the threads' behavior as explained in Section 3.2.2.1. While negative or hooked threads tend to maintain contact, an unzipping effect tends to occur when positive flank angles are used. This reduces the number of threads in contact and results in an increasing load distribution.

When increasing the wall thickness of the pin, less load appears to be carried by the pin tip (threads 1 through 3). The load is shifted to the end of the vanishing threads. Increasing the wall thickness of the pin can be compared with relatively weakening the box, similar to reducing the yield strength of the box material By strengthening the pin, more load is transferred to the critical section of the box which is located near the pin tip. This causes less deformation and less changes in elongation of the pin. This way, more load is transferred towards the pin tip, leading to an increased axial load distribution in the complete threads. Despite the reduced plastic deformation resulting in a lower load transferred through the vanishing threads, an equal amount of threads (four to five) appear to fail by plasticity and potential jump-out.

For the case of taper variation, the load distribution reaches its maximum at the end of the vanishing threads and increases with increasing taper angle. Since a steeper taper angle implies a faster growth of the threads, less threads are likely to fail. An interesting observation is that steeper taper angles tend to shift the load from the vanishing threads to the complete as is shown in Figure 5–25. This figure indicates that this is the case for all make-up cases. While this may be beneficial since the vanishing threads which are often susceptible to failure are relieved, this also implies that relative movement between both the pin and the box may be expected over an increased portion of the threaded length. This in turn may cause difficulties when trying to design a reliable thread seal.

When further investigating the effects when changing the box material, similar conclusions as the ones related to make-up (see Section 2.2) are found. Similar to make-up, increasing the yield strength of the box tends to shift the load from the complete threads towards the vanishing threads. In turn, the maximum load on the last engaged thread is increased and is more likely to fail. Once the strength of the box equals or exceeds the strength of the pin, the distribution converges as mentioned above.

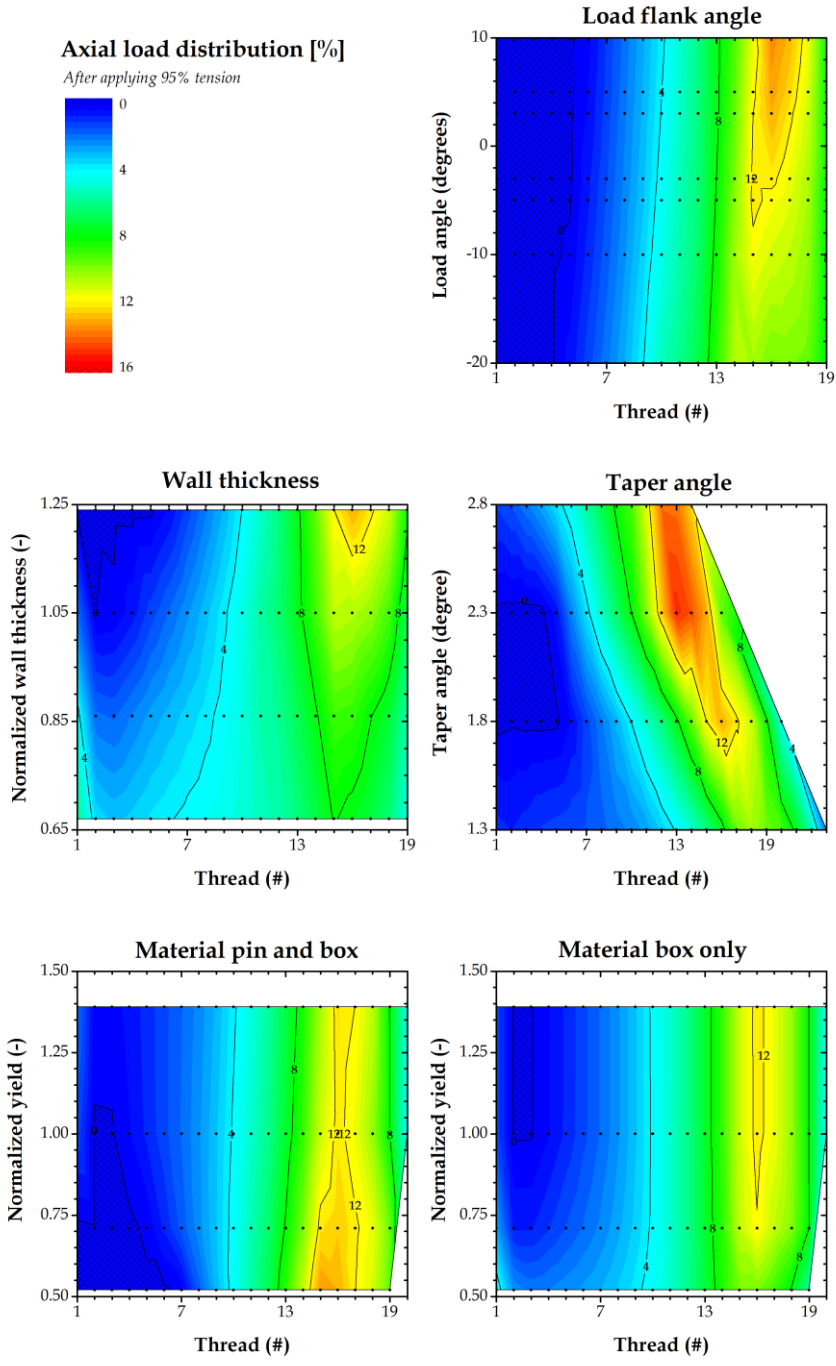

Figure 5–24: Effect of parameter modification on the axial load distribution after applying initial make-up and axial tension.

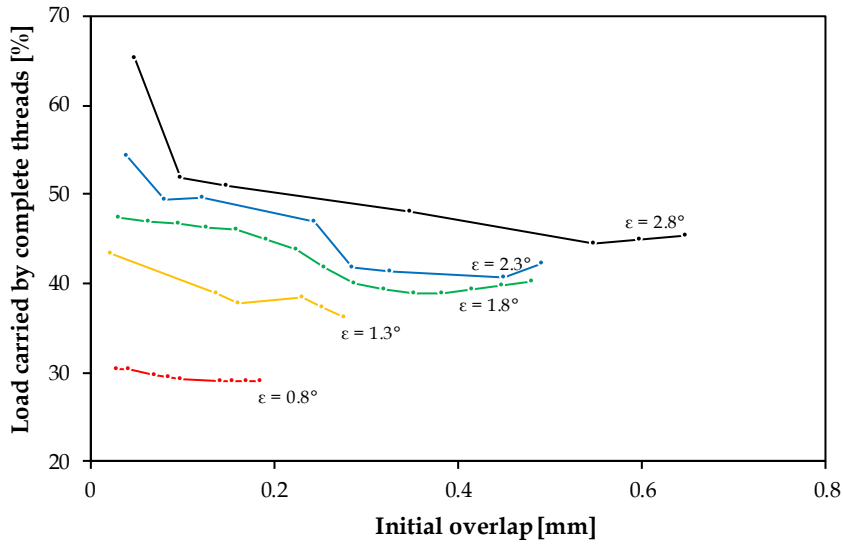

Figure 5–25: Effect of taper angle combined with make-up (radial overlap) on the portion of load carried by the complete threads.

In contrast, when increasing the yield strength of both the pin and the box material, the maximum near thread 16 tends to decrease. This is best explained by assessing the applied axial tensile load more closely. The external tensile load represents 95% of the pipe body strength. When a 95% load of a weak material such as GradeB is applied, the induced strains are considerably smaller than when the same 95% load is applied calculated based on a higher strength material such as P110. The differences in axial strains in the pipe body were approximately 1440 με and 3665 με for GradeB and P110 respectively. Since the geometry of both connections is the same, larger deformations are induced using the high strength material. By applying larger deformations, the total axial load is distributed over an increased amount of (mainly vanishing) threads.

3.4 Gap Size

3.4.1 Absolute gap size

After applying 95% of the maximum tensile load, the gap between the load flanks and stab flanks is extracted and is shown in Figure 5–26 and Figure 5–27 respectively. For the load flanks, very little clearance in all the cases is observed. When comparing these results with the results of the axial load distribution, previously shown in Figure 5–24, it is clear that when the load distribution is zero or negative, an axial clearance still exists. However, this clearance does not exceed 20 μm and will likely be clogged with thread

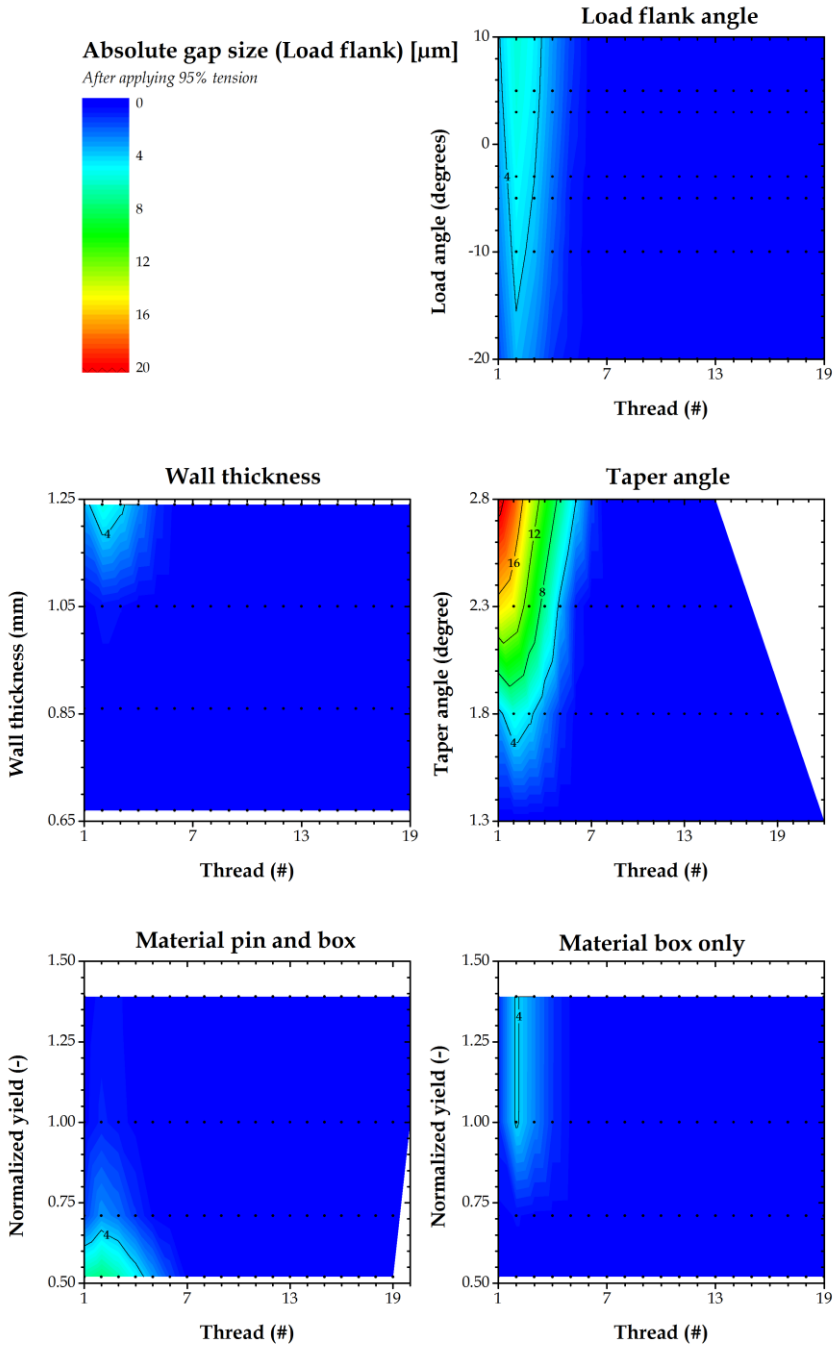

Figure 5–26: Effect of parameter modification on the absolute gap size at the load flank after applying initial make-up and axial tension.

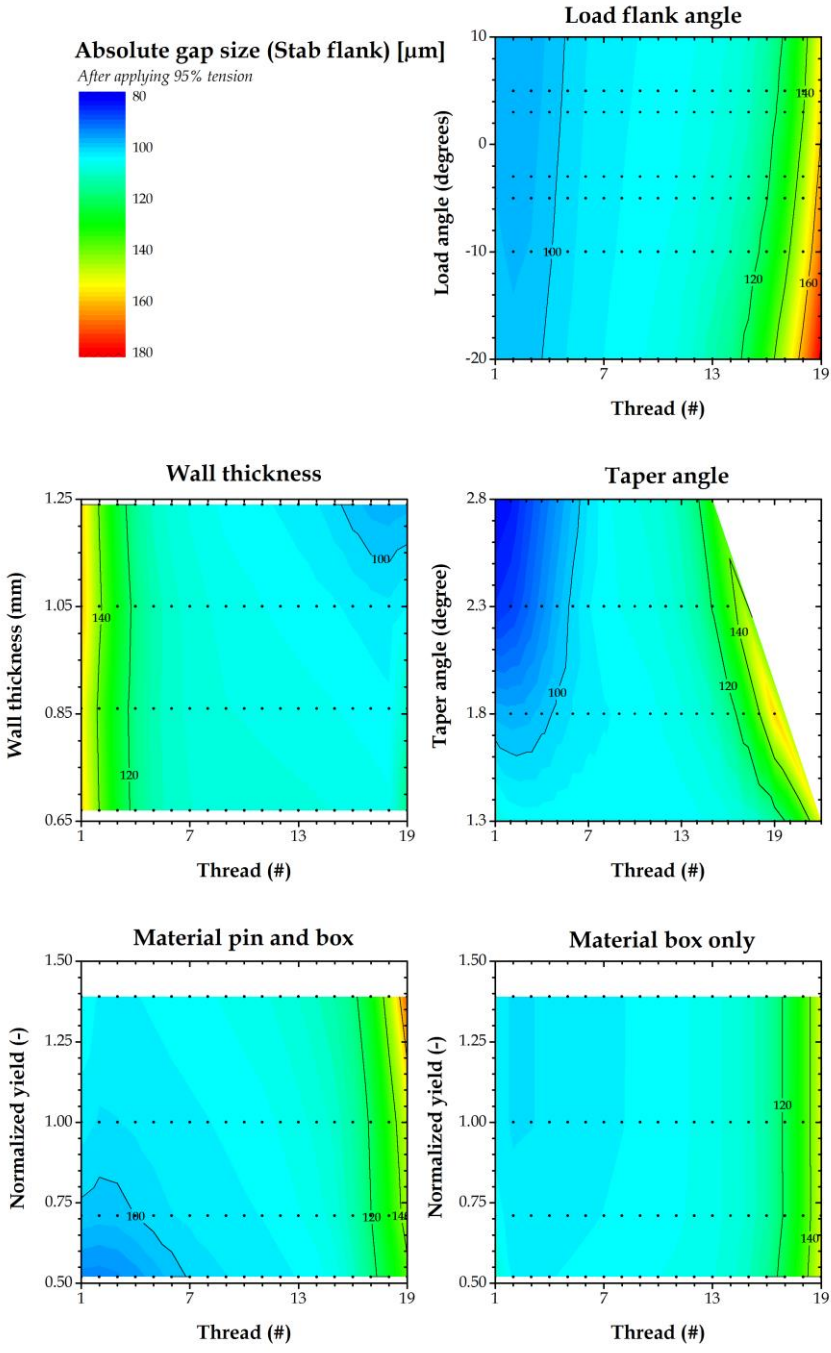

Figure 5–27: Effect of parameter modification on the absolute gap size at the stab flank after applying initial make-up and axial tension.

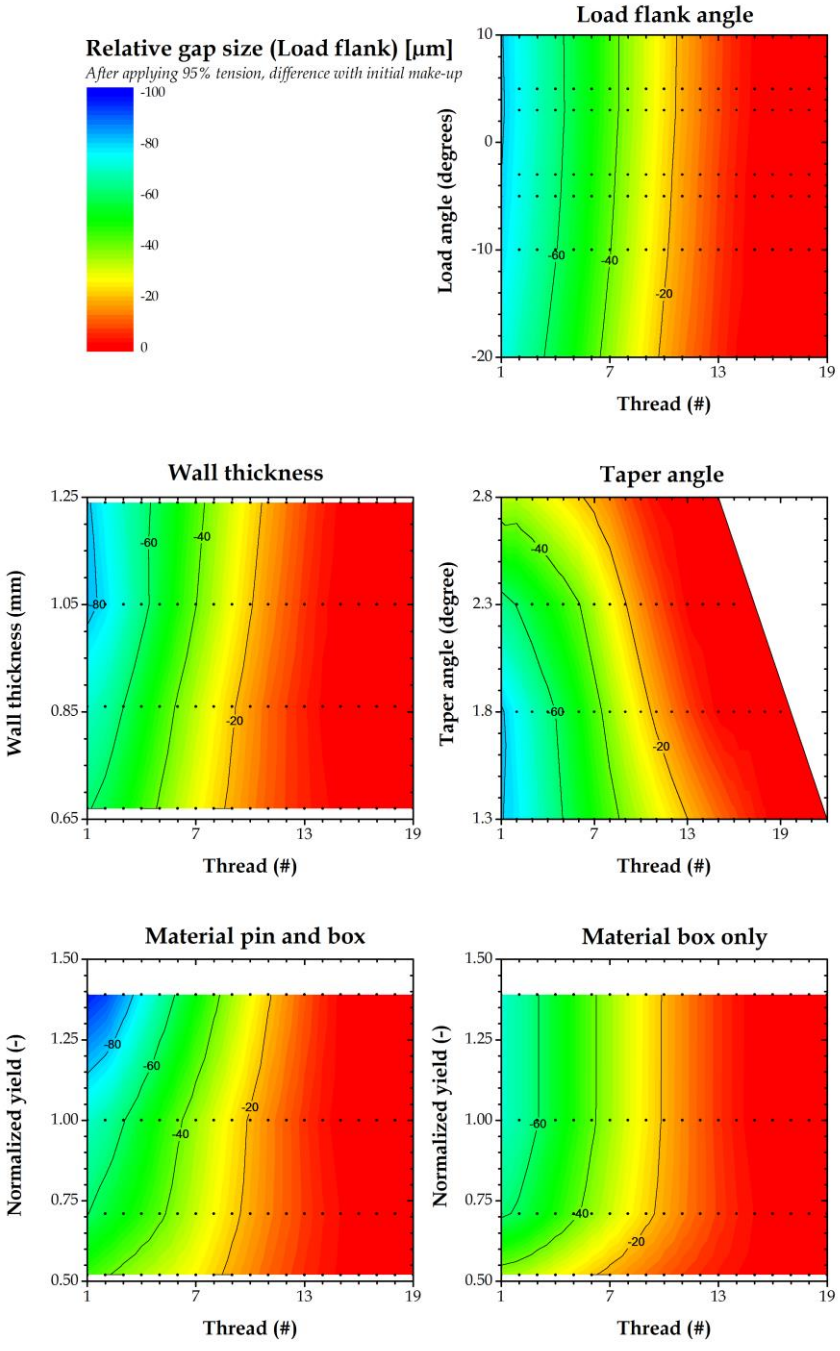

Figure 5–28: Effect of parameter modification on the relative gap size at the load flank after applying initial make-up and axial tension.

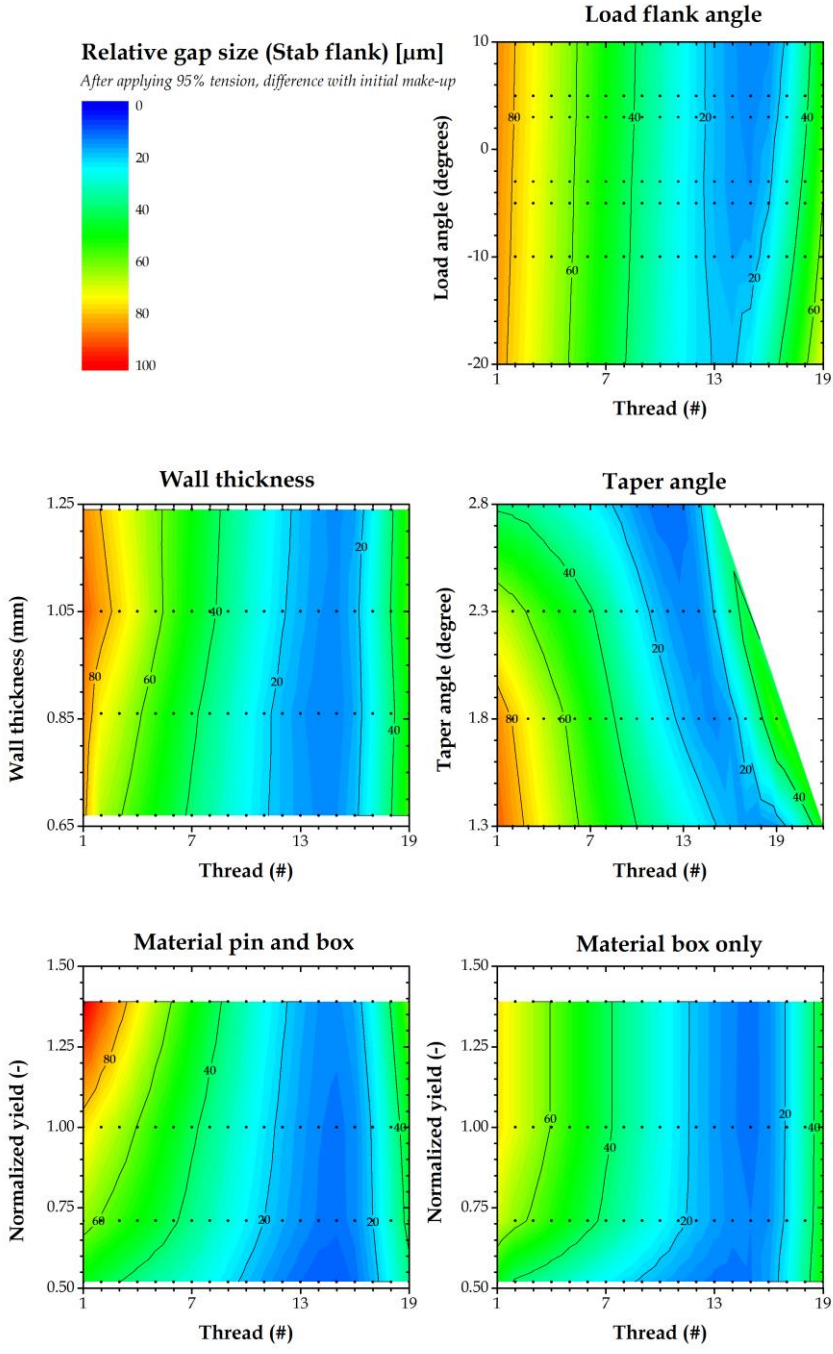

Figure 5–29: Effect of parameter modification on the relative gap size at the stab flank after applying initial make-up and axial tension.

compound, resulting in a thread seal. As expected, the gap sizes at the stab flanks show a similar, yet opposite behavior. It should be noted that the summation of the stab gap with the corresponding load gap does not equal the initial clearance exactly as the result of deformations during the make-up and during the application of the external loads.

3.4.2 Relative gap size

Finally, the relative gap size for the load and stab flanks are summarized in Figure 5–28 and Figure 5–29. It is interesting to notice that for the load gap, the highest negative values are situated near the pin tip. Despite the absence of acting loads, the gap sizes at this location are still susceptible to changes because of the deformation of the box. In contrast, the vanishing threads remain in contact and no changes are observed between the load flanks. The relative movement between pin and box at the stab flanks appear to be more complex. A local minimum is observed along the first half of the vanishing threads adjacent to the complete threads. This is caused by the failure of the threads succeeding this zone as was earlier noticed by a reduction of the axial load distribution. Due to the limited size of the load flanks among the last vanishing threads, the threads tend to slide over each other as a result of plastic deformation. While these changes appear to be very limited when modifying the load flank angle, wall thickness and the box material once a normalized yield ratio of 0.75 is reached, the two other parameters appear to have a significant effect. The relative clearance can be reduced when applying a steeper taper angle or when reducing the yield limit of the entire assembly. While the changes as a result of taper angle modification can be explained considering the lower initial clearance inherent to the larger taper angles, the increased initial make-up is responsible for the behavior when increasing the material strength. When considering to keep the thread clearance at both the stab flank and the load flank to a minimum, larger taper angles and the use of low steel grades appear to be more suitable. While the first can be explained by the contribution of the vanishing threads (see Section 3.3.2), the latter can be explained by the reduction of elastic deformation which directly influences the relative thread clearance.

4 Conclusions

This chapter has shown the applicability of the developed numerical modelling approach which was described in chapter 4. ThreadGenBT was first used to assess the effect of make-up on trapezoidal threaded connections. This study showed that by applying make-up, the axial load tends to shift from the complete threads to the vanishing threads while the radial load remains equally distributed over the threaded length. Additionally, leak paths long the thread flanks can be blocked by considering the Poisson effect.

Consecutively, the scripts post-processing capabilities using the predefined output parameters were shown by examining the effects of various connection parameters in combination with initial make-up. The investigated parameters were:

- The load flank angle.
- The wall thickness of the box.
- The taper angle.
- The material of both pin and box.
- The material of only the box.

For all cases, the external loads have to be considered when estimating the maximum make-up position in order to limit the overall plasticity. No significant changes were observed when considering the radial load distribution. In contrast, the axial load distribution could be influenced significantly by changing the wall thickness. When increasing the thickness of the box, similar effects as increasing make-up were observed. Considering the clearance along the thread flanks, taper angle and material strength of the entire assembly appear to be of major importance while only minor changes are induced by the other three variables.

To conclude, it was found that changing the taper angle has effect on both the mechanical performance as on the economic aspect such as the rig time during make-up. Furthermore, it was shown that increasing the strength of the box material offers benefits, but once the pin becomes the weakest member, further increasing the material yield strength does not offer any advantages, nor mechanical disadvantages. Instead of changing the strength of the material, it was indicated that by applying changes to the wall thickness, similar results could be obtained.

The knowledge obtained within this chapter will be used to develop a new type of connection. This process is further explained in the next chapter.

References

[5.1] Mazzaferro, G.M., Coppola, T., Amato, S., et al., *Threaded connection with improved root thread profile*, United States Patent, US 20140182426 A1, 2014

[5.2] Sivley, R.S., and Reynolds, H.A., *Helical groove for a tubular connection*, United States Patent, US 7607333 B2, 2009

[5.3] Pollack, J., *Pipe connection*, United States patent, US 20140300104 A1, 2014

[5.4] American Petroleum Institute, *API 5B: Specification for threading, gauging and thread inspection of casing, tubing and line pipe threads*, fifteenth edition, 2008

[5.5] American Petroleum Institute, *API 5L: Specifications for line pipe*, forty-fifth edition, 2013

[5.6] ISO specification 13679, *Petroleum and Natural Gas Industries – Procedures for Testing Casing and Tubing Connections*, European Committee for Standardization, 2006

Chapter 6

Development of a new type of connection: the ‘LS95R’

<< *This page intentionally left blank* >>

Table of Contents

1 Introduction

Before defining the criteria the new type of connection has to fulfill, it is important to point out that this is only a theoretical design to illustrate the capabilities of the developed numerical approach, including the finite elements model and post processing procedures. Since geometric tolerances and irregularities as a result of the manufacturing are not within the scope of this work, they are not explicitly taken into account. The starting point for this new thread design is the 4.5 inch connection with a standard API buttress thread [6.1]. By using this reference, the results gathered during the performed parametric study (see Chapter 5) can directly be used for the design considerations. The pipes which are to be connected are 114.3 mm (4.5 inch) pipes of TN80 steel grade with a wall thickness of 7mm. This decision is based on the fact that this is the smallest standardized casing size and imposes the least requirements on testing equipment when experiments have to be conducted..

Section 2 starts with an overview of the design intentions, explicitly mentioning the targeted enhancements to solve some of the problems seen today. Next, the global parameters are quantified based on the results obtained during the parametric study performed in Chapter 5. In addition to these variables, the local thread parameters are further enhanced by performing an additional 1200 numerical simulations. Based on these results, section 5 encloses the geometry of a new, modified connection which is believed to have a better performance when applying axial tension and internal pressure up to 95% of the pipe body strength compared to the standard buttress connection.

In order to demonstrate the potential benefits of the developed connection, a case study is included in section 6 where a standard connection is compared with its proposed successor. Finally, some remarks together with a word of caution is formulated and the chapter is ended by summarizing the main conclusions.

2 Design criteria

In order to design an improved connection, several prerequisites have to be fulfilled. First of all, it is desirable that the connection is able to contain pressurized fluids without leaking. Since the *API Modified* thread compound is used in this research, a gap size of 125µm is assumed to be able to seal the connection [6.2]. However, when loads are applied and relative movement between pin and box is initiated, it is unsure whether the formed leak paths will heal after the thread compound is dried out. For this reason, it is desired to have contacting surfaces at both the load and the stab flank. This way, a helical leak path will not freely exist and this is believed to increase the connection's sealing capabilities. In order to create contacting flanks without drastically increasing frictional forces during make up because of the

previously defined *k*-value (see Chapter 3), a root-crest contact is preferred. Therefore, it is opted to maintain a limited gap size between the stab flanks of pin and box. The size of this gap has to be determined by applying an iterative assessment of the gap size at the stab flanks near the pin tip during make-up. By using the effect of the Poisson's ratio of the steel, the gap at the first engaged thread can be closed due to the members' elongation. This requirement will also impose a minimum make-up position. Since this principle is much more complicated than only the Poisson effects due to deformations caused by make-up and additional working loads, an iterative process is required using previously determined values for the other parameters.

Apart from a better leak resistance, the outer diameter should be kept to a minimum for the reasons mentioned in Chapter 1 and a fast make-up is desirable to reduce rig times. The latter can be incorporated by reducing difficulties related to stabbing and by reducing the required number of power-tight turns. Both these criteria can be fulfilled by increasing the thread size or by applying a steeper taper angle.

A last requirement for the suggested connection is that it needs to have a 100% rating compared to the pipe body performance of the connected pipes for all four extremes of the von Mises envelope as defined in the ISO 13679 standard [6.3].

3 Design Considerations

1.1 Selection of box material

In order to select an appropriate material, two aspects have to be taken into account. Firstly, when tension is applied, the critical section of the assembly has to be identified and assessed. Secondly, when internal pressure is applied, the box will be expanded even further than during initial make-up while the pin will be pushed back to its initial state. This means that the material should be chosen so that the critical section is located on the pin, probably somewhere within the area containing the vanishing threads. This way, connection ratings of over 100% can be achieved. Additionally, a sufficient elastic energy reserve has to be foreseen in the box. While it is advantageous to reduce the outer diameter of the connection as much as possible, the selection of an appropriate material should be based heron. Since plasticity should be avoided according to the ISO 13679 testing procedures, only the yield strength of the material is of interest for this study.

1.2 Wall thickness

Based on the findings related to the wall thickness ratio obtained in Section 3.3 of Chapter 5, the ratio of box-to-pin wall thickness could be reduced up to 0.81 while a make-up value of a little below 1 turn is still possible.

In order to take into account the safety margin defined when assessing the required thread clearance (see further in section 1.5), it is opted to slightly increase the pin-to-box ratio up to 0.9. This way, a make-up of 1 powerturn should still be possible. Considering the wall thickness of the pin is 7mm, the section of the box near the first engaged thread has to be at least 6.3 mm. The reason this value is less than the wall thickness of the pin can be explained by considering the 12.5% tolerance on the wall thickness of the pipe. Due to this tolerance, the burst pressure is only 87.5% of the nominal value. Since the custom design of the box does not necessarily have the same tolerances, this adjustment does not have to be taken into account, resulting in a reduced wall thickness.

Taking into account the threaded length on the pin and the matching taper, the proposed wall thickness at the last engaged thread of the box would lead to an insufficient outer diameter at the box tip to include threads. Since it is desirable to keep the total amount of vanishing threads, the wall thickness at the critical section is slightly increased to 6.7 mm, resulting in an increase of 8.7 mm with respect to the outer pin diameter of 114.3 mm as is shown in Figure 6-1. Note that this is much smaller than the standard 17.8 mm, defined by the API [6.1].

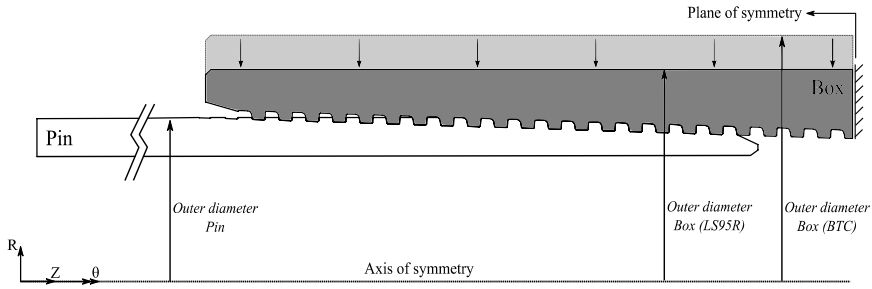

Figure 6-1: Schematic representation of the reduced outer diameter of the LS95R connection compared to the standard BTC connection.

1.3 Taper Angle

In order to determine an appropriate taper, the results in Figure 6-2 are considered. Because one of the prerequisites is containing a thread seal, a small taper angle is beneficial since this creates a larger neutral zone near the pin tip on which no external forces are working. In contrast, a large taper angle is suited to reduce the number of make-up turns required during assembly. This reduces the rig time and is economically more efficient. The obtained data from the simulations using a 0.25 mm radial overlap is consolidated in Figure 6-2. It was mentioned before that a thread seal is assumed to be effective when a critical gap size is not exceeded in 3 to 5 consecutive threads. In order to reduce the chances of damaging the dried out thread compound at these locations, it is decided to reduce the impact of external loads at these locations.

Using the plotted data in Figure 6-2 and keeping in mind that the results are based on a slightly higher amount of make-up turns than required, the upper limit for the thread seal (5 consecutive threads) is considered to be the upper limit of the taper angle for the proposed connection. This way, the maximum applicable taper angle is considered 2.41 degrees. Related to this angle, a maximum of about 1.05 powerturns can be applied. It is beneficial to achieve the required make-up in as little time/rotations as possible together with the previously determined amount of make-up turns to ensure sufficient axial elongation of the pin to create a thread seal. For these reasons, the 2.4 degrees value is used as the actual taper angle. This angle coincidently matches the angle defined in the API standard for connections of sizes 16 inch and larger.

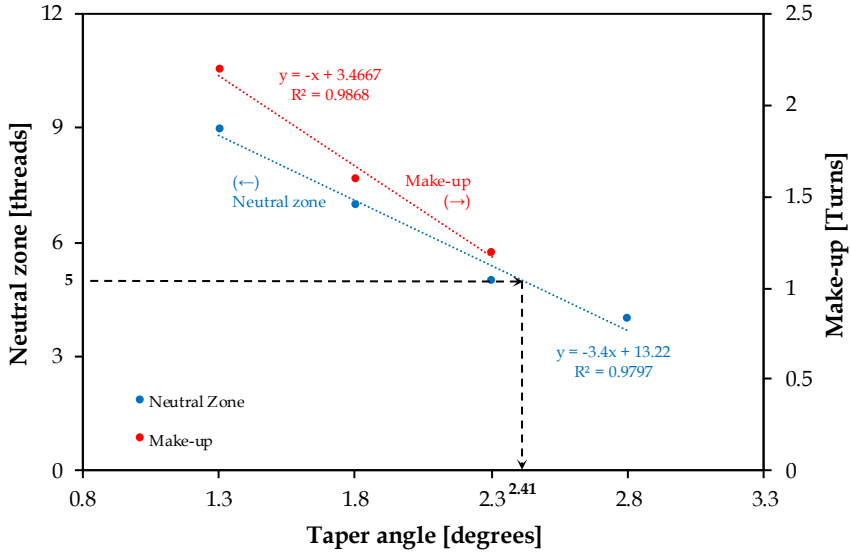

Figure 6-2: Determination of an appropriate taper angle

1.4 Flank Angles

Based on the results of the numerical study in Chapter 5 where it was shown that modifying the load flank angle of a standard trapezoidal threaded connection did not have any significant effect when combined with an initial, radial make-up, it is decided not to apply any changes to the load flank angle. It should be noted once again that this assumption is not valid for premium connections and/or connections containing other make-up mechanics.

The root and crest flank angles are modified with the intention of minimizing the frictional multiplier (k-value, see Chapter 3) in an effort to reduce the required make-up torque. Appropriate angles were determined to be 0 degrees for both root and crest flank angle. This modification reduces the k-value to its minimum value, 1, and is also used in the standardized BTC

connection for sizes of 16 inch and larger. For smaller standardized sizes, having 1.8 degrees angles, this value is only marginally larger.

1.5 Clearance between Threads

It should be mentioned that due to the complex interaction of the mechanisms described in section 3 of Chapter 5, it is very hard to calculate the appropriate gap size when designing connections and therefore, an iterative, numerical design approach is required.

In an effort to determine an appropriate gap size between the stab flanks, which is required to limit the required make-up torque, the average opening between the flanks in a standard buttress connection is evaluated and shown in Figure 6-3. From this analysis, it is clear that when the stab flank clearance reduces, the clearance at the opposing load flank increases. This means that it is impossible to seal both helical paths at the same time when applying make-up.

It was mentioned before that this theoretical coupling geometry does not take into account tolerances. However, in reality, these tolerances may be beneficial. Due to the random nature of these geometric deviations, they may obstruct the possible leak paths. This assumption is based on the report of a study that investigates the possible reasons why buttress connections started to leak [6.4,5]. It was revealed that deviations in the geometry might have a beneficial result on the leak resistance of the connection. Thanks to better machining methods, these deviations reduced and caused the connections to leak.

It is believed that at least two threads without gap are required to manufacture a thread sealing [6.6]. For this reason, three consecutive threads at both ends are investigated: the first three complete threads are supposed to seal the stab flank helix while the gap sizes of the last three complete threads seal the load flank helix. The average relative changes of gap sizes for a standard buttress threaded connection at the defined thread flanks are given in Figure 6-3. The reason why the average gap size was considered rather than the maximum gap size, which is used when considering leak resistance, is because the maximum gap sizes are often located at the extents of the flanks near the thread radii. Therefore, this would give an overestimation of the overall gap size and might require a too high number of make-up rotations causing excessive contact pressures and early plastic deformation. From this figure, it is observed that for make-up turns over about 1.8 power turns, the gap sizes remain constant. The reason for this is a combination of plastic deformation on the one hand and a complete closure of the gaps at the stab flanks at the other hand. After considering the allowable tolerance on the present gap size between stab flanks to be 25 μm [6.1], it is found that this value corresponds with the relative gap size increase for the third and limiting complete thread when about 1 make-up turn is applied. Considering the

maximum value for the tolerance is usually not reached, it is decided to take into account a 20 % reduction in gap size, reducing the target make-up position from 1 turn to 0.8 powerturns. This also allows some extra margin of error resulting from changes made to the taper (see further). Using this value as the proposed make-up position, the maximum gap size at the stab flanks near the pin tip that can be closed is 51 µm. This value is considered to be the initial, nominal thread clearance of the newly designed connection.

It should be noted that this calculation is based on a taper angle of 1.8 degrees. When the taper angle deviates from this value, it is possible that the gap size needs to be adjusted. Since changes to the taper angle also change the maximum make-up position, adjustments of the gap size are based on a series of preliminary simulations rather than on a theoretical approach using found trends.

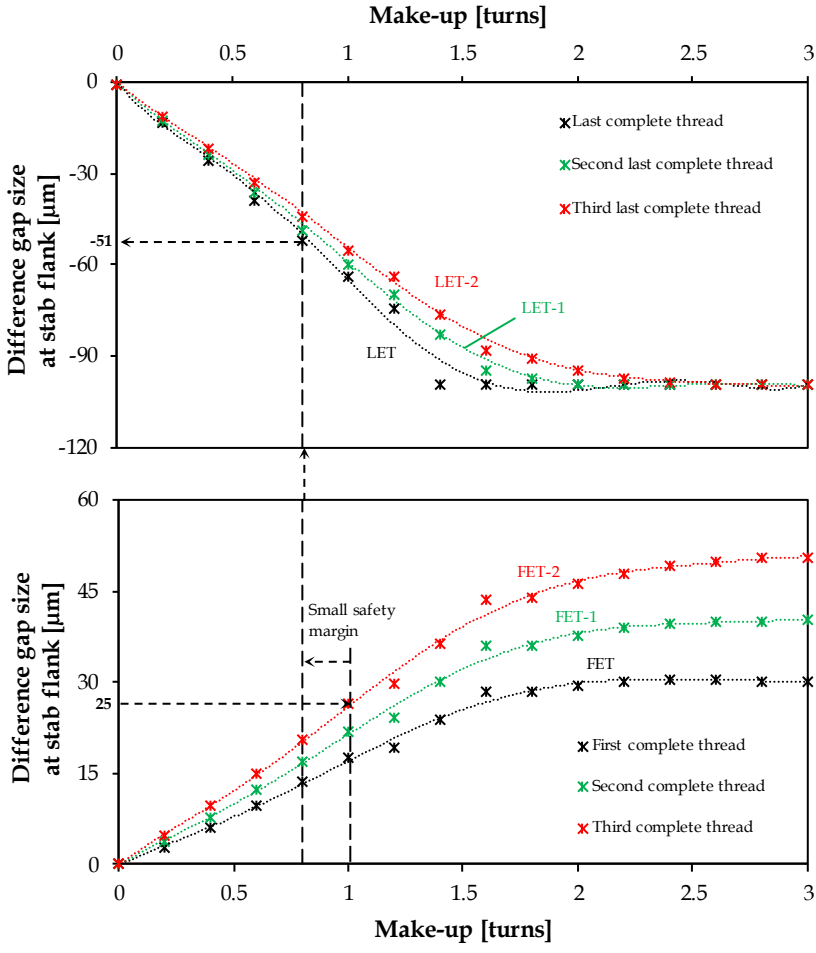

Figure 6-3: Determination of required gap size at stab flank

4 Adjustments of thread parameters

The identification of the appropriate thread parameters to match the requirements mentioned in section 2 is partly based on the numerical study performed in Chapter 5. Since that study was based on the standard buttress connection as a starting point, not all the information may be readily available for use in the development of a custom connection. While the found trends may be used, the exact values may not be directly applicable. An example of this is the determination of the required gap size in combination with the taper angle. Since this gap size is based on a 1.8 degrees taper angle, the proposed taper angle of 2.4 degrees may have different make-up characteristics resulting in a different required gap size. One of the possibilities is performing the numerical study of the standard buttress connection with this modified value. However, in this case, assuming these values will not significantly vary because of the slight taper deviation, it was opted not to rerun over 2000 simulations but to use the values found using the standard taper and to make adjustments after evaluating the performance of the connection using the defined values. In order to determine possible enhancements, an additional study is performed on the thread parameters using the previously selected global parameters.

4.1 Effect of thread size modification

When considering connections with smaller diameters such as tubing connections, smaller threads (usually scaled down, resulting in more threads per inch) are often used. One of the assumed benefits of using smaller threads is an improved load distribution [6.7]. In order to investigate this claim, the pre-defined thread geometry is down-scaled in various sizes ranging from 5 threads per inch (tpi) to 10 tpi. The frequently used values of 6 tpi [6.8] and 8 tpi [6.9] are also considered. When scaling the threads, an additional boundary condition is defined to ensure a unique result after scaling. This is incorporated by using the pitch line. This straight, imaginary line connects the middle positions of the load flanks of the thread and is held at the same location for all threads.

Using the calculated friction independent holding torque based on the simulated contact pressures, it is shown in Figure 6-4 that the required make-up torque increases with increasing number of thread per inch (which leads to a decreasing thread size). Based on the range of tested sizes, this relationship between maximum holding torque and thread size appears to evolve towards an asymptotic value. This suggests that further reducing the threads will not have much effect on the required make-up torque, nor on the holding torque. Based on these results, it can be concluded that smaller threads tend to lead to a tighter joint. This can be explained by the observation that an increased number of threads leads to a small reduction of plastic deformation

and a limited increase of overall contact surface in the threaded region, generating additional friction forces.

The absolute radial load distribution shows no significant differences when the thread size is changed. Because the total thread length and overlap remain the same, the magnitude of contact pressure on the root and crest flanks is the same. The lower radial load distribution for the smaller thread is evident since more threads are located in the threaded surface.

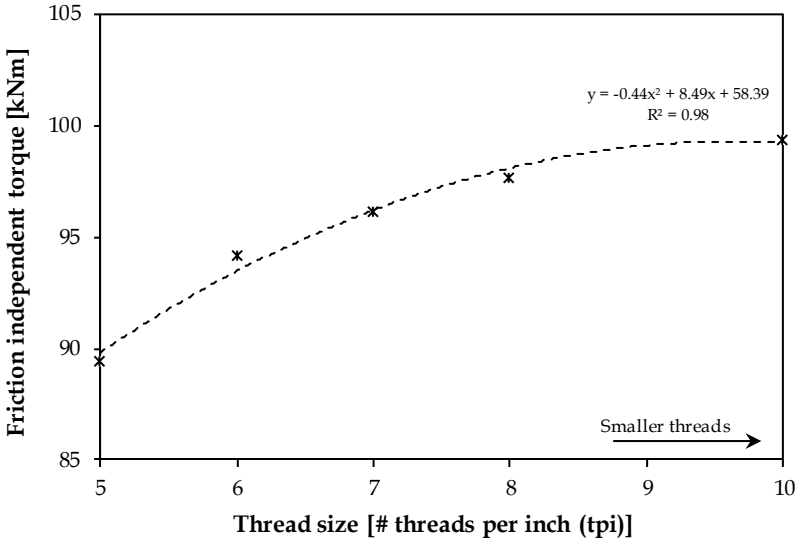

Figure 6-4: The effect of thread size on the numerically predicted friction independent torque.

For the axial load distribution shown in Figure 6-5, it is interesting to notice how the load distribution is more equally distributed when the thread size is reduced. When considering Figure 6-5.A, it is seen that the axial load behavior of the complete threads is independent of their size. All sizes follow the same tendency as observed when using the smallest thread size. The only difference is the cut-off position.

Additionally, when a limited number of threads is present, more load is present on the first engaged thread. It appears that when more complete threads are in contact, a lower portion of the load is present near the vanishing threads. Despite having a lower relative axial load on the vanishing threads, Figure 6-5.B suggests that failure is likely for all threads located in the first 15 mm of the threaded area, regardless of the number of threads present. This can be understood by the assumption that a reduced thread size fails at a lower critical load as a result of the reduced amount of material in the critical shear sections. Overall, it is concluded that a reduced axial load per thread can be

obtained while maintaining the same amount of radial overlap by reducing the thread size.

The effect of scaling the threads on the gap size when an axial load of 95% of the pipe body yield strength is applied is illustrated in Figure 6-6. Based on these results, a translation of the thread clearance at both the stab and load flanks is visible. This indicates that the gap sizes at load and stab flanks are

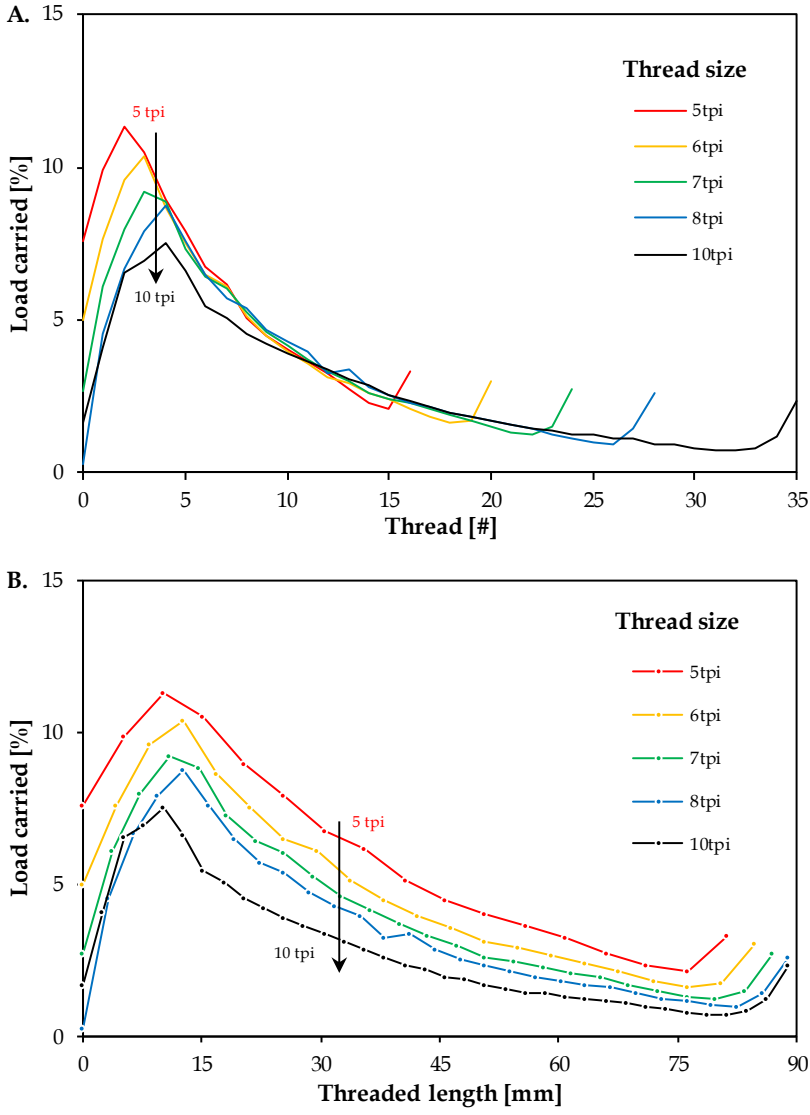

Figure 6-5: Effect of thread size on the axial load distribution plotted in function of threads (A) and in function of the location among the threaded area (B).

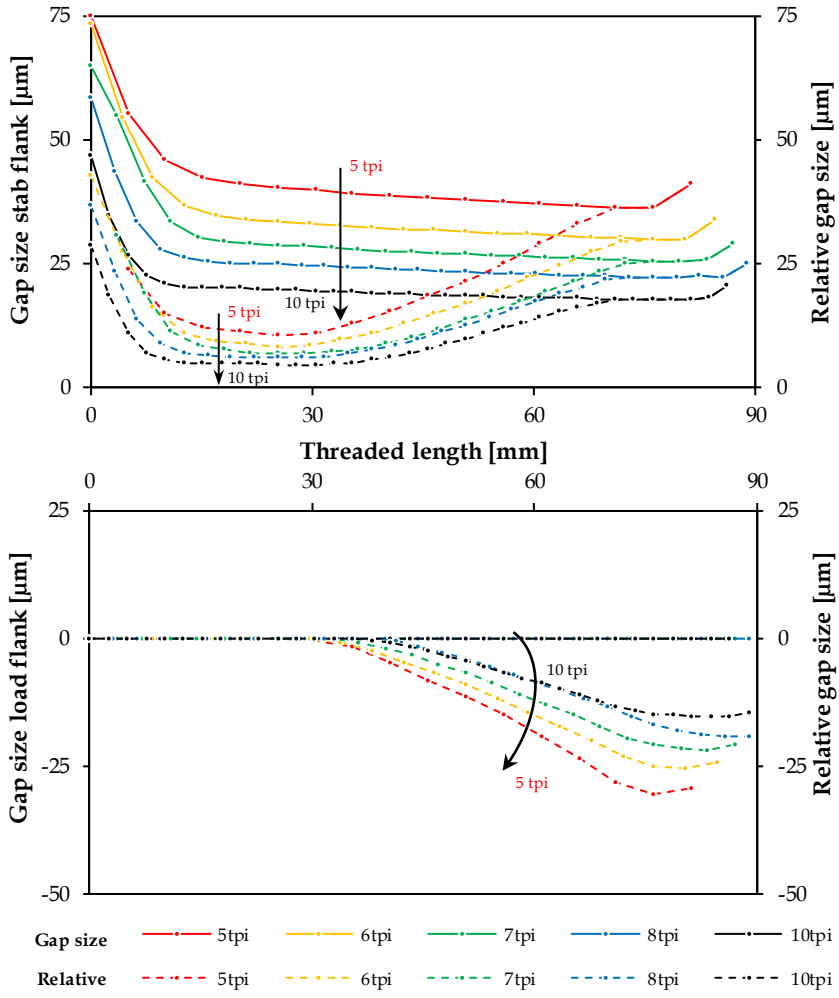

Figure 6-6: Effect of scaling thread size on gap size behavior.

similar for all cases and can be predicted using the scaling factor of the threads. The results for any thread size can be approximated by, for example, multiplying the results of the smallest thread size with the geometrical scaling factor. An example of this approach, using the thread size of 10 tpi as a reference, is shown in Figure 6-7. Using the data obtained for the smallest threads to gain as many data points as possible, a good correspondence is observed for the complete threads. The underestimations present near the vanishing threads can be neglected since a thread seal at this location is not likely. In addition to the gap size being proportional to the scaling factor, also the length of the leak path is proportional. Since a longer leak path increases the likeliness of obstructing possible leak paths, smaller threads are beneficial.

When consulting literature, it is suggested that the use of smaller threads leads to an improved load distribution [6.7]. Based on this assumption, it would make sense to apply the smallest threads possible. However, when the threads are too small, the likelihood of jump-out and damage caused by stabbing and cross-threading increases significantly. For this reason, it is not advisable to scale the threads down by a factor 2 (10 tpi). Doing this would mean that the thread height is only 0.79 mm instead of the standard 1.57 mm. Focusing on existing premium and standard connections, threads with pitches leading to 10 tpi or more are only used for triangular threads. When trapezoidal threads are applied, pitch lengths implying 2 tpi through 6 tpi and thread heights of about 0.8 mm up to 1.8 mm can be found in literature [6.10-13]. An optimal thread height suggested by ref [6.14] was found to be 1.20 mm. Based on the numerical findings and available literature, the threads for the connection are adjusted to 6 tpi instead of the standard 5 tpi.

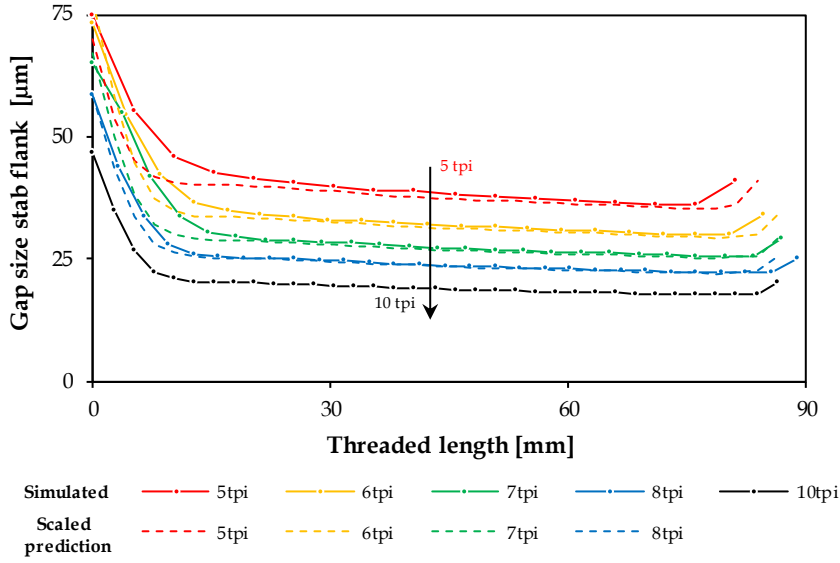

Figure 6-7: Difference between numerically calculated and scaled gap sizes at the stab flank

4.2 Effect of reducing initial gap size modification

In a standard API Buttress connection, the nominal stab-flank clearance is 100 µm. Taking into account possible tolerances on the nominal values, the actual clearance is defined to be between 30 µm and 180 µm. When a thread seal is desired, the ideal clearance between threads would be 0 µm. However, due to tolerances and machinability, this is not possible and maximum three thread flanks can be in contact when tightening to a handtight position. Once make-up turns are applied, the maximum amount of contacting flanks per

thread is reduced to two. The choice which flanks remain in contact can be manipulated using an initial clearance between thread flanks. To prevent wedging of the threads, allowing achievable radial make-up, a clearance near the stab flanks is preferred in the designed connection.

As mentioned before, a clearance as small as possible is often preferred when a thread seal has to be created. However, no optimal values for the flank clearances are currently defined and proposed values, described in literature, generally range from 10 µm up to 300 µm [6.15]. If the stabbing flank clearance is smaller than 10 µm, the clearance is so small that tightening of a threaded joint becomes unstable, and also galling might become an issue. On the other hand, if the stabbing flank clearance is larger than 300 µm, the clearance is so large that external or internal pressures can easily penetrate the threads, pushing the thread compound away and creating a leak path. Some examples of proposed values are: between 51 µm and 254 µm with a preferred clearance of 102 µm [6.16], 150 µm or less [6.17] or between 50 µm and 76 µm [6.18-20]. When different pitch lengths are used for stab and load flanks, values as low as 2 µm are being proposed [6.21].

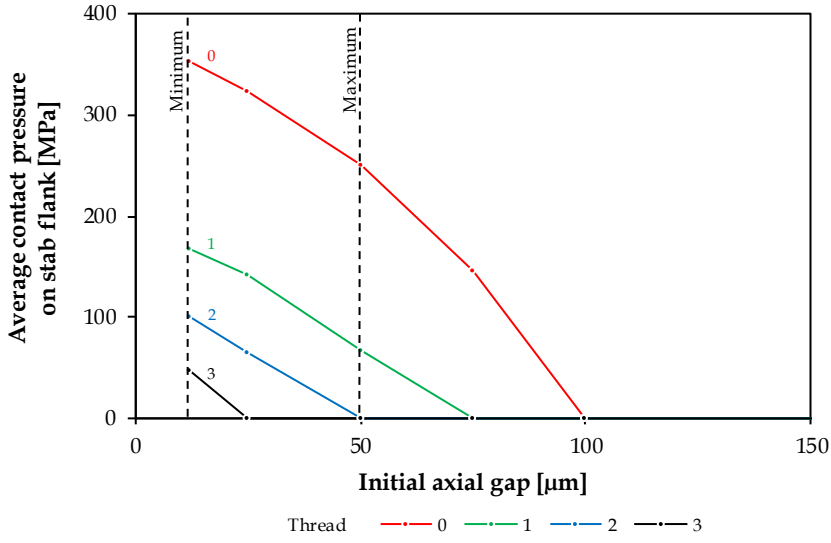

Figure 6-8: Contact pressure on the stab flank after make-up based on the initial, hand tight thread clearance.

Using the numerical results, the effect of initial clearance on the average contact pressure along the stab flank is shown in Figure 6-8. Based on these results, it could be concluded that a smaller axial gap size is better since more contacting stab flanks and higher contact pressures are generated. As mentioned before, perfectly matching threads might be ideal in theory, but they are impossible to manufacture. In order to establish the limits for an initial

gap size, a lower limit and upper limit ought to be established. As a lower limit, the minimal value found in literature of 10 μm is considered. As an upper limit, the previously mentioned criterion which proposed that no leakage occurs when 3 to 5 thread pitches are in contact is used. Once a gap size of less than 50 μm is present, three threads are in contact and the upper limit of the proposed criterion is fulfilled, while contact pressure does not exceed the yield strength of the material. This value also corresponds with the proposed lower boundary of the majority of the patents described above. Using this limit, a 40 μm interval is created which can be used to incorporate geometric tolerances for manufacturing. Since the tolerances are not addressed in this study, a nominal value of 30 μm is considered as a design parameter of the proposed connection.

Despite a slight increase in required torque, no significant changes can be observed which occur as a result of the reduced initial axial clearance.

5 Connection details

The used parameters can be found in Table 6-1. In addition to the newly designed connection, giving an overview of the initial and modified parameters, the parameters for a standard BTC connection and SR23 connection are provided as well for comparison purposes.

Table 6-1: Nominal dimensions of the connections

Parameter	BTC	SR23	Initial design	Final design
Outer diameter box [mm]	132.08	132.08	123.00	123.00
Taper angle [°]	1.8	1.8	2.4	2.4
Load angle [°]	3	3	3	3
Stab angle [°]	10	10	10	10
Crest angle [°]	1.8	1.8	0	0
Root angle [°]	1.8	1.8	0	0
Pitch length [mm]	5.080	5.080	5.080	4.233
Thread size pin [mm]	2.502	2.515	2.502	2.117
Gap size box [mm]	2.604	2.591	2.555	2.147
Length full threads [mm]	56.286	56.286	56.286	56.286
Make-up loss [mm]	87.320	87.320	79.565	79.565

6 Case Study: BTC and SR23 versus LS95R

As a final investigation, a comparison is made between the proposed, enhanced geometry and the standard Buttress connection as defined by the

API. It should be kept in mind that only static loads incorporating internal pressure, axial tension and combinations hereof are considered in combination with a make-up level which corresponds with both the minimum and the maximum positions.

6.1 Plasticity

Using the aforementioned procedures applied to the data visualized in Figure 6-9, the minimum and maximum make-up positions of the LS95R connections are found to be respectively 0.55 turns and 1.65 turns, compared to 0.57 turns and 1.70 turns for the standard BTC connection. After considering external loads comprised of axial tension and internal pressure, these upper limits are reduced to 1.34 and 1.37 for the LS95R and BTC connection respectively.

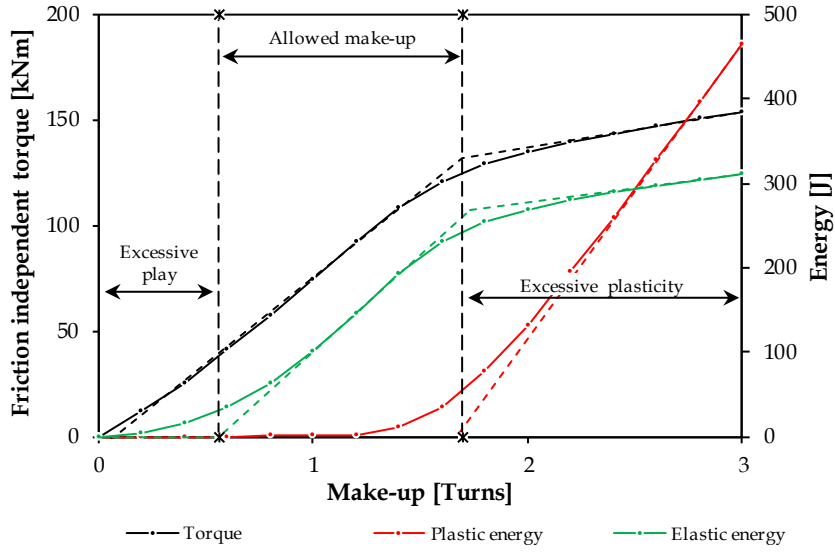

Figure 6-9: Overview of energy and required torque for the make-up positions up to 3 make-up turns using the LS95R connection

When comparing the effects caused by make-up for both connections, it is required to take into account the difference in taper. Since the state of the connection after make-up is mainly influenced by the amount of radial overlap, it is beneficial to express make-up as the amount of radial overlap rather than the amount of power turns. The distinction between these variables becomes clear in Figure 6-10. While Figure 6-10.A indicates that the maximum allowed make-up position is reduced, Figure 6-10.B suggests that a significantly larger radial overlap can be reached using the proposed connection. The reduced

torque observed for the new connection is mainly caused by the reduced amount of vanishing threads.

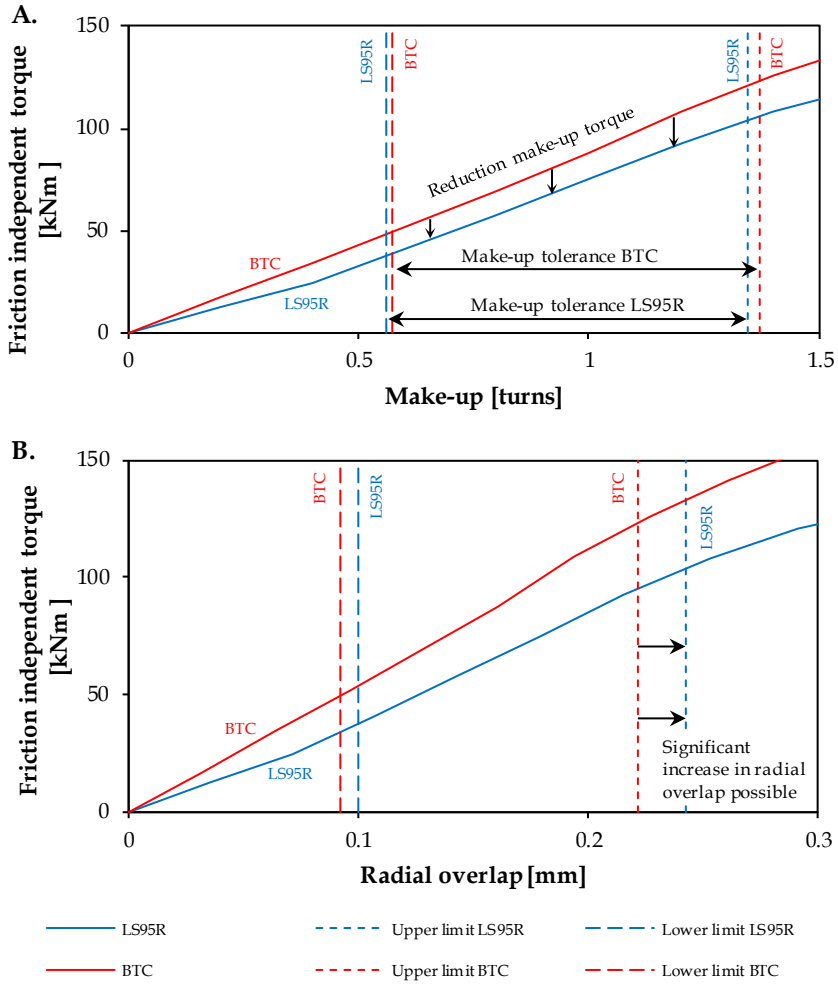

Figure 6-10: Effect of make-up, expressed in amount of power turns (A) and radial overlap (B)

The advantages of this increased overlap become visible in Figure 6-11. Without inducing plastic deformation, the steeper taper angle allows higher contact pressures on the crest flanks in the region containing the complete threads. This increase in contact pressure might be beneficial when it is assumed that, apart from flank clearance, contact pressure will influence the sealing capabilities. This assumption was already mentioned in Chapter 4, but is not known to be significant for connections using a thread seal. While this

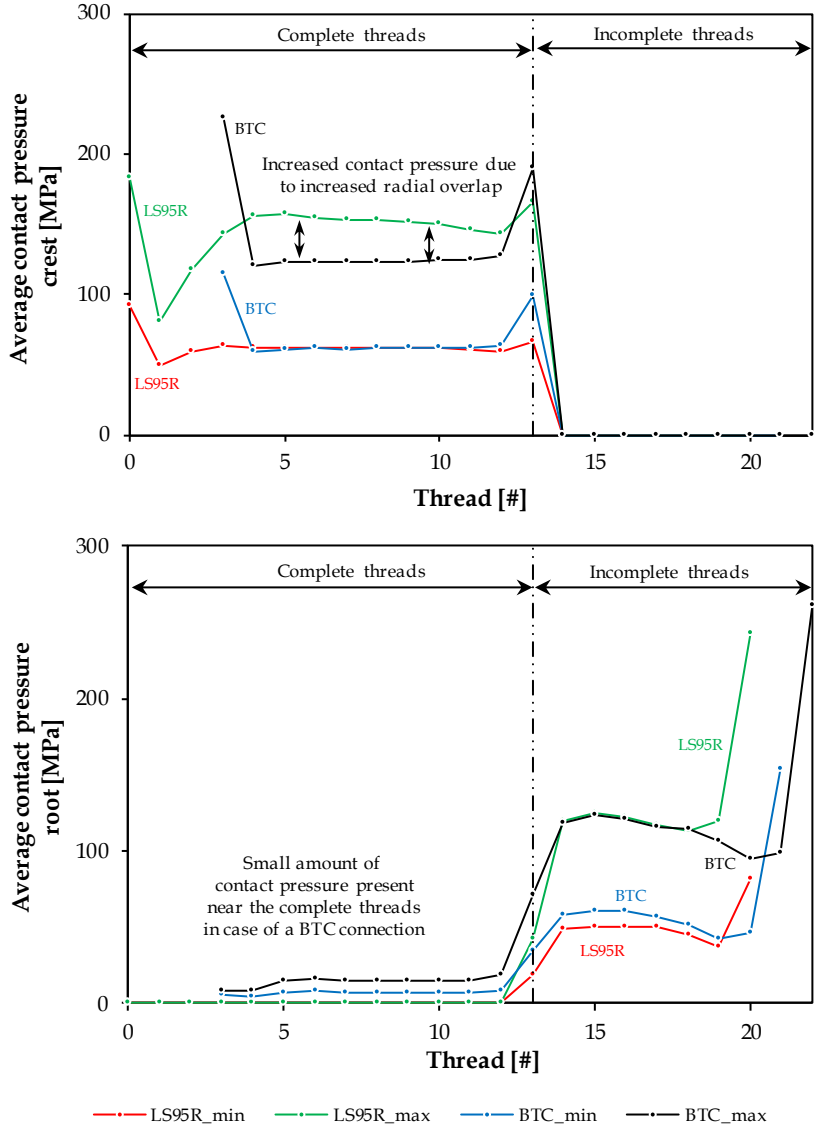

Figure 6-11: Effect of make-up and geometry on the contact pressure at crest and root

additional radial overlap can be beneficial for the overall stress-strain state of the connection, it is noteworthy to focus the attention of the increased risk of potential galling when insufficient thread compound is applied. In addition to the increased contact pressure in threads 4 through 12, a reduction is visible in threads 1 through 3. This is caused by the intended engagement of the stab flanks near the pin tip (see Chapter 5, Section 2.2) to increase the likeliness of creating a thread seal.

For the root flanks, two distinct tendencies can be identified. For the lower limits, the LS95R connection shows a slightly lower average contact pressure in the section containing the vanishing threads. This is most likely caused by a combination of the steeper taper and the root flank angle, as was intended in an effort to reduce the amount of required make-up torque. For the complete threads, no contact pressure is present on the root flanks as a result of the neutral flank angle for both root and crest.

To conclude, Figure 6-12 gives an overview of the suggested maximum torque when a certain percentage of the pipe body load has to be reached. A similar tendency can be observed for both connections. While the lower limit is approximately identical, the upper limit shows a small offset, suggesting a lower number of maximum make-up turns for the new connection.

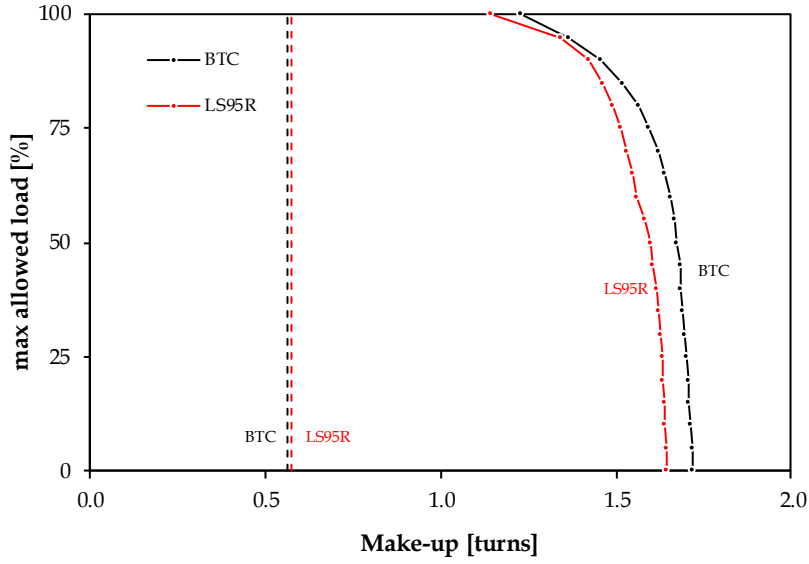

Figure 6-12: Maximum and minimum allowed make-up position for both the standard Buttress connection and the proposed LS95R.

6.2 Load distribution

Very little difference can be observed when assessing the relative radial load distribution which is shown in Figure 6-13.A. The only difference worth mentioning is the pronounced decrease of load carried by threads 1 through 3. This decrease, becoming more pronounced with increasing make-up is the result of the engaging stab flanks at the pin tip, as mentioned before. When considering the total radial load shown in Figure 6-13.B, the load per thread of the new connection is lower while the amount of radial overlap is higher. This is simply caused by the reduced thread size, 6 threads per inch instead of the commonly used 5 threads per inch for standard API buttress connections.

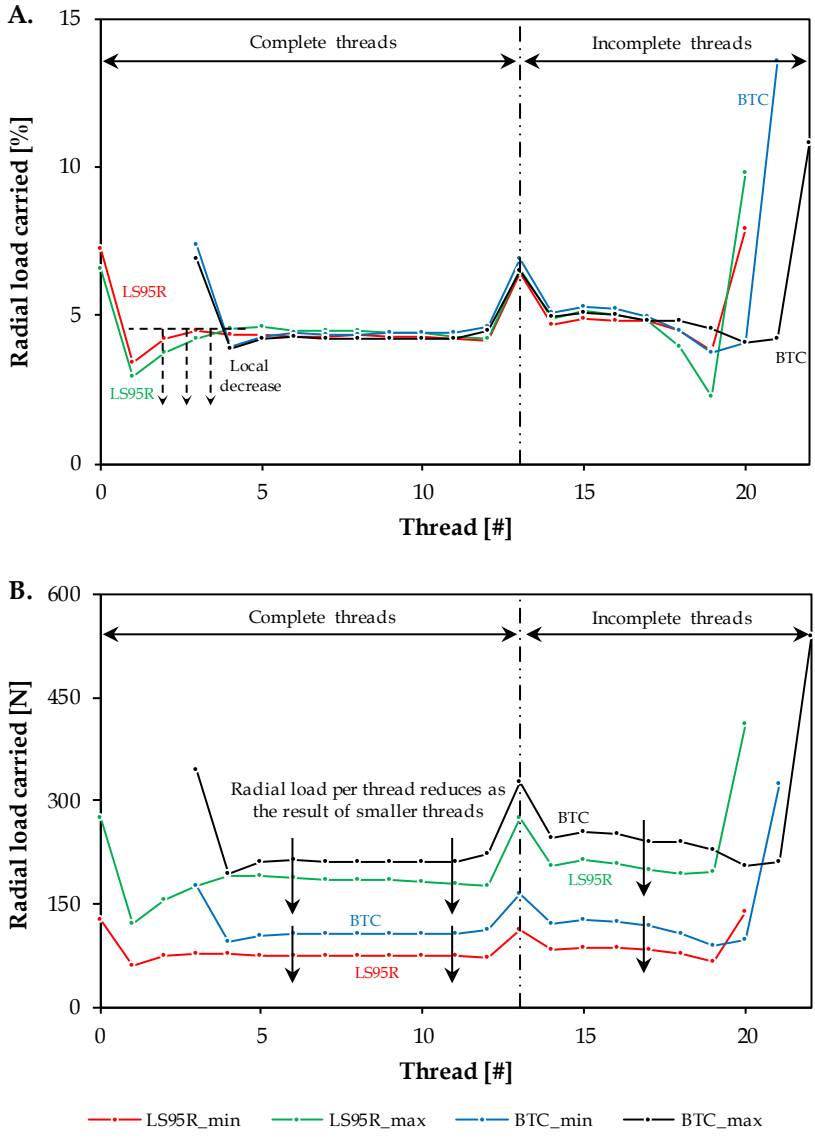

Figure 6-13: Radial load distribution after make-up for both the designed LS95R and standard BTC connections.

The axial load distribution in case axial tension is applied is given in Figure 6-14. Due to the steeper taper used in the LS95R connection, less vanishing threads are present. From Chapter 5, it was found that by increasing the taper leading to a reduced number of vanishing threads, more axial load is taken by the complete threads. For the investigated situations, the relative load taken by the complete threads almost doubles when comparing the LS95R with the

BTC connection. While only 29% of the load is carried by the complete threads of the BTC connection, 51% is carried when using the LS95R connection. Due to this shift in load, the peak load of 12% (see Figure 6-14, when minimum make-up is applied) can be reduced to 8% using the new design. An additional advantage of a steeper taper angle is the faster increasing amount of material present in the critical zone near the root flanks (see also Figure 5-20 of Chapter 5). When more material is present, the likelihood of failure due to local plasticity decreases. This tendency can be seen in Figure 6-14 when considering the amount of failed threads. While the four last threads of the BTC connection show signs of failure, only three threads are predicted to fail using the LS95R connection. Taking into account the reduced pitch length of the latter, this results in a reduction of approximately 40% of damaged thread length, from at least 20 mm to 12 mm.

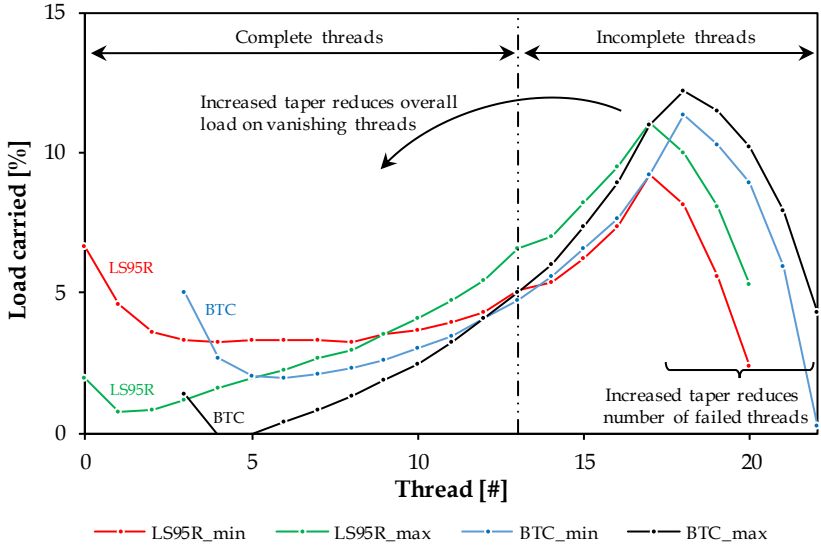

Figure 6-14: Comparison of the axial load distribution of a standard BTC and the LS95R connection.

6.3 Gap size

The comparison of the gap size might be one of the most important criteria within this case study. While it is fairly easy to assess whether or not a connection will keep pin and box together based on FEA, the exact sealing integrity cannot be predicted using only FEA. However, since sealing capabilities are often linked to the combination of thread clearance and particle size in the thread compound, it is possible to indicate whether one connection is likely to maintain its sealing capabilities easier than another. As mentioned before in Chapter 4, it is assumed that when the maximum particle size present

in the thread compound is twice the size of the flank clearance, the thread compound is almost certain to seal the connection.

The newly designed LS95R connection has a significant advantage over its competing BTC connection due to the reduced initial gap size. While the BTC connection was designed keeping in mind production methods and tolerances of the late 1950's, the design of the LS95R connection is designed keeping in mind possible manufacturing tolerances using CNC machinery.

Within Figure 6-15, the gap sizes between load and stab flanks after applying an axial tensile force equal to 95% of the pipe body strength are presented with full lines. The dashed lines represent the relative clearance between the threads and are calculated by subtracting the initial gap size after make-up from the final gap size. It is opted to use the relative gap size rather than the clearance after make-up because it might provide a better insight in the connection. After make-up, the thread compound is dried out. Once a leak tight thread seal is established, larger relative changes are more likely to induce cracks within this seal. While large absolute clearances combined with small relative changes might occur, visualizing the difference between the make-up and the end of the simulation is considered more indicative.

The clearance at the stab flanks is shown in Figure 6-15.A. From this figure, the effect of the initially designed clearance is immediately visible. The decision of reducing the initial gap size with 75% (see section 1.5) results in a final gap size which is reduced by about 70%. While this reduction was to be expected, it is more interesting when considering the relative clearance. When making a distinction between the LS95R connection on one side and the BTC connection on the other, it can be observed that the relative gap size appears to be more dependent on the initial make-up torque for the standard buttress connection, while the proposed connection appears to be almost independent of this variable. In addition, the slightly larger relative clearance for all the make-up positions for the case of the buttress connection might suggest that a leak path along the flanks is less likely to occur when the developed LS95R connection is used.

In case of the load flanks, all the existing gaps which were created during make-up are removed. As was also the case with the stab flanks, the relative clearance of the BTC connection is larger and more dependent on initial make-up than the new design. However, since this involves reduction of the clearance, this is less likely to have any effect on the sealing capabilities of the connection. If the connection were to be loaded in compression, this clearance is of more importance and could lead to a leaking connection.

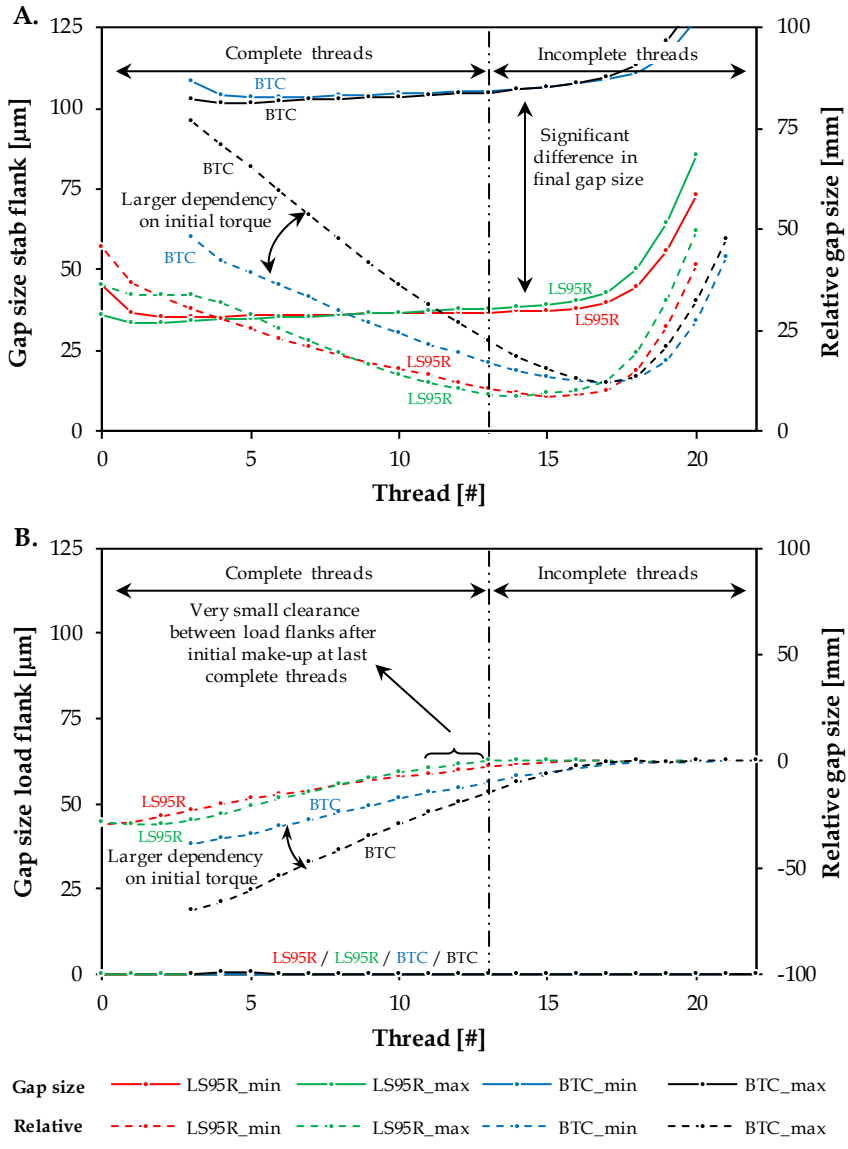

Figure 6-15: Initial (full lines) and relative (dashed lines) gap size at the stab flanks (A) and load flanks (B) for the extreme make-up positions combined with axial tension.

7 Remarks

First of all, the reduction of 40% on the excess outer diameter may appear to be a lot. However, it should be noted that this calculated outer diameter does not incorporate a safety factor. The standardized tolerance on the wall

thickness of tubular members is 12.5% [6.22]. This would mean that in order to compare to the standardized API coupling, a wall thickness of 7.1 mm should be considered. Using this new value, a total reduction of excess outer diameter of approximately 30% is attained. In addition to a reduced outer diameter, also a significant weight reduction of about the same percentage is achieved.

While improvements appear to be made, this geometry is not the optimal geometry for threaded couplings having a high performance rating. When considering the designs of companies which are actively seeking to enhance sealing threads, additional aspects should be considered before implementing the suggested design. Figure 6-16 shows various aspects of the thread which are taken into account designing the TopTorq connections of a small company, named Reliable Pipe Threads. An enhanced thread which is commercially available as a TopTorq connection is shown within this picture. It is claimed that these couplings form a gas-tight connection solely relying on the thread seal. Taking a look at the geometry of this connection, it is immediately apparent that a crest-to-root gap is incorporated while a stab flank clearance is present in the suggested, improved thread of the LS95R connection. This observation indicates a design principle which was mentioned, but not studied within the proposed framework: a different pitch length for stab and load flanks. It was mentioned in Chapter 3 that applying this principle unlocks the possibility to remove the axial play in a threaded connection. The reason this was not investigated is that by applying this method, an axial make-up needs to be induced. The conducted research focusses on make-up relying on the generation of radial forces. While this approach is worth investigating, this fundamentally different approach is situated out of the scope of this work. It can also be seen that a negative load flank is applied. While the load flank angle does not make much difference when an axial gap is still present, it appears to be beneficial when wedging the threads. This way, jump-out is unlikely to occur while applying torque and/or axial tension. Further, the size of the stab flanks are increased to facilitate the stabbing procedures and thread radii are increased to improve fatigue strength. While the first enhancement is implicitly incorporated in the proposed design by increasing the taper angle and choosing neutral crest and root angles, the latter was not considered since dynamic loads leading to fatigue failure were not the principal aim of this research.

Furthermore, while the design was investigated using a validated numerical approach, experiments are advised before applying the proposed connection. The main reason for this is to take into account criteria which cannot be predicted such as the behavior of the applied thread compound which is vital to create a thread seal. Not only is the thread seal affected by the applied thread compound, also the make-up, holding and break-out torque depends on this substance. This is because these three torque levels are partially a function of the coefficient of friction, which is in turn dependent on

the applied thread compound. It cannot be guaranteed that fresh thread compound has the same coefficient of friction as a dried out compound. Therefore, it is impossible to predict the exact make-up, holding and break-out torque. The values calculated using the friction-independent holding torque (CTRQ) are only an indication. When it is desirable to know these three torque-levels, it is mandatory to perform a series of make-up tests.

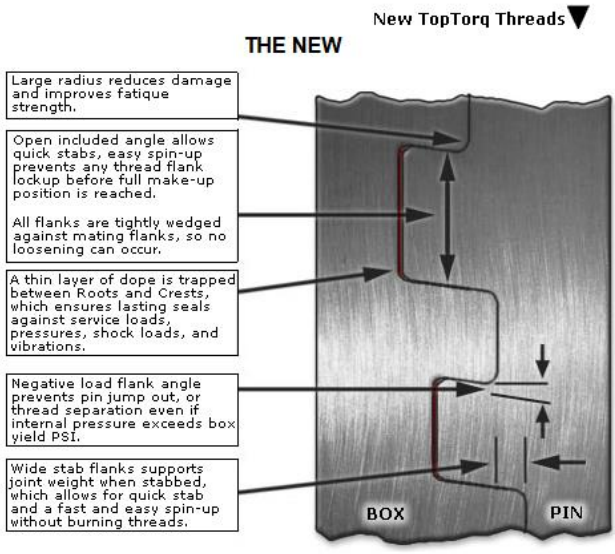

Figure 6-16 Commercial representation of the *TopTorq* threads as provided by the company '*Reliable Pipe Threads*' [6.23]

As a final note, it should be mentioned that an enhanced Buttress connection already exists. In the late 1990's, an addition to the API 5B standard was suggested in which the buttress thread was redefined in an effort to increase its sealing capabilities. This enhanced connection is known as the Buttress SR23 connection. Compared to the standard buttress connection originating from 1956 and patented by Samuel Webb (see Chapter 1), the only change is a reduction of the clearance located at the stab flank. In general and with the exception of the clearance after make-up, previous research by the author, but not included within this dissertation, indicated that no differences between this enhanced version and the original could be observed when applying internal pressure and axial tension [6.24]. This is one of the reasons why it was opted to compare the newly created connection with the original buttress connection. A second reason is that the numerically determined clearance at the stab flanks when assembling the connection into a hand tight position is similar to the nominal 25 µm used for the SR23 connection. This would result in marginal enhancements when addressing the gap sizes in section 6.3. In order to demonstrate the usability of the developed methodology, it was considered justified to use the original connection. By independently

determining a new, optimized thread clearance which is similar to a previously found enhancement, suggested in the SR23 connection, the reliability of the applied approach increases. A final reason not to use the enhanced API buttress connection is based on an economical point of view. While this connection is defined in a supplementary note within the API standard, it is not clear whether or not this connection is currently being produced. While it is obvious that the original connection is available everywhere, no apparent indication suggesting any distinction between the original BTC and its successor are present. Since the existence of this connection is not widely mentioned throughout (commercial and scientific) history, the author has reason to believe that the SR23 connection is likely not commercially available.

8 Conclusions

In the previous chapter, the effects of various parameters were investigated. As a result of this study, a connection is designed at ***L***aboratory ***S***oete with a ***95***% rating incorporating a ***R***educed outer diameter: the *LS95R*. After comparing this connection with a standard Buttress connection, it is believed to have better performance, especially related to its ability to maintain pressurized fluids. In addition, one of the greatest advantages is the significant reduction of the outer diameter. When it is the objective to design connections which have the same outer diameter of the pipe body (flush-type connections) containing a 100% rating, the proposed connection is a step in the right direction.

Despite the apparent success of the connection, several disadvantages have to be taken into account. Slightly higher contact pressures within the threaded area may result in a higher risk of galling. However, due to the smaller clearances, a thread compound with smaller particle sizes compared to the API modified thread compound can be used to prevent galling. Additionally, for practical reasons, the connection was designed to be usable up to loads equal to 95% of the pipe body strength instead of the wanted 100%. Related to this reduced performance, it should be mentioned that no safety factors were taken into account.

Finally, tolerances were not taken into account since the exact determination of these uncertainties is beyond the scope of ThreadGenBT.

References

[6.1] American Petroleum Institute, *API 5B: Specification for threading, gauging and thread inspection of casing, tubing and line pipe threads*, fifteenth edition, 2008

[6.2] Watts, J.D., and Ramos, B. W., *Wedgethread pipe connection*, United States patent, US 6682101 B2, 2004

[6.3] ISO specification 13679, *Petroleum and Natural Gas Industries – Procedures for Testing Casing and Tubing Connections*, European Committee for Standardization, 2006

[6.4] American Petroleum Institute, *API Report 86-53 Document Information, Investigation of Leak Resistance of API Buttress Connector*, report, 1987

[6.5] American Petroleum Institute, *WI 2317: Tech Report on LTC/BTC Performance Properties and Leak Resistance: Thread compounds - Rev SS-2006*, report, 2006

[6.6] Reynolds, H., *Downhole threaded connection with scalloped wedge threads*, United States Patent, US7717478B2, 2010

[6.7] Newport, A., *Stress and fatigue analysis of threaded tether connections*, PhD dissertation, Department of mechanical engineering, University college London, 1989

[6.8] Morotti, M., Dell'Erba, D., and Della Pina, G, *Threaded joint for tubes*, United States Patent, US 6921110 B2, 2005

[6.9] Moyer, M., Powers, J.P., Ashley, R.A., *Tubing connection with eight rounded threads*, United States patent, US 5411301 A, 1995

[6.10] Reynolds, H.A., *Treating method and design method for tubular connections*, United States Patent, US 7497481 B2, 2009

[6.11] Huston, F.N., *Threaded connection for oil field applications*, United States Patent, US 7510219 B2, 2009

[6.12] Verger, E., De Montlebert, D. and Thoreau, E., *Threaded tubular connection with progressive axial thread interface*, United States Patent, US 7661728 B2, 2010

[6.13] Noel, T., Roussie, G. and Varenne, E., *Tubular threaded connection joint with trapezoid threads having convex bulged thread surface*, United States Patent, US 20040195835 A1, 2004

[6.14] Santi, N.J., *Threaded joint with high radial loads and differentially threated surfaces*, United States Patent, US 8215680 B2, 2012

[6.15] Hamamoto, T., Sumitani, K., Sugino, M., et al., *Tubular threaded joint*, United States Patent, US 20090200798 A1, 2009

[6.16] Hashem, G.J., *High torque modified profile threaded tubular connection*, United States Patent, US 6767035 B2, 2004

[6.17] Maillon, B., Martin, P., and Durivault, J., *Threaded connection*, United States Patent, US 20120286507 A1, 2012

[6.18] Roussie, G., Massaglia, J., Granger, S., et al., *Threaded tubular connection which is resistant to bending stresses*, United States Patent, US 8220842 B2, 2012

[6.19] Franz, W.F., *Threaded tubing joint*, United States Patent, US 3109672 A, 1963

[6.20] Maillon, B., Martin, P., and Durivault, J., *Threaded connection*, United States Patent, US 8678448 B2, 2014

[6.21] Martin, P., and Maillon, B., *Threaded connection*, United States Patent, US 20130069364 A1, 2013

[6.22] American Petroleum Institute, *API 5L: Specification for line pipe*, forty-fifth edition, 2013

[6.23] Reliable Pipe Threads, *TopTorq: Wedge threads*, 2010, accessed 28 April 2015, <http://www.reliablepipethreads.com>

[6.24] Galle, T., De Waele, W., Van Wittenberghe, J., et al., *Optimal Make-Up Torque for Trapezoidal Threaded Connections Subjected to Combined Axial Tension and Internal Pressure Loading*, Proceedings of the 2014: pressure vessels & piping division conference, 2014

Chapter 7

Conclusions, future work and personal reflections

<< *This page intentionally left blank* >>

Table of Contents

1 Conclusions

Within this thesis, a numerical modelling approach was proposed with the intention of adding various aspects to public literature. These novelties include:

- Developing **a framework to enable pursuing a general, consistent approach (see section 1.1)** in order to express and analyze the '*behavior*'. Literature suggests the use of 2D models to conduct studies on threaded connections. However, apart from strain comparisons and vague approximations of initial make-up, no detailed validation methods and procedures regarding the validity of these models has been provided.
- Obtaining accurate information about the **influence of various geometric features on the behavior (see section 1.2)** of the connection. While lots of different designs are available claiming to have an inherent better resistance to a variety of loads, the exact influences of these geometric features, nor a set of features that can be used to uniformly compare the various kinds with each other are described in public literature.
- **Enhancing existing connections or creating new connections (see section 1.3)** with a certain performance ratio compared to the strength of the pipes of the coupling connections. Using the parameters describing the connection's behavior combined with the determined effects of the various geometric parameters, it is thought to be possible to manipulate the strength of the assembly to a predefined strength. In addition, this approach could also be used to incorporate other objectives such as ease of use, weight reduction, outer diameter reduction, …

1.1 Numerical modelling methodology

Throughout this research, numerical modelling was preferred over experiments, for several reasons. First of all, the use of numerical models implies that certain conditions are simplified such as uniform material properties, equal wall thickness, perfect alignment,… However, these simplifications also imply a reduction of uncertainties when the effect of a certain parameter is investigated. Due to the high degree of uncertainties, it is rather impossible to determine the effect of small changes such as deviating flank angles by using experiments only. Secondly, the performance of parametric studies is economically not possible using only experiments. When changing a feature of the thread, custom made tools should be developed and an excessive amount of experiments should be conducted. Thirdly, it is not possible to repeatedly achieve certain requirements such as an accurate, predefined make-up position. Due to the uncertainty related to the coefficient

of friction and geometric tolerances, it is impossible to know the exact make-up position. This implies that experiments requiring certain make-up positions cannot be performed in a practical way. Finally, using experiments limits the amount of achievable output. No information about contact pressure, stresses and data situated at inaccessible locations can be directly obtained.

The modelling methodology is schematically shown in Figure 7-1. Throughout the research, a two dimensional, parametric script named '*ThreadGenBT*' was developed and validated using a limited number of experiments and a full three dimensional, numerical model. After simulating an initial, (API-)standardized design, three performance parameters are assessed. Based on the outcome of these parameters, changes are made to geometric variables based on their isolated effects. This process is repeated until the desired performance is achieved. This iterative process is considered the *optimization* of the connection.

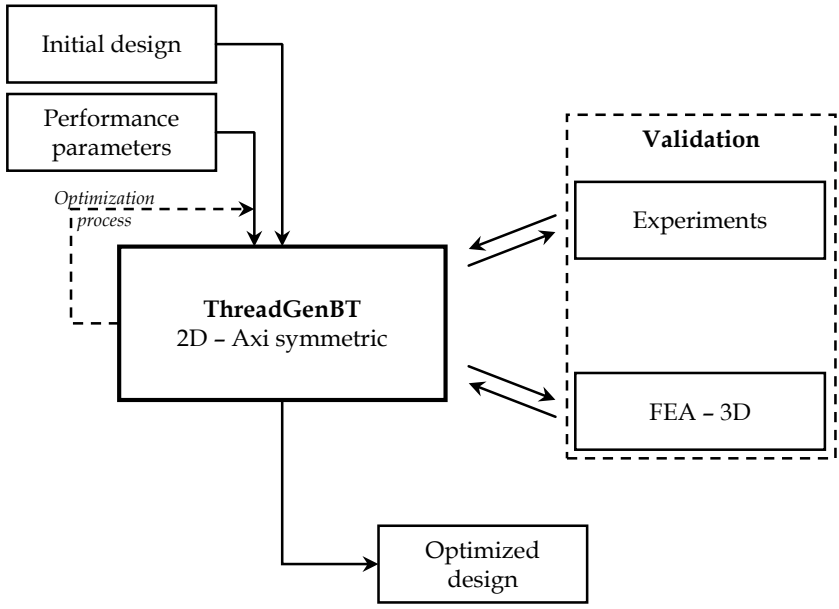

Figure 7-1: Overview of the proposed modelling strategy

Note that the term *optimization* and not *finalization* is used. While the numerical program offers a cheap, fast and fairly reliable output, certain disadvantages might still be present. Examples of such flaws are anything related to handling, tolerances, uninvestigated load combinations, failure mechanisms … Therefore, additional steps such as experiments should be conducted to confirm their actual performance before using a new design in in the field.

Despite the fact that two dimensional models have been used for decades to simulate threaded connections, several distinct additions to current literature have been made from a numerical point of view:

- ✓ The **comparison of make-up conditions with a 3D** FEA model including the thread helix;
- ✓ The **use of field measurements**, including temperature, to compare experiments with the numerical model;
- ✓ The **estimation of required make-up torque** based on the axi-symmetric model.

1.2 Effect of geometry and make-up

During this research, three performance indicators were identified as adequate:

- **Plasticity (P)**;
- **Load distribution (LD)**;
- **Clearance or the gap size between load and stab flanks (GS)**.

By consistently applying these parameters on the results of a parametric study in chapter 5, the effects of isolated parameters in combination with initial make-up could be determined and are summarized in Table 7-1.

Table 7-1: Isolated effects of make-up, global and some local thread parameters on plasticity (P), axial load distribution (LD) and flank gap size (GS)

Parameter	*Effect*	
Make-up	**P:**	Increase of make-up increases plasticity in the weakest section of the connection
	LD:	By increasing make-up, a greater part of the applied tensile load is transferred between the members by the vanishing threads and contact pressure increases
	GS:	Additional make-up increases load flank pressure at the last engaged threads and reduces stab flank clearance near the first engaged threads

Table 7-1 (continued)

Parameter	*Effect*	
Yield strength coupling and pipe	**P:**	Increasing yield strength of material delays plastic deformation, but no changes in distribution
	LD:	More threads transfer load when materials with a higher yield strength are used. Use of low yield strength materials can transfer the entire load by using only a part of the threaded area
	GS:	Higher strength materials are able to close larger stab flank clearances since they admit higher make-up levels
Yield strength coupling	**P:**	Increasing coupling strength reduces plasticity. Once pin and box have the same yield strength, no more changes occur
	LD:	Increasing coupling yield reduces equal distribution over the threads, shifting the load towards the vanishing threads
	GS:	While the clearances at the complete threads are equal for the maximum applied load, more axial movement is present due to larger initial stab gap sizes when using higher strength materials.
Wall thickness box	**P:**	Reducing the wall thickness of the box changes the critical load combination from tensile to internal pressure, increasing plasticity in the central zone of the box instead of the pin.
	LD:	Increasing wall thickness stiffens the box, leading to a more uniform load distribution over the entire threaded area.
	GS:	Increasing the relative strength of the box leads to reduced axial compression and limits the initial gap size near the stab flanks.

Table 7-1 (continued)

Parameter	*Effect*	
Taper angle	**P:**	An increase of taper reduces the area containing vanishing threads, reducing plasticity and reducing the number of threads likely to fail in the critical shear zones
	LD:	By reducing the vanishing threads, more loads are transferred by the complete threads. This reduces failed vanishing threads and in turn reduces the amount of failed threads
	GS:	Increase of taper reduces the stab gap size at the complete threads and reduces axial movement
Size threads	**P:**	Reducing thread size results in a reduction of plasticity and strengthens the critical section as a result of an local increase of material thickness
	LD:	While the shape of the load distribution remains equal, smaller threads lead to a more uniform distribution of load transferred per thread
	GS:	While the reduction of the final gap size matches the scaling factor, the relative clearance tends to saturate once a certain value is reached (8tpi for the stab flank)
Load flank angle	**P:**	Negative angles tend to increase likelihood of shear failure near the last engaged threads
	LD:	Hand tight: negative angles lead to an increased load at vanishing threads Made-up: No significant effects
	GS:	Hand tight: Negative angles reduce the unzipping effect/jump out of the threads Make-up: No significant changes

Table 7-1 (continued)

Parameter	*Effect*	
Initial thread clearance	**P:**	Reducing thread clearance while maintaining the same levels of make-up tends to increase plasticity due to a wedging effect of the threads
	LD:	No significant changes are observed
	GS:	Reducing initial clearance reduces overall gap size and increases the number of thread pitches for which the stab flank contact is present

1.3 Improved BTC connection: the LS95R

Finally, all the observed effects of the various variables were taken into account and changes were made starting from an API Buttress threaded connection. The result was merged in a new connection: the LS95R threaded connection. This connection is shown in Figure 7-2 and is believed to resist combined loads (consisting of internal pressure and axial tension) with an equivalent force of at least 95% of the pipe yield strength (hence a 95% performance rating). It also has a significantly smaller outer diameter compared with standard buttress connections. This makes the connection easier to use in the field and is one step closer to the objective of creating a connection with a 100% rating having an outer diameter equal to the outer diameter of the pipes it connects. In addition, this connection can be assembled using a reduced make-up torque compared to standard connections.

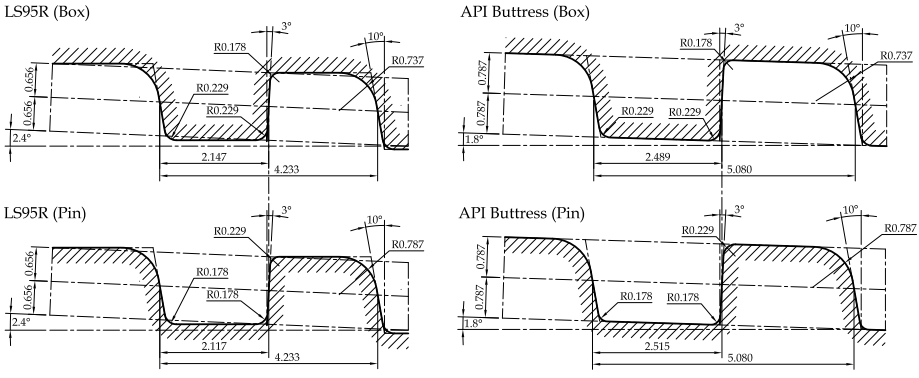

Figure 7-2: Overview of the thread geometry of the LS95R connection (left), compared to the API Buttress connection (right) for both pin (bottom) and box (top)

2 Suggested future work

2.1 Combined effects

The conducted research attempted to investigate the effects of parameters on the performance of the coupling by evaluating specific performance parameters. The considered parameters were deemed sufficient to create a new connection suitable of connecting two given pipes. Based on individual effects, design decisions were taken and the proposed connection appears to be appropriate up to the intended 95% performance rating.

This new connection is the result of the combination of isolated cases in which single parameters were changed and in which their effects on the performance parameters were evaluated. While this approach shows that it is possible to enhance an existing product based on isolated observations, further research is required to analyze the combined effects of various parameters. It is possible that once the interactions are more clearly, even better connections can be designed.

2.2 Additional geometric parameters

2.2.1 Geometric and material tolerances

One of the major disadvantages of the developed program is the inability to apply tolerances to the various geometrical dimensions and material properties. Therefore, it is suggested to implement this in the model as well. In order to do this, it might be possible to apply a random deviation to all points which are used to create the nominal thread profile. The limits of this deviation can then be related to the tolerances. While this may appear to be a geometric problem, it should be noted that this involves a statistical study as well, since it is highly unlikely that the statistical distribution will be the same for all parameters.

This statistical study might also be used to reduce the safety factors, which are a direct result of the existence of uncertainties such as the tolerances. By introducing the correct statistical distributions, it would be beneficial to extend the study with a *Load and Resistance Factor Design (LRFD)* approach, which is gaining interest for the development of pressure vessels [7.1] and piping [7.2]. The main advantage of this approach is that it could lead to a significant reduction of currently applied conservatism and that it can be used in addition to currently used procedures [7.3].

2.2.2 Taper mismatch

Another addition which is strongly recommended is the introduction of non-uniform taper mismatch. Based on the experiments conducted in chapter 3, it was indicated that taper mismatch can have significant effects, especially

during make-up. In addition to the experiments, preliminary simulations conducted in chapter 4 showed that assuming a continuous, equal taper mismatch over the entire threaded area is not the answer to this problem. While it is not entirely clear how to express this problem using a parametric approach, a start could be to segment the threaded area. By doing so, the geometry of the thread in each segment could be altered using custom taper angles, obtained by experimentally measuring the manufactured connection. Also, the tapers between pin and box should not necessarily be equal.

2.2.3 Third generation threads

While the original '*ThreadGen*' [7.4] script was designed to create models containing triangular threads, the developed successor '*ThreadGenBT*' allows generating trapezoidal threaded connections. In order to keep up with modern day demands and trends, it is advisable to further enhance this script with the required parameters to generate semi-premium and premium connections. The additional parameters required for this modification have been mentioned in Chapter 6. Once these modifications are applied, the proposed methodology can also be applied to the enhanced premium connections, which are believed to have the possibility of exceeding a 100% performance ratio.

In addition to the geometric changes, also the ability to change the material properties of distinct sections should be included to provide the possibility to simulate the presence of coating surfaces on the threads. This modification is strongly suggested since the dope-free technologies are most likely going to be the next step in the field of threaded connections due to the various advantages mentioned (see further in section 2.4).

2.2.4 (Semi-) Premium connections

2.2.4.1 Pin–to–Pin

A semi-premium connection is defined as a threaded connection with a torque shoulder or an equivalent feature such as the nose of the opposite pin. When using T&C type connections, one of the possibilities is to use the pin tip of the accompanying pin member as a torque shoulder located at the center of the connection. When this geometry has to be simulated, two major changes are required.

First of all, the symmetry conditions at the mid-plane have to be eliminated and the model has to be mirrored over its center plane. In addition, a contact surface has to be defined over both pin tips and an initial numerical overlap at this location has to be resolved prior to applying additional external forces. To do this, a small pin tip will have to be added to the geometry in order to be able to modify the amount of numerical overlap independently of the make-up applied to the threads. This can be done by applying a section with a certain length between the current connection and newly added pin tip. An

alternative for the numerical overlap can be considered by adding a small amount of thermal elements which can be expanded when a temperature field is applied as is done in reference [7.8]. However, it should be noted that when applying the latter, the ability of performing thermal might lead to wrong make-up characteristics.

Secondly, it might be possible that the field and mill ends have different torque values. While it was shown (see Chapter 4) that this difference does not have a lot of influence on the numerical results of standard buttress connections, it is advised not to neglect this when calculating pin-to-pin geometries since the area of interest is located at and near the center region of the connections. Furthermore, it is strongly suggested to conduct a preliminary study to better understand and predict the effect of make-up on the elongation at the pin tip caused by the Poisson's ratio.

2.2.4.2 Torque Shoulder and/or Sealing Surface

When the threaded connections design does not rely on the pin-to-pin concept, a torque shoulder is implemented to gain similar mechanics in the semi-premium connection. When complemented with a sealing surface, the connection is defined as a premium connection. In order to create these models, a similar approach as described in section 2.2.4.1 is suggested with the exception that the symmetry conditions at the center of the box can be maintained to reduce calculation times.

This approach is already widely used in literature. However, when consulting the available literature, the make-up aspect remains unclear often. The simulated connection after make-up is often linked to a certain amount of torque. While this approach is not possible for standard threaded connections due to the unknown coefficient of friction, this might be plausible for (semi-)premium connections. The required make-up of the latter type of connections is mainly generated by the axial wedging between threads at one side and the torque shoulder at the other side, rather than radial expansion/compression of pin and box. For this reason, make-up is (presumably) often introduced by resolving an initial overlap at the torque shoulder only [7.10]. The problem of applying this methodology is that this does not conform with the typical torque turn diagram for premium connections. Based on these diagrams, a torque is initiated by the contact between the threads before the torque shoulder is engaged. Despite the indication of a mixed make-up containing both thread and torque shoulder, limited to no information about the distinction and combination of those is described in literature. By using the developed model in its current shape, the geometry associated with the make-up caused by the threads can easily be generated. Once this action is performed, the shoulder and possible sealing surface can be added.

2.2.4.3 Feasibility Study

When designing a sealing surface at the nose of the pin, the geometry is dependent on the chosen seal type. In general, the sealing mechanism is a ball-to-ball, cone-to-cone or ball-to-cone geometry. Depending on the geometry, the parameters defining the sealing index (contact pressures and contact lengths) as previously mentioned in Chapter 4 will vary. In order to cover all possible geometries, several different parameters should be considered when adapting the parametric script. A similar design approach should be considered for the torque shoulder. A graphical overview containing the minimum amount of additional variables for the pin and box member are shown in Figure 7-3.

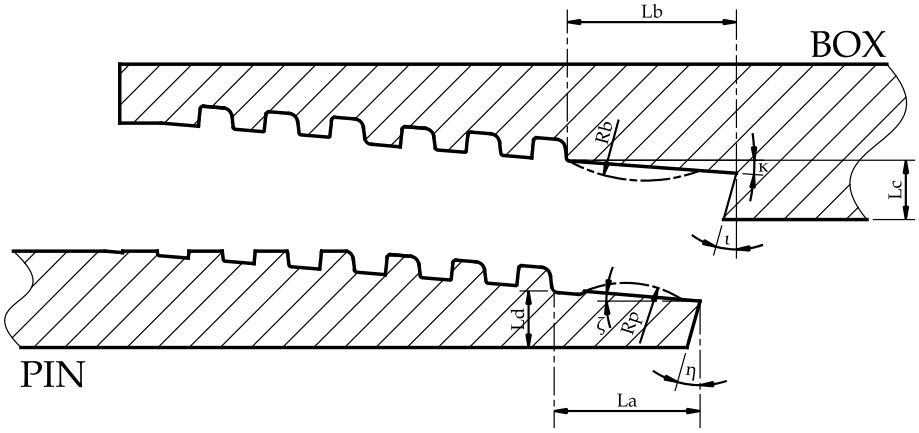

Figure 7-3: Overview of the minimum required parameters to implement the ability to simulate premium connections. The sealing surface can be modelled using a radius or straight line.

Figure 7-4 indicates that it is feasible to calculate premium connections using the same methodology used for standard connections. The main difficulty involved in defining the appropriate make-up position is the unpredictable behavior of the overlap at the shoulder. When neglecting the make-up applied on the threads, it is possible to establish a relation between make-up and initial overlap. This way, the amount of applied make-up can simply be altered by changing the overlap at the pin tip. When make-up is applied at the threads as well, the Poisson's ratio induces an elongation of the pin. This induces an additional axial force on the shoulder surface, increasing the torque. Therefore, the amount of make-up on the threads and torque shoulder should not be defined independently. This can be done by expressing the make-up position in rotations as is done in the current numerical model and by modifying the length of the pin nose. This means that the amount of overlap is directly calculated based on the manufactured geometry combined with the amount of applied power turns. This is in contrast with the often applied method in which the amount of overlap is calculated using a certain

amount of torque assuming that the coefficient of friction is known and assuming no make-up is applied on the threads [7.11].

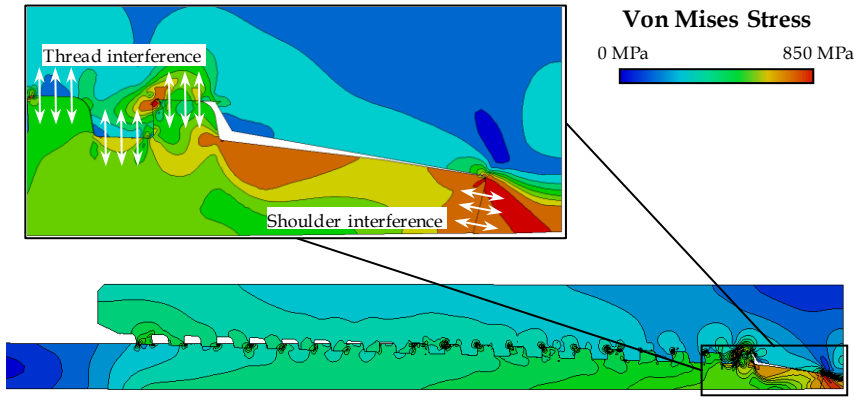

Figure 7-4: Example of the simulation of a premium connections using make-up at both the threads and the torque shoulder.

It should be noted that when simulating (semi-) premium connections, the performance parameters need to be redefined and reinterpreted. For example, the thread clearance in those connections is not related to the sealing capabilities of the coupling. Also, a uniform, axial load distribution might not be the most desirable shape. For those connections, it might be beneficial to transfer all working loads through the threads before the pin tip is reached. This way, the sealing surface will only be dependent of initial make-up and working conditions will have nearly no effect on its performance.

2.3 Indirect validation of contact pressure

2.3.1 Relation contact pressure – friction

While information is present in literature about the validation of numerical models using experimentally measured strains, to date, no validation of the local contact pressure between the threads is ever published. It was suggested by a preliminary study in chapter 6 that this contact pressure could be linked with the visible temperature at the outside of the box. This temperature originates from frictional energy during make-up which is mainly dependent on the coefficient of friction and contact pressure. For the experimentally used thread compound, *API modified*, a contact pressure dependency is known to affect the coefficient of friction and this relationship is given by a graph. Despite its apparent validity, very little is publically known about how exactly the data was generated and little interpretation is given to explain the odd behavior for lower contact pressures. Therefore, it is suggested to recreate these experiments and to obtain the contact pressure dependency of the coefficient of friction for various thread compounds.

2.3.2 Relation contact pressure – temperature

Temperature is generated in a connection as the result of two different kinds of energy: frictional energy and deformation energy. While deformation energy is the main occurring source during service, frictional energy is predominant during make-up.

A first step in relating the contact pressure to the visible temperature is by obtaining all required thermal material parameters such as specific heat and conductivity. It is possible that temperature dependency of these values has to be taken into account. Once the material parameters are known, it should be possible to calculate the deformation energy and the evolution of the generated heat based hereon.

The second part consists of the transformation between frictional energy and heat input using the previously determined relationship between contact pressure and the coefficient of friction. When applying the heat inputs or temperatures to the different elements in the contact surface, the progression of the temperature throughout the connection can be visualized.

When combining the two energy sources, additional parameters can be validated quantitatively rather than qualitatively, especially during make-up.

2.3.3 Implementation

A potentially valuable addition to the numerical model is the introduction of coupled thermo-mechanical simulations. During the testing of the connections (see Chapter 3), it was shown that thermal variations could be measured during make-up and during the tensile limit load test. When the thermal properties of the used steels are known, it is potentially possible to validate parameters which cannot be measured directly such as the contact pressure and the exact location of failure starting within the threaded area. Throughout Chapter 4, the thermal measurements were considered as an indirect method for validating the numerical model. While the assumptions were based on intuitive and physically understandable criteria, no direct validation could be linked to these measurements yet.

Energy leading to a temperature increase and decrease is induced in the connections when external loads are applied. When performing make-up tests, heat is generated as the result of friction and deformation caused by the applied torque, which is the only externally applied force. During the limit load test, elastic deformation causes the connection to cool down while plastic deformation causes the connection to heat up.

While this approach has not been suggested in literature yet, it is assumed to be possible to turn the measurement of temperature from a secondary variable into a primary variable which can be directly used to enhance the validation of the developed model. For the make-up tests, temperature acted

as a secondary variable to validate the contact pressure since the frictional energy, which is the source for the observed temperature increase, is strongly dependent of the contact pressure along the threaded contact surface. Once the relation between contact pressure and temperature can be identified, it is possible to apply a certain temperature to the elements containing a certain contact pressure. If consecutively the steady state temperature is calculated, it is possible to simulate the temperature distribution throughout the connection. Once this distribution is known, it is possible to compare the measured temperature with the simulated temperature at the visible locations, validating the origin of the temperature increase and/or decrease, being the contact pressure since the heat generated by deformation is negligible (see Chapter 3). For the limit load test, a similar approach can be applied. During this test, temperature is mainly dependent on the deformation energy which is directly related to the stress-strain state of every element. When applying the appropriate thermal properties to the material behavior, the thermal steady state situation for every load situation can be calculated and validations can be performed using the data obtained both numerically and experimentally at the visually accessible locations.

2.3.4 Feasibility Study

2.3.4.1 Overview FEA model

As part of the feasibility study to link the predicted contact pressure to the measured temperature, a simplified thermo-mechanic numerical model of the box which was tested and measured in Chapter 3 is created. This model consists of a 3D model in which the thread helix is neglected. Because of this simplification, a 2D axisymmetric model could be used as well. Since no contact is modelled, it is possible to use larger elements without losing accuracy and therefore, a 3D model using about 12.000 C3D8T elements to model a quarter of the connection in combination with cyclic symmetry was chosen to facilitate visual assessment of the results.

Since it is the objective of the study to find a relation between the contact pressure in the threaded region and the temperature at the outer surface of the box, the pin member is opted to be negligible because temperatures are used input parameters, not a certain amount of heat. If a relationship between contact pressure and temperature exists, it should be possible to replace the contact-boundaries with thermal boundaries. In practice, this means that it should be possible to extract the occurring contact pressures from the previously defined axi-symmetric model (see chapter 4) and replace those by thermal boundary conditions in the thermo-mechanical model. These additional boundary conditions represent a certain temperature which is generated during make-up as the result of friction and are therefore directly related to the contact pressure. The properties of the originally used grade B steel is expanded with the conductivity (48 W/mK), thermal expansion

coefficient (1.2E-8/K) and specific heat (4800 J/kgK). These values are adopted from a steel used in reference [7.5]. Since no large temperature variations are expected based on the results of the temperature measurements conducted in Chapter 3, no temperature dependency of the material parameters is taken into account.

An overview of the model can be found in Figure 7-5. In this figure, it is visible that the boundary condition used to indicate symmetry at the mid plane of the box is replaced by a boundary condition limiting all movements in all possible directions. This is possible because only one side of the box is made up during the test and no temperature increases, nor decreases influencing the results are expected. The only thermal boundary condition applied is the surface film at the outside of the connection. This is the area through which heat is transferred to the surrounding environment, inducing a cooling effect.

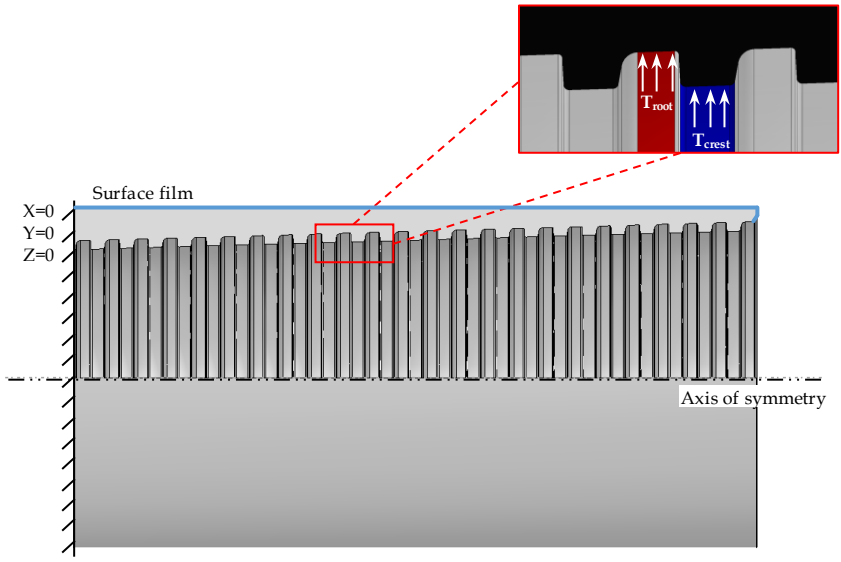

Figure 7-5: Illustration of the location where the temperature loads are applied

Instead of mechanical loads, temperature fields are applied to simulate the heat generated by the rotational movement combined with the friction in the contact area. A first field elevating the connections temperature to 293 K (20 °C) is applied to the entire model during initiation. In addition, a temperature proportional to the calculated contact pressure at those locations is applied to every root and crest surface as indicated in Figure 7-5. The limited amount of contact at the load flanks of the connection near the tip of the box is not taken into consideration due to the likelihood of numerical errors, limited contact area and possible cooling effects of excessive, liquid thread compound in the

clearances. Taking these three criteria into account, it was not opted to be beneficial for this feasibility study.

Since it is unknown how much contact pressure will result in how much heat generation, equation 7.1 was used arbitrarily to calculate a temperature. An overview of the average contact pressures, based on FEA modelling, can be found in Figure 7-6.

$$T = C_{p,AVG} + 293 \qquad \text{(Eq. 7.1)}$$

It should be noted that this simple equation does not represent the actual temperature representing the actual heat input generated by the frictional energy. However, by using this formula, it is believed to provide an insight in the shape of the curve measured during the experiment at the outer surface of the box in the assumption that a first order relationship exists between contact pressure and temperature [7.6] as the result of a uniform and constant sliding velocity and coefficient of friction. Furthermore, the deformation energy is considered negligible [7.7]. Since this thermal simulation is only a preliminary analysis to evaluate the feasibility, the simplifications can be considered to be acceptable at this point. Future research should primarily focus on the determination of the relationship between contact pressure and heat generation.

2.3.4.2 Results

After applying all boundary conditions and loads as described in section 2.3.4.1, the steady state situation of the thermal behavior is calculated. The results can be seen in Figure 7-6.

Within this figure, the red curve represents the previously measured temperature at the outer surface of the box using infrared thermography (see Chapter 3) and the crosses represent the average contact pressure for all threads. The black line represents the shape of the calculated temperature profile taking into account the previously mentioned assumptions. Since the temperatures used to represent the contact pressures are not correct, a scaling factor is applied in which the maximum and minimum values of the numerical and experimental data approximate. By scaling the entire curve, everything is still kept in proportion and might provide realistic insights in the temperature distribution given the validity of a first order relationship between contact pressure and temperature. The scaling of the data points was conducted using equation 7.2.

$$T_{calc} = (T_{FEA} - T_i)\frac{1.15}{6.5} \qquad \text{(Eq. 7.2)}$$

While a quantitative comparison between the numerical and experimental data is not possible as a result of the scaling factor which was applied, an important aspect is visible assessing the shape of the curve in relation with the occurring contact pressures. In Chapter 3, it was concluded that the temperature increase was caused by frictional energy rather than deformation energy after comparing the temperatures taken by infrared thermography with the occurring strains measured using the digital image correlation method. Comparison of these datasets showed that the maximum temperature was at an entirely different location as the maximum deformation. Additionally, a minor offset was observed when comparing the measured temperature with the simulated contact pressures, as is shown again in Figure 7-6. Taking into account all the applied assumptions, this offset could have been the result of an inaccuracy in estimated location, geometrical deviations causing slightly different contact pressures,… Despite satisfying results, the performed thermal analysis shows that this mismatch was not accidentally observed. When smoothing the waviness seen between the 70 mm and 90 mm position on the outer surface of the box, it is confirmed that the experimentally observed mismatch is a direct result of temperature and thus the frictional energy rather than deformation energy.

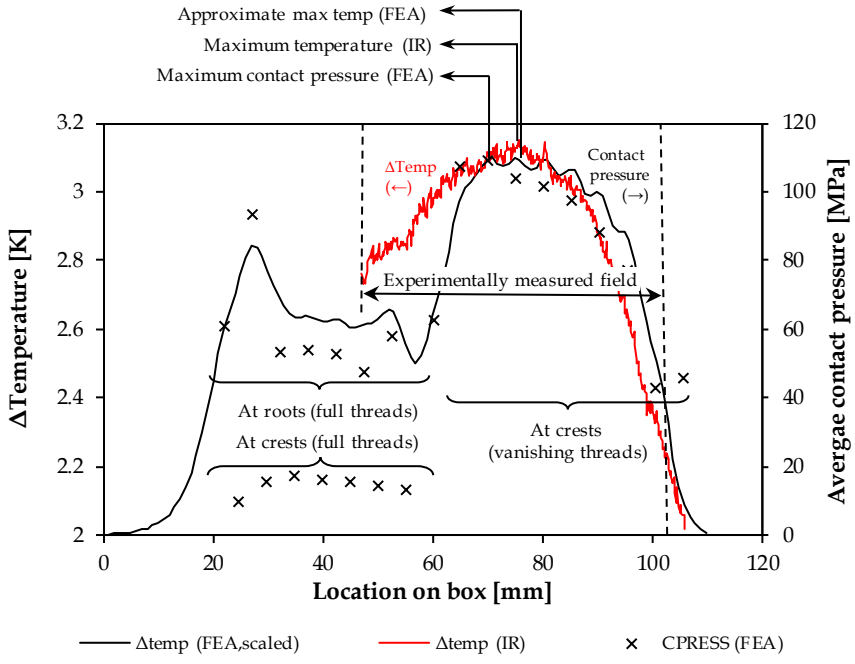

Figure 7-6: Overview of the experimentally measured temperature increase during make-up together with the simulated average contact pressure per thread and temperature at the outer surface of the box

2.3.4.3 Further required enhancement

Based on the results described above, it appears feasible to establish a relationship between the contact pressure along the threads and the measurable temperature at the outer surface of the box. While quantitatively no conclusions can be drawn, the temperature distribution, illustrated in Figure 7-7, could be readily used.

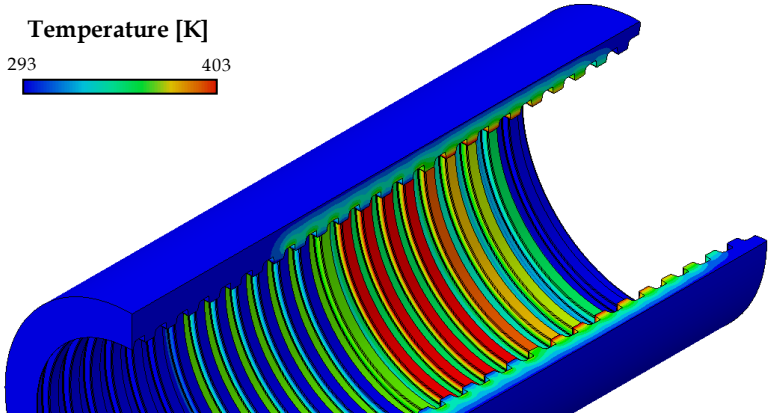

Figure 7-7: Calculated temperature distribution during make-up when assuming that the frictional heat is proportional with the contact pressure.

However, several enhancements requiring further, extensive research need to be considered. First of all, referring back to Figure 7-6, a large deviation between the experimental data and numerical data is visible near the location containing the last full threads. This deviation is likely the result of deviations in the thermal properties of the material such as specific heat and conductivity, which were not based on experimentally measured values. Secondly, a strong cooling effect is visible at the outer surface of the box, shown in Figure 7-7. While this is likely to occur in reality, it is beneficial to further examine the heat transfer from the steel to the surrounding air by means of experiments in an effort to accurately quantify the film coefficient applied to these transition regions. Thirdly, another part of the research should focus on the establishment of a relationship between contact pressure and temperature or amount of induced heat. While the temperatures within the promoted simulation are believed to be proportional with the obtained contact pressure, scaling is still required. Once the exact relationship is found, it should be possible, taking into account that the material properties are correctly defined, to recreate the temperature distribution without additional manipulation as was the case in this example.

Finally, it should be mentioned that while this simulation is based on the steady-state situation using temperature inputs, it might be beneficial to use heat instead of temperature. In that case, the combined influence of contact pressure and make-up speed could potentially be linked with heat

inputs/fluxes rather than absolute temperatures. Within this preliminary simulation, a constant temperature is assumed, rather than energy generated by an external force (torque in the case of make-up).

2.4 Dope-free Connections

2.4.1 Industrial Significance

From an economical point of view, the use of threaded connections combined with a thread compound to ensure the intended make-up is considered an aged technology. Figure 7-8 shows the economic tendencies related to new and aging technologies. For the old, conventional doped connections, it can be seen that the economic growth has passed and maturation is already in progress for a while. Furthermore, it can be seen that in order to make additional, limited technological advances related to doped connections, a lot of time and investments is required. From an economical point of view, it is not beneficial to further investigate this technology.

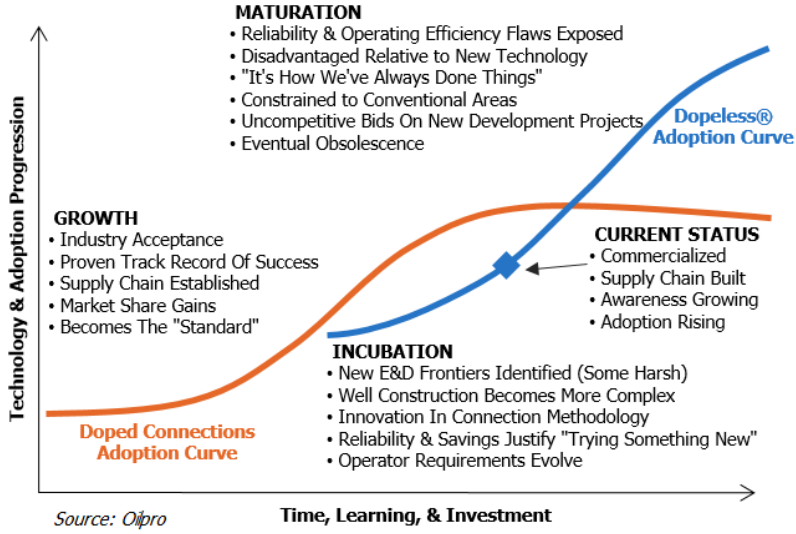

Figure 7-8: Advances in technology compared with the required resources in function of its lifespan [7.13]

Since a few years, a drastic shift occurred within this field for the first time in over a century. In the early 2000's, dope-free threaded connections which use coatings instead of thread compounds have been proposed, tested and put to use for the first time. From Figure 7-8 it is visible that this technology has just passed its incubation period. This means that it should be possible to make tremendous and profitable progress with limited resources compared to the costs and time it took to develop and implement this technology for the first time. The beneficial prospects related to dope-free connections can further be

explained taking into account the criteria a new technology requires in order to grow and be profitable (see Chapter 2).

A first important criterion is that these couplings allow unlocking difficult-to-access resources. Examples of these reservoirs are the ones which can be found in harsh environments such as the sub-zero areas (such as Alaska, Russia, Canada and nowadays the Arctic regions) where preheating of thread compound is required nowadays. Other examples are the remote geographical areas since applying dope before transport is often hard to do. Apart from the locations itself, the increasing complexity of the current wells is easier to establish. Throughout history, the use of thread compound has always caused a certain degree of uncertainty. Excessive dope could lead to pressure build ups and a lack of thread compound potentially increases the coefficient of friction and might even lead to galling. In both cases, make-up cannot be guaranteed. Taking this into consideration, the use of dope-free technology provides more reliable and more uniform joints.

The second criterion is the improvement in exploration and production economics. Runtimes on the rigs are improved because no doping is required. As an average value, the decrease of required runtime per connection is estimated to be about 25%, from 11 to 14 connections in an hour [7.13]. This reduces both the overall costs and the time required for the first oil to be produced. In addition, the costs related to the supply chain and storage requirements can be made because less re-make-ups and rejects occur as a result of the increased reliability. Finally, a reduction in environmental impact is achieved. Improvements related to this last criterion have already been implemented by using the so-called *green dopes*. Within these dopes, the polluting lead is not present, reducing the environmental fingerprint. However, this enhancement proved to have limitations when used in certain environments such as reduced lubrication in arctic areas. The advantage of the dope-free technology is that it does not contain lead, nor any other substances, and it can be used in all possible places and applications. Since no additional elements are added to the connection, the risks for corrosion are also reduced leading to lower chances of leaks occurring in the string during its lifetime.

Despite the promising prospective for this new approach, special attention should be given to its development for obvious reasons. Until today, only a limited number of wells are constructed using these connections which means that it is inevitable that certain flaws are yet to be discovered.

2.4.2 Feasibility Study

From the previous section, it is clear that the importance of dope-free technologies is increasing because of ease of use, environment friendliness and reliability. In order to implement this technology within the developed model, very little changes are required. Currently, an outer layer along the threads is used to drastically reduce the element size of the contact elements. The size of

this zone can be changed when defining the parameters of the models. This means that the size of this zone can be adjusted to match the thickness of the coating which is applied to the threaded area of connections fit for dope-free use, as is indicated in Figure 7-9. These types of connections can be simulated by simply applying the material characteristics, such as the young's modulus, stress-strain curve and frictional properties, of the coating to these areas.

Preliminary simulations using connections made of a steel with a yield strength of 850 MPa combined with a coating have been conducted and have proven the ability to perform these types of simulations.

Based on a patent filed by Tenaris [7.14], it was found that layers containing phosphates are applied to threads that do not require thread compounds. Since the mechanical characteristics of the coating are not explicitly revealed, a Young's modulus equal to 100GPa [7.15] is used within this study. Apart from a suggested hardness of 50 – 250 HV [7.16] or 70-140 on the Rockwell M scale [7.17], no data could be found regarding the characteristics of these coatings when loads are applied. For this reason, the coating is considered elastic.

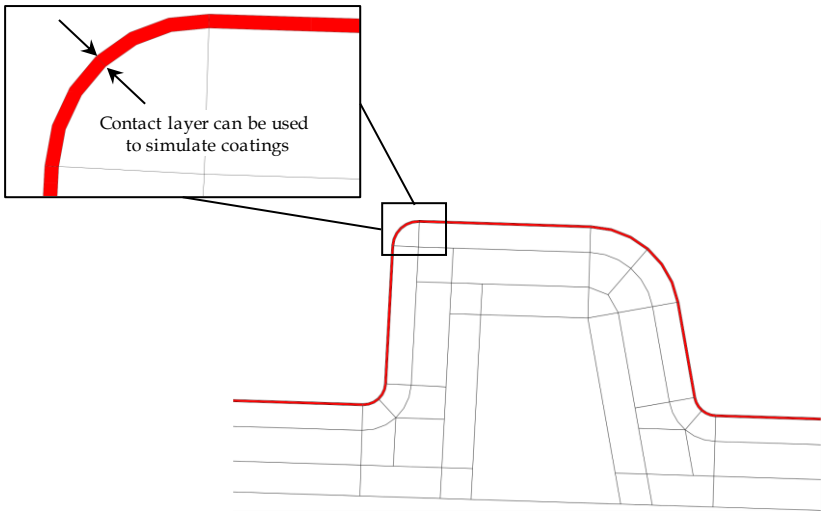

Figure 7-9: Indication of the contact layer which can be transformed in a coating layer when suitable material properties are assigned.

In Figure 7-10, a detail of the results of two simulations can be seen. Figure 7-10.A represents the principal strains at the load flank/crest of a full pin thread after 0.6 turns make up. From this figure, unexpected discontinuities are visible between the strains in the layer containing the coating and the base material. Therefore, it is advised to apply a small transition layer between both materials in an effort to limit these discontinuities. Another difficulty might arise when applying a lower Young's modulus as can be seen in Figure 7-10.B.

When the outer layer becomes too soft, for example when using a Young's modulus of 1 GPa as was used for this simulation, excessive deformation of the mesh occurs when resolving initial overlap. This imposes limitations on the coatings that can be simulated using the proposed methodology. While it is likely for the coating to get damaged when it is too soft or too high make-up levels are applied, further research is required in this case. A possible work-around would be the use of thermal elements to simulate the make-up stage of the assembly using axisymmetric models, as was suggested earlier in Chapter 4. Another alternative would be to use full three dimensional models, but at this time, these were found to be too time consuming to be an effective substitute. Finally, the latter figure also shows a sudden change in stress levels between the coating and the base metal. While this might appear a fluke in the model, this is normal considering the different material properties of both materials.

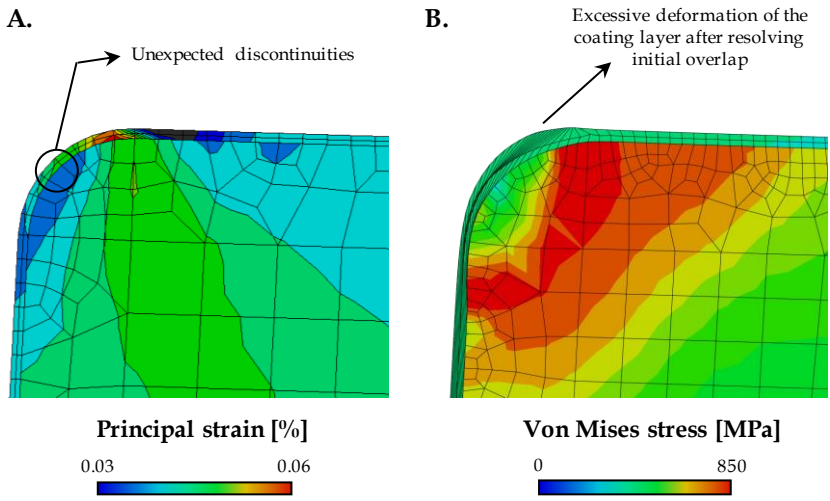

Figure 7-10: Expected difficulties when using a soft layer over the threads consist of discontinuities (A) and excessive deformations of the mesh (B)

3 Personal reflections and opinion of the author

In a final message to the reader, the author wishes to elaborate on the difference between the apparent, current public opinion and his own opinion and interpretation regarding premium connections and its use. It should be stressed that this section is only a personal opinion after performing research on the subject for four years and could be controversial but should not be considered the absolute truth.

Figure 7-11 shows the difference between public belief according to literature and personal opinion. Nowadays, the ability to seal is of increasing importance in the oil- and gas industry. In order to achieve this prerequisite,

premium connections appear to be a popular tool. Current research, indicated by '*current tendency*', is usually based upon these connections and possibilities of modifying the thread geometry or applying coatings to avoid the use of thread compounds is explored. This tendency also imposes that the performance of premium connections will increase while the performance of standard connections remains constant. Popular belief is based on pressure ratings obtained by combining the *API modified* thread compound and standard API buttress connections. However, both the *API modified* thread compound and the API buttress connections can be considered outdated. While the author does not question the performance of these connections, it is his understanding that these premium connections are often used in conditions where standard connections could be used, given their performance is enhanced.

The publically accepted maximum pressure rating for standard connections at 275 bar is ill chosen since it is based upon the assumption that an *API Modified* thread compound, which is nowadays known to be inferior, is used. Currently, much better thread compounds are commercially available and should be considered. With current technologies, it is possible to apply thread compounds which are able to cure leak paths using temperature, pressure and even microscopic growth. There are even records of the fact that thread compounds are responsible for the sealing capabilities of premium connections. These examples show that thread compounds may be responsible for sealing capabilities rather than the sealing surface of premium connections. Instead of making the transition from standard to premium connections, changing the thread compound could prove to be sufficient.

Additionally, the tolerances of API defined standard connections are based upon outdated machining tolerances. With gap sizes exceeding 100 µm, creating reliable thread seals is almost impossible. In order to create reliable thread seals, these connections should be redesigned and CNC machining techniques should be taken into account. By doing so, tolerances could be reduced leading to less clearance between the threads.

Therefore, while the current commercial market related to threaded connections focusses on profitable premium connections, a serious reconsideration should be made as indicated by '*suggested method*' in Figure 7-11 and more focus should be put on the reassessment of these outdated, standard connections by taking into account the progress made in the field of thread compounds and production technologies. Otherwise, these connections cannot be used to their full potential. While this does not mean that premium connections are likely to become obsolete, it could lead to a significant reduction of rig development costs and faster and easier manufacturing of threaded connections for oil and gas wells.

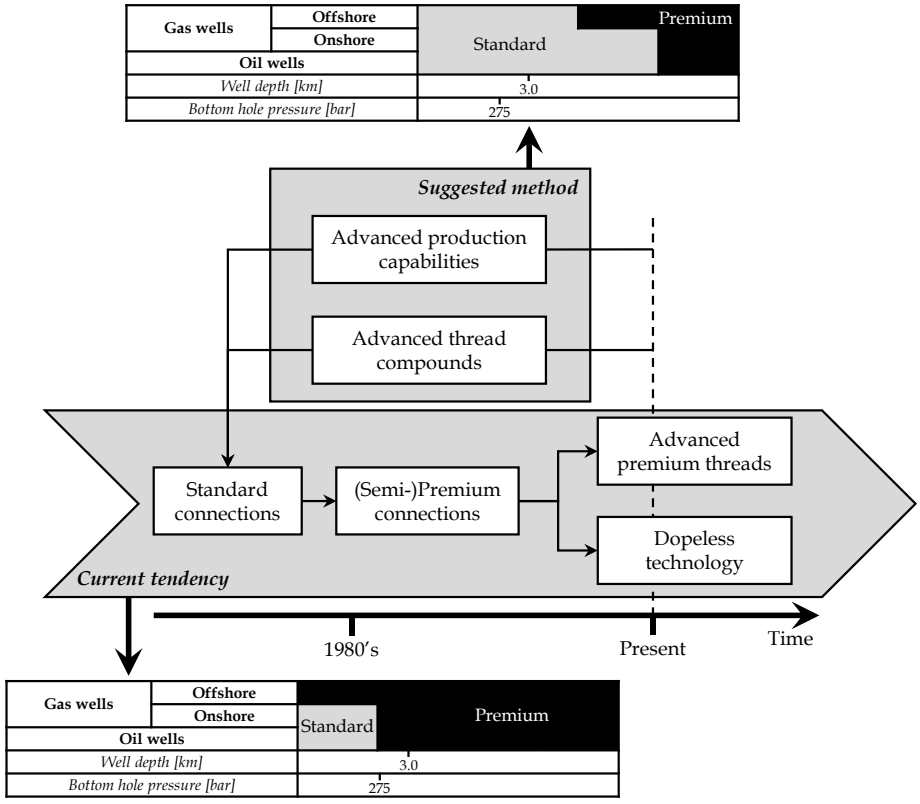

Figure 7-11: Potential increase of applicability of standard connections

References

[7.1] Cai, B., Liu, Y., Liu, Z., et al., *Exploratory study on load and resistance factor design of pressure vessel for subsea blowout preventers*, Engineering Failure Analysis, 27, pp. 119–129, 2013

[7.2] Echtermeyer, A.T., and Lasn, K., *Safety approach for composite pressure vessels for road transport of hydrogen. Part 2: Safety factors and test requirements*, International Journal of Hydrogen Energy, 39(26), pp. 14142–14152, 2014

[7.3] ASME, *Development of Reliability-Based Load and Resistance Factor Design (LRFD) Methods for Piping*, book, 2007

[7.4] Van Wittenberghe, J., *Experimental analysis and modelling of the fatigue behavior of threaded pipe connections*, doctoral thesis, 2012

[7.5] Day, A. J., *An Analysis of Speed, Temperature, and Performance Characteristics of Automotive Drum Brakes*, Journal of Tribology, vol. 110, pp. 295–305, 1988

[7.6] Kennedy, F.E., and Baker, Y.L., *Contact temperatures and their influence on wear during pin-on-disk tribotesting*, Tribology International, 303 (1-2), pp. 622-631, 2013

[7.7] Assanelli, A. P., and Dvorkin, E. N., *Finite Element Models of OCTG Threaded Connections*, Computers & Structures, 47(4), pp. 725-734, 1993

[7.8] Takano, J., Yamaguchi, M., and Kunishige, H., *Development of Premium Connection "KSBEAR" for Withstanding High Compression, High External Pressure, and Severe Bending*, Kawasaki steel technical report, 47, 2002

[7.9] Ferjani, M., Averbuch, D., and Constantinescu, A., *A computational approach for the fatigue design of threaded connections*, International journal of fatigue, 33 (4), pp. 610-623, 2011

[7.10] Xu, H., Shi, T., Zhang, Z, et al., *Loading and Contact Stress Analysis on the Thread Teeth in Tubing and Casing Premium Threaded Connection*, Mathematical Problems in Engineering, 2014

[7.11] Dvorkin, E.N., Toscano, R.G., *Finite element models in the steel industry: Part II: Analyses of tubular products performance*, Computers & Structures, 81(8–11), pp. 575–594, 2003

[7.12] Triepke, J., *Understanding oilfield technology lifecycles*, OCTG case study, oilpro, 2014

[7.13] Tenaris, *Dopeless technology: Quantifying operational, well productivity and HSE benefits*, Report, 2012

[7.14] Ribalta, J.C., Dell'erba, D.N. and Carcagno, G.E., *Joints having improved sealability, lubrication and corrosion resistance*, United States Parent, US 20120018081 A1, 2012

[7.15] Kash, E.C. and Kash, J.E., *Rust resistant well perforating gun with gripping surfaces*, United States Patent, US 20130037255 A1, 2013

[7.16] Anraku, T., Goto, K., Matsumoto, K., et al., *Threaded joint for steel pipes*, United States patent, US 20040195825, 2004

[7.17] Reynolds, H.A., *Treating method and design method for tubular connections*, United States Patent, US 7497481 B2, 2009

Appendix A

Numerical model: 3D - Model

Table of Contents

1 Creation of a 3D model

In order to be able to predict the behavior of a threaded connection under real working conditions, a full 3D model is developed and examined using ABAQUS™/Explicit. This study is limited to the make-up stage because of two reasons. First of all, the make-up stage is the only stage where axi-symmetry is counterintuitive. Since a 3D simulation and 2D simulation can be considered as identical with exception of the thread helix, any effects this thread helix may cause could be visible when comparing both modelling approaches. Additionally, the make-up torque of the actual process using the thread helix may be compared with the approximated 2D approach. Secondly, excessive calculation times combined with convergence problems encountered when attempting to reliably apply external loads. Since the considered load combinations (internal pressure combined with axial tension) are of an axi-symmetrical nature, no further attempts were made to further investigate these issues.

The model, illustrated in Figure A-1, consists of an API defined 114.3 mm (4.5 inch) pin [A.1] and a matching box, representing an integral connection. Each of the members is connected to a reference point (RP) by a kinematic

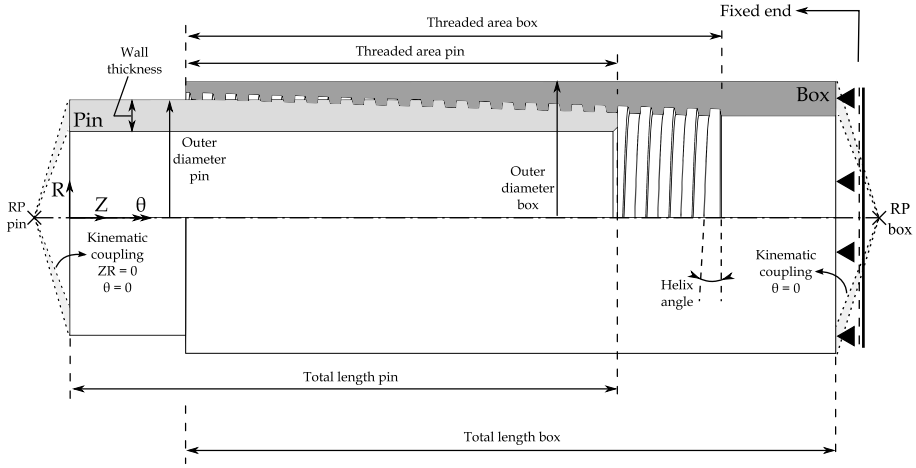

Figure A-1: Schematic overview of the 3D model

coupling which is used to apply the required boundary conditions and loads. When applying a displacement using Abaqus™/Explicit, a smooth step is often advised. For the simulations performed, the amplitude of the applied rotational displacement was chosen to be linear, but combined with an initial velocity applied to the pin, matching a make-up speed of 60 rpm. This speed was chosen higher than the usual maximum of 14 rpm [A.2] to limit the required step time and to significantly speed up the calculation process. This

artificial adjustment is allowed when considering quasi-static conditions (see further in Section 1.4.2).

1.1 Boundary Conditions

Within the assembly, the pin is assumed to be the rotating part and its end is connected to a reference point on the pipe axis (see Figure A-1) by using a kinematic coupling. As such, angular displacement (θ) of the connected nodes is restrained relative to the reference point within the cylindrical coordinate system of the pin. The box is clamped and acts as a static part. In order to achieve this state, all possible degrees of freedom of the box end are constrained and a second reference point (RP_{box}) is connected to the fixed area with the help of a kinematic coupling.

It should be noted that angular displacement of the pin axis relative to the box axis, as illustrated in Figure A-2, has been observed to occur when applying coefficients of friction of 0.05 or higher, especially when combined with higher

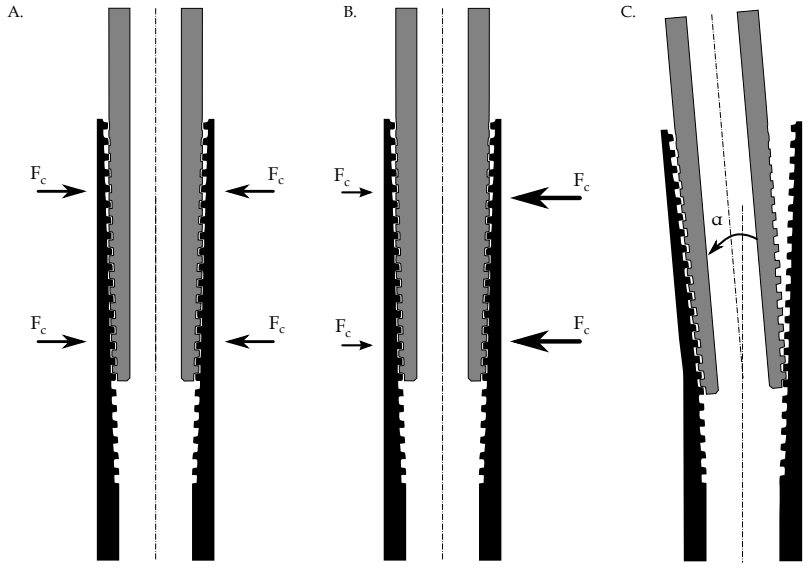

Figure A-2: Unrealistic deformation as the result of uneven distribution of contact forces

make-up levels. Normally, the contact forces resulting from friction between contacting nodes are distributed evenly over the circumference of the contact surface (Figure A-2.A) and no resultant radial force is applied to the box. However, the frictional forces generated by the contacting nodes are not equally distributed over the circumference of the contact surface (Figure A-2.B) when a coarse mesh is being used. This will generate a resulting radial force, leading to misalignment of the pin axis relative to the box axis (Figure

A-2.C). This misalignment will further increase the magnitude of the resulting radial forces leading to excessive, plastic deformation. This early plasticity reduces the torque to turn ratio (see Section 6.1 of chapter 4) and therefore results in erroneous torque values, invalidating the performed simulations. In an effort to prevent the tendency of misalignment without exponentially increasing calculation times by reducing mesh size, an additional boundary condition which disables the movement of the pin nodes in the θ direction relative to the reference point was added. This restriction is valid based on the assumption of plane strain behavior which follows from the generally assumed (quasi-) axi-symmetry, which is by definition a plain strain condition, in a threaded connection. This way, no torsion is allowed in the pin body, resulting in a suppression of the swinging motion of the pin.

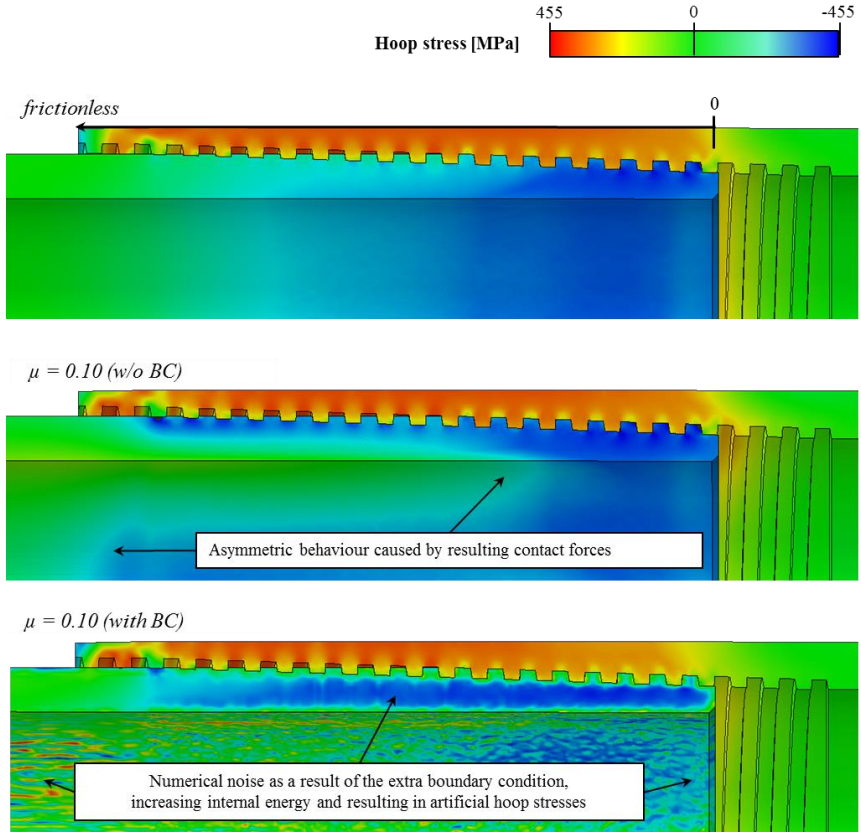

Figure A-3: Example of hoop stresses without friction, when friction increases and when the pin movement is restricted. The figures represent a 90 degrees section of the assembly and are cyclic symmetric for all cases.

Figure A-3 shows the influence of friction and the additional boundary condition on the simulated stresses within the connection. Despite a good correspondence in the axial direction, the hoop stresses in the pin member are greatly influenced and show signs of excessive scatter throughout the entire body, most likely caused by the applied rotational displacement to this part. For the box however, stress variations appear to be negligible in both directions. In addition to the noticeable effects on the stress distribution, Figure A-4 indicates that the internal energy, consisting of elastic and plastic energy, of the assembly increases drastically by applying the additional boundary condition mentioned before in an effort to restrict the pin movement. While this increase is probably related to the resistance against torsion, no straightforward explanation for this behavior could be found.

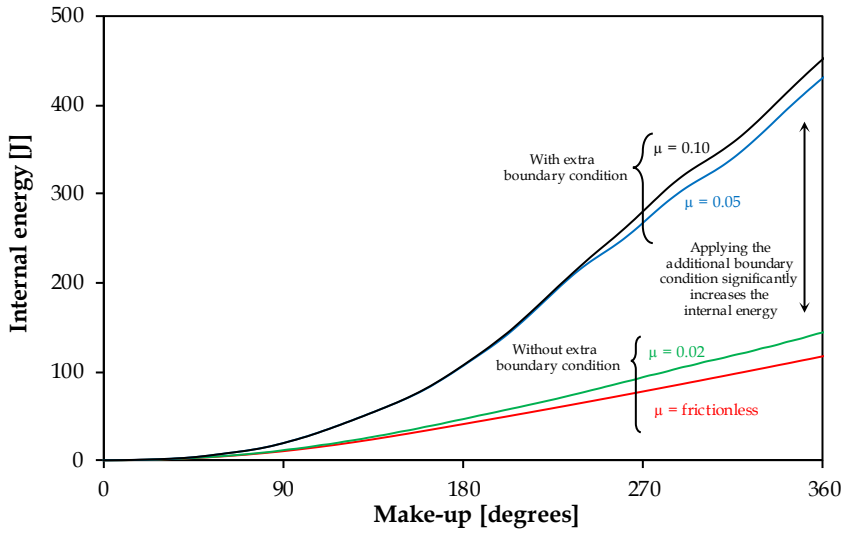

Figure A-4: Effect of additional boundary condition on the internal energy of the simulation.

1.2 Contact Definitions

A surface-to-surface contact is defined between pin and box. Based on make-up simulations using coefficients of friction ranging from 0 through 0.10, covering the entire range of the *API modified* thread compound, frictionless contact provides the most uniform results for the strains over the circumference for both pin and box. This tendency was already visible earlier in Figure A-3.

1.3 Applied Mesh

Every thread consists of a 5x3 elements cross section, which is equivalent to a maximum element size of 0.5 mm. The element size is not based on a convergence study since this is practically not possible due to excessive

calculation times and difficulties when creating the model. Therefore, a similar element size as mentioned in reference [A.3] is adopted. As a result of computational limitations, large elements have to be used and no detailed studies can be performed. While the overall stress/strain distribution in the material is believed to be acceptable (see further, Figure A-6), conclusions related to contact pressures should be formulated with caution. The applied mesh consists of C3D8R elements, which are three dimensional, continuum (solid), 8-node, hexahedral elements with reduced integration. A detail of the mesh is given in Figure A-5. In an effort to avoid problems with excessive deformation of critical elements, a structured mesh is used. When this is not possible, it is, based upon experience of the author, advised to use the sweep algorithm to maintain an optimal mesh quality. Additionally, the use of C3D8R brick elements is strongly advised for the aforementioned reasons. In total, 2,200,000 elements are used in this model.

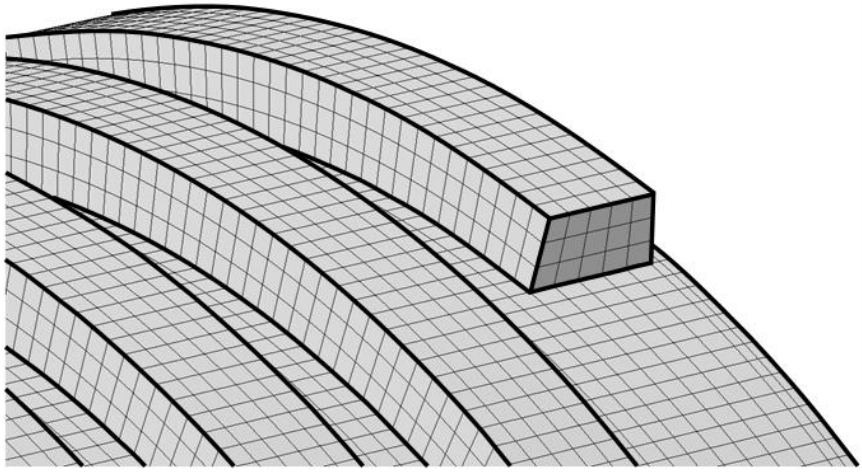

Figure A-5: Example of the used 3D mesh.
Brick elements of approximately 0.5 mm x 0.5 mm x 0.5 mm were used.

1.4 Hypotheses

1.4.1 Geometric simplifications

A major disadvantage when attempting to create a full 3D model is the increase of elements required. For this reason, defeaturing and increasing the element size in comparison with the 2D axi-symmetric model is mandatory to limit the total amount of elements used, speeding up the process. For the performed simulations, thread radii and the chamfer at the pin tip were removed.

1.4.2 Quasi-static conditions

When simulating the make-up process, a rotational displacement of 360 degrees is applied to the reference point of the pin. Special attention should be paid to the velocity of this displacement. In order to minimize dynamic effects caused by excessive speeds, a quasi-static modelling approach should be maintained. A commonly accepted approach to assume quasi-static conditions is conducted by monitoring the global energy balance. During the simulations, the ratio of the kinematic energy to the total internal energy should be between 5 and 10% [A.4]. This ratio is mainly influenced by two parameters: the applied rotational speed and the use of virtual mass scaling. The latter is, without going into detail, used to significantly reduce calculation times. In order to set an appropriate mass scaling, convergence of the stresses at different sections over the circumference of the coupling is preferred. Figure A-6 shows the effect of mass scaling on the Von Mises stresses at the inner surface of the pin (frictionless contact) taken at four different locations evenly distributed over the circumference of the pin. From this picture, it can be seen that the convergence is reached when the mass scaling is reduced up to 1E-6 and an optimal value was found to be 8E-7. When further reducing the mass scaling, very limited benefits are obtained and the required calculation time is increased excessively.

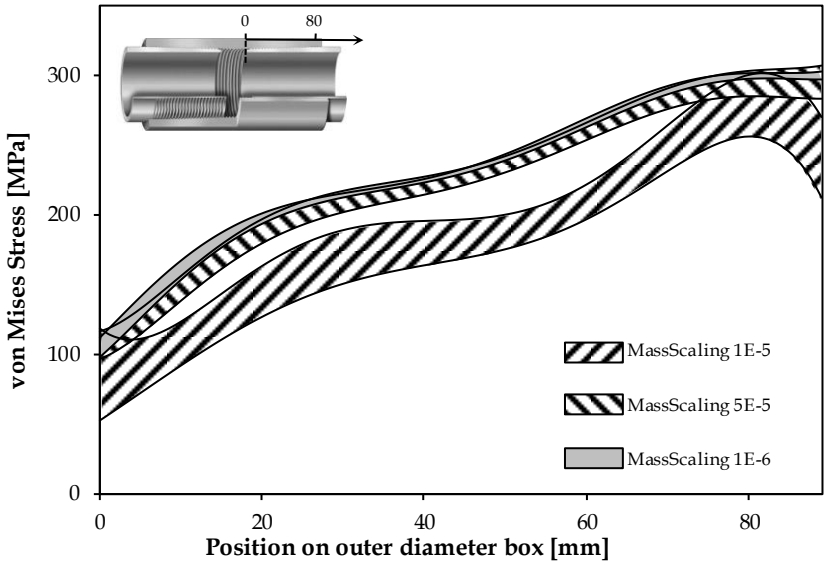

Figure A-6: Effect of mass scaling on the von Mises stresses along the outer surface of the box

Apart from the mass scaling to decrease the calculation time, the rotational velocity of the pin also influences the energy balance. Using the 60 rpm rotational velocity together with a mass scaling of 8E-7, the resulting kinematic to internal energy ratio for the simulations was found to be between 2.5 % and 7.4 %, which is less than the advised maximum value. For this reason, the dynamic effects such as vibrations, torsion, wobbling,… can be neglected.

2 Validation using the 2D model

2.1 Comparison of strains

During the make-up phase of a standard BTC connection, the pin is compressed while the box is expanded. This results in a strain state where the hoop strains are of primary importance. The results for a 2D model and a 3D model with coefficients of friction of 0, 0.02 and 0.10 are shown in Figure A-7. For the 3D models, the strains were extracted at nodes spaced 36 degrees around the circumference and the borders of the indicated areas represent the minimum and maximum values encountered. It is noticeable that the scatter increases with increasing friction coefficient, as a direct result of the resulting contact forces (see section 1.1). When the contact-induced frictional forces are neglected, which is the case for the frictionless simulation, an almost perfect match between 3D and 2D simulation results is visible. This indicates that the

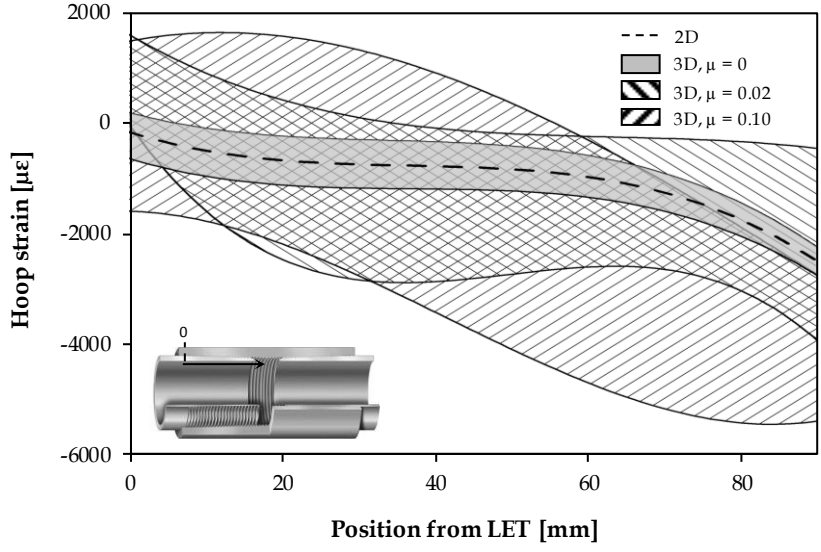

Figure A-7: Comparison of the hoop strains at the inside of the pin using the 2D and 3D models.

strain state after make-up of the investigated type of connections is mainly dependent on the geometry and not on the friction between both members. When the mesh is further refined, an even better agreement should be obtained. However, within the scope of this study, this refinement of the mesh was not deemed necessary.

2.2 Torque-turn diagram

It has been shown that when the strain state of the connection has to be investigated, a frictionless 3D simulation provides similar information as a 2D axi-symmetric simulation in which the initial overlap is resolved. During make-up, the required torque consists of both frictional and deformation torque. While the frictional torque is dependent on the contact pressure and coefficient of friction, the deformation torque can be linked to the internal energy of the assembly as will be shown later. The results of the 2D frictional torque and the total 3D applied torque are given in Figure A-8. From this figure, it can be seen that a very good correspondence occurs when low values of friction are applied. For increased values however, the required torque obtained by the 2D model is higher than the torque obtained by the 3D model. This difference can be explained as a result of the increased plasticity when misalignment between pin and box axis occurs because of the contact forces, rather than an increase in required torque.

In addition to the frictional torque, the 3D model also takes into account the deformation torque based on the internal energy of the connection. It has been mentioned that the strain state after make-up is independent of the friction coefficient and therefore, the frictionless simulation can be used as an estimate for this component. It should be noted that in most cases, especially for standard buttress connections, the effect of the deformation energy is very limited and is often neglected [A.5]. In the case studied (μ=0.02) and illustrated in Figure A-9, the effect of the deformation energy on the torque value was about 4% when plasticity occurred and even less for the advised make-up levels of up to 180 degrees.

Taking into account both the frictional component and the component caused by deformation of the connection, the following equation can be used to provide the link between 2D and 3D prediction of the make-up torque:

$$T_{3D} - \frac{E_i}{MU} = T_{2D} \qquad \text{(Eq. 4.21)}$$

With T_{3D} the torque obtained by the 3D model, T_{2D} the frictional torque calculated using the 2D model, E_i the internal energy of the connection and MU the amount of applied make-up in radians. The actual torque T derived from the 2D simulations becomes:

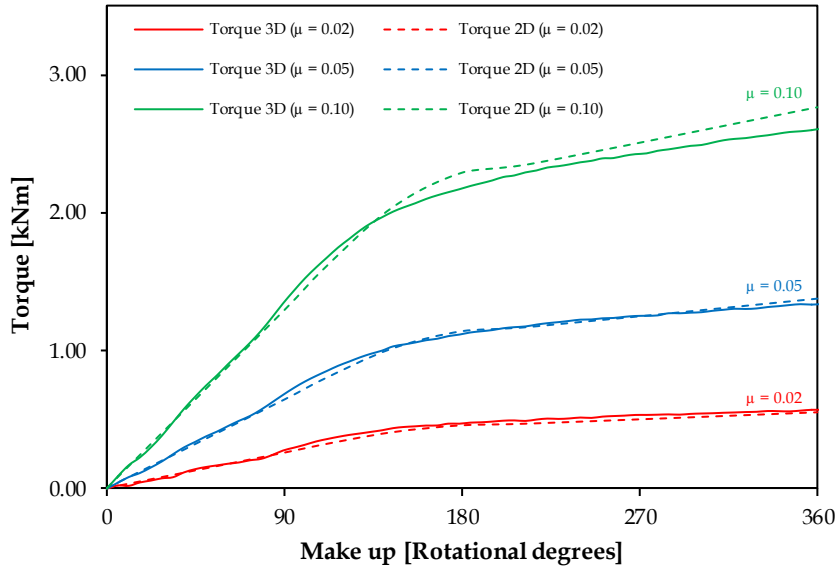

Figure A-8: Comparison of make-up torque obtained using 3D and 2D models for various coefficients of friction (0.02, 0.05 and 0.10)

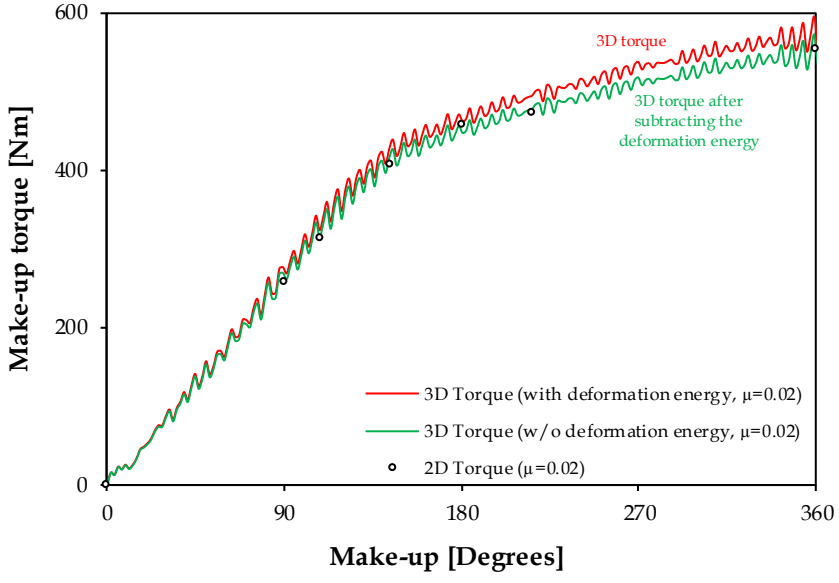

Figure A-9: Comparison of required make-up torque based on 2D and 3D numerical simulations and the influence of the connection's internal energy

$$T = \sum_{i=1}^{n} \mu_i \iint r_i^2 \, p_{c,i} \, ds_i \, d\theta + \frac{E_{int}}{MU} \qquad \text{(Eq. 4.22)}$$

In this equation, μ_i is the contact pressure dependent coefficient of friction, r_i the distance from the element to the centerline of the coupling, $p_{c,i}$ the contact pressure in the element, s_i the axial location of the element, θ the rotational angle ranging between 0 and 2π and n the number of contact elements. After applying this energetic correction for the case with μ = 0.02, the torque levels obtained from both simulations are almost identical.

References

[A.1] API specification 5B, Specification for Threading, Gauging, and Thread Inspection of Casing, Tubing and Line Pipe Threads, American Petroleum Institute, 1996

[A.2] Rivero, G.J., Dunn, T.E., and Parker, C.W., *Position make-up indicator system*, United States Patent, US 20120210552 A1, 2012

[A.3] Chen, J., and Shih, Y., *A Study of the Helical Effect on the Thread Connection by Three Dimensional Finite Element Analysis*, Nuclear Engineering and Design, 191, pp. 109-116, 1999

[A.4] Jaurrieta, M. A., *Explicit FE Simulations of Large-scale Tests on Beam-to-RHS Column Connections*, Tubular Structures X: Proceedings of the 10th International Symposium, pp. 511-518, 2003

[A.5] Assanelli, A. P., and Dvorkin, E. N., *Finite Element Models of OCTG Threaded Connections*, Computers & Structures, 47(4), pp.725-734, 1993

Appendix B

Numerical model: Fracture estimation

Table of Contents

1 Introduction

When developing the design methodology using finite elements, a damage/fracture criterion was not included. Therefore, simulations can only be considered reliable when loads up to the material's yield strength are applied. When applying higher loads, up to fracture, damage is likely to initiate in the threads due to excessive shear forces. As is often the case in reality, the vanishing threads, starting with the last engaged thread, will be damaged and fail before necking and eventually fracture occurs through the entire wall thickness of the pin or box, whichever is the weakest.

The currently proposed model does not include any damage criterion. While finite element programs such as Abaqus, which was used in this research, do offer the possibility to include these advanced models, it has been a deliberate choice not to include them. This way, advanced knowledge of damage and failure methods is not required on the one hand and at the other hand, no extensive experimental procedure has to be conducted to obtain and include all required material parameters.

While it is not possible to simulate the fracture near the threads with the current method, the contact area can be modified by excluding certain edges of the thread, creating a discontinuous contact surface which represents the failure of the thread. This methodology is comparable with element deletion techniques, which are not included for the aforementioned reasons. When these modifications are not applied, erroneous results can be obtained as was the case with the experimentally tested connection mentioned in Chapter 3. Figure B-1 shows the simulation of the connection in which a full contact surface (A.) and a modified contact surface was used (B.). From this picture, it

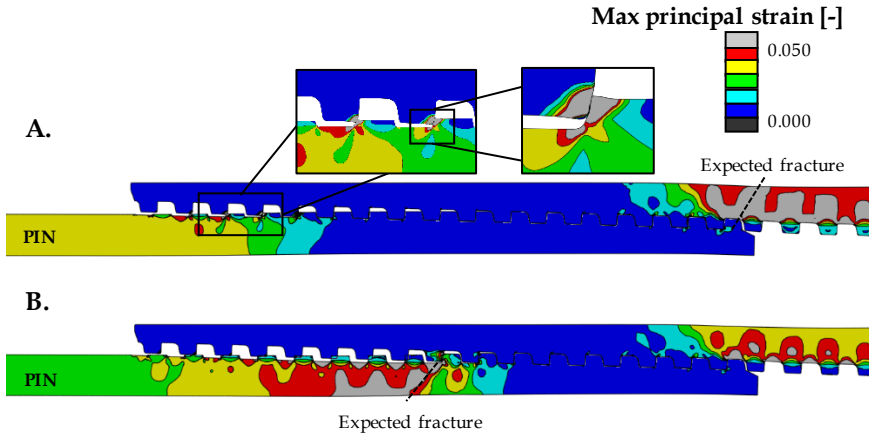

Figure B-1: Effect of modified contact area after 5.5mm axial displacement for full contact (A) and reduced contact (B)

is visible that the location of necking, which will eventually lead to fracture, occurs in different locations depending on the contact surface used. Failure in the box is expected for the case a full contact is used, while failure in the pin is predicted when the modified contact area is implemented. Considering the experimentally determined location of fracture, near LET-7 at the pin (see Chapter 3), the urge to apply this modified approach becomes clear since this takes into account the partial failure of the vanishing threads, resulting in a more realistic estimation of the critical section of the assembled connection.

2 Feasibility study

From Figure B-1.A, it is clear that when using the entire threaded region as a contact area, excessive strains are reached near the roots of the pin threads, especially near the last engaged threads. These high strains cause 45 degrees shear bands and the fracture strains are likely to be exceeded. However, due to the lack of a failure criterion, no damage is numerically initiated and instead of local jump-out, the threads remain intact and resist a significant amount of the axially applied loads. Figure B-2 shows that this results into a higher, non-conservative estimation of the maximum load the connection can withstand when axial tension is applied. Also visible in this figure is that there is only a minor difference between using the entire threaded surface as a contact surface compared with a contact surface in which up to three threads are omitted. This is explained by the fact that for the last vanishing threads (from the LET to the LET-2), the threads tend to slide over each other rather than to hook behind each other. This mechanism is still possible when using the full contact.

In the above explanation, it is suggested that a reduced contact method is preferred once loads exceeding the yield limit of the connection are applied. Currently, it remains the question how many threads have to be omitted from the contact area. In order to determine this, an iterative process has to be conducted.

Referring back to Figure B-1, two different failure locations are considered: or the connection will fail in the critical wall section of the pin/box, or the connection will fail in the shear bands near the roots of the vanishing threads.

In case the latter failure location appears first, it is assumed that the calculations past this critical load are not reliable anymore, since the failed thread still takes up a part of the applied load while in reality it does not. Therefore, this thread has to be omitted from the contact surface. In order to determine whether or not a thread has failed, the maximum principal strains are taken into account. It is assumed that once a path is formed with strains exceeding the experimentally determined maximum strain, the thread or wall section is considered to fail. The amount of axial displacement at which this occurs is given in Figure B-3 for various modified contact areas. From the latter

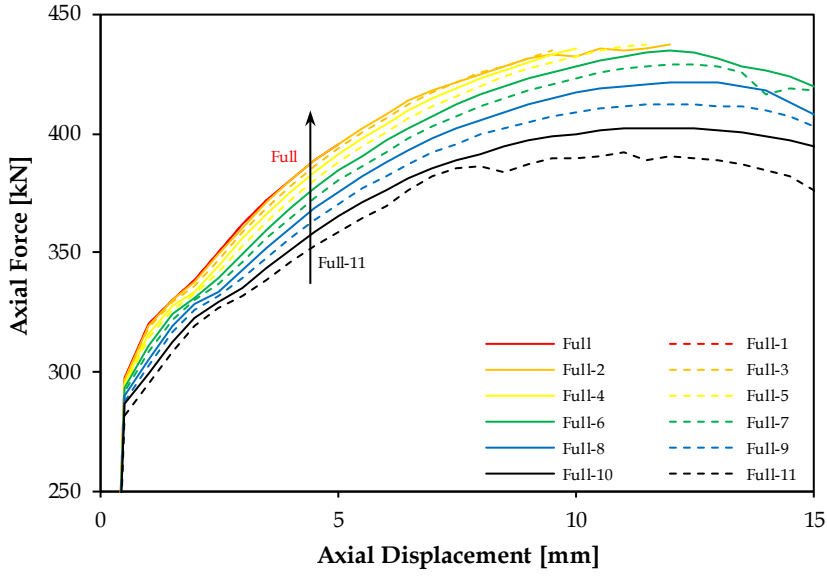

Figure B-2: Effect of reduced contact on the maximum estimated load

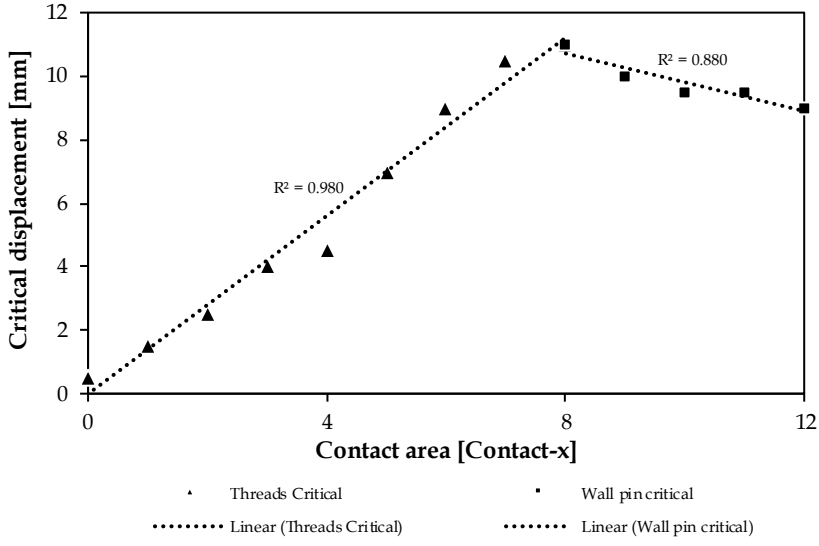

Figure B-3: Location of critical section related to use of contact modification

figure, two linear trends can be observed. In the first part, for a contact area ranging from full contact to the case in which 8 threads (up to LET-7) are omitted from the contact area, a gradual failure of consecutive threads is observed with increasing axial displacement. Once 8 threads have failed, by local jump-out or fracture, failure is observed through the wall of the pin rather than in the vulnerable section of the threads. This failure occurs sooner when the area of contact is further reduced as the result of the tapered thread shape. Since the weakest member is the pin, the wall thickness of the critical section located at the last fully engaged thread reduces and the critical load is reached with less axial displacement. The value at the intersection, approximately x=8 in case of the situation shown in Figure B-3, of these two trends can be assumed to be the last stable contact area and should be used when trying to determine at what location the connection will finally fail.

In the case of the specimen which was experimentally tested in Chapter 3 and which is mentioned here, Figure B-3 indicates that a contact area omitting eight threads (up to LET-7) should be used. When using this contact definition and observing the results displayed in Figure B-1.B, the critical section is located near LET-7 in the wall of the pin. This location also proved to be the weakest point during the experiment.

The full black line in Figure B-4 represents the force-displacement curve using the previously explained approach up to a displacement of 15mm. Since the only objective of this modification is to locate the critical section of the connection and 15 mm exceeds the elongation for which the maximum force is reached and necking starts, it is not required to calculate further data. This

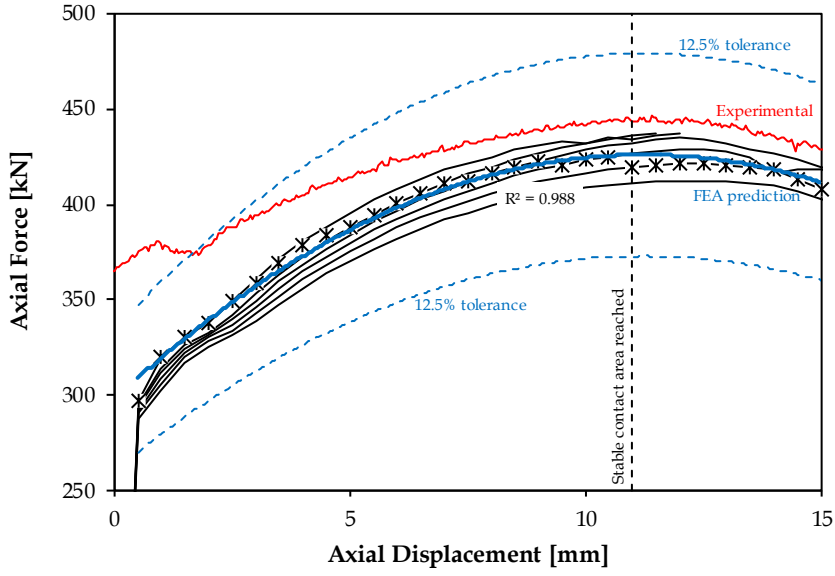

Figure B-4: Proposed Force-Displacement curve

curve was derived based on several simulations taking into account different contact areas which are indicated in grey. Every time a thread failed, a switch between curves was made until a stable contact area was reached. Finally, a second order polynomial trend line was fitted through the results. In order to compare the numerical results with the experimental results, the experimentally obtained curve is added to the graph after matching the maxima of both curves, making corrections taking into account possible axial clearance. When comparing both curves, it is evident that the experimental values are significantly higher than the predictions. This is likely the result of the large tolerances of up to 12.5% which are allowed to the wall thickness of the pin and box. When taking these tolerances into account, the obtained results appear to be plausible once all play is removed from the connection.

When further analyzing the difference between the predicted and measured curves using Figure B-5, it can be observed that the difference with the FEA prediction remains a constant value once an axial displacement of 8mm is reached. This observation suggests that the proposed methodology is plausible for high axial loads, taking into account an initial and constant offset of approximately 18kN or 4.3%. Since this offset is likely caused by the tolerance on the wall thickness. In that case, a constant value is expected and, when not including any damage criterion, this can only be obtained using the modified contact approach as shown in Figure B-5.B. The larger deviations prior to a displacement of 8 mm are possibly caused by the gradual resolving of the occurring play along the thread.

Despite promising results assessing the force-displacement curve, it should be noted that this proposed method is only intended to locate and visualize the critical section in which the connection will fail when excessive axial tensile loads are applied. Therefore, it should not be used to predict the exact strains and stresses since it is not possible to modify the contact surface throughout the simulation, as is the case in reality. In order to calculate reliable stress-strain fields and the exact location where fracture occurs, a more advanced fracture and/or damage model is required.

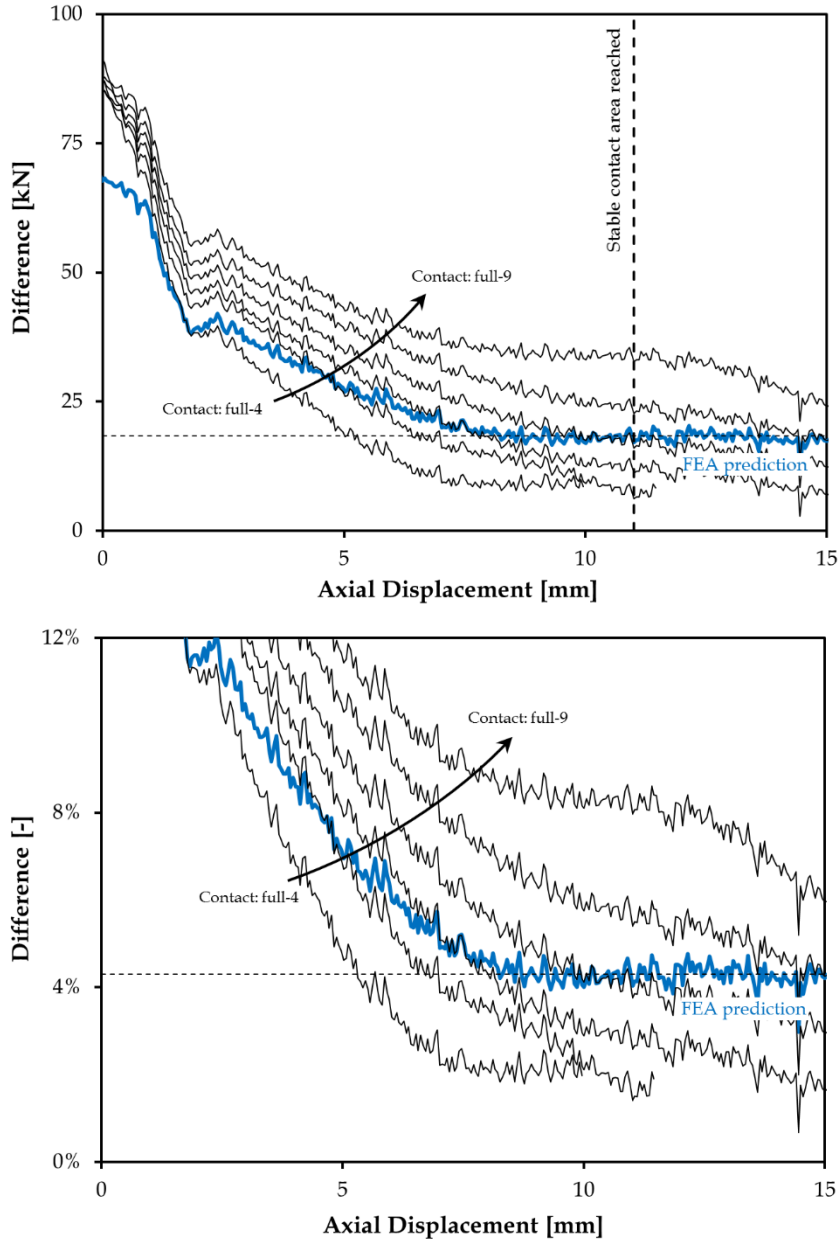

Figure B-5: Difference force-displacement curves